BSEE Contract No. E14PC00007

Final Report

Model Testing to Evaluate Degradation of Axial Capacity from Cyclic Loading

Prepared for Bureau of Safety and Environmental Enforcement

Proposed Research on Renewable Energy of Oil and Gas Operations in the U.S. Outer Continental Shelf

engineers • scientists • innovators	Date of Issue	22 March 2016

Bureau of Safety and Environmental Enforcement

Altan Aydin	Contracting Officer's Representative
Herma Banks	Contracting Officer

Bureau of Ocean Energy Management

Sid Falk, P.E.	Structural Subject Matter Expert
Daniel O'Connell, P.E., G.E.	Geotechnical Subject Matter Expert

Geosyntec/MMI

Christopher Hunt, Ph.D, P.E., G.E.	Senior Principal / Project Manager
Tom McNeilan, P.E., G.E.	Geotechnical Consulting Board / Project Director
Jacquelyn Allmond, Ph.D.	Senior Staff Engineer

University of California, Davis

Bruce Kutter, Ph.D.	Professor
Dan Wilson, Ph.D.	Associate Director, Center for Geotechnical Modeling
Bao Li Zheng, M.S.	Graduate Student Researcher

EXECUTIVE SUMMARY

The project "Model testing to evaluate degradation of axial pile capacity from cyclic loading" for jacket and tripod foundations for Offshore Wind Turbine Structures (OWTS) was awarded to MMI Engineering, Inc. (MMI) by the Bureau of Safety and Environmental Enforcement (BSEE) in response to a solicitation for the BSEE Technology Assessment Program (TAP) on Renewable Energy in the US Outer Continental Shelf (OCS) (Broad Agency Announcement number: E14PS00003). Specifically, the BSEE solicitation stated: "*Degradation of axial pile capacity from cyclic loading needs to be better understood. Model or full scale axial cyclic load tests are needed to confirm recent analytical methods.*"

This report documents the successful execution and results of four multi-stage centrifuge tests performed at the University of California, Davis (UC Davis) Center for Geotechnical Modeling (CGM) using the 1-m radius Schaevitz centrifuge (also referred to as the small centrifuge) while spinning at 80 g. The centrifuge is useful for scale modeling of any large-scale nonlinear problem for which gravity is a primary driving force. Consistent with centrifuge scaling laws, at 80 g a 149 mm model pile represents an 11.9 m long prototype pile, and 100,000 cycles of load can be applied at high frequency (~20 Hz) in under 1.5 hours.

The centrifuge testing program included the following primary goals:

1. Evaluate the potential for obtaining meaningful results using centrifuge testing to measure and evaluate changes in strength, stiffness and load transfer of a single pile subjected to a combination of low amplitude high-cycle loads meant to emulate cyclic loads imposed by an operating OWTS, and large amplitude low-cycle loads associated with environmental loading during storms.
2. Develop an initial data set from scale centrifuge testing of piles subjected to one-way (tension) and two-way (tension and compression) cyclic axial loading.
3. Use the data set to develop an interaction diagram (e.g., Jardine and Standing, 2000; Tsuha, et al., 2013) relating the average static axial load and applied cyclic axial loads to tested maximum pile load and applied number of cycles.
4. Assess the data set relative to recently proposed methods (i.e., Seidel and Uriona, 2011, Stuyts, et al., 2011) for evaluating impacts of cyclic degradation on predicted pile performance.
5. Provide guidance on implications of the findings and recommended next steps (e.g., further testing, additional modeling, etc.).

The approach and scope to achieving these goals were aligned to maximize the results within the available budget for the program. The small centrifuge at the UC Davis CGM, which was used for this program, allows for testing to be completed in a relatively short time, requires minimal material and staffing resources, and is significantly less costly than use of a larger centrifuge. This testing program recognized that the size of the small centrifuge would limit the size of pile and model geometry, and add complexities to the conduct of the testing program. However, the challenges overcome during this program (i.e., testing model piles at very low cyclic load amplitudes over very large numbers of cycles for the first time) enhanced the capabilities of the actuator, controller, and data collection system on the small centrifuge, making it more useful for future testing.

The program results showed that significant value can be obtained from testing in the small centrifuge, specifically in the area of developing failure criteria and interaction diagrams that center on measured behavior (load and displacement) at the pile head. However, for some of the technical goals, specifically related to understanding stiffness and load transfer along the pile shaft, and for developing more complex models such as multi-piled structures, the larger (and more costly) 9-m radius centrifuge at the UC Davis CGM will be required. The implications of the results relative to choice of centrifuge size for future testing are discussed in the report.

The four multi-stage centrifuge tests performed typically included three stages of loading (load packets), beginning with an initial low amplitude load applied for each of 100,000 cycles, followed by a higher amplitude load applied for 10,000 cycles, and a final very large amplitude load applied for 500 cycles. The majority of the load packets consisted of one-way tensile loading only, although two load packets did include two-way loading that cycled between loading in compression and tension. Static pullout tests were conducted prior to, and after each load packet to evaluate changes in axial capacity as a result of cyclic loading. The tests showed that the response of a single pile to the various load packets depends on the ratio of both the applied static and cyclic loads to the tensile capacity of the pile, the number of cycles applied, the history of pile loading, and whether or not the cyclic loads include stress reversals (i.e., two-way loading). In general, low amplitude high-cycle load packets resulted in very little residual pullout of the pile, and very small reductions in tensile capacity, and increasing load amplitude resulted in greater pullout and capacity reduction. The two two-way load packets both resulted in an increase in pile capacity. The full data set is included in the report and its appendices.

Results from one multi-stage test were analyzed using the RATZ computer program (Randolph, 2003) which implements a load transfer approach (i.e., t-z method) with the applied cyclic loading history to compute the degradation of shaft friction and the corresponding reduction in pile capacity. Separately, the four multi-stage tests were analyzed using a linear damage law and interaction diagrams following the approach of Stuyts et al. (2011) which focuses on failure based on conditions at the pile head, and ignores the details of cyclic degradation at depth. While both analytical methods provided insight into the behavior of single piles subject to cyclic loading, neither was able to fully capture the observed behavior from the centrifuge program. Both are considered useful tools, but more test data and more development of the models will be needed to develop and calibrate them for design of OWTS.

Several key implications of the testing program and associated analyses include:

- The current set of tests indicates that, while limited, degradation of pile capacity can still occur under low amplitude high-cycle loading. Current methods of design for OWTS pile foundations do not account for this effect and small changes in capacity may result in changes to the stiffness of the foundation system, which in turn may have implications on the frequency response of the OWTS.

- Current analysis tools are not able to account for the increase in capacity seen in the two-way loading tests in this program. An increase in capacity may also have an impact on the stiffness of the foundation system, and as such this observed condition should be investigated further.
- Because of the above consideration, foundation design may result in either less conservatism than desired or more conservatism than required. Such uncertainty has direct implications relative to the long-term performance and costs of offshore wind turbines. Removal of excess conservatism has the potential to improve the economics of offshore wind. Further evaluation and research is warranted.

Based on the above, the report outlines a recommended research program including both small and large centrifuge testing. The small centrifuge program would be used to enhance our understanding of failure conditions in different loading regimes, as well as different soil types. However, given the complexity of design for OWTS, an understanding of failure conditions is not enough. The large centrifuge program would be used to improve our understanding of soil-pile-structure interaction under operating and shutdown conditions which would in theory be performed at some distance from the failure conditions identified with the small centrifuge. This understanding from the large centrifuge tests would be used to further calibrate and develop analytical tools such as RATZ to improve our ability to design these systems with appropriate degrees of conservatism.

Table of Contents

Figures

Tables

The project "Model testing to evaluate degradation of axial pile capacity from cyclic loading" for jacket and tripod foundations for Offshore Wind Turbine Structures (OWTS) was awarded to MMI Engineering, Inc. (MMI) by the Bureau of Safety and Environmental Enforcement (BSEE) in response to a solicitation for the BSEE Technology Assessment Program (TAP) on Renewable Energy in the US Outer Continental Shelf (OCS) (Broad Agency Announcement number: E14PS00003).

1 INTRODUCTION

Understanding the influence of the soil-pile interface is critical for reliable operations of offshore wind turbines. The foundation and support structure for an offshore wind turbine must satisfy a number of criteria including limits on stiffness, displacement, tilt, and other characteristics that can influence the behavior of the entire system. These requirements are particularly challenging for offshore wind turbines due to their complex dynamic loading conditions. The effects of cyclic loading on multi-piled support structures represent a major gap in the current state of the practice for offshore wind. These structures involve unique design challenges due to:

- The potential for complete load reversal within the piles due to the relatively low gravity loads in the system.
- The fact that the support structures and foundations may be loaded near peak demand during normal operation (i.e., the operating wind load may generate mudline overturning moment close to or in some cases greater than during the design storm condition).
- The substantial number of load cycles that occur due to the almost continuous operation of the rotor.

Significant degradation in soil-pile resistance could lead to excessive deformation, or tilt, of the system, thereby rendering the turbine inoperable. Axial degradation would also result in a softening of the overturning resistance of the system, which would reduce the system vibration frequencies potentially to the point where resonant conditions would occur with rotor frequencies.

There is a substantial amount of prior testing and analysis that has been generated to study axial pile performance for oil and gas applications. While a significant amount of this work is applicable, and has been applied, to offshore wind, the differences in load amplitudes and cycles makes it very difficult to apply this information with the level of confidence that is needed, particularly in light of the aforementioned performance requirements.

This research addresses a critical gap in the design and analysis of offshore wind turbines supported by jacket and tripod structures. Specifically, the project was designed to advance the state-of-the-art for understanding the influence of repeated cyclic loading on axial capacity of this type of foundation within an offshore wind loading environment by:

1. Evaluating the potential for obtaining meaningful results using a centrifuge to measure and evaluate changes in strength, stiffness and load transfer of a single pile subjected to a combination of low amplitude high-cycle loads meant to emulate cyclic loads imposed by an operating OWTS, and large amplitude low-cycle loads associated with environmental loading during storms.
2. Developing an initial data set from scale centrifuge testing of piles subjected to one-way (tension) and two-way (tension and compression) cyclic axial loading.
3. Using the data set to develop an interaction diagram (e.g., Jardine and Standing, 2000; Tsuha, et al., 2013) relating the average static axial load and applied cyclic axial loads to tested maximum pile load and applied number of cycles.
4. Assessing the data set relative to recently proposed methods (i.e., Seidel and Uriona, 2011, Stuyts, et al., 2011) for evaluating impacts of cyclic degradation on predicted pile performance.
5. Providing guidance on implications of the findings and recommended next steps (e.g., further testing, additional modeling, etc.).

2 CENTRIFUGE TESTING PROGRAM

The scaled model testing program was performed at the University of California, Davis (UC Davis) Center for Geotechnical Modeling (CGM) using the 1-m radius Schaevitz centrifuge (also referred to as the small centrifuge[1]). Four series of model tests were performed on the centrifuge while spinning at 80 *g*. The centrifuge is useful for scale modeling of any large-scale nonlinear problem for which gravity is a primary driving force. Soils have nonlinear mechanical properties that depend on the effective confining stress and stress history. The centrifuge applies an increased "gravitational" acceleration to physical models to produce identical self-weight stresses in the model and prototype. The one to one scaling of stress enhances the similarity of geotechnical models and makes it possible to obtain accurate data to help solve complex problems such as soil-structure interaction.

2.1 Model Pile

Three centrifuge proof tests were performed on dummy piles to optimize the cyclic loading actuator control system, verify the model pile installation method, and design an adequate coating to protect strain gauge instrumentation. The extensive preliminary test sequencing was critical to building a robust and reliable testing program.

The final pile used for all tests was made from Aluminum 6061-T6 tubing with 40,000 psi yield strength manufactured by Vita Needle Company. The tubing had a diameter of 7.94 mm (5/16 inch), and a wall thickness of 0.51 mm (0.020 inch). The fabricated full length tube was cut to 19.05 cm (7.5 inches) at the centrifuge facility, and fitted with a pointed tip to minimize installation disturbance and improve instrumentation survivability. The model pile properties are provided in Table 1 in both model and prototype scale, and were chosen based on the following criteria:

- The total length of pile above ground prior to installation and the height of the actuator were limited by the clearance in the centrifuge.
- The depth of installation was limited in order to limit the influence of the rigid base of the container.[2]
- L/D ratio near 20, within range of a prototype offshore structure.
- Material strength and wall thickness with enough rigidity to prevent bending, buckling, or compression failure of the pile during installation, but with enough flexibility to capture potential progressive failure at depth.

[1] The UC Davis CGM has both a small (1-m) and a large (9-m) radius centrifuge. As with this program, the small centrifuge is often used for initial fundamental research due to lower cost and relative speed with which experiments can be assembled. The large centrifuge has significantly greater capabilities due to increased model size and greater number of instruments that can be tested, but is both more costly and requires more time to prepare.
[2] If the pile is embedded too deeply in the container the pile tip response can be influenced by the container base.

Instrumentation was installed on the final model pile using with the following steps:

1. Four full strain gauge bridges were mounted on the outside of the model pile to measure axial load at different depths.
2. Strain gauge wires were routed through the aluminum tubing.
3. The pile was loaded in compression beyond installation stress (buckle check), strain gauges calibrated and checked for cross-axis, drift, and temperature sensitivity.
4. Sealant-sand mixture was adhered to the aluminum tube and strain gauges to roughen the pile surface and to prevent the wires from being scraped off the gauges during pile installation and testing.
5. A plug was installed at the pile tip (closed tip condition) to protect the sensor wires inside the pile.

Figure 1 shows the final instrumented pile, including locations of the four strain gauges, displacement gauge, axial load cell, actuator, and accelerometers.

2.2 Sand Specimen

The uniformly graded fine sand, Ottawa F-65, was used as the model soil material. The soil model was dry-pluviated using hoppers and funnels to a target relative density of between 65% and 70% to produce strain softening behavior following a peak strength, while preventing pile yielding during in flight installation. It is possible to perform this test in a saturated or unsaturated condition, however a dry sand model is easier to construct to a consistent relative density and produces more reliable instrumentation performance. A dry sand model was therefore the preferred condition for this fundamental research. After the first full test, the bottom 7 mm of the container was lined with modeling clay, covered by 18 mm of a looser relative density sand layer to prevent pile buckling during installation. This 25 mm thick looser base layer was assumed to have a limited effect on the pile response as the pile shaft did not penetrate the lift (see Figure 1), and the loading conditions were predominantly in tension. The properties of the Ottawa F-65 Sand are provided in Table 2 and the achieved specimen relative densities are shown in Table 3.

Scaling of soil particles is an important issue to consider in centrifuge modeling. The main requirement is to have a sufficient number of particles across the dimensions of the model so that the soil can be considered a continuum and modeled as such. The acceptable ratio of the diameter of the model (D_{model}) to the diameter of the particle (D_{particle}) depends on the problem being studied. For this test, the $D_{\text{pile}}/D_{\text{particle}}$ is approximately 40.

2.3 Test Sequencing

The testing program consisted of five separate centrifuge model tests, each with a prescribed set of loading scenarios. A hydraulic actuator and load cell attached to the pile head controlled both in flight pile installation and the cyclic and static loading conditions. The first test was designed to establish baseline static pile capacity, test the pile installation method, test the cyclic loading system and general pile response, and troubleshoot any identified issues.

The remaining four tests were designed to progress from:

1. A small cyclic amplitude, high-cycle, high frequency scenario, corresponding to normal operating conditions in calm seas where the major cyclic loads applied to the foundation come from rotor unbalance force (at the rotor frequency) and the aerodynamic interaction of the rotor blades and the tower (at 3 times the rotor frequency), with static loads at 30-40% of pile capacity and cyclic loads at 2-5% of capacity; to
2. A higher cyclic amplitude, moderate-cycle, high frequency scenario, corresponding to operating conditions in higher seas where the cyclic loads applied to the foundation are dominated by normal wave action, with similar static loads as in case 1, while cyclic loads increased to 10-20% of pile capacity; to
3. A very large cyclic amplitude, small-cycle, low frequency scenario, corresponding to a design storm condition where the turbine is shut down and the structure is subjected to the design storm wind and wave loading, with static loads decreased to 20-30% of pile capacity and cyclic loads increase to 30-40% of capacity.

As such, the maximum load the piles saw (static plus cyclic) was 40% to 60% of pile capacity (i.e., design factor of safety of approximately 2).

The complete load sequencing for each centrifuge test is shown in Table 4. At the start and end of each test, the load cell and strain gauges were calibrated to measure their initial readings. Before and after each load packet, a pullout test was performed to identify the change in capacity associated with the previous load packet[3]. These pullout tests were performed by retracting the pile 2 mm with the displacement controlled actuator and recording the resulting tensile load as measured by the load cell at the pile head. The results from these tensile capacity tests are provided in Appendix A, and are summarized in Table 4.

As shown in Table 4, while the pile used in all tests was the same, small variations in initial density of the sand samples, and possibly small deviations during pile installation at this small scale, resulted in measured initial tensile capacities ranging from 180 N to 320 N, and possibly up to approximately 450 N (inferred for Test 4). These variations demonstrate the importance of comparing the tests after normalization by pile capacity.

[3] For Test 2A, after 86,000 cycles of loading, the adapter from the pile to the loading actuator failed and the test was halted. As such, no pullout test was performed at the end of this test.

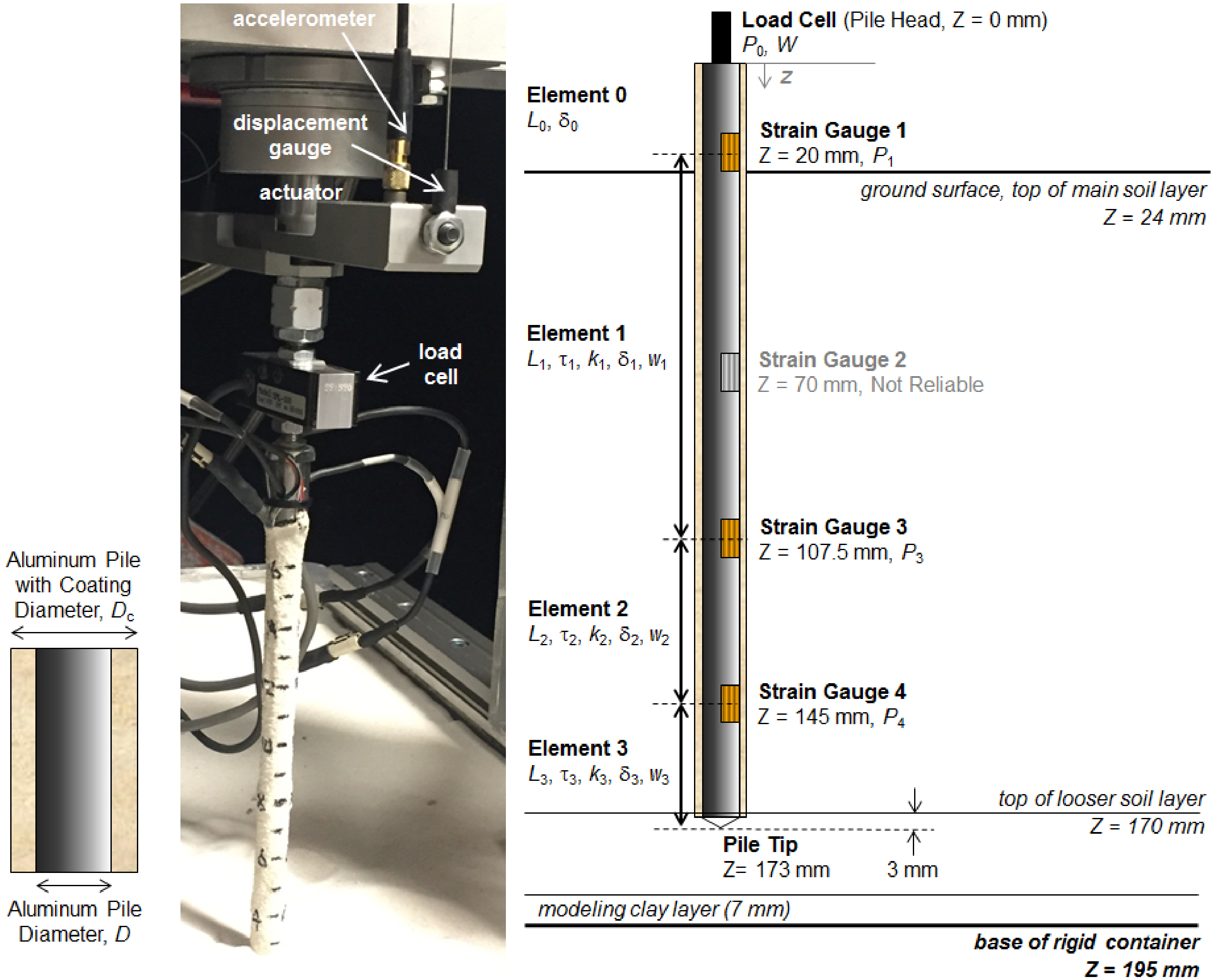

Figure 1. Model pile with sensor instrumentation.

Table 1. Model Pile Parameters (model and prototype scale)

	Model	Prototype (at 80 g)
Diameter, D	7.9 mm	0.64 m
Thickness, t	0.5 mm	40 mm
Embedded Length, L	149 mm	11.92 m
Embedded L/D	18.8	
Material	Aluminium	
Yield Strength	40,000 psi	

Table 2. Material Properties of Ottawa F-65 Sand*

Soil Description	Pale Brown Poorly-Graded Sand
Specific Gravity, Gs	2.67
Minimum Void Ratio, e_{min}	0.54
Maximum Void Ratio, e_{max}	0.76
Minimum Dry Density, $\rho_{d,min}$	1515 kg/m^3
Maximum Dry Density, $\rho_{d,max}$	1736 kg/m^3
Grain Size, D_{10}	0.13 mm
Grain Size, D_{30}	0.18 mm
Grain Size, D_{60}	0.23 mm
Coefficient of Uniformity, C_u	1.7
Coefficient of Curvature, C_c	1.1
% Fines	0.9%

**Carey et al. (2015).*

Table 3. Specimen Relative Density

Centrifuge Test	Sand Specimen Number	Relative Density, D_R	
		Main Layer (top 146 mm)	**Looser Layer** (bottom 15 mm)
Test 2A	1	65%	65%
Test 2B	2	66%	46%
Test 3			
Test 4	3	70%	43%
Test 5	4	70%	44%

Table 4. Centrifuge Test Sequencing of Load Packets and Tensile Tests

Test	Type	ID	N_{cycles} = 1,000 cycles	Q_{static} / Q_T	Q_{cyclic} / Q_T	Static Load (N)	Cyclic Load (N)	Tensile Capacity (N)	Residual Pullout (mm)	Residual Pullout Rate (RPR) (mm/1,000 cycles)
Test 2A	*Calibration at 1g, Calibration at 80g, Pile Installation*									
	Tensile Test							205		
	Load Packet	2A-I	86	0.38	0.05	78	10		0.0	0.00
	Pile-Actuator Adapter Failed, Test Halted									
Test 2B	*Calibration at 1g, Calibration at 80g, Pile Installation*									
	Tensile Test	A						285		
	Load Packet	2B-I	100	0.39	0.02	110	6		0.0	0.00
	Tensile Test	B						275		
	Load Packet	2B-IIA	10	0.43	0.11	118	29		0.2	0.02
	Tensile Test	C						230		
	Load Packet	2B-IIB	10	0.30	0.22	70	51.5		9.5	0.95
	Tensile Test	D						175		
	Retract Pile, Calibration at 80g									
Test 3	*Calibration at 1g, Calibration at 80g, Pile Installation*									
	Tensile Test	A						180		
	Load Packet	3-I	100	0.32	0.06	58	10.5		0.0	0.00
	Tensile Test	B						175		
	Load Packet	3-II	10	0.29	0.10	50	17.5		0.0	0.00
	Tensile Test	C						170		
	Load Packet	3-III	0.5	0.19	0.42	33	71.5		0.0	0.00
	Tensile Test	D						180		
	Retract Pile, Calibration at 80g									
Test 4	*Calibration at 1g, Calibration at 80g, Pile Installation*									
	Tensile Test	A						281 (450)*		
	Load Packet	4-I	100	0.24	0.02	109	11		0.0	0.00
	Tensile Test	B						454		
	Load Packet	4-II	10	0.24	0.08	109	36		0.0	0.00
	Tensile Test	C						411		
	Load Packet	4-III	0.5	0.20	0.19	81	77.5		0.7	1.35
	Tensile Test	D						373		
	Retract Pile, Calibration at 80g									
Test 5	*Calibration at 1g, Calibration at 80g, Pile Installation*									
	Tensile Test	A						320 (400)*		
	Load Packet	5-IA	10	0.14	0.08	55	31		0.0	0.00
	Load Packet	5-IB	1	0.14	0.07	55	27		0.0	0.00
	Tensile Test	B						340		
	Load Packet	5-II	0.5	0.16	0.23	56	78		0.2	0.40
	Tensile Test	C						375		
	Load Packet	5-III	0.05	0.29	0.21	107	79		2.7	54.00
	Tensile Test	D						200		
	Retract Pile, Calibration at 80g									

**After installation, 2 mm pullout displacement was insufficient to fully mobilize pile capacity. Tensile capacities in parentheses were selected based on a review of test progression in tandem with the subsequent pullout test.*

3 CENTRIFUGE TEST RESULTS

3.1 Interaction Diagrams

The target load packets for centrifuge tests 2 through 5 are shown superimposed on the Tsuha, et al. (2012) interaction diagram in Figure 2, where the target load packets are shown in Table 5. N_{cyc} values are shown next to the load packets, where N_{cyc} corresponds to the total number of applied cycles in the load packet (N_i) divided by 1,000 (e.g., 100,000 cycles corresponds to N_{cyc} = 100 and 500 cycles corresponds to N_{cyc} = 0.5, etc.).

Tests 2 and 3 were designed to capture both the stable and meta-stable regimes described by Tsuha, et al. (2012) in both one-way (tension only) and two-way (tension and compression) loading. Tests 4 and 5 were then developed based on a preliminary study of the Test 2 and 3 results. The goals of test 4 and 5 were to capture more data in (1) the lower loading, higher cycle regime to target the progressive failure mechanisms of small amplitude loading over many thousands of cycles, (2) the one-way, tension only, side of the meta-stable regime, where significant pull out was observed in Test 2, and (3) the two-way loading regime, where improved performance over one-way loading was observed in Test 3.

On the interaction diagram shown in Figure 2 and throughout this report, the boundaries of stable, meta-stable, and unstable zones are presented consistent with the boundaries included in Tsuha et al. (2012). As described by Tsuha et al., the stable zone is "where axial displacements stabilize or accumulate very slowly over hundreds of cycles, under either [two-way] or [one-way] (in this case, tensile) loading. It was noted that such cycles can improve shaft capacity." This zone is characterized by Tsuha et al. as having cyclic failure in greater than 1000 cycles (N_f > 1000). The meta-stable zone is described as "where displacements accumulate at moderate rates over tens of cycles without stabili[z]ing. Cyclic failure develops with 100 < N_f <1000." The unstable zone is described as "where displacements accumulate rapidly under [one-way] and [two-way] cycling." Note that Tsuha et al. state that the "pattern" of the interaction diagram is likely to change with differing soil conditions and pile parameters.

The achieved load interaction diagram for Tests 2 through 5 is shown in Figure 3, with the load values shown in Table 6. In the figure, the N_{cyc} values and the Residual Pullout Rates (RPR) are shown next to the load packets. The RPR is defined herein as the residual pile head pullout (positive) normalized by N_{cyc}. Negative residual pile head pullout (insertion) values are reported as zero in Table 6, with measured values provided in Appendix B. The RPR should be considered an index of relative deformation, as it only considers total displacement from load packet start to finish and does not capture progressive failure throughout cycling. The RPR is considered a surrogate for "failure" within the interaction diagram regimes from the literature; however failure criteria and damage (i.e., loss of capacity) will be discussed in later sections. In general the load packets in the stable regime (relatively low amplitude cyclic loading) away from the stable/meta-stable boundary all have nearly zero RPR values with very little residual pullout or insertion. In the case where the static load is over 40% of the tensile capacity (i.e., 2B-IIA, 10 N_{cyc}) the RPR (0.02) has begun to increase. For the two load packets which went into compression (two-way loading) in the meta-stable region, very different RPR values were observed over 500 cycles. For Test 3-III a small residual pullout was measured, but is considered to be near the tolerance of the string potentiometer used for measurement, and so was assigned a residual pullout of 0 mm and hence an RPR of 0. For Test 5-II, a larger RPR of 0.4 was calculated. This variation for two-way loading tests may be an indication of the importance of loading history on the observed response of an OWTS system.. Finally, in the one-way loading meta-stable regime (or close to the stable/meta-stable boundary), where the pile is loaded purely in tension at medium cyclic and static loads (2B-IIB, 4-III, and 5-III), the highest RPR values were recorded (0.95, 1.35, and 54, respectively).

3.2 Soil-Pile Response

The progressive loading and displacement of the pile can be summarized through plots of axial load vs time, pile head displacement vs time, and axial load vs pile head displacement. Axial load was measured by the load cell at the top of the pile, and pile head displacement was measured by a string potentiometer attached to a beam connected to the pile head (see Figure 1). Time histories are provided in Appendix B.

Three different types of pile displacement response were observed in this testing series. For cases where the pile was two-way loaded in both tension and compression (Test 3-III and Test 5-II), there is a notable difference in stiffness and displacement. The axial load vs displacement figures for Test 3-III and Test 5-II show more complex loops of stiffening and softening as the pile moves in and out of compression-tension loading. The softer response observed in the compression zone could be due to global changes in density as the pile moves in and out of compression, closure of the gap under the pile tip as the pile is inserted, or loading into looser material which has filled the gap under the pile tip.

Additionally, ratcheting of the pile was observed in cases with pure tension loading. The axial load vs displacement figures of Test 2B-IIA and Test 4-III, show a fairly consistent stiffness throughout loading. Their displacement vs time plots also show gradual displacement at the pile head over time as the pile is cycled, with small residual displacements. In these cases, the pile is likely ratcheting out of the soil due to the prolonged exposure to cyclic tensile loads. In the case of Test 4-III, had the test continued past 500 cycles it is likely that the residual displacements would have been significantly higher as the pile continued to ratchet out of the ground.

Finally, “failure” of the pile, considered herein as pullout approaching (Test 4-III) or exceeding (Tests 2B-IIB and 5-III) 10% of the pile diameter, was observed in cases of one-way tensile loading where cyclic loading was on the order of 20% of the initial capacity, resulting in significant capacity reduction during cycling. The most extreme case is Test 5-III. As shown in the axial load vs displacement figure in Appendix B, the overall stiffness for Test 5-III is fairly consistent throughout cycling and the majority of the displacement is observed when the pile is at the maximum applied tensile load. The initial tensile capacity of the pile was 375 N, however the pullout test following 5-III indicates a significant drop in tensile capacity to 200 N. In this case, perhaps in part due to densification during the preceding two-way loading in Test 5-II, the pile appears to have undergone rapid degradation of capacity, such that it was being loaded to near the final tensile capacity of 200 N over much of the duration of the test, and pulling out at this load with each cycle.

Table 5. Target Load Packets

Test-Load Packet	N_{cyc} =1000 cycles	$\frac{Q_{stat}}{Q_T}$	$\frac{Q_{cyc}}{Q_T}$
2-I	100	0.40	0.02
2-II	10	0.40	0.10
2-II	0.5	0.30	0.30
3-I	100	0.30	0.05
3-II	10	0.30	0.20
3-III	0.5	0.20	0.40
4-I	100	0.40	0.05
4-II	10	0.40	0.16
4-III	0.5	0.30	0.30
5-I	10	0.20	0.10
5-II	0.5	0.20	0.30
5-III	0.5	0.40	0.30

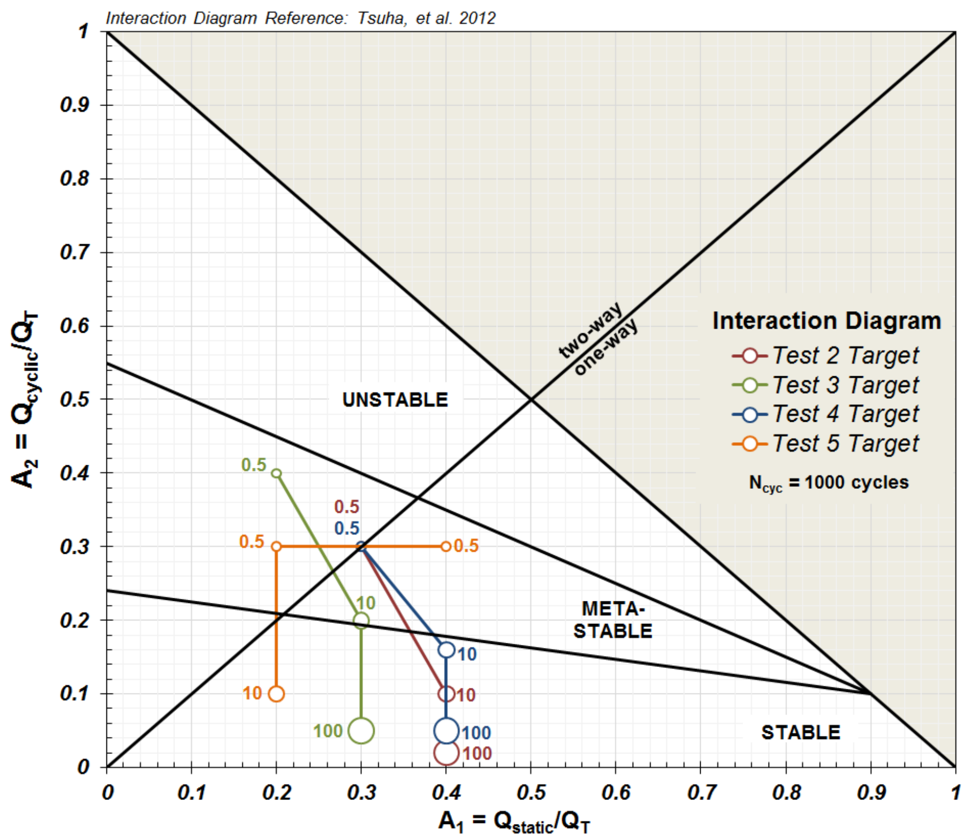

Figure 2. Target Interaction Diagram

Table 6. Achieved Load Packets

Test-Load Packet	N_{cyc} =1000 cycles	Q_{stat}/Q_T	Q_{cyc}/Q_T	Static Load (Q_{stat}) (N)	Cyclic Load (Q_{cyc}) (N)	Pre Tensile Capacity (N)	Post Tensile Capacity (N)	Residual Pullout (mm)	Residual Pullout Rate (RPR) (mm/1,000 cycles)
2A-I	86	0.38	0.05	78	10	205	--	0.0	0.00
2B-I	100	0.39	0.02	110	6	285	275	0.0	0.00
2B-IIA	10	0.43	0.11	118	29	275	230	0.2	0.02
2B-IIB	10	0.30	0.22	70	51.5	230	175	9.5	0.95
3-I	100	0.32	0.06	58	10.5	180	175	0.0	0.00
3-II	10	0.29	0.10	50	17.5	175	170	0.0	0.00
3-III	0.5	0.19	0.42	33	71.5	170	180	0.0	0.00
4-I	100	0.24	0.02	109	11	450*	454	0.0	0.00
4-II	10	0.24	0.08	109	36	454	411	0.0	0.00
4-III	0.5	0.20	0.19	81	77.5	411	373	0.7	1.35
5-IA	10	0.14	0.08	55	31	400*	400*	0.0	0.00
5-IB	0.5	0.14	0.07	55	27	400*	340	0.0	0.00
5-II	0.5	0.16	0.23	56	78	340	375	0.2	0.40
5-III	0.05	0.29	0.21	107	79	375	200	2.7	54.00

Assumed value since 2mm displacement for pullout test was insufficient to fully mobilize pile capacity.

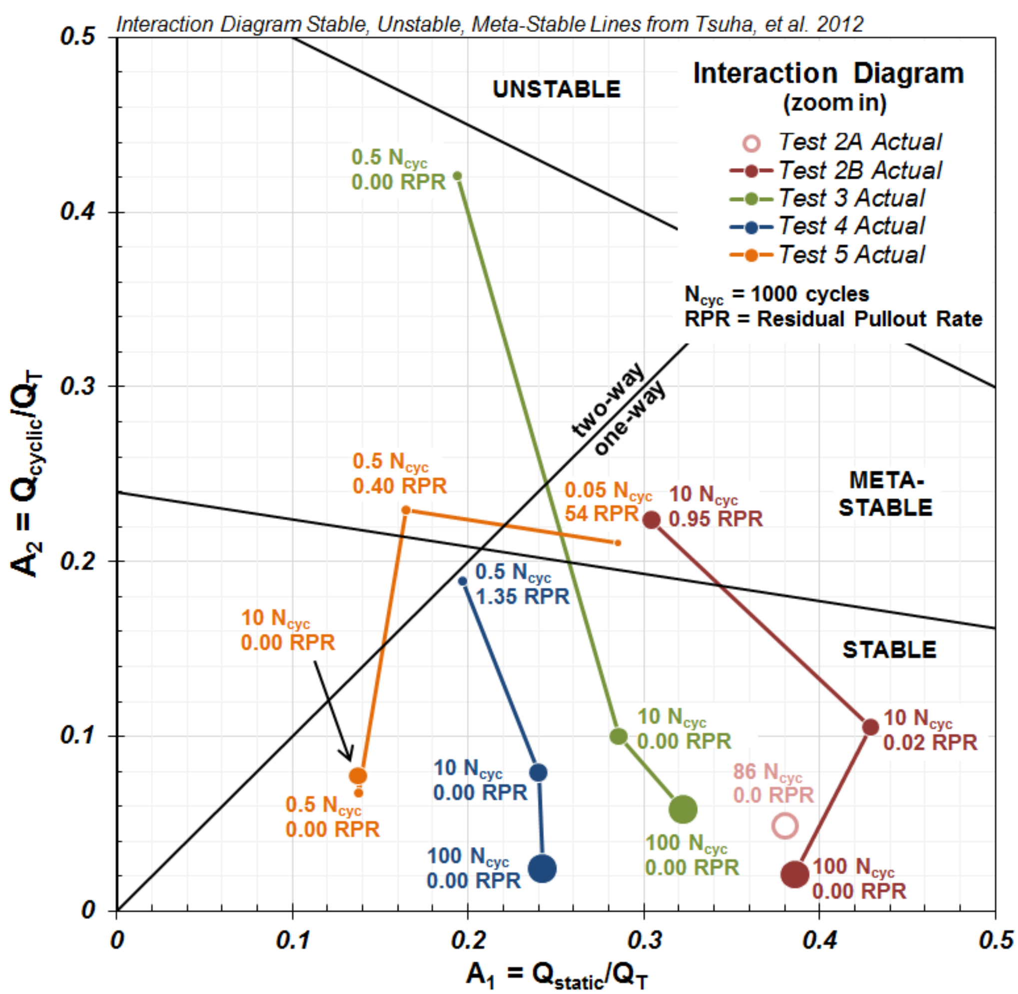

Figure 3. Achieved Interaction Diagram

3.3 Where is Cyclic Degradation Occurring?

3.3.1 Cyclic Axial Loads with Depth

Cyclic degradation with depth was captured between load packets using the calculated cyclic axial loads from the strain gauges. The cyclic axial loads at each strain gauge were compared to the loads measured by the load cell at the pile head, and to pre- and post-tensile capacities of the pile. The results are plotted in Appendix C.

Each time history plot provides a snapshot of the cyclic load (top figure) measured by the Load Cell (LC), Strain Gauge 1 (SG1, above soil), Strain Gauge 3 (SG3), and Strain Gauge 4 (SG4) (see Figure 1 for strain gauge locations). Due to its proximity to the load cell and position above the soil, the cyclic load of SG1 closely matches the load cell. SG3 and SG4 consistently show shedding of the cyclic load with depth. SG2 results are not considered reliable, and hence are not included in any of the analyses. The bottom figure on each time history plot shows the cyclic strain gauge load normalized by the cyclic load from the load cell. A value of 1 would indicate a perfect match to the load cell reading. The normalization becomes unstable as the cyclic load cell reading approaches zero (i.e., dividing by zero). As such, the normalized values were developed only over a range of data near the peaks of each cycle. The plots show the percentage of the total applied cyclic load (i.e., load cell reading) measured at the depth of each strain gauge, and can be evaluated over the entire time history.

Using the location of the strain gauges, a representative cyclic load (Q_{cyc}) for the load cell and each strain gauge has been plotted in three additional ways for each test in Appendix C. The first figure of cyclic load vs. depth indicates a decrease of cyclic load with depth, consistent with the time history plots. The second figure shows strain gauge Q_{cyc} normalized by the load cell Q_{cyc}. In all cases, SG3 shows an increased percentage of the total cyclic load over the course of each test, although the percentage increase varies significantly between tests (e.g., ~20% increase in Test 2B vs ~5% increase in Test 4). The third figure for each test shows the strain gauge Q_{cyc} normalized by the pre- and post-tensile capacities of the pile (Q_T). Normalization by the post-tensile capacity tends to move the lines to the right, indicating that the value of Q_{cyc} is a larger component of the reduced total capacity at the end of the load packet. Stuyts et al. (2012) observed that based on the large-scale testing at Dunkirk, cyclic loading at greater than 25% of the pile capacity resulted in densification of soil surrounding the pile, and corresponding degradation in radial effective stress and reduction in shaft friction, and that cyclic loads under 25% could be beneficial to pile capacity. Most of the cyclic loads at depth fall well below the 25% capacity level in these tests, but the pile capacity was typically reduced even at these lower cyclic demands. Only for the two load packets with two-way loading (3-III and 5-II), an increase in pile capacity is reflected in a reduced normalized Q_{cyc}/Q_T.

Overall, very little change in cyclic load at depth was observed in the strain gauges over the duration of each load packet. This may be consistent with observations by others (e.g., Tsuha, et al., 2012) that most degradation occurs at shallow depths which are not captured by SG3 and SG4. Given the higher shaft resistance at depth corresponding to the higher confinement, a significant reduction in capacity at shallow depth may be consistent with the relatively small percentage increase in demand noted in the strain gauges at depth.

3.3.2 Soil-Pile Stiffness and Local Displacement with Depth

Local displacements and soil-pile stiffness at depth were evaluated as additional indicators of potential cyclic degradation over the duration of loading. The soil-pile stiffness along the pile was calculated using the measured loads from the strain gauges and displacement measured at the pile head. Mobilized shaft resistance (τ) along the pile can be calculated as:

$$\tau = \frac{P}{\pi D L} \qquad \textbf{EQ. 1}$$

where P is the total axial load acting on the pile, D is the diameter of the pile, and L is the pile length. Equation 1 can then be applied to each segment (i.e., element) along the model pile (parameters and elements shown in Figure 1):

$$\begin{bmatrix} \tau_1 \\ \tau_2 \\ \tau_3 \end{bmatrix} = \begin{bmatrix} (P_1 - P_3)/\pi D_c L_1 \\ (P_3 - P_4)/\pi D_c L_2 \\ P_4/\pi D_c L_3 \end{bmatrix} \qquad \textbf{EQ. 2}$$

where P_x is the load measured by the strain gauge x, D_c is the composite diameter of the pile (i.e., including the sand and epoxy coating), L is the pile element length, and the tensile load at the pile tip is assumed to be zero[4]. The axial deformation at the center of each element due to loading (δ) was calculated by using the average load acting on the element as follows:

$$\begin{bmatrix} \delta_1 \\ \delta_2 \\ \delta_3 \end{bmatrix} = \sum \frac{PL}{EA} = \begin{bmatrix} \dfrac{\left(\dfrac{P_0 + P_1}{2}\right) L_0}{(EA)_c} + \dfrac{\left(\dfrac{3P_1 + P_3}{4}\right)\dfrac{L_1}{2}}{(EA)_c} \\ \delta_1 + \dfrac{\left(\dfrac{P_1 + 3P_3}{4}\right)\dfrac{L_1}{2}}{(EA)_c} + \dfrac{\left(\dfrac{3P_3 + P_4}{2}\right)\dfrac{L_2}{2}}{(EA)_c} \\ \delta_2 + \dfrac{\left(\dfrac{P_3 + 3P_4}{4}\right)\dfrac{L_2}{2}}{(EA)_c} + \dfrac{\dfrac{3P_4}{4}\dfrac{L_3}{2}}{(EA)_c} \end{bmatrix} \qquad \textbf{EQ. 3}$$

Where E is the Young's modulus of the pile, A is the area of the pile, and $(EA)_c$ is the composite axial stiffness (i.e., including the sand and epoxy coating, estimated as 1.6 times the EA of the aluminum tubing). The local displacement at each element (w) can then be calculated by subtracting the axial deformation from Equation 3 from the total displacement measured at the pile head (W):

---

[4] In two-way loading when the pile is in compression, the load at the pile tip will not be zero. This introduces recognized discrepancies in applying this approach to the two load packets where two-way loading occurs.

$$\begin{bmatrix} w_1 \\ w_2 \\ w_3 \end{bmatrix} = W - \begin{bmatrix} \delta_1 \\ \delta_2 \\ \delta_3 \end{bmatrix} \qquad \textbf{EQ. 4}$$

Finally, the soil-pile stiffness (*k*) at the center of each element is then defined as the ratio of the mobilized shaft resistance (Equation 2) and the local displacement (Equation 4):

$$\begin{bmatrix} k_1 \\ k_2 \\ k_3 \end{bmatrix} = \begin{bmatrix} \tau_1/w_1 \\ \tau_2/w_2 \\ \tau_3/w_3 \end{bmatrix} \qquad \textbf{EQ. 5}$$

After transforming the cyclic strain gauge load measurements to shaft friction at each element using Equation 2, the static shaft friction was calculated by averaging the time history over a set of cycles (e.g., averaging was performed over 10 and 5 cycles for the high frequency (~20 Hz) and low frequency (0.5 Hz)[5] cyclic loading conditions respectively). This averaging process was performed 5 times at equally spaced intervals within a single load packet, at each pile element, and at the pile head. The interval shaft friction values were then used in Equation 4 to compute the local displacement, and then Equation 5 was used to compute the soil-pile stiffness at the same intervals.

The interval soil-pile stiffnesses are shown for each test in Figure 4, along with the tensile capacity measured between load packets. In general, the soil-pile stiffness degrades as the tests progress within a load packet and throughout sequential load packets. This is consistent with a reduction in mobilized shaft resistance, or an increase in displacement, over the course of the test. For one-way loading scenarios, the tensile capacities also degrade.

For two-way loading, tensile capacities are seen to increase after the load packet is complete. In Test 3-III, a small increase in tensile capacity is paired with an increase in soil-pile stiffness over the duration of the load packet. In test 5-II however, a larger increase in tensile capacity is paired with an initial increase in stiffness and then a decrease throughout the remainder of the load packet. The interpretations of this analysis are further complicated in two-way loading by the presence of compressive loads at the pile tip during part of each cycle, which is admittedly neglected by the procedure for computing stiffness as outlined above.

The soil-pile stiffness can also be compared to the cyclic local displacement for each test, as shown in Figure 5. These plots show a clear trend that as the measured cyclic local displacements increase, the soil-pile stiffness decreases. The change in soil-pile stiffness with displacement is also typically greater with depth (i.e., the slope of the trend line for Element 3 (deepest embedment) is typically steeper than the slope of the trend line for Element 1 (shallowest embedment)).

[5] The 0.5 Hz loading frequency used in Load Packets 3-III, 4-III, 5-II, and 5-III, falls outside the frequency range of both the accelerometers and string potentiometer. The averaging process described above does not account for non-linearity in the instrument; therefore the discrete values of soil-pile stiffness provided in Figure 4 for these loading packets are very sensitive at small displacements.

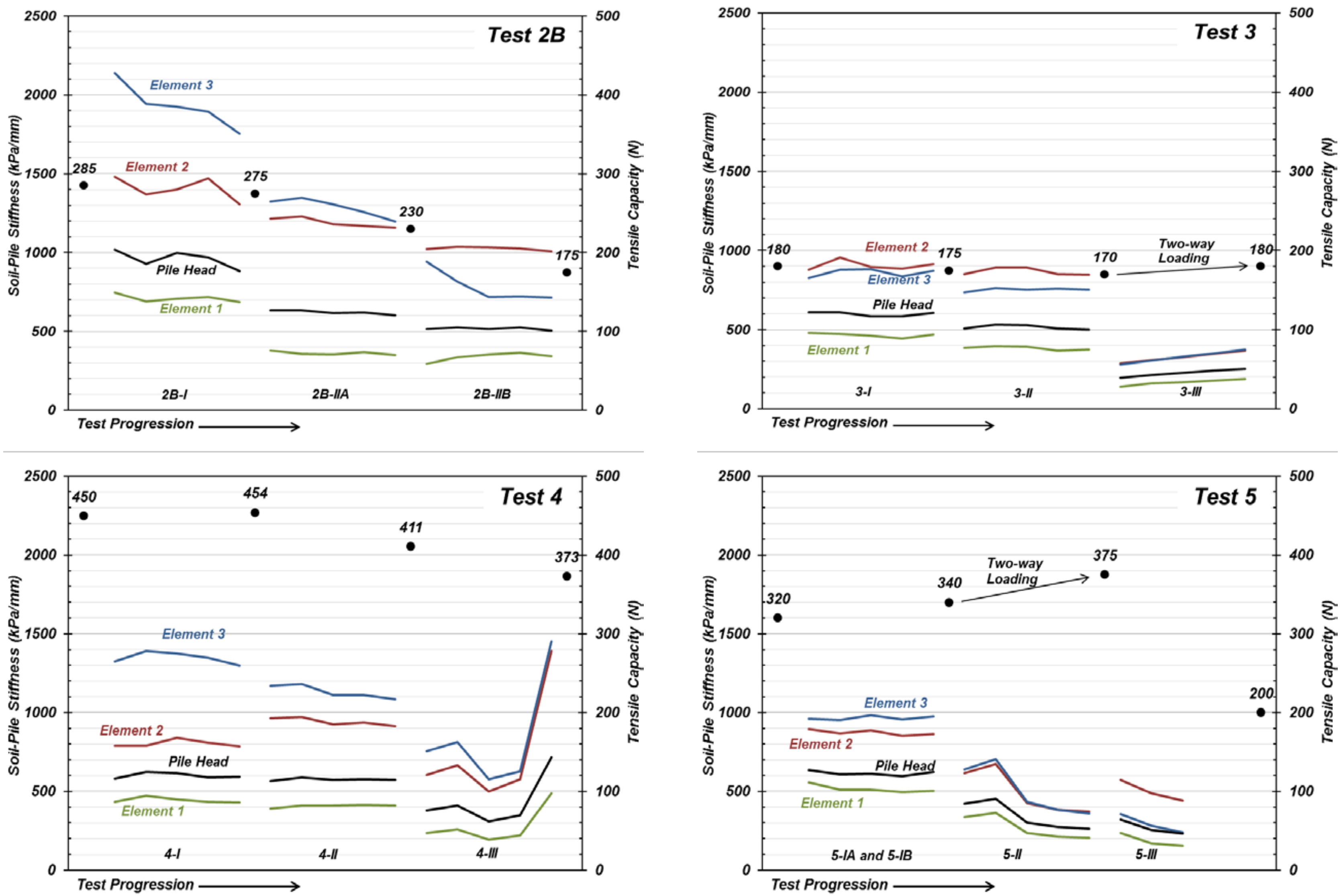

Figure 4. Soil-Pile Stiffness and Tensile Capacity with Test Progression

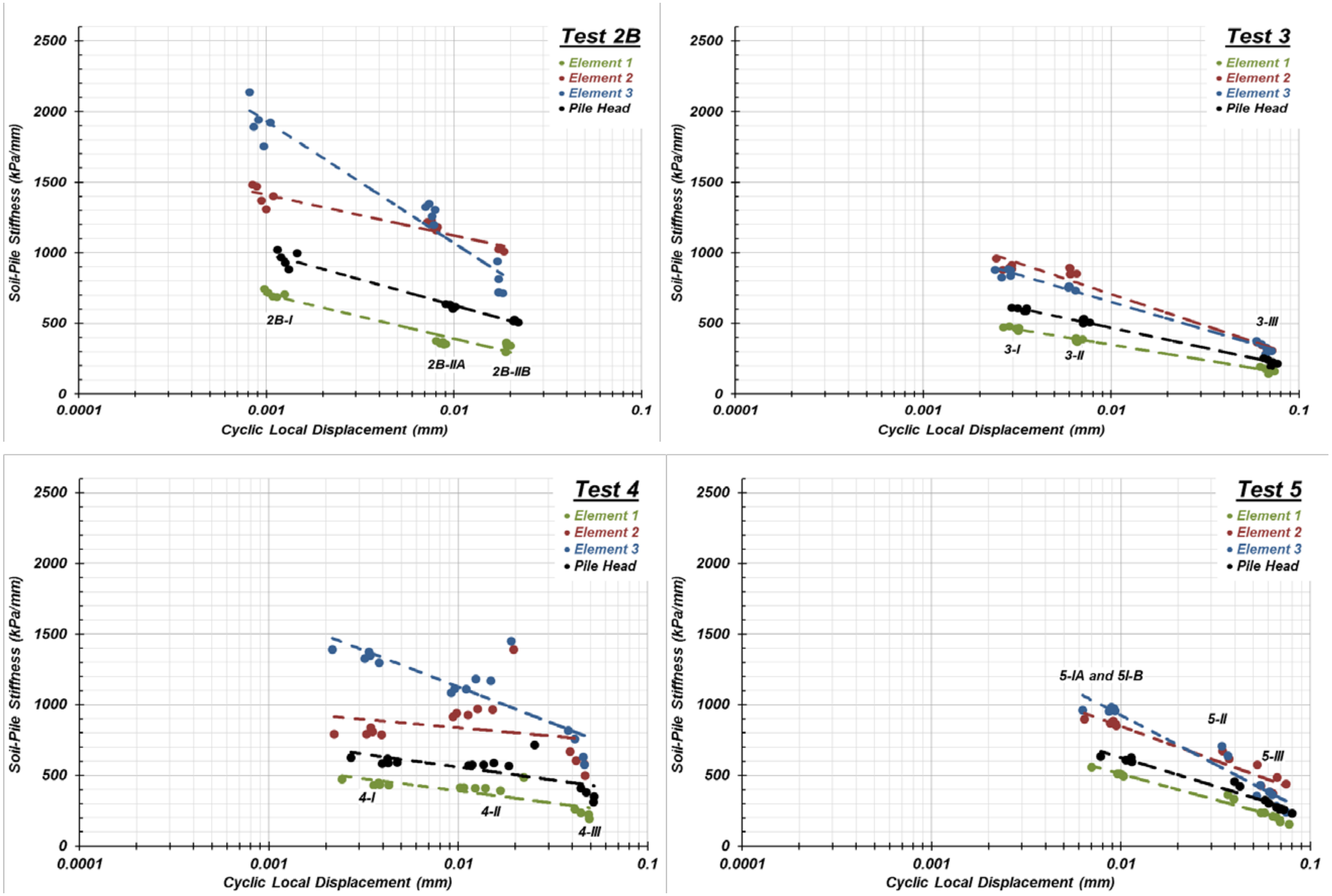

Figure 5. Soil-Pile Stiffness and Cyclic Local Displacement (Semi-Log, Model Scale)

4 COMPARISON WITH ANALYTICAL METHODS

4.1 RATZ Analysis

The approach presented by Seidel and Uriona (2011) involves use of existing realistic (i.e., not conservative) static pile capacity methods to develop initial shaft friction capacity conditions for the pile. Seidel and Uriona use the Imperial College Pile (ICP) method to develop shaft friction capacity. Then the RATZ computer program (Randolph, 2003) which implements a load transfer approach (i.e., t-z method) is used with the applied cyclic loading history to compute the degradation of shaft friction and the corresponding reduction in pile capacity.

In this study, the RATZ computer program was used to model the loading conditions associated with the complete Test 4 Load Packet from the centrifuge data set. Test 4 was selected because the pile was not subjected to the more complex two-way loading condition, but degradation was observed. The static pullout tests from the centrifuge program were used in place of ICP predictions for evaluation of initial pile capacity. The pile and soil parameters used in the analysis are provided in Table 7.

Stiffness in the centrifuge tests was observed to be dependent on the amplitude of the cyclic strains. In order to match the initial pile-head stiffness in RATZ to the experimental results, reduction of the theoretical shear modulus was required for each load packet, sequentially.[6] The largest cyclic strains were accumulated before Load Packet 4-III, therefore the shear modulus reduction would be greatest for Load Packet 4-III (i.e., development of strain results in an expected reduction in shear modulus).

Modeling of the residual displacement in RATZ may be possible, but it was not attempted in this comparison exercise. Instead, the comparison focused on cyclic load transfer along the pile. The predicted cyclic shaft friction and cyclic axial load with displacement from the RATZ model are shown in Figure 6 and Figure 7 for Load Packet 4-II adjacent to the measured values from the data set for the first and last 50 cycles of the load packet, respectively. For comparison, the RATZ model results shown are from nodes located at depths similar to the mid-depth of the discretized model pile elements (e.g., mid-way between strain gages), and show reasonable agreement with the measured values.

Reduction in secant stiffnesses (i.e., pile-head force-displacement and shaft friction-local displacement) were modeled by RATZ. However, the RATZ model appears to be incapable of modeling stiffening behavior. This limits the RATZ model as a viable method to model piles under cyclic loading if the stiffness has the potential to either increase or degrade.

The complete set of results from the RATZ analysis with the associated comparison plots from the Test 4 data are provided in Appendix D.

[6] RATZ assumes a parabolic shape of the local stress-displacement relationship; the stiffness at any point on the loading curve is a function of the stress level, independent of the magnitude of cyclic loading.

Table 7. Input Parameters to RATZ model (Test 4, model scale)

PILE PARAMETERS					
Pile Length, Embedded	L_e	=	150 mm		
Pile Diameter	D	=	6.92 mm		
Pile Diameter with Composite	D_c	=	9.37 mm		
[1]Modulus of Pile with Composite	E_c	=	41.7 GPa		
Number of Elements	N	=	40		
SOIL PARAMETERS BY LOAD PACKET			**4-I**	**4-II**	**4-III**
Load Transfer Parameter	ζ	=	4	4	4
Yield Parameter	χ_i	=	0	0	0
[2]Normalized Modulus	G/G_{max}	=	1/2	1/6.5	1/15
[3]Initial Tensile Capacity	$Q_{T,i}$	=	[5]450 N	454 N	411 N
[4]Final Tensile Capacity	$Q_{T,f}$	=	[6]450 N	411 N	373 N
[7]Shaft Friction Ratio (Residual/Peak)	τ_r/τ_{peak}	=	1	0.905	0.908
[8]Displacement to Residual	Δw_r	=	0.937 mm	0.937 mm	0.937 mm
Strain-Softening Parameter	η	=	1	1	1
[9]Cyclic Shaft Friction Ratio (Residual/Peak)	$\tau_{cyc,r}/\tau_p$	=	1	0.905	0.908
LAYER GEOMETRY AND PARAMETERS			**Layer 1** *Dense Sand*	**Layer 2** *Loose Sand*	**Layer 3** *Modeling Clay*
Layer Depth (top)	z_{top}	=	0 mm	154 mm	161 mm
Layer Depth (bottom)	z_{bottom}	=	154 mm	161 mm	168 mm
Layer Thickness	Δh	=	154 mm	18 mm	7 mm
Initial Density	ρ_0	=	1665	1603	--
Initial Void Ratio	e_0	=	0.604	0.693	--
Initial Relative Density	$D_{R,0}$	=	70.7%	42.9%	--

NOTES:
1. E_c=F$(EA)_{pile}/A_c$, where F=1.6, observed increase in axial stiffness.
2. Matched initial pile head stiffness, G, with experimental data. G_{max} is obtained from empirical correlations.
3. The maximum tensile capacity is assumed as the measured residual tensile capacity before the packet.
4. The residual tensile capacity is assumed as the measured residual tensile capacity after the packet.
5. After installation, 2 mm pullout displacement was insufficient to fully mobilize pile capacity. A tensile capacity of 450 N was selected based on an assumption that limited degradation occurred during the course of the test.
6. The measured post-packet tensile capacity was 454 N, but set $Q_{T,f} = Q_{T,i}$ to satisfy $Q_{T,f} \leq Q_{T,i}$ in RATZ.
7. Estimated to be equal to the ratio $Q_{T,f}/Q_{T,i}$.
8. $\Delta w_{r} = 0.10D$ = required displacement to reach residual conditions.
9. Assumed no cyclic softening.

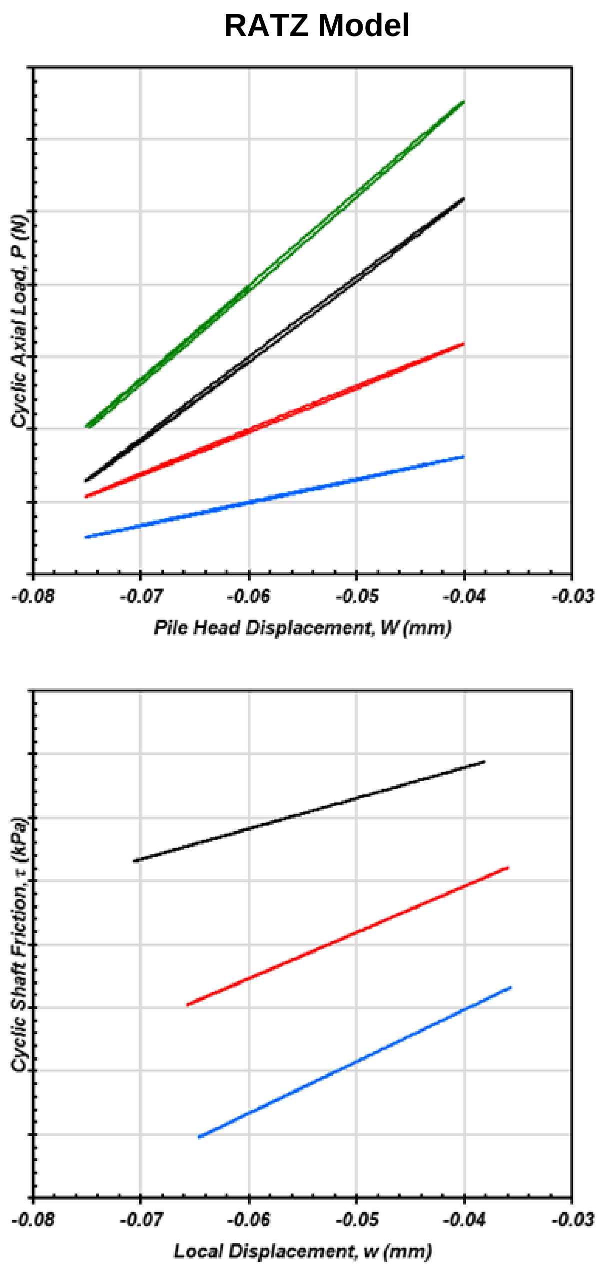

Figure 6. Comparison between the Predicted Cyclic Shaft Friction and Cyclic Axial Load with Displacement Using the RATZ Model and the Measured Test-Load Packet 4-II Data (1-50 cycles, first 50 cycles in the full load packet).

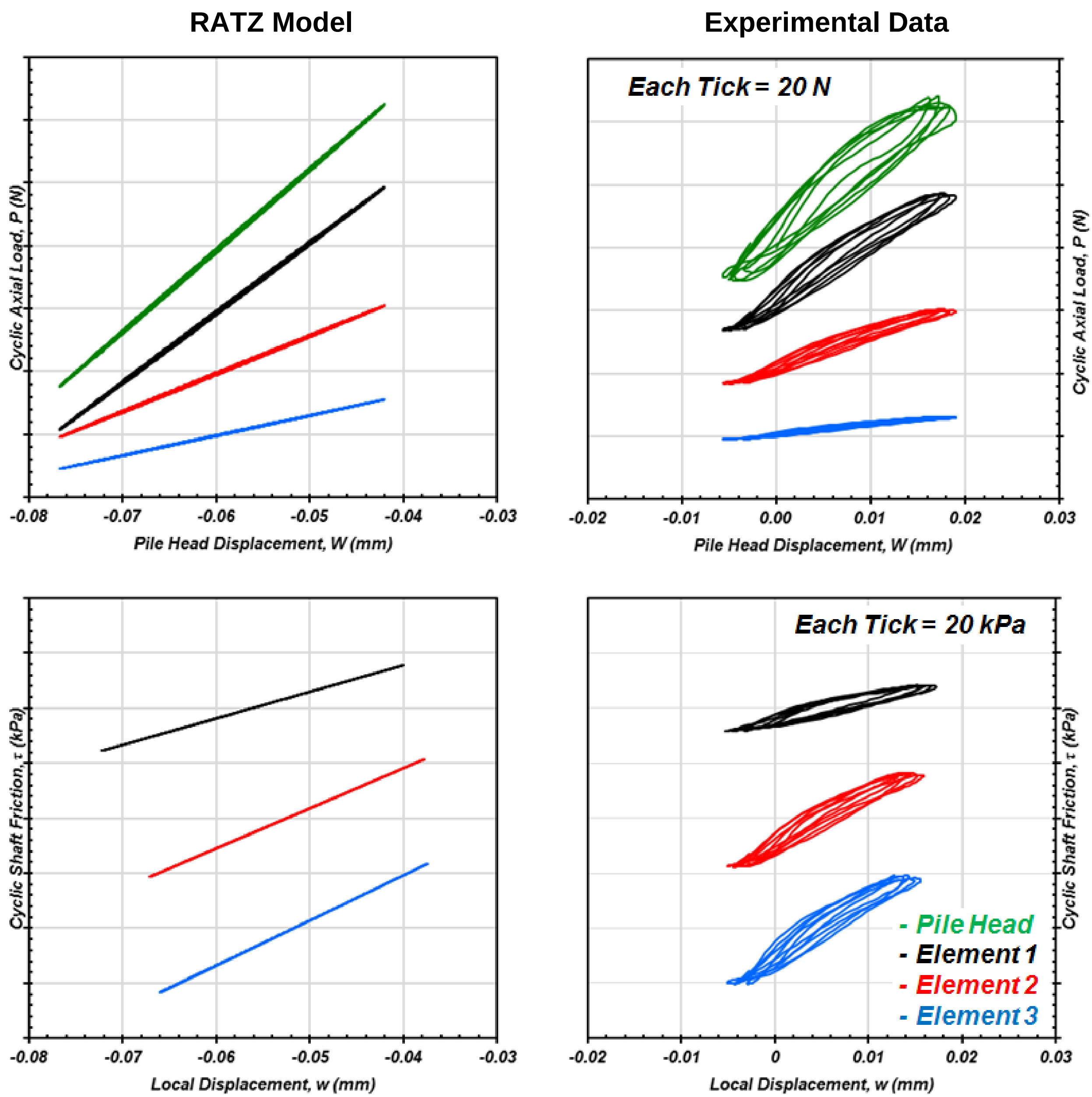

Figure 7. Comparison between the Predicted Cyclic Shaft Friction and Cyclic Axial Load with Displacement Using the RATZ Model and the Measured Test-Load Packet 4-II Data (9,950-10,000 cycles, last 50 cycles in the full load packet).

4.2 Simplified Damage Law Analysis

The simplified approach presented by Stuyts, et al. (2012) uses an iterative procedure to evaluate incremental pile capacity degradation as a result of combinations of discrete cyclic loading events (e.g., 1000 cycles of low amplitude loading, followed by 200 cycles of intermediate amplitude loading, followed by 20 cycles of high amplitude loading), where for each discrete packet of cyclic loads, the following steps are performed:

1. Use an interaction diagram with number of cycles to failure (N_f) curves to evaluate the N_f value for a combination of applied static and cyclic axial loads.
2. Use a damage law to establish the relationship between increment of damage (D_i) and the associated ratio (N_i/N_f) of applied number of load cycles (N_i) to the number of cycles to failure (N_f).
3. Use the following degradation equation to relate the increment of damage (D_i) to the associated pile capacity reduction ($\Delta Q_{T,i}$):

   $$\Delta Q_{T,i} = D_i\left(Q_{T,i} - Q_{max,i}\right) \qquad \text{EQ. 6}$$

   where $Q_{T,i}$ is the initial pile capacity prior to the current increment of cyclic loads and $Q_{max,i}$ is the maximum load applied during the cycle (i.e., $Q_{cyc} + Q_{static}$).
4. Update the previous pile capacity using the new pile capacity reduction:

   $$Q_{T,i+1} = Q_{T,i} - \Delta Q_{T,i} \qquad \text{EQ. 7}$$

5. Repeat for all load packets.

This simplified analysis to predict final capacity can either be accomplished using a known loading combination and interaction diagram, or by using the cycles to failure from the centrifuge testing program in unison with a damage law. The analyses described herein compare the measured data from the testing series with the predicted final capacity using the simplified method with the Jardine, et al. (2000) and Kirsch, et al. (2011) interaction diagrams. The full calculation package is provided in Appendix E.

4.2.1 Implementation with Centrifuge Data

When rearranged, the degradation equation (Equation 6) defines the increment of damage as the ratio between available load before failure ($Q_{T,i}$ - Q_{max}) and the pile capacity reduction ($\Delta Q_{T,i}$). Assuming a linear damage law (Stuyts, et al. 2012), the damage suffered during a load packet is defined as:

$$D_i = \frac{N_i}{N_f} \qquad \text{EQ. 8}$$

where a D_i of 1 indicates failure (i.e., $N_i = N_f$). Using Equation 8 as the damage law in Equation 6, the number of cycles to failure can be defined as:

$$N_f = \frac{N_i}{\Delta Q_{T,i}}\left(Q_{T,i} - Q_{max,i}\right) \qquad \text{EQ. 9}$$

An N_f value can then be computed for each load packet using Equation 9 and the first initial measured pile capacity before testing ($Q_{T,i}$), the maximum applied load ($Q_{max,i}$), the number of cycles (N_i), and the measured change in capacity (Q_T before and after the load packet). The resulting N_f values were evaluated for each load packet and a "selected" N_f value ($N_{f\text{-}c}$) was used in the forward analysis.[7]

The back calculated $N_{f\text{-}c}$ value can then be used in the simplified analysis where the damage suffered in each load packet is calculated using $N_{f\text{-}c}$ in Equation 8. This computed incremental damage is then used as input to Equation 6 to calculate the final capacity at the end of each load packet. Each sequential initial capacity thereafter is then taken as the capacity change (i.e., capacity loss from damage) subtracted from initial capacity of the load packet. Comparison between the measured final capacity and the final capacity using the simplified damage law is provided in Table 9. This analysis is essentially calibrated to the centrifuge data, because the known capacity change was used to compute $N_{f\text{-}c}$. Similar final capacities between this exercise and the measured values indicate appropriate implementation of the simplified damage law. This calibration exercise is included in Appendix E.

4.2.2 Implementation with Interaction Diagram N_f Curves

Jardine, et al. (2000) and Kirsch, et al. (2011) each developed interaction diagrams with envelopes of constant N_f relative to the standard axes of Q_{static}/Q_T and Q_{cyc}/Q_T. For these diagrams, Q_T was defined as the pile capacity at the beginning of the cyclic load packet ($Q_{T,i}$). This allows N_f to be computed independently for each load packet, and in theory independently of the prior loading history.

The Jardine interaction diagram was developed for N_f values ranging from 1 to 400 cycles based on load testing performed at the Dunkirk site (Jardine, et al., 2000). Kirsch extended and modified the Jardine interaction diagram for N_f values ranging from 1 to 1,000,000 cycles. The majority of the data from the centrifuge testing series presented herein exists in a low Q_{cyc}/Q_T range, falling below the lowest line on both the Jardine and Kirsch diagrams. In this analysis, both interaction diagrams were therefore extrapolated or extended by adding additional lines of constant N_f extending to $Q_{cyc}/Q_T = 0.1$. For the Jardine interaction diagram, extrapolating results in N_f = 8,100 cycles at $Q_{cyc}/Q_T = 0.1$, and for the Kirsch interaction diagram, extending resulted in N_f = 2,000,000 cycles at $Q_{cyc}/Q_T = 0.1$.[8] For both "extended" diagrams, any load packet falling below the $Q_{cyc}/Q_T = 0.1$ line is assigned an N_f = 2,000,000. The extended interaction diagrams were used to interpolate N_f for a given loading condition (Q_{cyc} and Q_{static}).

[7] Selection of an $N_{f\text{-}c}$ value followed two primary criteria: (1) values were rounded to the nearest 1,000 cycles; and (2) computed negative N_f values correspond to a measured increase in pile capacity, which was ignored in this analysis by selecting $N_{f\text{-}c}$ equal to 10,000,000 cycles to prevent capacity reduction

[8] For the Jardine interaction diagram, extrapolation followed an approximately logarithmic extension from the existing N_f lines down to $Q_{cyc}/Q_T = 0.1$ at N_f = 8,100 cycles. For the Kirsch interaction diagram, one additional constant N_f line for 2,000,000 cycles was added at $Q_{cyc}/Q_T = 0.1$, as extrapolation would have resulted in an order of magnitude increase to 10,000,000 cycles, which would be inconsistent with the observations from the centrifuge program.

Following the Stuyts, et al. (2012) simplified approach, a full test can be simulated using the extended interaction diagrams with the following inputs: (a) the initial capacity at the start of testing (first load packet), (b) the prescribed number of loading cycles, and (c) the known static and cyclic loading conditions. The initial capacities for subsequent load packets are then taken as the capacity change (i.e., capacity loss from damage) subtracted from initial capacity of the prior load packet. An example of this analysis is provided in Table 8 for Test 5, with load packets overlain on the Jardine and Kirsch extended interaction diagrams plotted in Figure 8a and b, respectively. Results for all the tests are provided in Appendix E.

Table 8. Example – Computing Final Capacity using Interaction Diagrams (Test 5)

Load Packet	Number of Cycles, N_i	Initial Tensile Capacity, $Q_{T,i}$ (N)	Q_{static} (N)	Q_{cyc} (N)	Cycles to Failure, N_f	Damage, $D_i = N_i / N_f$ *Linear, failure if >1*	Q_{max} ($Q_{static}+Q_{cyc}$) (N)	Capacity Degradation, ΔQ_T D_i ($Q_{T,i}$ - Q_{max}) (N)	Final Capacity, $Q_{T,f}$ ($Q_{T,i} - \Delta Q_T$) (N)
Jardine, et al. (2000) Extended Interaction Diagram									
5-IA	10000	400	55	31	2,000,000	0.005	86	2	398
5-IB	500	398	55	27	2,000,000	0.000	82	0	398
5-II	500	398	56	78	2,608	0.192	134	51	348
5-III	50	348	107	79	1,169	0.043	186	7	341
Kirsch, et al. (2011) Extended Interaction Diagram									
5-IA	10000	400	55	31	2,000,000	0.005	86	2	398
5-IB	500	400	55	27	2,000,000	0.000	82	0	398
5-II	500	400	56	78	1,009,899	0.000	134	0	398
5-III	50	400	107	79	699,391	0.000	186	0	398

Note: Highlighted cells are centrifuge data used as input to the analysis.

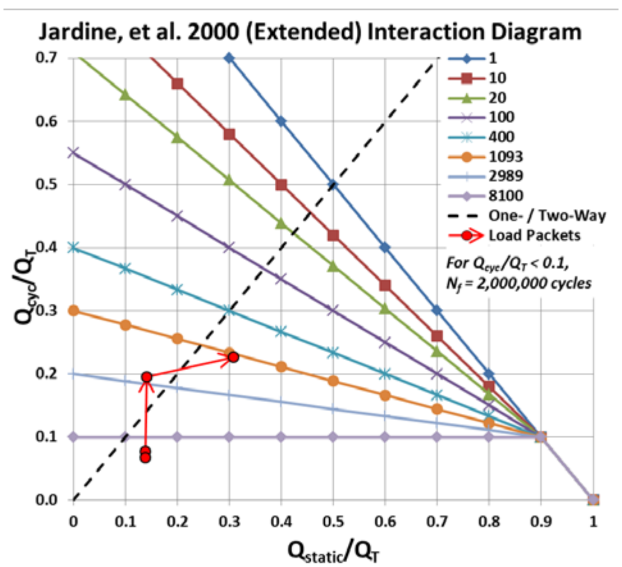

(a)

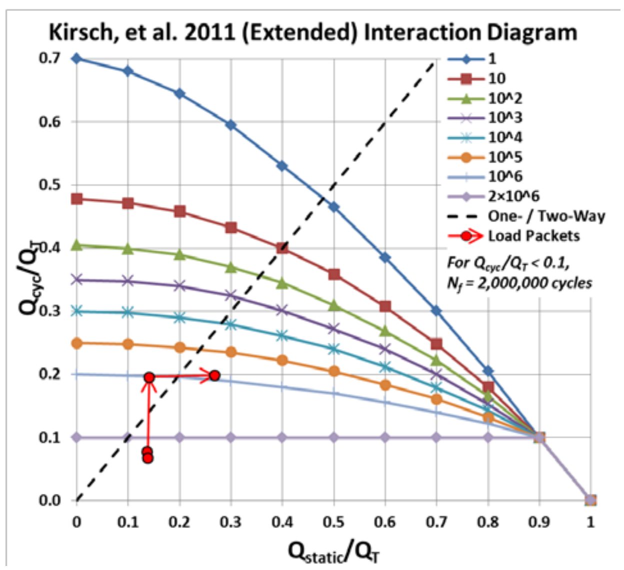

(b)

Figure 8. Example – Computing Final Capacity using Interaction Diagrams (Test 5)

4.2.3 Results

The Stuyts, et al. (2012) simplified approach was used to predict final capacity of the pile at each load packet for each test. The results from this analysis are summarized in Table 9, which includes: (1) the measured capacity from the centrifuge tests, (2) the predicted capacity using the calibrated damage law with a known capacity change, (3) the predicted capacity using the extended Jardine, et al. (2000) interaction diagram and failure curves, and (4) the predicted capacity using the extended Kirsch, et al. (2011) interaction diagram and failure curves.

The predicted capacities using the calibrated damage law with a known capacity change match well with the measured capacities. This is expected since the damage is calibrated to the measured change in capacity, and the similarity indicates appropriate implementation of the simplified damage law. The variations between measured and predicted capacity stem from using the selected cycles to failure, and not accounting for increases in capacity.

Both the Jardine and Kirsch extended interaction diagrams do a reasonable job of predicting the minor degradation from the first load packets. This is largely due to assigning an N_f value of 2,000,000 cycles for Q_{cyc}/Q_T < 0.1 in both interaction diagrams. In general, the Jardine extended diagram predicts more degradation than was observed, and may be a conservative representation based on this set of centrifuge data (with the exception of Load Packets 4-II, 4-III, 5-IB and 5-III). The Kirsch extended diagram tended to predict less degradation.

Table 9. Pile Capacity Evaluations (Actual vs. Predicted)

					Final Capacity, $Q_{T,f}$			
Test-Load Packet	**Number Of Cycles, N_i**	**Total Cycles**	Q_{stat}/Q_T	Q_{cyc}/Q_T	**Measured (N)**	**Calibrated** *using known capacity change* **(N)**	**Jardine, et al. (2000) Interaction Diagram (N)**	**Kirsch, et al. (2011) Interaction Diagram (N)**
--	0	0	--	--	285	285	285	285
2B-I	100,000	100,000	0.39	0.02	275	277	277	277
2B-IIA	10,000	110,000	0.43	0.11	230	233	147	276
2B-IIB	10,000	120,000	0.30	0.22	175	177	122	274
--	0	0	--	--	180	180	180	180
3-I	100,000	100,000	0.32	0.06	175	174	174	174
3-II	10,000	110,000	0.29	0.10	170	169	68	174
3-III	500	110,500	0.19	0.42	180	169	0	105
--	0	0	--	--	450	450	450	450
4-I	100,000	100,000	0.24	0.02	454	447	434	434
4-II	10,000	110,000	0.24	0.08	411	404	432	432
4-III	500	110,500	0.20	0.19	373	363	386	432
--	0	0	--	--	400	400	400	400
5-IA	10,000	10,000	0.14	0.08	400	400	398	398
5-IB	500	10,500	0.14	0.07	340	347	398	398
5-II	500	11,000	0.16	0.23	375	347	348	398
5-III	50	11,050	0.29	0.21	200	186	341	398

5 OBSERVATIONS

The centrifuge testing series and analyses presented herein were designed to begin to fill a current knowledge gap and advance the state of the art for understanding the influence of repeated cyclic loading on axial capacity of OWTS performance by: (1) evaluating the potential for obtaining meaningful results using a small centrifuge for this application; (2) developing an initial data set from scaled centrifuge testing of piles subjected to one-way (tension) and two-way (tension and compression) cyclic axial loading; (3) using the data set to develop interaction diagrams (e.g., Jardine and Standing, 2000; Tsuha, et al., 2013) relating the average static axial load and applied cyclic axial loads to tested maximum pile load and applied number of cycles; (4) assessing the data set relative to recently proposed methods (i.e., Seidel and Uriona, 2011, Stuyts, et al., 2011) for evaluating impacts of cyclic degradation on predicted pile performance; and (5) providing guidance on implications of the findings and recommended next steps. The following observations are made based on the results from the program:

Centrifuge Test Results

- In general the load packets in the stable regime (relatively low amplitude cyclic loading) away from the stable/meta-stable boundary on the interaction diagrams all have nearly zero RPR values with very little residual pullout or insertion. In the case where the static load is over 40% of the tensile capacity (i.e., 2B-IIA, 10 N_{cyc}) the RPR (0.018) has begun to increase. Note however that while residual pullout was minimal, some tensile capacity reduction was observed in two of the three low amplitude high-cycle packets, specifically in Tests 2B-I and 3-I with over 30% static load.
- For the two load packets which went into compression (two-way loading) in the meta-stable region, very different RPR values were achieved over 500 cycles (0 RPR for 3-III; 0.4 RPR for 5-II) and tensile capacities were observed to increase. This variation for two-way loading tests may be an indication of the importance of loading history on the observed response of an OWTS system.
- In the one-way loading meta-stable region (or close to the stable/meta-stable boundary), where the pile is loaded purely in tension at medium cyclic and static loads (2B-IIB, 4-III, and 5-III), the highest RPR values were recorded (0.95, 1.35, and 54, respectively) pullout approached or exceeded 10% of the pile diameter, and tensile capacity reductions were significant.
- Three general types of soil-pile response were observed: (1) pile ratcheting over prolonged cyclic loading; (2) stiffening and softening as the pile moves in and out of compression-tension loading; and (3) residual pullout approaching or exceeding 10% of pile diameter (generally considered failure) with cyclic loading near 20% of the initial tensile capacity of the pile.
- Observations of strain gauges SG3 and SG4 indicated very little change in cyclic load at depth over the duration of each load packet. This may be consistent with

observations by others (e.g., Tsuha, et al., 2012) that most degradation occurs at shallow depths which are not captured by SG3 and SG4. Given the higher shaft resistance at depth corresponding to the higher confinement, a significant reduction in capacity at shallow depth may be consistent with the relatively small percentage increase in demand noted in the strain gauges at depth.

- The centrifuge test results are likely dependent on the specifics of the soil profile tested. The density of the soil and the soil's tendency to dilate or contract can have a significant impact on capacity and response to loading. Saturated vs. unsaturated conditions may not be as important in sands where loading would be drained, but would certainly be important in clay soils, and potentially in silty or clayey sands subject to pore pressure build up during significant loading events. The method of pile installation within these soil profiles can also be expected to have an impact on the pile response, and would have to be evaluated. We recommend further testing to evaluate the magnitude of these effects.

RATZ Model Analysis

- The RATZ model is designed to account for the flexibility of the pile and the variation of the soil displacement along the length of the pile. Theoretically, it can account for the progression of degradation along the length of the pile. However, the simplified degradation approach currently implemented in RATZ was not designed to account for millions of small amplitude load cycles. The current RATZ degradation approach can model reduction in strength, but it cannot model the strengthening and stiffening of the soil response observed in some of the tests herein, which would be important for the response of OWTS.
- Stiffness in the centrifuge tests was observed to be dependent on the amplitude of the cyclic strains, which is inconsistent with the formulation of RATZ. To capture the observed reduction in shear modulus with increasing cyclic strains, a shear modulus reduction with strain was assumed and calibrated for each load packet.
- With the reduced shear moduli, the cyclic stiffnesses were captured reasonably well with the RATZ model.

Simplified Damage Law Analysis

- Predicted capacities using the calibrated damage law with a known capacity change match well with the measured capacities, indicating appropriate implementation of the simplified damage law.
- The Jardine, et al. (2000) extended interaction diagram appears to be a conservative representation based on these limited tests, but there were exceptions (Test 4-II) and failure cases (4-III and 5-III).
- There is not enough data to develop an interaction diagram with N_f curves based on this dataset alone. However, it would be worth the effort to do more testing to

develop such a diagram(s), especially in the high-cycle, low Q_{cyc}/Q_T regime where the Jardine, et al. (2000) and Kirsch, et al. (2011) diagrams were extended for this analysis.

- A key limitation of this approach is that all of the information (number of cycles, load, and displacement) applies only at the pile head, and, as noted by others, the associated interaction diagrams are expected to change with both pile and soil properties, and so need to be developed for a range of combinations. Calibrated interaction diagrams required for application of the simplified damage law approach will need to be developed through additional experimental work.

<u>Implications to Current Design Practices for OWTS</u>

- The testing program illustrates the complexity of the load capacity and stiffness of foundation piles when subjected to long duration cyclic operating loads and larger cyclic storm loads. The program also identifies many variables that can affect the foundation and soil response. This indicates a need for structure-specific analyses that appreciates the complexities and uncertainties associated with foundation behavior.
- The current set of tests indicates that, while limited, degradation of pile capacity can still occur under low amplitude high-cycle loading. Current methods of design for OWTS pile foundations do not account for this effect and small changes in capacity may result in changes to the stiffness of the foundation system, which in turn may have implications on the frequency response of the OWTS.
- Current analysis tools are not able to account for the increase in capacity seen in the two-way loading tests in this program. An increase in capacity may also have an impact on the stiffness of the foundation system, and as such this observed condition should be investigated further.
- The test results illustrate the conceptual appropriateness of damage law analyses and interaction diagrams. However, the analyses suggest that the boundaries between “meta-stable” and “stable” boundaries, as described by Tsuha, et al. (2012) and further developed by Tsuha, et al. (2015), may be overly simplistic, require further evaluation, and likely need adjustment for application to OWTS design, in particular in the low amplitude high-cycle regime. While the degradation measured within the low amplitude “stable” zone was limited, it was not insignificant. When considering that these effects will be compounded over the millions of cycles that an OWTS will be subjected to, the importance of understanding this mechanism becomes apparent.

- The design (and performance) of OWTS is complex.[9] Current methods, by necessity, include significant assumptions and simplification relative to the soil response to the complex and long-term cyclic loads. As shown by the cyclic tests conducted herein, soil response is complex and depends on many factors. Caution is therefore appropriate relative to design practices.
- Because of the above consideration, foundation design may result in either less conservatism than desired or more conservatism than required. Such uncertainty has direct implications relative to the long-term performance and costs of offshore wind turbines. Removal of excess conservatism has the potential to improve the economics of offshore wind. Further evaluation and research is warranted.

[9] Final structural design analyses of OWTS includes: (1) the development of storm loading time histories for appropriate storms; (2) structural analyses to define stresses, load-deformation behavior, and the structural frequency of the structure conventionally under ultimate, serviceability and fatigue limit states; (3) the use of pile head load-deformation from those structural analyses to model the soil-structure interaction of the foundation in a geotechnical model; (4) comparison of pile head displacements and moments at the interface between the geotechnical and the structural models; and (5) iterative adjustment of the structural properties of the foundation system until an appropriate convergence is obtained between the results of the two analytical models.

6 RECOMMENDATIONS FOR FUTURE WORK

This testing program provides insight into a current knowledge gap surrounding the influence of repeated cyclic loading on axial capacity and OWTS foundation performance. In this program, observations were developed from the test results, and the data were assessed relative to recently proposed analysis methods.

There are two suggested testing programs to further enhance the understanding of OWTS performance. To supplement these programs, we recommend further evaluation of the cyclic load history of actual OWTS. Thus, the loading regime in the testing program can appropriately emulate the loading regime of installed wind turbines.

Small Centrifuge Testing Program

The smaller, 1-m radius centrifuge at the UC Davis CGM, which was used for this program, allows for testing to be completed in a relatively short time, requires minimal material and staffing resources, and is significantly less costly than use of a larger centrifuge. The recent testing program enhanced the capabilities of the actuator, controller, and data collection system for low amplitude high-cycle testing. Hence, future testing will require minimal trouble shooting of the loading system. However, the scale of the small centrifuge limits the amount of instrumentation that can be placed on the pile, and requires the use of sealant sand around the strain gauges to protect them during installation and testing.

Thus, in our opinion, the most appropriate testing program with the small centrifuge machine should focus on conducting many tests on simplified piles (i.e., load cell and pile head displacement measurements only) in different soil types and under different loading regimes. The results from this testing series can be used to develop more complete interaction diagrams across the range of combinations of static and cyclic loading, and develop improved failure criteria, especially in the low amplitude high-cycle regions where the existing interaction diagrams were heavily extended as a result of the limited data from this study.

Large Centrifuge Testing Program

The larger (but more expensive) 9-m radius centrifuge at the UC Davis CGM would allow testing to be completed on a much larger scale with an extensively instrumented model, and would eliminate, or reduce, many of the challenges encountered in the current study due to the size limitations of the smaller centrifuge. Improvements associated with use of the larger size centrifuge and associated data acquisition system include:

- Moving strain gauges to the interior of the pile, removing the need for the sand sealant coating.
- Increasing the number of instruments and their robustness to better capture behavior along the pile shaft.
- Using longer (more than double the embedment length) and more flexible piles.

- Testing under saturated conditions.
- Testing multi-piled OWTS system models (i.e. building a full multi-piled system instead of cyclically loading one pile).
- Simultaneous testing of multiple models.

The most effective testing program with the large centrifuge might include 3 or 4 interesting cases developed from the current (and potentially additional) tests conducted in the small centrifuge. The results from an appropriately scoped testing program in the larger centrifuge should provide enhanced understanding of pile capacity degradation, local displacement and stiffness changes with depth, cycle frequency effects, and multi-pile system response.

Summary

As described above, the small centrifuge program would be used to enhance our understanding of failure conditions in different loading regimes, as well as different soil types. However, given the complexity of design for OWTS, an understanding of failure conditions is not enough. The large centrifuge program would be used to improve our understanding of soil-pile-structure interactions under operating and shutdown conditions which would in theory be performed at some distance from the failure conditions identified with the small centrifuge.

With additional testing, research, and concurrent development of the analytical models, we envision a design methodology where a damage law model is used as a check to ensure the structure is not designed near a failure condition, and the RATZ-type model would then be used to optimize the OWTS foundations within the anticipated range of loads. Alternatively, a future combined model could be developed with a RATZ-type component to account for the distribution of load and local displacement along the pile shaft, and an empirical damage law component to account for the overall changes in capacity and stiffness. These tools would result in an improved ability to design these systems with appropriate degrees of conservatism.

7 REFERENCES

Carey, T.J., Kutter, B.L., Manzari, M., Zeghal, M., and Vasko, A. "LEAP Soil Properties and Element Test Data", 2015, https://nees.org/resources/13689.DOI: 10.17603/DS2WC7W.

Jardine, R. and Standing, J. *Pile Load Testing Performed for HSE Cyclic Loading Study at Dunkirk, France*. Offshore Technology Report – OTO 2000 008, July 2000.

Kirsch, F. and Richter T. "Cyclic Degradation of Pile Foundations for Offshore Wind Turbines." Proceedings of the 36th Annual Conference on Deep Foundations, 2011.

Randolph, M. *RATZ Version 4-2: Load Transfer Analysis of Axially Loaded Piles.* 2003.

Seidel, M. and Uriona, M. "A New Approach for Assessing Offshore Piles Subject to Cyclic Axial Loading." Geotechnik, Volume 34, Issue 4, December 2011.

Stuyts, B., Cathie, D., Falepin, H., and Burgraeve, A. "Axial Pile Capacity of Wind Turbine Foundations Subject to Cyclic Loading." Offshore Site Investigation and Geotechnics, Society of Underwater Technology, September 2012.

Tsuha, C.H.C., Foray, P.Y., Jardine, R.J., Yang, Z.X., Silva, M., and Rimoy, S. "Behaviour of displacement piles in sand under cyclic axial loading." Soils and Foundations, Volume 52, No.3, June 2012.

Tsuha, C.H.C., Yang, Z.X., Silva, M., Rimoy, S., and Jardine. R. "Advanced Laboratory Investigation of Axial Cyclic Loading in Silica Sands." Proceedings of Soil Mechanics 2015, November 2015.

APPENDIX A: TENSILE LOAD TESTS

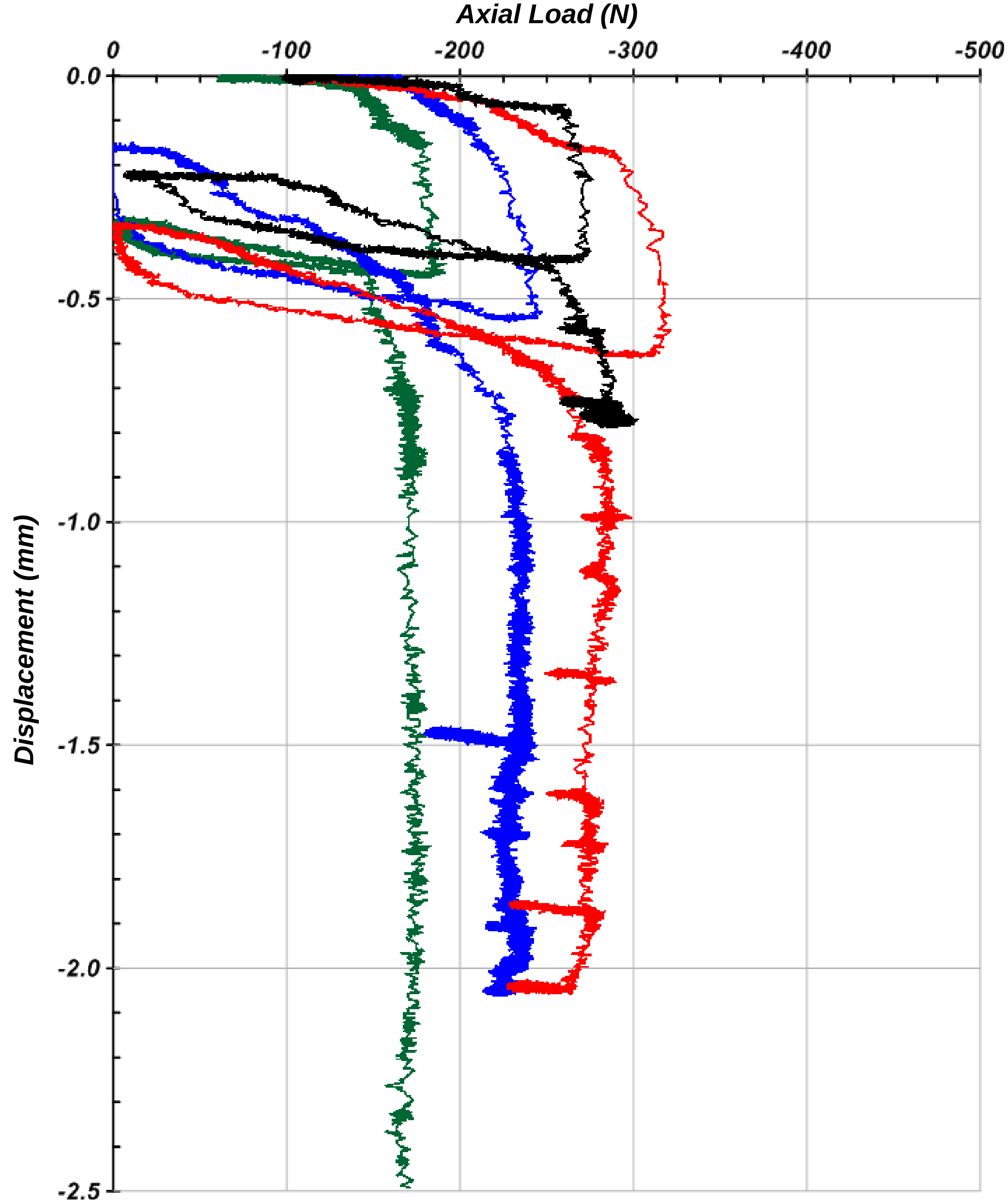

Tensile Capacity Test	Peak Tensile Capacity (N)	Residual Tensile Capacity (N)
2A	285	285
Load Packet 2B-I		
2B	320	275
Load Packet 2B-IIA		
2C	245	230
Load Packet 2B-IIB		
2D	185	175

Tension Load = Negative
Retract Displacement = Negative

All Tensile Capacity Tests (Load Cell Measurement Only)
Centrifuge Test 2

March 2016

A-2

MMI
engineers • scientists • innovators

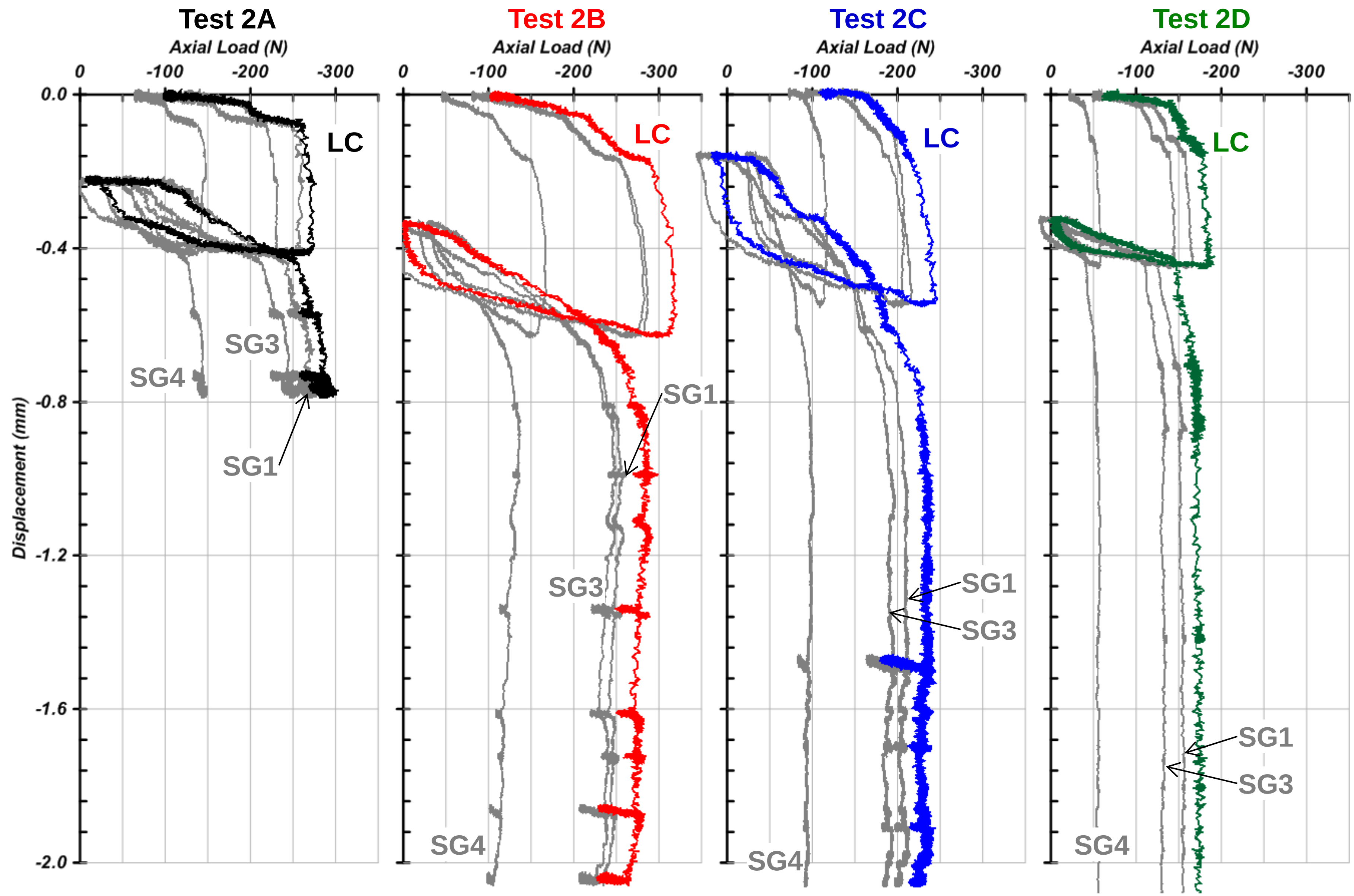

Single Tensile Capacity Tests (Load Cell and Strain Gauge Measurements)

Tensile Capacity Test 2A, 2B, 2C, and 2D

March 2016

A-3

MMI

engineers • scientists • innovators

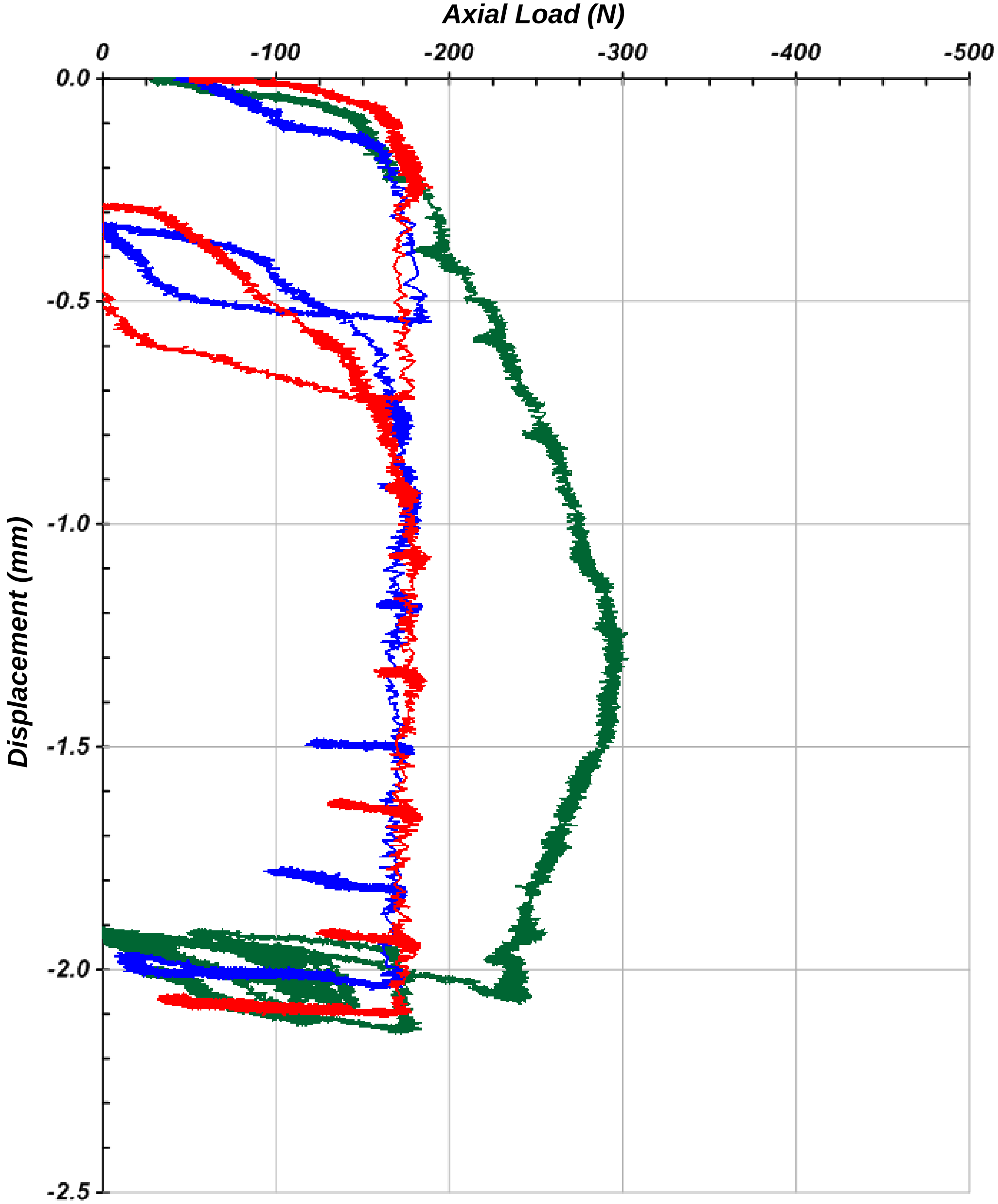

Tensile Capacity Test	Peak Tensile Capacity (N)	Residual Tensile Capacity (N)
3A*	180	180
Load Packet 3-I		
3B	180	175
Load Packet 3-II		
3C	180	170
Load Packet 3-III		
3D	295	180

**after installation, but no fast data recorded, value from slow data acquisition system.*

Tension Load = Negative
Retract Displacement = Negative

All Tensile Capacity Tests (Load Cell Measurement Only)
Centrifuge Test 3

March 2016
A-4

MMI
engineers • scientists • innovators

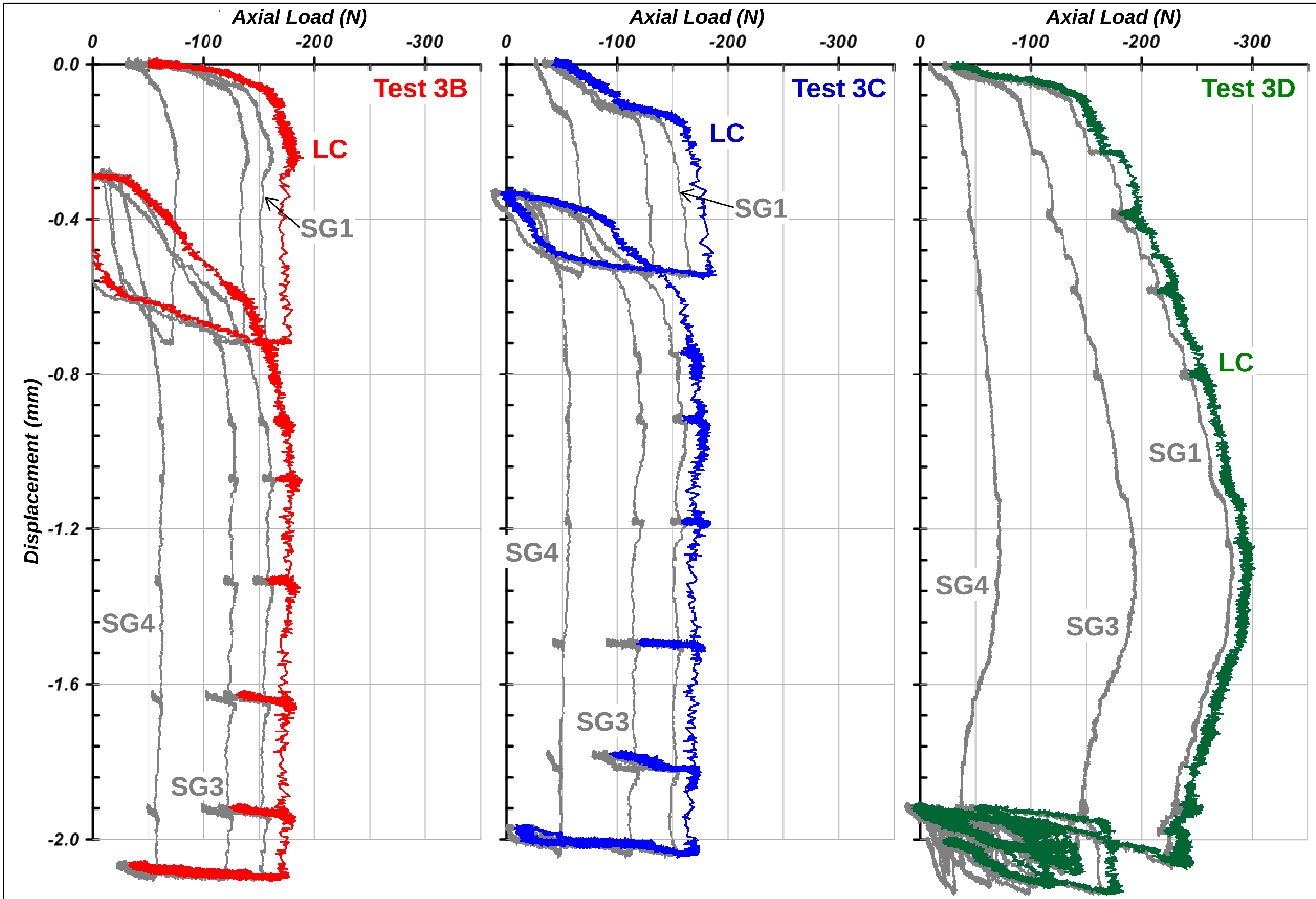

Single Tensile Capacity Tests (Load Cell and Strain Gauge Measurements)
Tensile Capacity Test 3B, 3C, and 3D

March 2016
A-5

MMI engineers • scientists • innovators

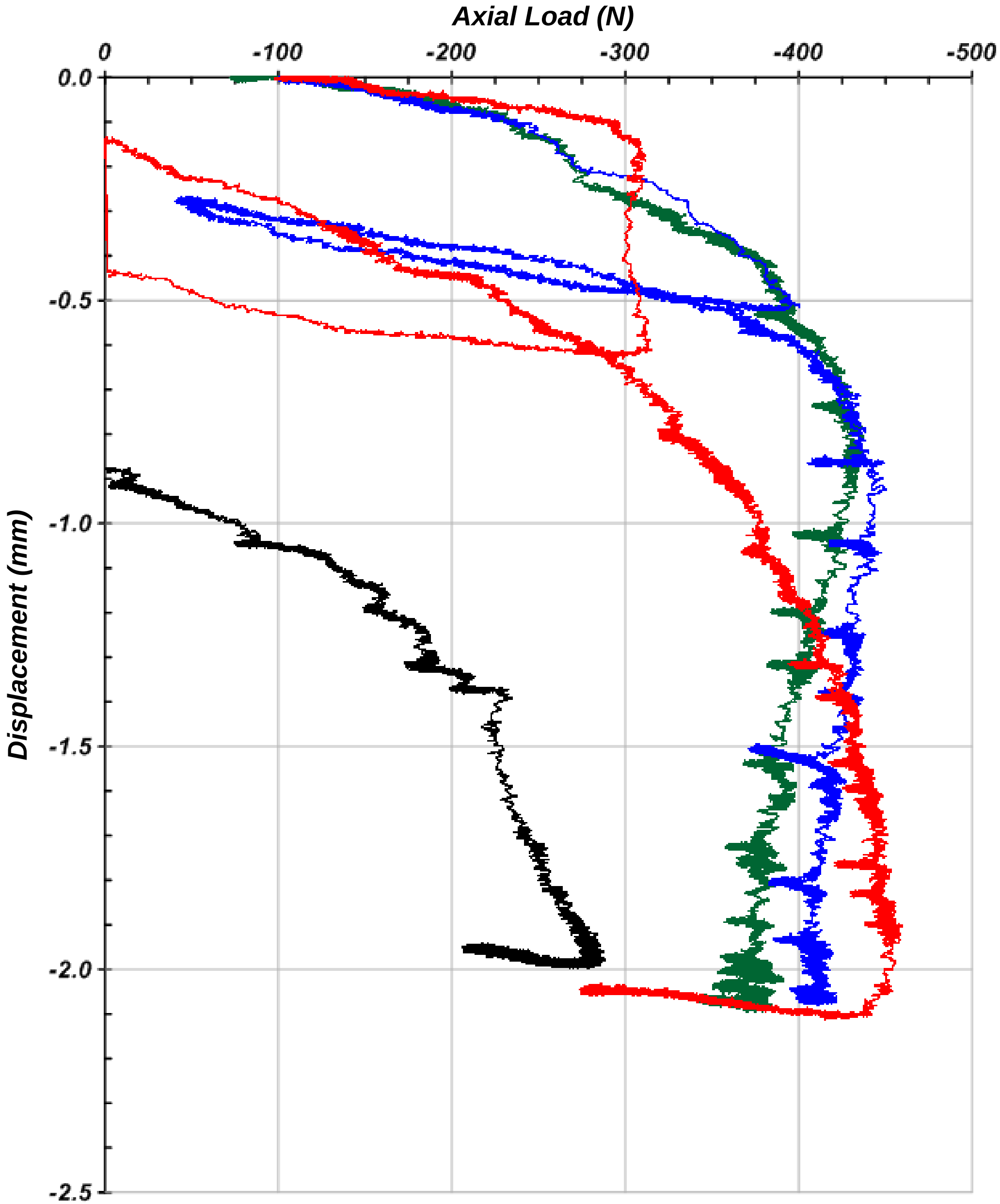

Tensile Capacity Test	Peak Tensile Capacity (N)	Residual Tensile Capacity (N)
4A*	281 (450)	281 (450)
Load Packet 4-I		
4B	454	454
Load Packet 4-II		
4C	445	411
Load Packet 4-III		
4D	432	373

**After installation, 2 mm pullout displacement was insufficient to fully mobilize pile capacity. A tensile capacity of 450 N was selected based on an assumption that limited degradation occurred during the course of the test and review of Test 4B.*

Tension Load = Negative
Retract Displacement = Negative

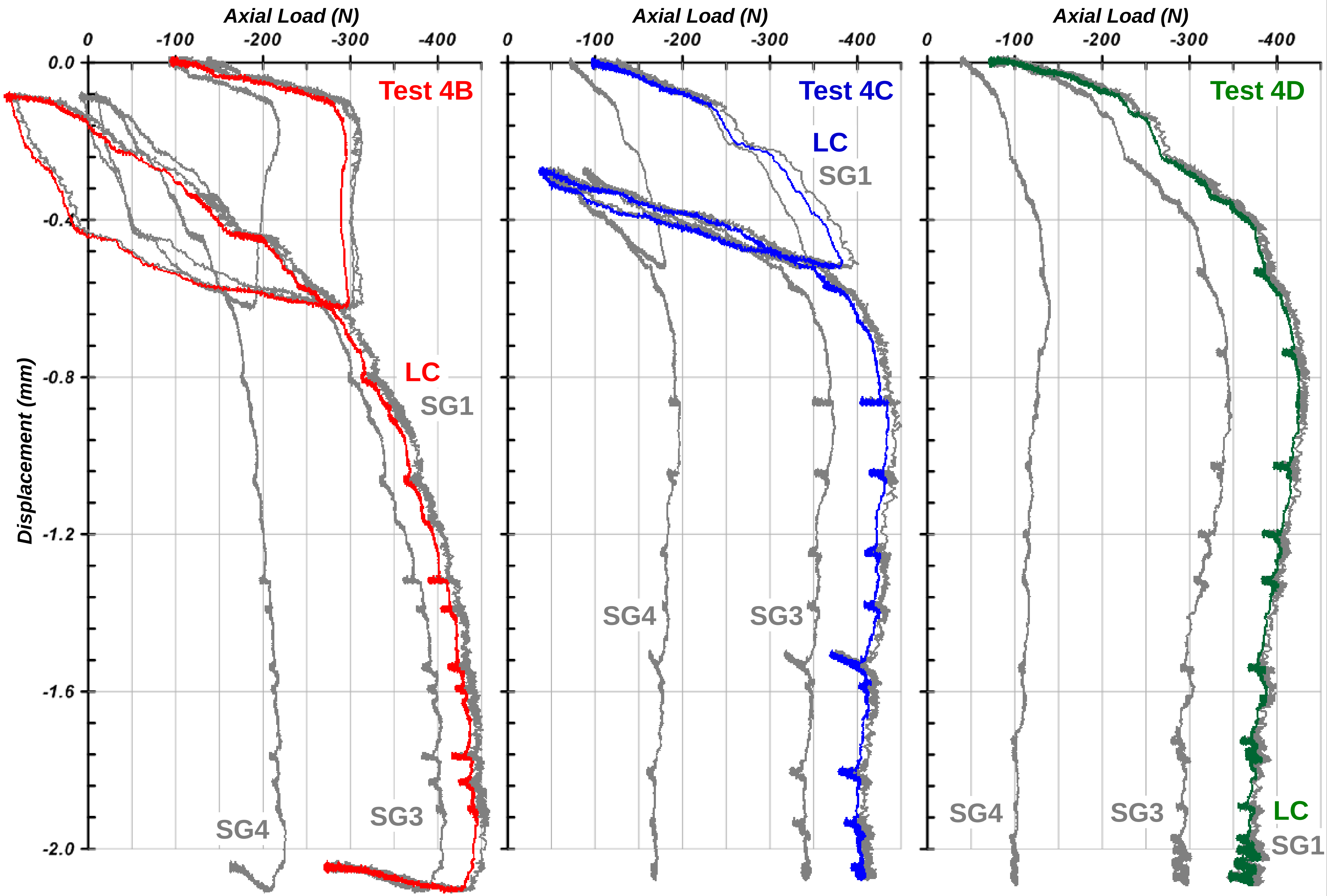

Single Tensile Capacity Tests (Load Cell and Strain Gauge Measurements)
Tensile Capacity Test 4B, 4C, and 4D

March 2016
A-7

MMI
engineers • scientists • innovators

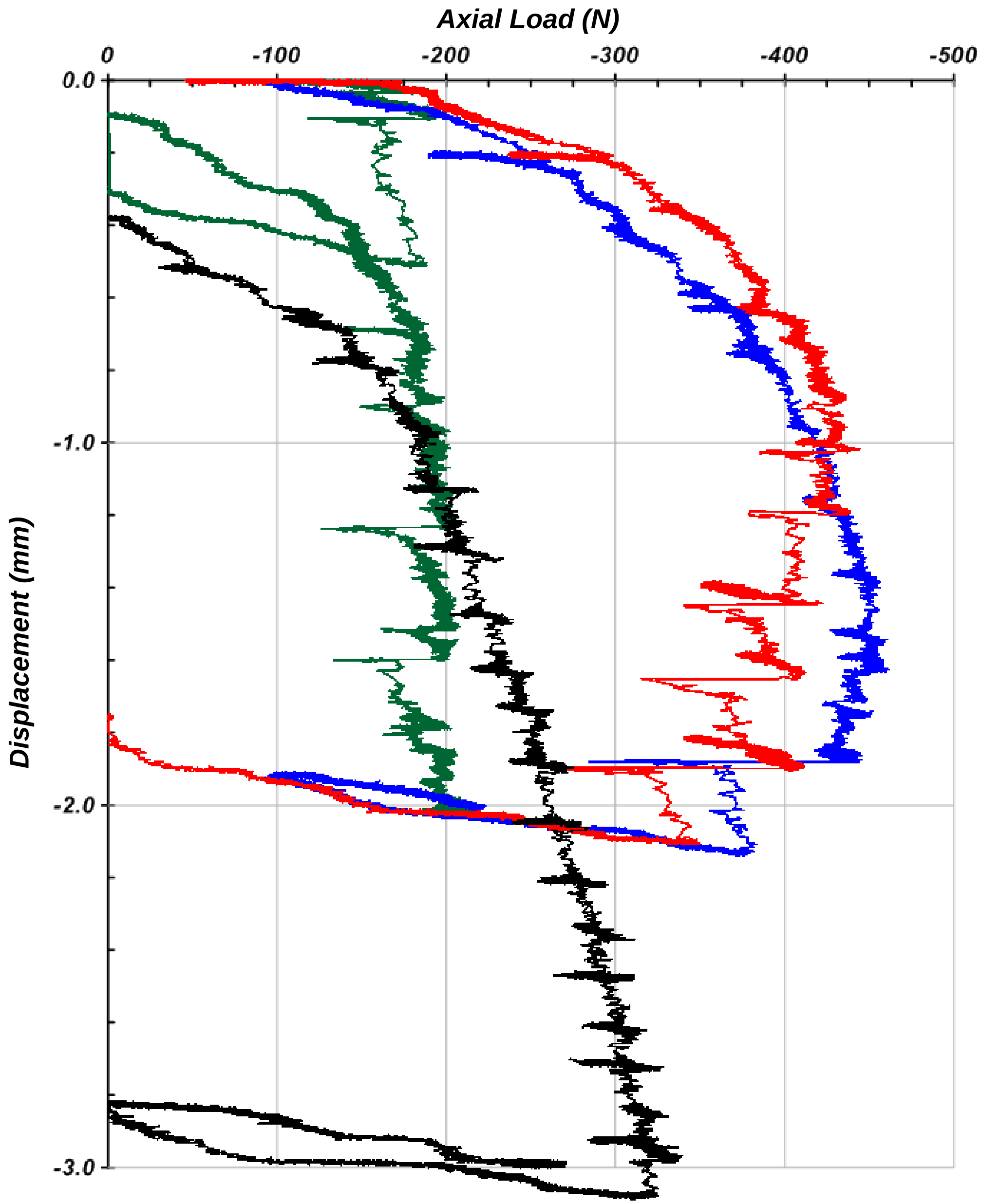

Tensile Capacity Test	Peak Tensile Capacity (N)	Residual Tensile Capacity (N)
5A*	320 (400)	320 (400)
Load Packet 5-IA		
Load Packet 5-IB		
5B	430	340
Load Packet 5-II		
5C	453	375
Load Packet 5-III		
5D	200	200

**After installation, 2 mm pullout displacement was insufficient to fully mobilize pile capacity. A tensile capacity of 400 N was selected based on an assumption that limited degradation occurred during the course of the test and review of Test 5B.*

Tension Load = Negative
Retract Displacement = Negative

All Tensile Capacity Tests (Load Cell Measurement Only)
Centrifuge Test 5

engineers • scientists • innovators

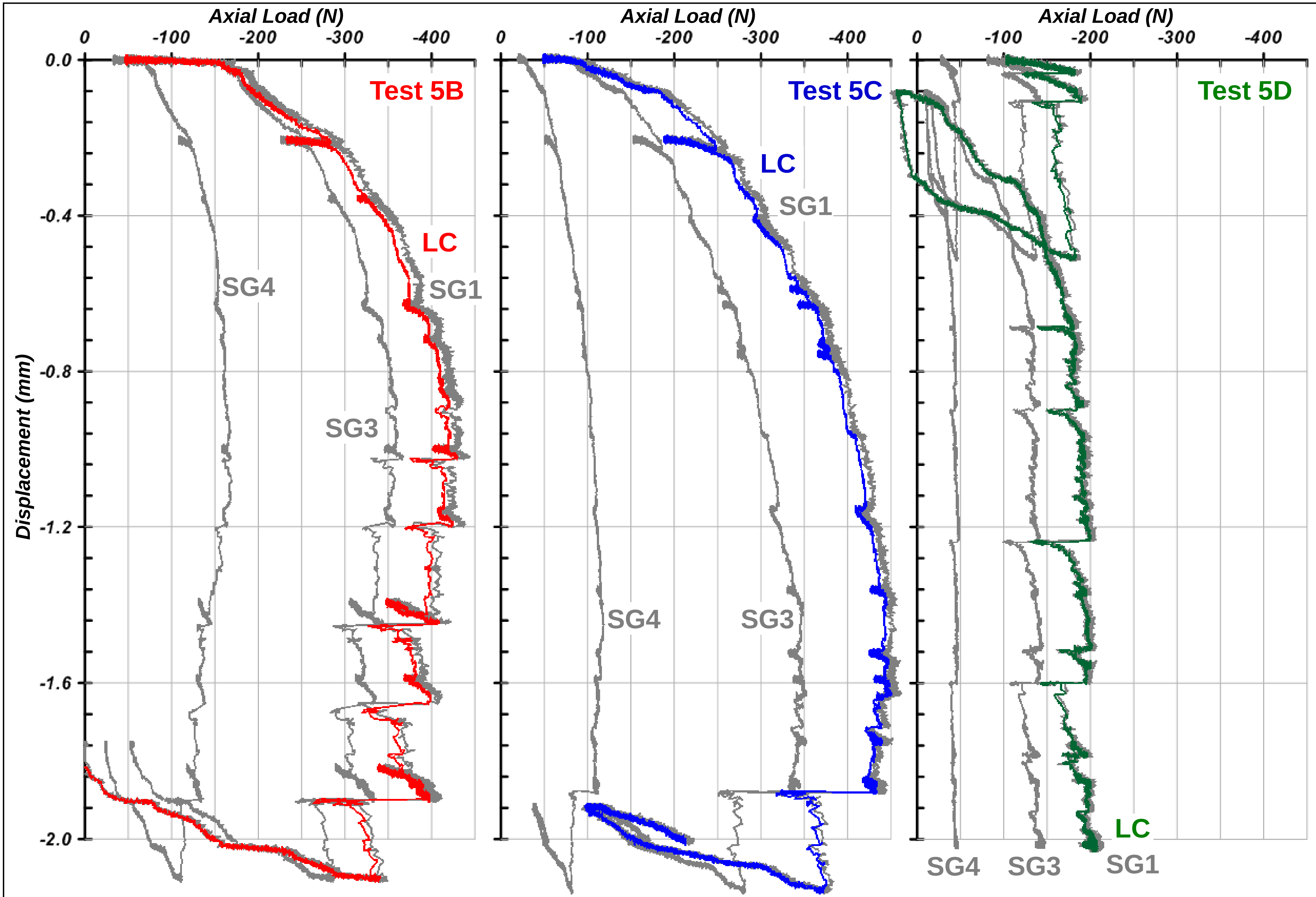

Single Tensile Capacity Tests (Load Cell and Strain Gauge Measurements)

Tensile Capacity Test 5B, 5C, and 5D

March 2016

A-9

MMI engineers • scientists • innovators

APPENDIX B: LOAD AND DISPLACEMENT TIME HISTORIES

CENTRIFUGE TEST 2A

Load Packet	N_{cyc} =1000 cycles	Frequency	Q_S/Q_T	Q_{cyc}/Q_T	Static Load (N)	Cyclic Load (N)	Pre Tensile Capacity (N)	Post Tensile Capacity (N)	Residual Pullout (mm)	Residual Pullout Rate (RPR) (mm/N_{cyc})
2A-I	86	23 Hz	0.38	0.05	78	10	205	--	-0.03	-0.00035

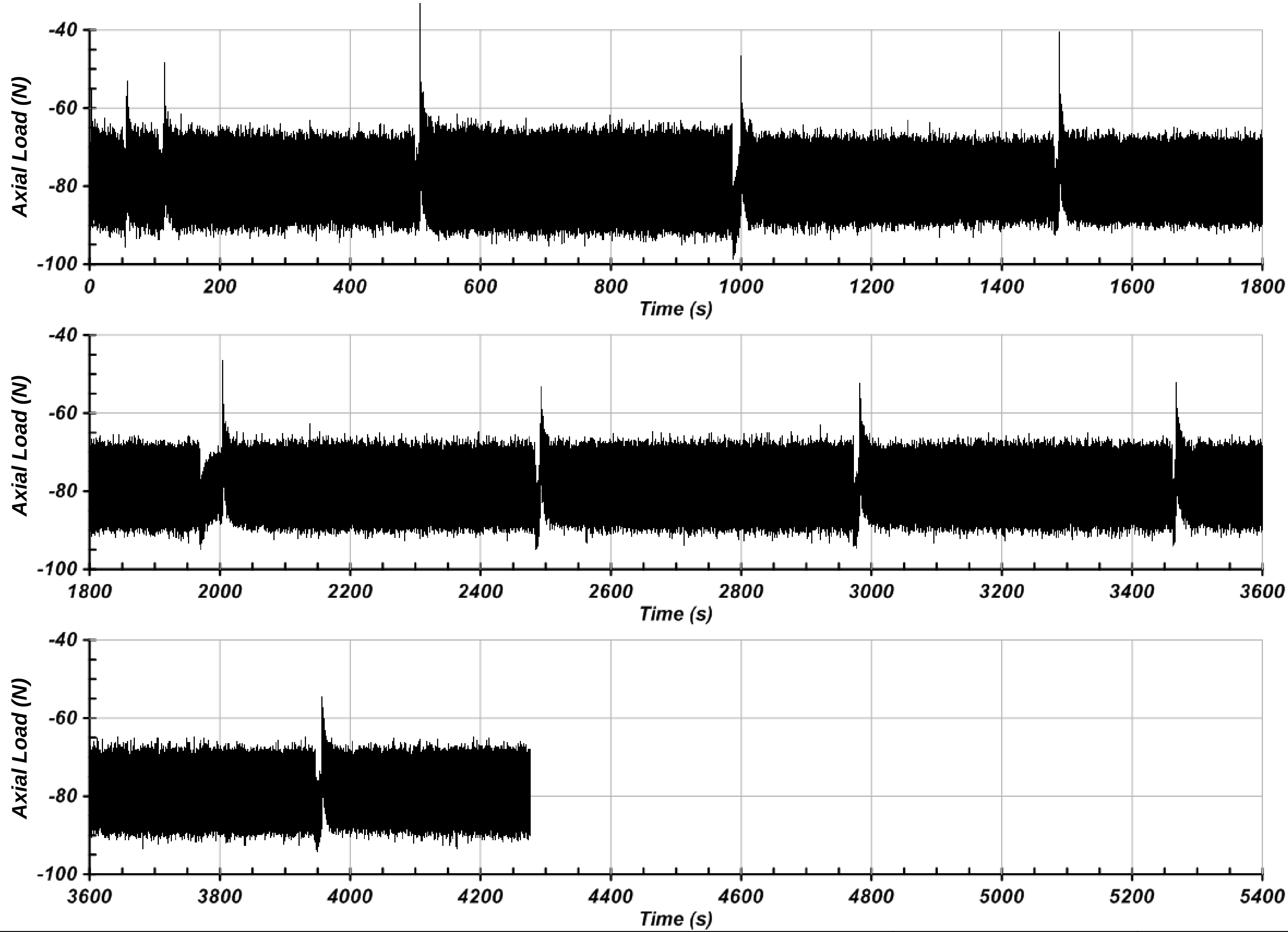

Axial Load vs. Time
Centrifuge Test 2A-I (86,000 cycles at 23 Hz)

March 2016

B-3

MMI
engineers • scientists • innovators

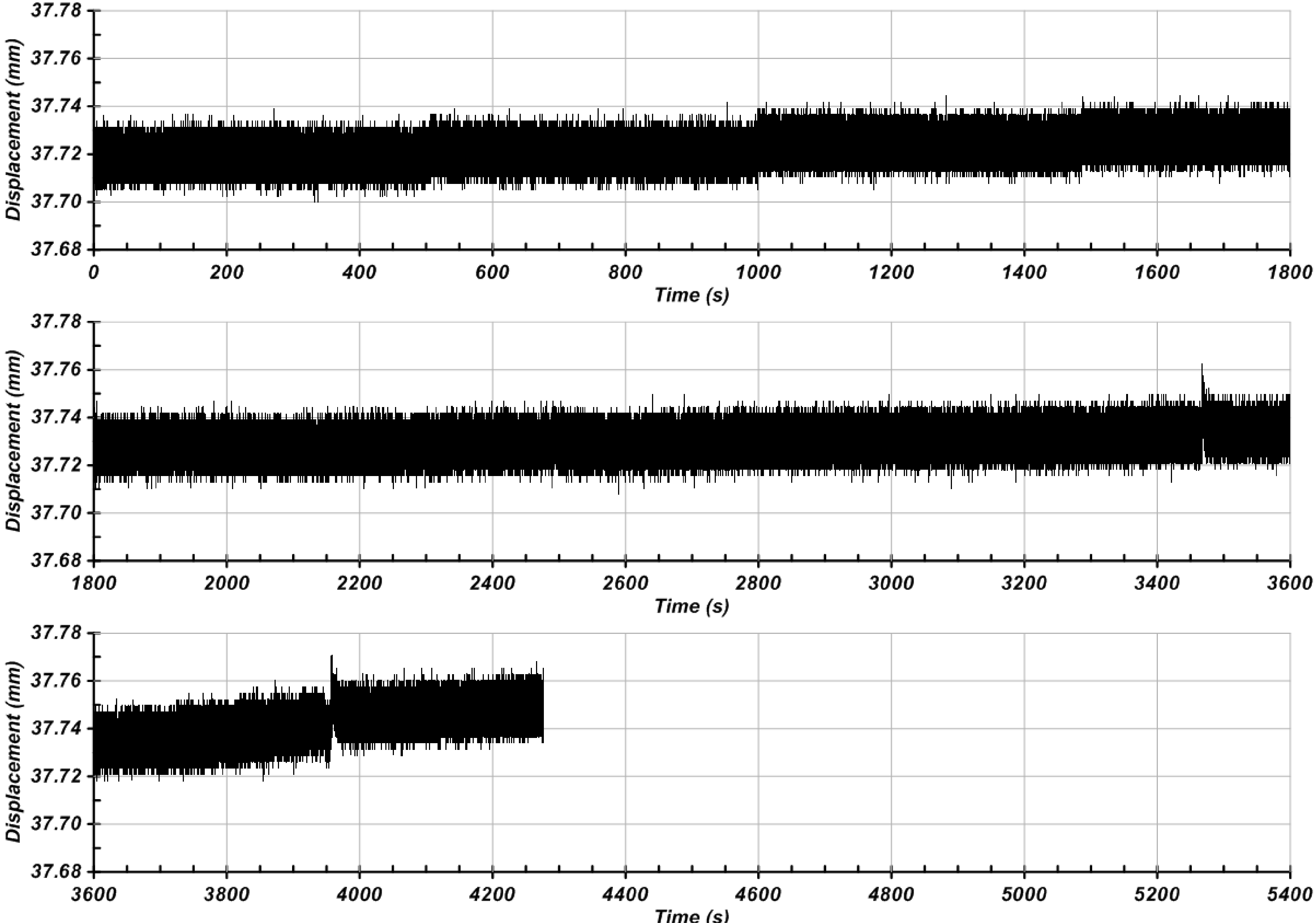

Displacement vs. Time
Centrifuge Test 2A-I (86,000 cycles at 23 Hz)

March 2016
B-4

engineers • scientists • innovators

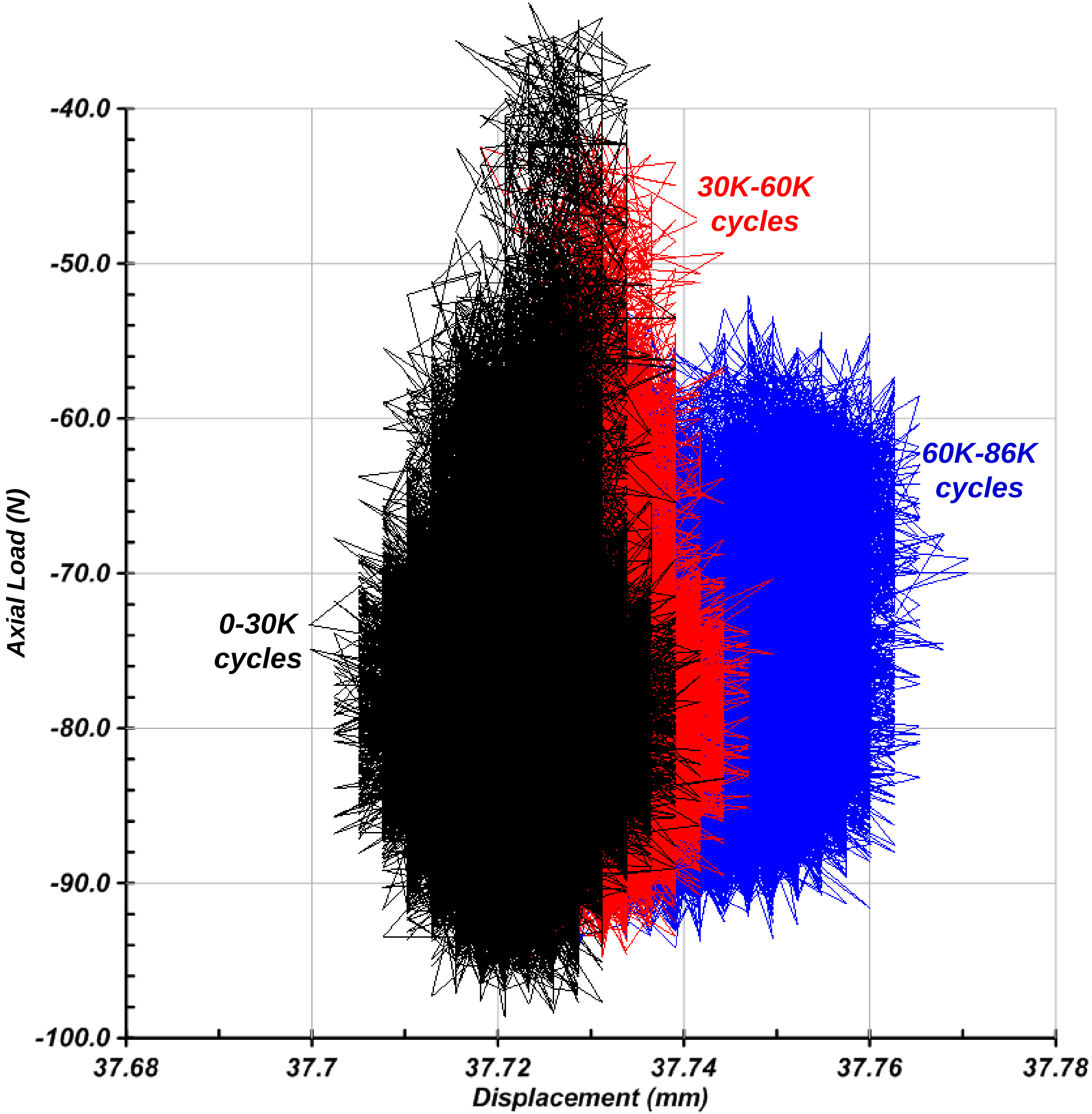

Axial Load vs. Displacement
Centrifuge Test 2A-I (86,000 cycles at 23 Hz)

March 2016

CENTRIFUGE TEST 2B

Load Packet	N_{cyc} =1000 cycles	Frequency	Q_S/Q_T	Q_{cyc}/Q_T	Static Load (N)	Cyclic Load (N)	Pre Tensile Capacity (N)	Post Tensile Capacity (N)	Residual Pullout (mm)	Residual Pullout Rate (RPR) (mm/N_{cyc})
2B-I	100	23 Hz	0.39	0.02	110	6	285	275	-0.06	-0.00055
2B-IIA	10	23 Hz	0.43	0.11	118	29	275	230	0.18	0.018
2B-IIB	10	23 Hz	0.30	0.22	70	51.5	230	175	9.50	0.95

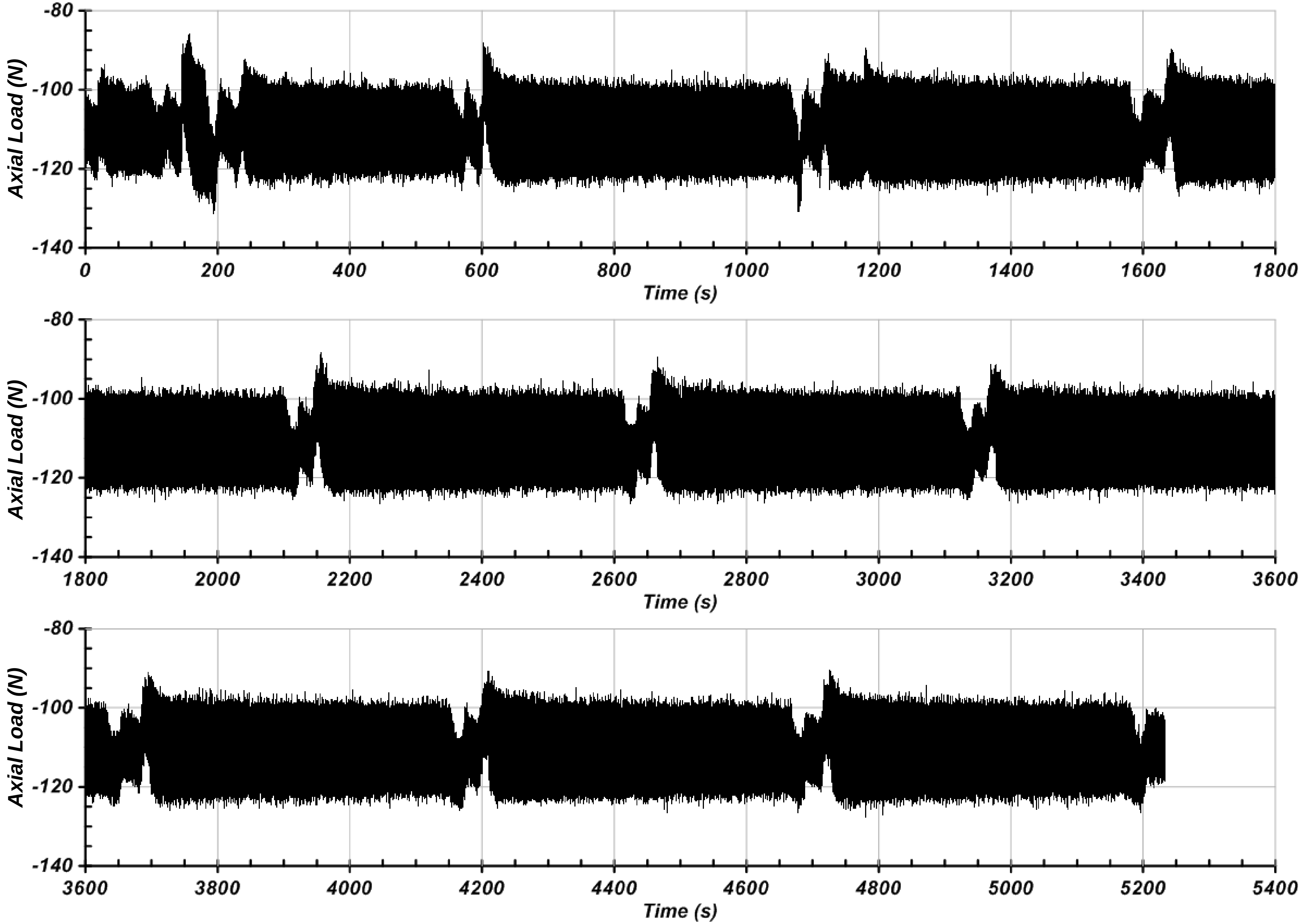

Axial Load vs. Time

Centrifuge Test 2B-I (100,000 cycles at 23 Hz)

March 2016

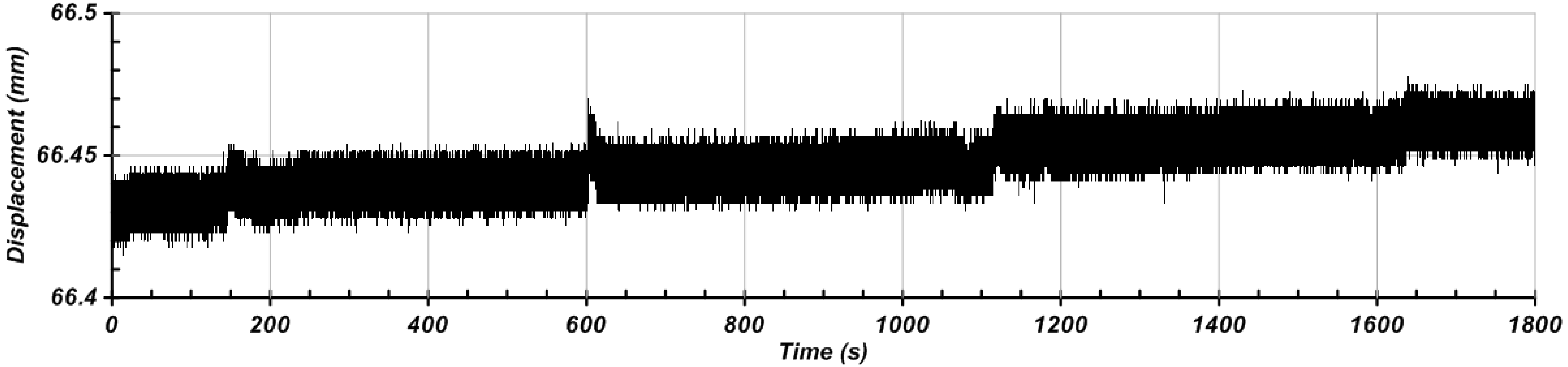

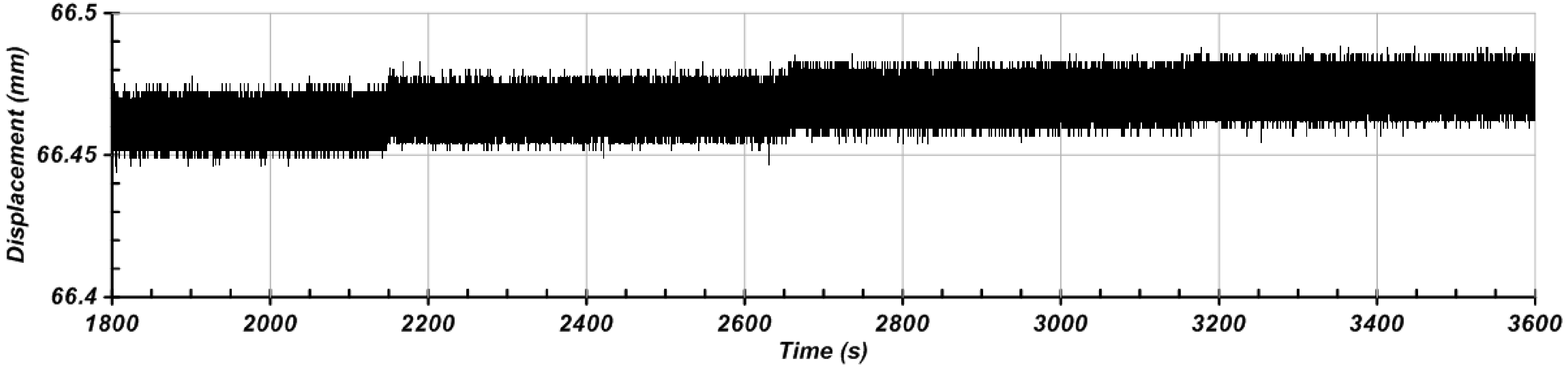

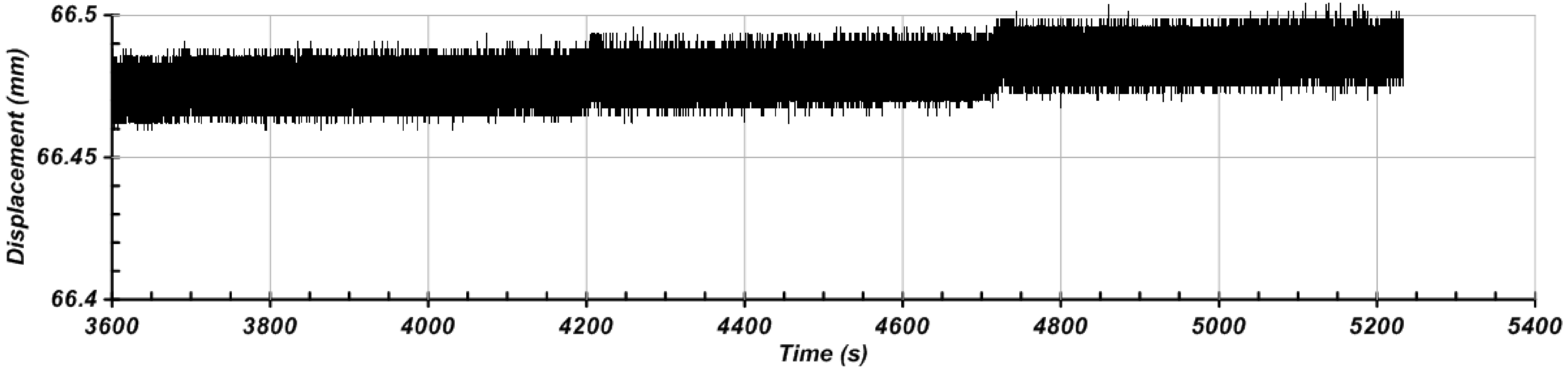

Displacement vs. Time
Centrifuge Test 2B-I (100,000 cycles at 23 Hz)

March 2016

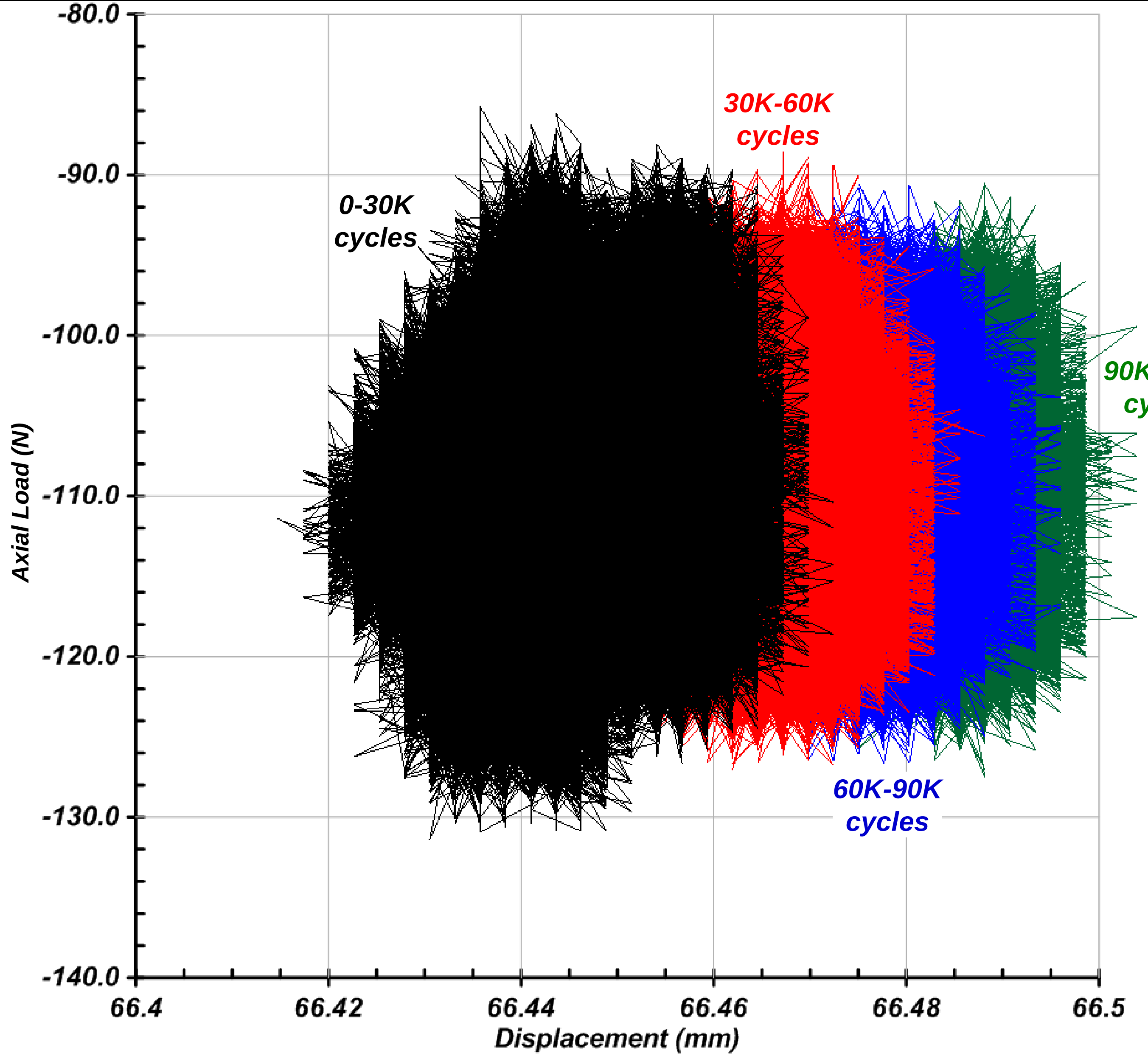

Axial Load vs. Displacement
Centrifuge Test 2B-I (100,000 cycles at 23 Hz)

March 2016
B-9

MMI
engineers • scientists • innovators

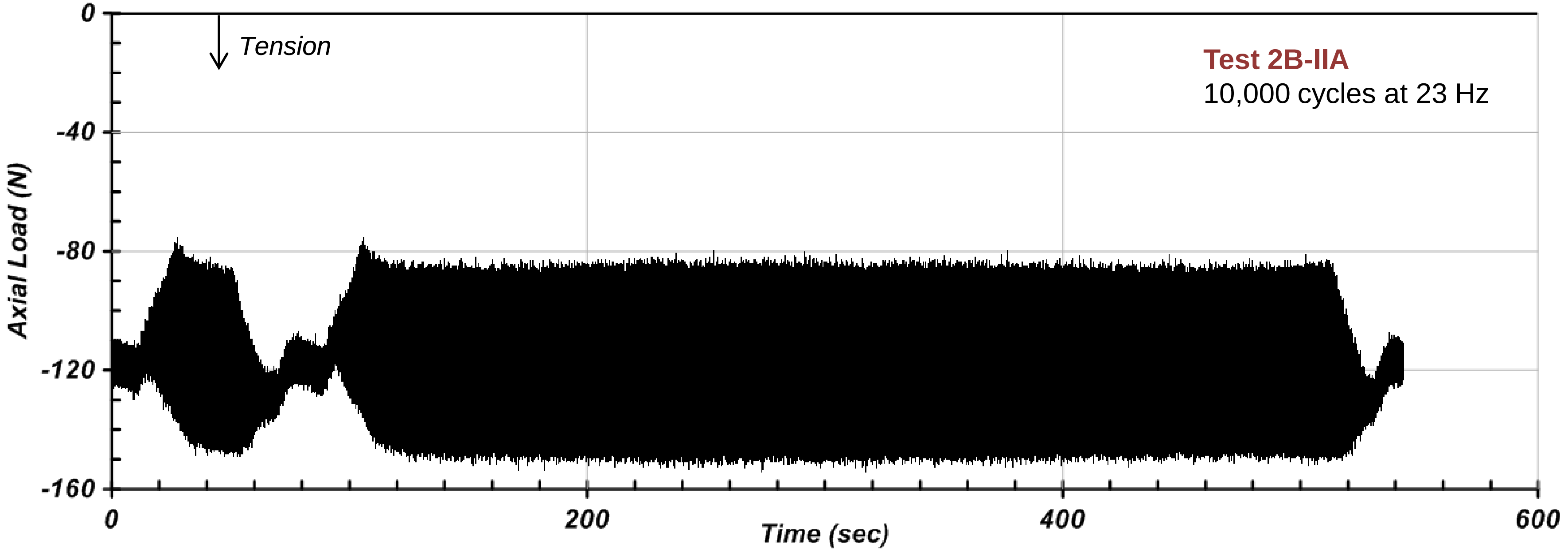

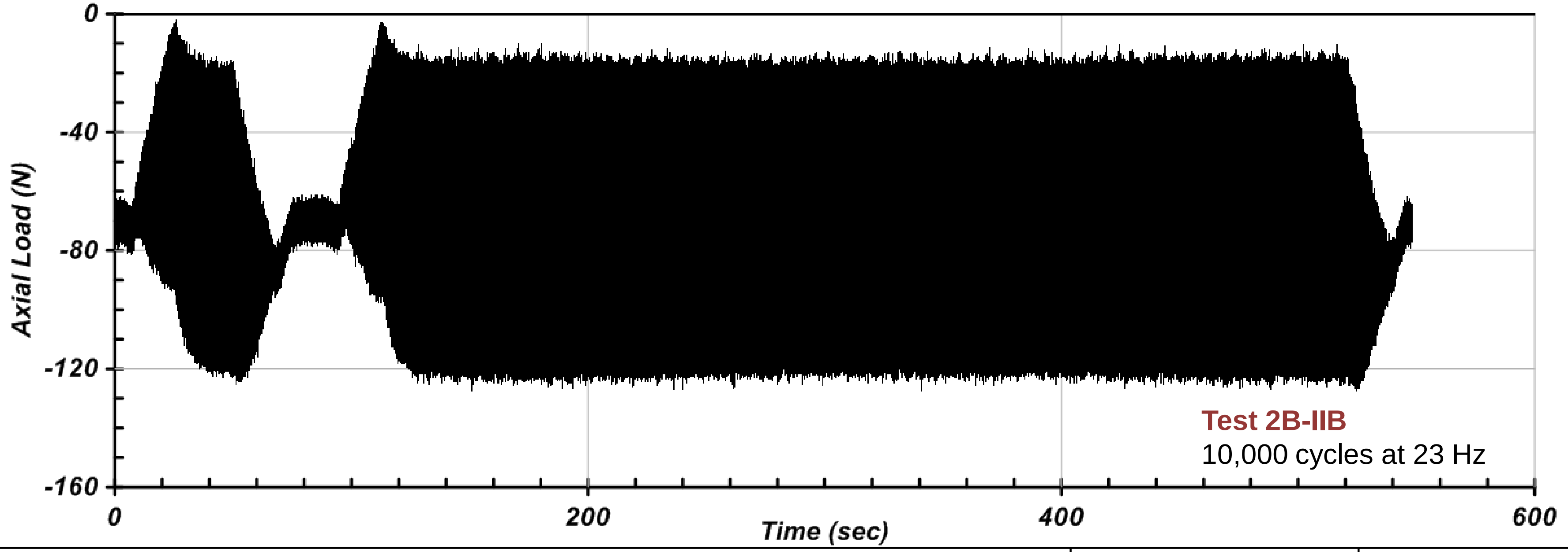

Axial Load vs. Time
Centrifuge Test 2B-IIA and 2B-IIB (10,000 cycles at 23 Hz)

March 2016

engineers • scientists • innovators

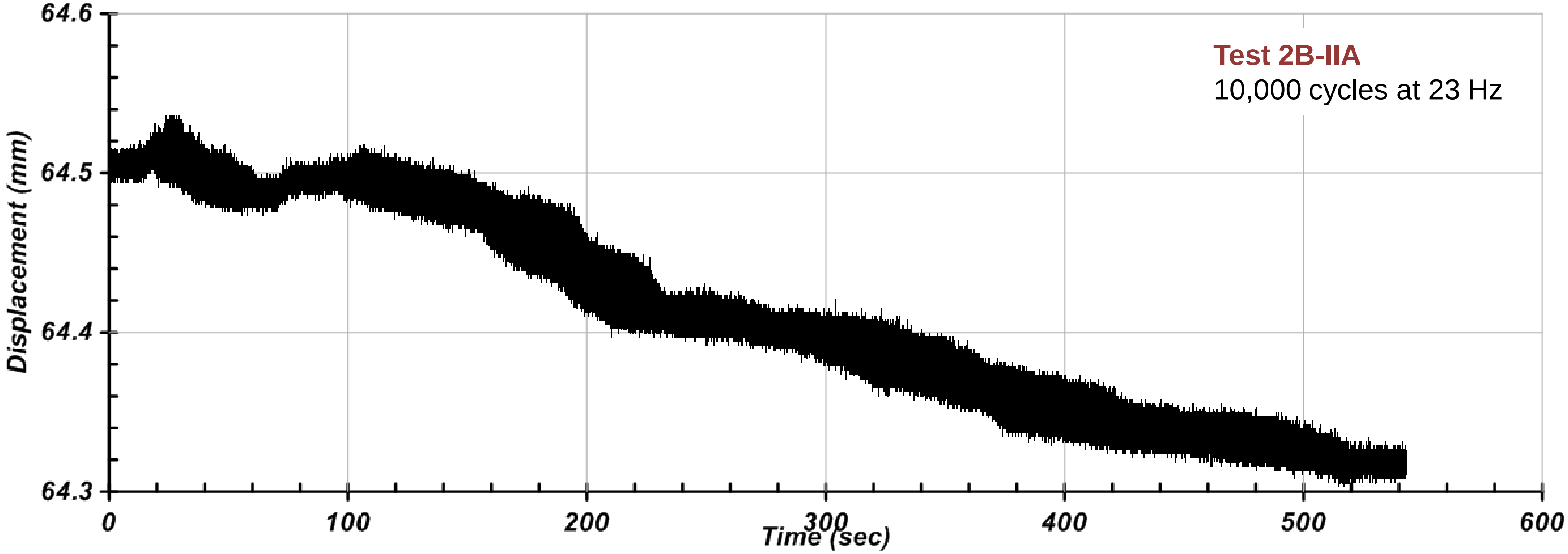

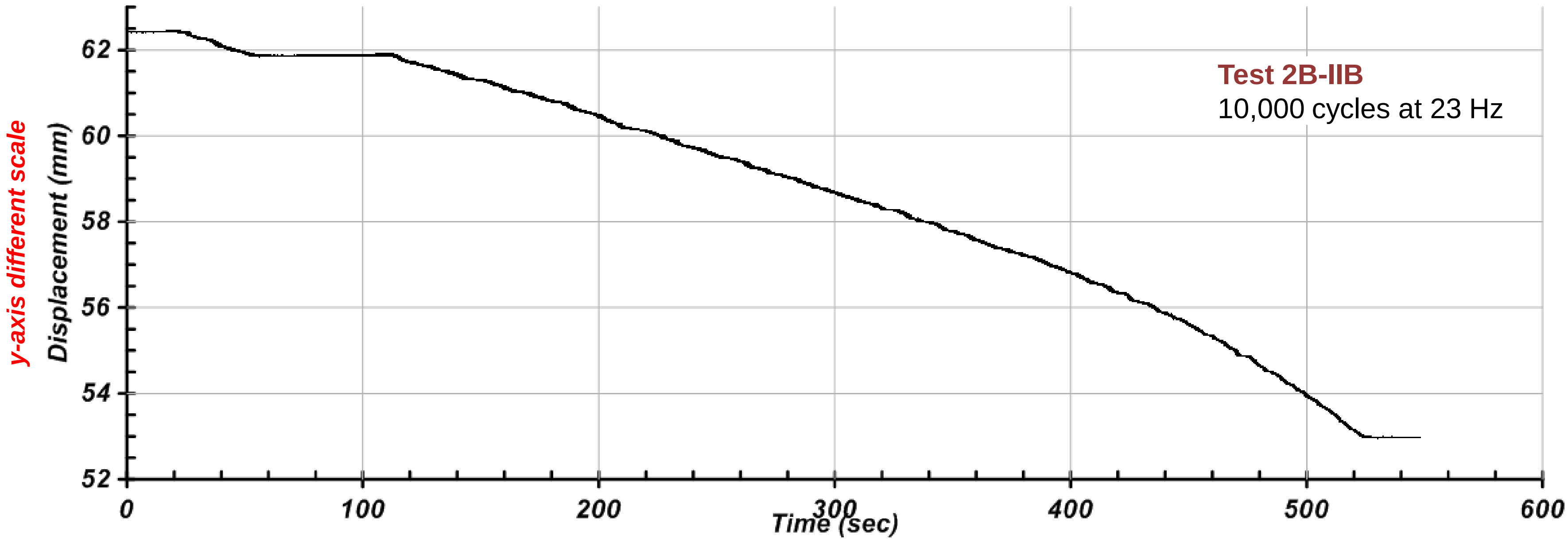

Displacement vs. Time

Centrifuge Test 2B-IIA and 2B-IIB (10,000 cycles at 23 Hz)

March 2016

MMI engineers • scientists • innovators

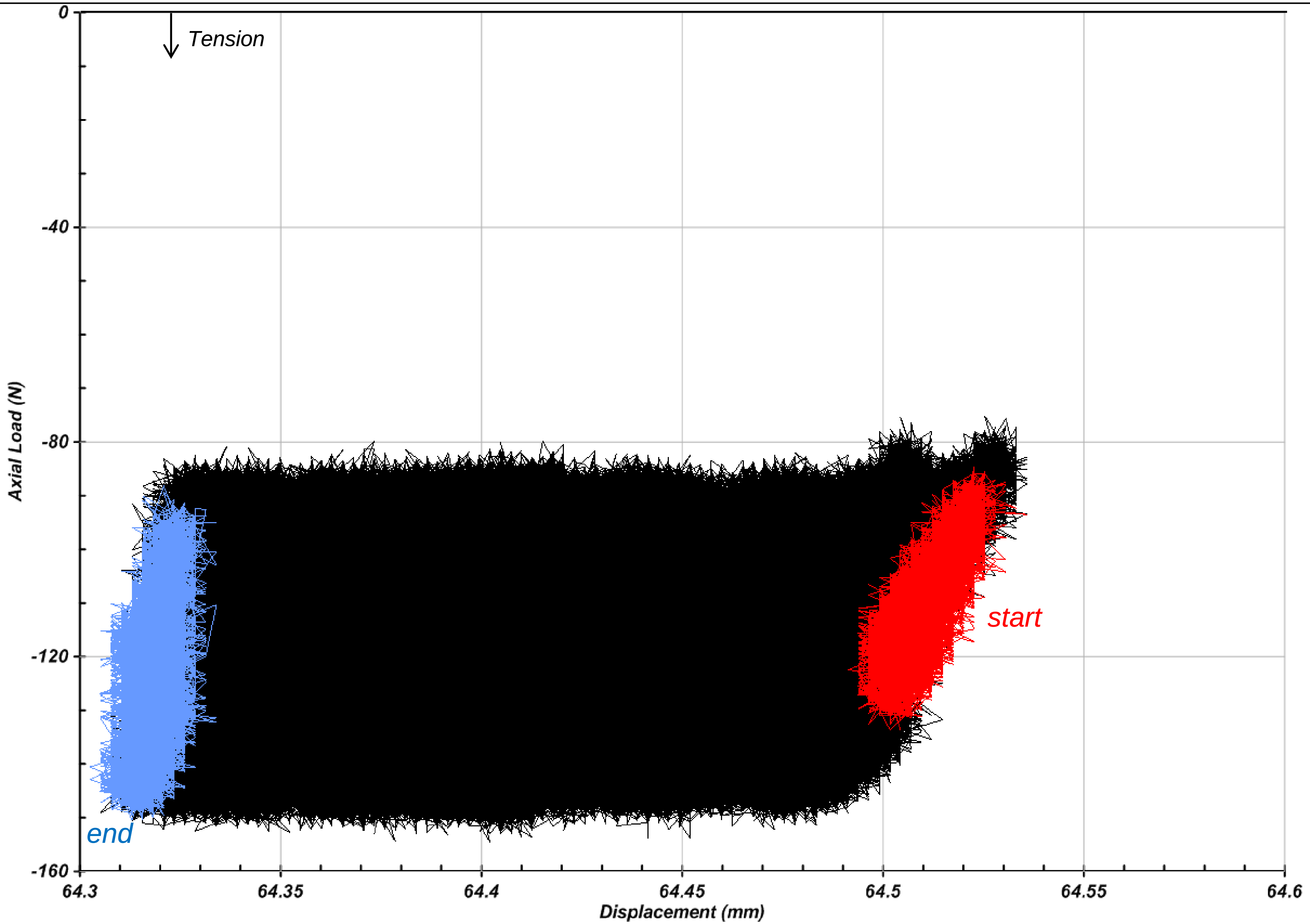

Axial Load vs. Displacement

Centrifuge Test 2B-IIA (10,000 cycles at 23 Hz)

March 2016

B-12

MMI
engineers • scientists • innovators

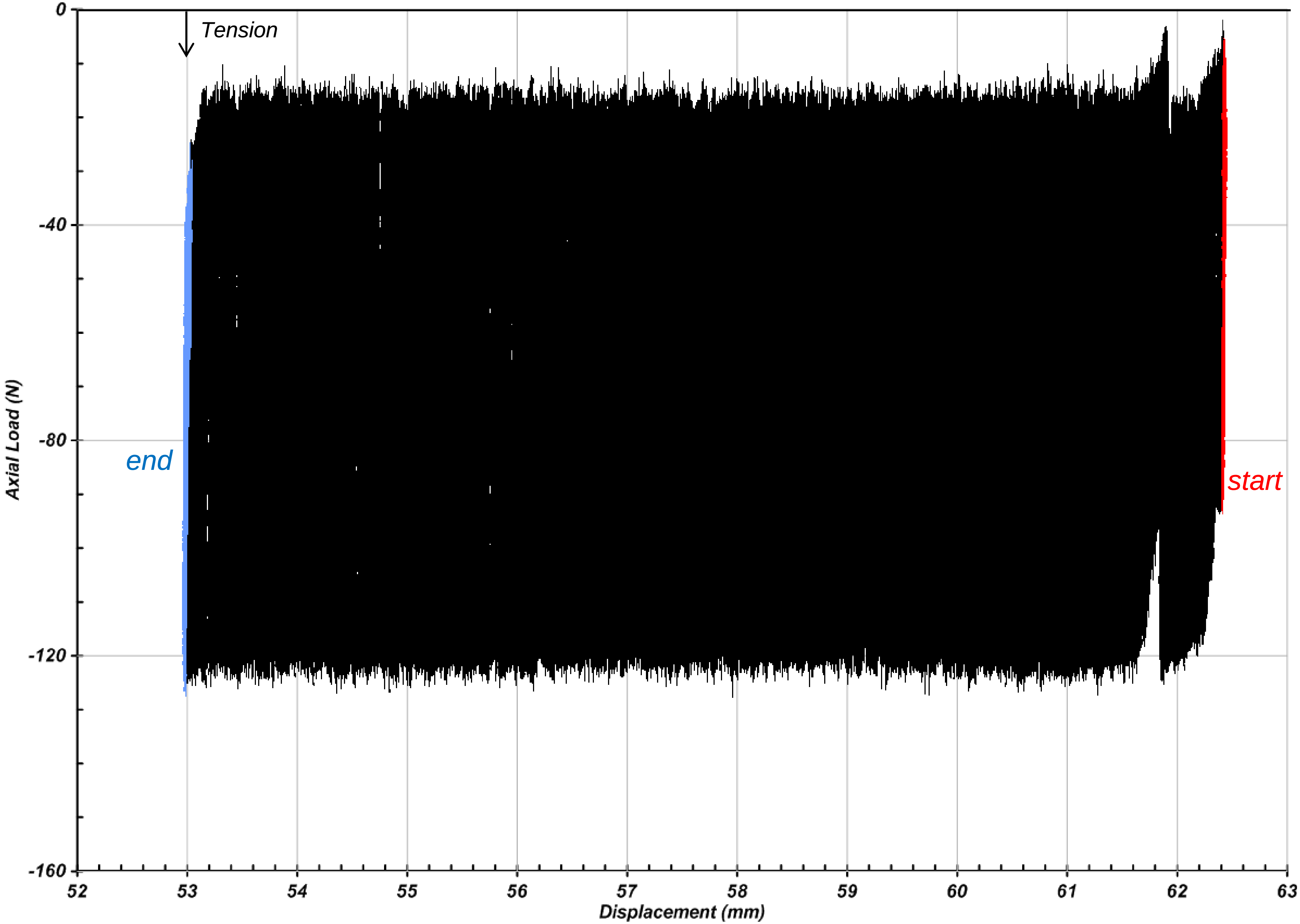

Axial Load vs. Displacement
Centrifuge Test 2B-IIB (10,000 cycles at 23 Hz)

March 2016
B-13

engineers • scientists • innovators

CENTRIFUGE TEST 3

Load Packet	N_{cyc} =1000 cycles	Frequency	Q_S/Q_T	Q_{cyc}/Q_T	Static Load (N)	Cyclic Load (N)	Pre Tensile Capacity (N)	Post Tensile Capacity (N)	Residual Pullout (mm)	Residual Pullout Rate (RPR) (mm/N_{cyc})
3-I	100	23 Hz	0.32	0.06	58	10.5	180	175	-0.13	-0.00125
3-II	10	23 Hz	0.29	0.10	50	17.5	175	170	-0.01	-0.001
3-III	0.5	0.5 Hz	0.19	0.42	33	71.5	170	180	0.02	0.04

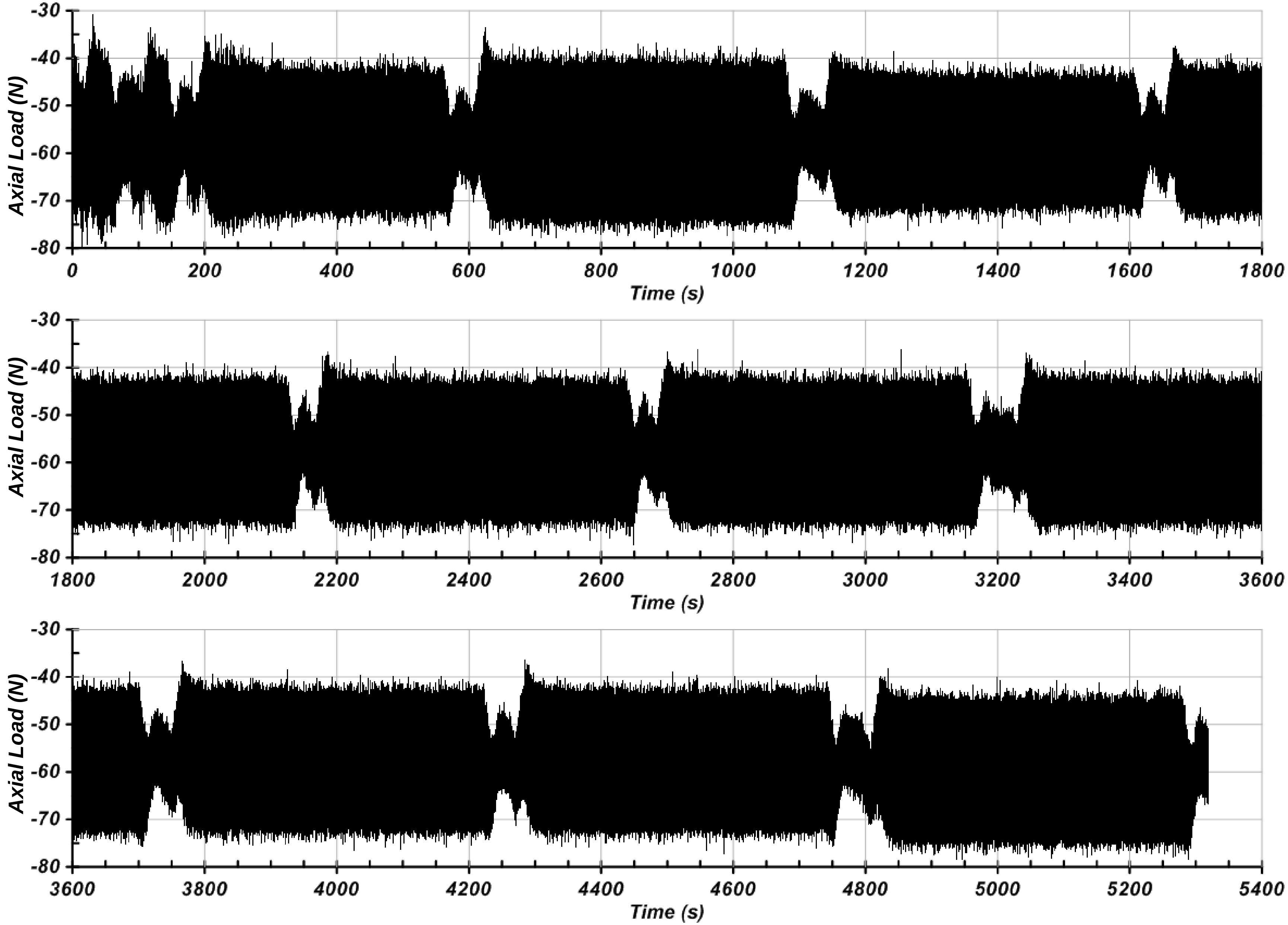

Axial Load vs. Time
Centrifuge Test 3-I (100,000 cycles at 23 Hz)

March 2016
B-15

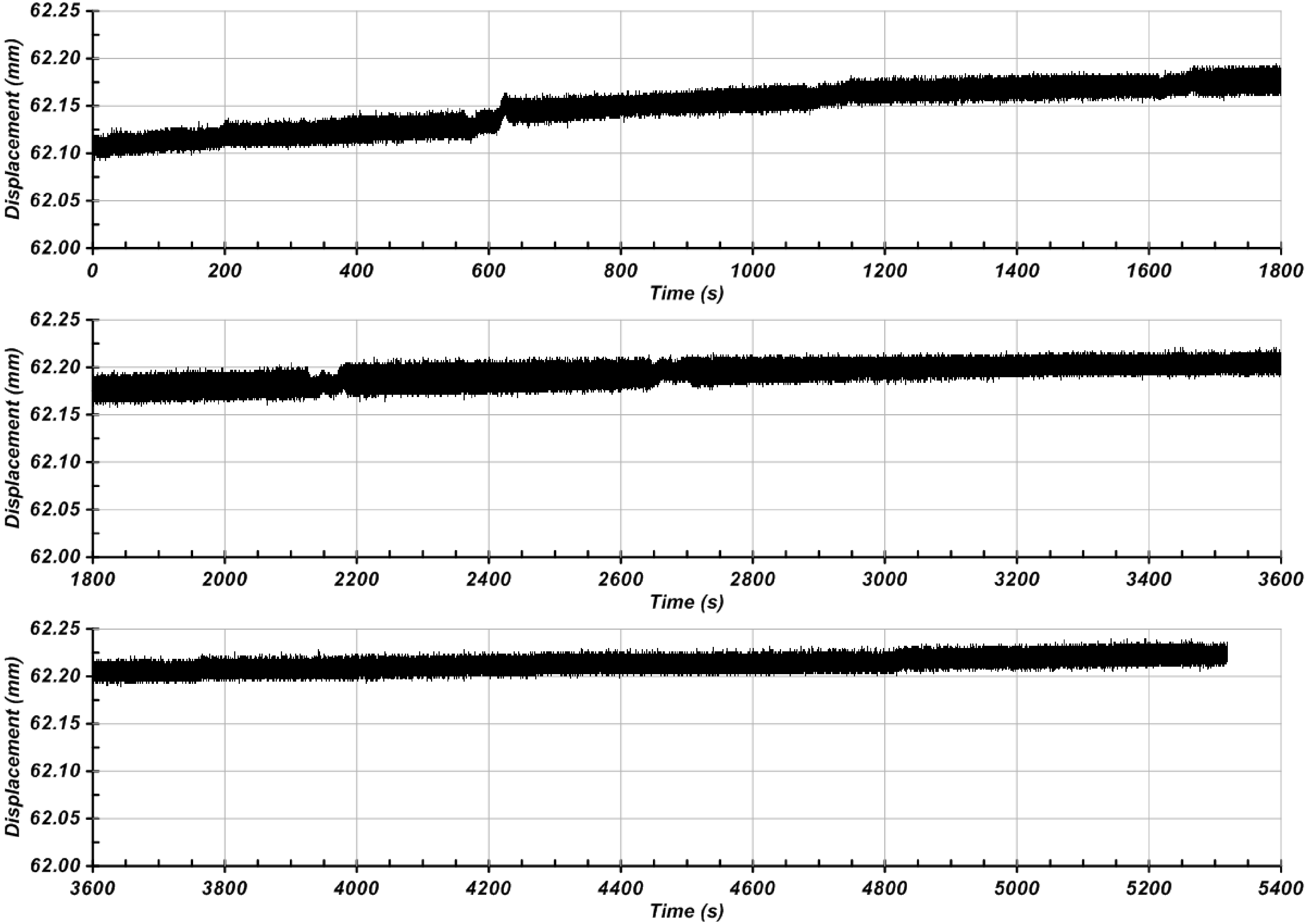

Displacement vs. Time
Centrifuge Test 3-I (100,000 cycles at 23 Hz)

March 2016

engineers • scientists • innovators

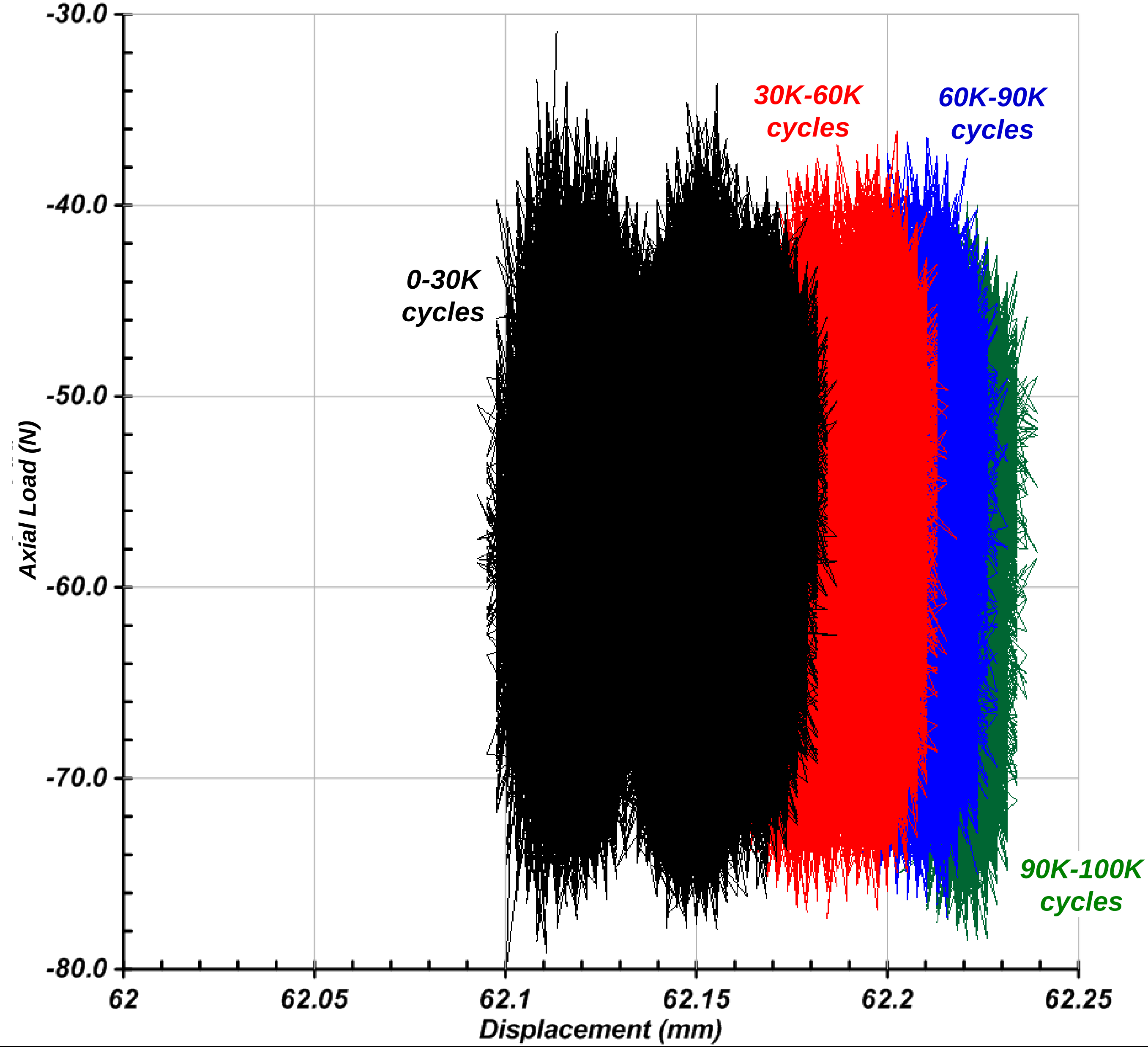

Axial Load vs. Displacement
Centrifuge Test 3-I (100,000 cycles at 23 Hz)

March 2016

MMI engineers • scientists • innovators

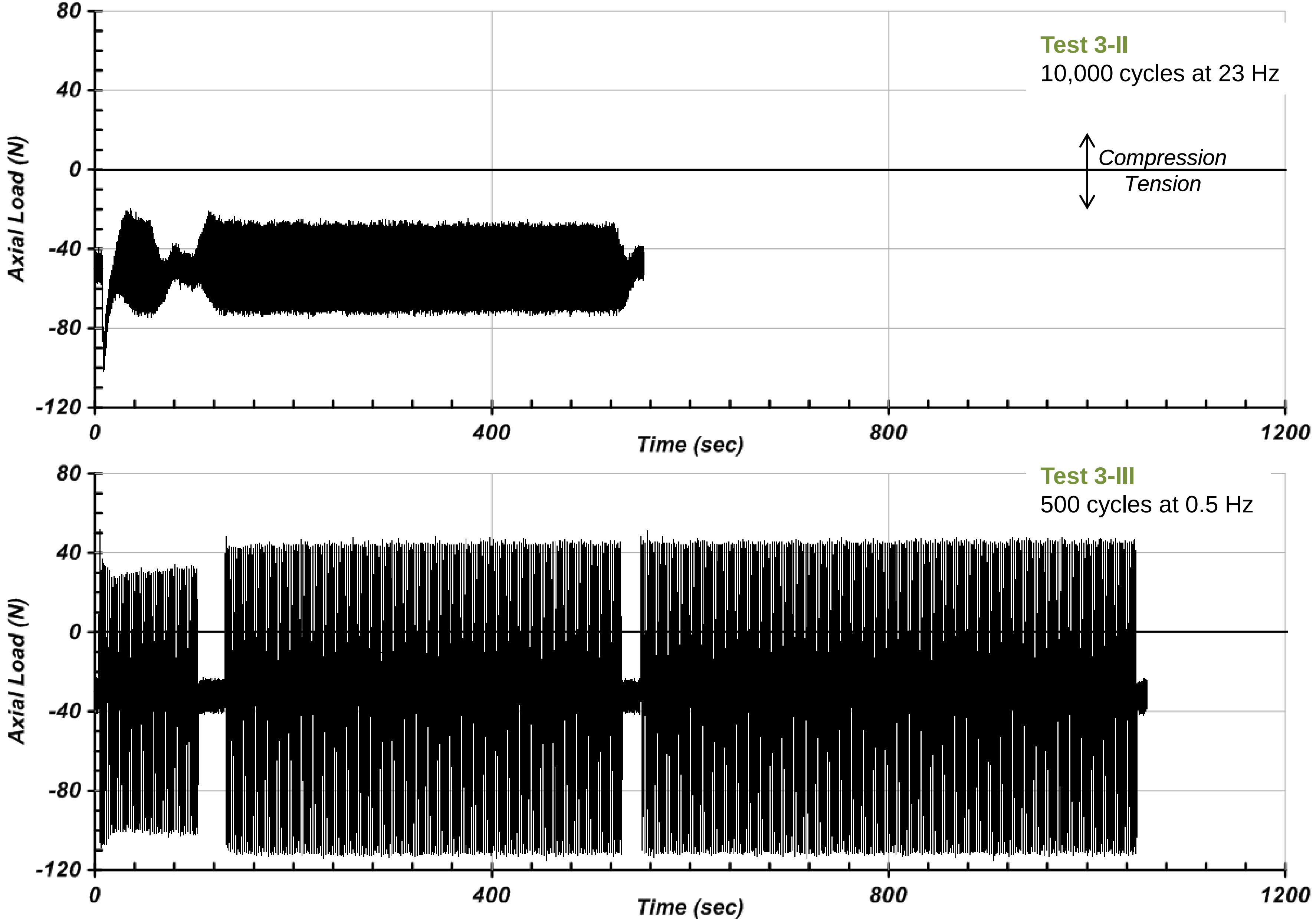

Axial Load vs. Time

Centrifuge Test 3-II (10,000 cycles at 23 Hz) and Test 3-III (500 cycles at 0.5 Hz)

March 2016

MMI engineers • scientists • innovators

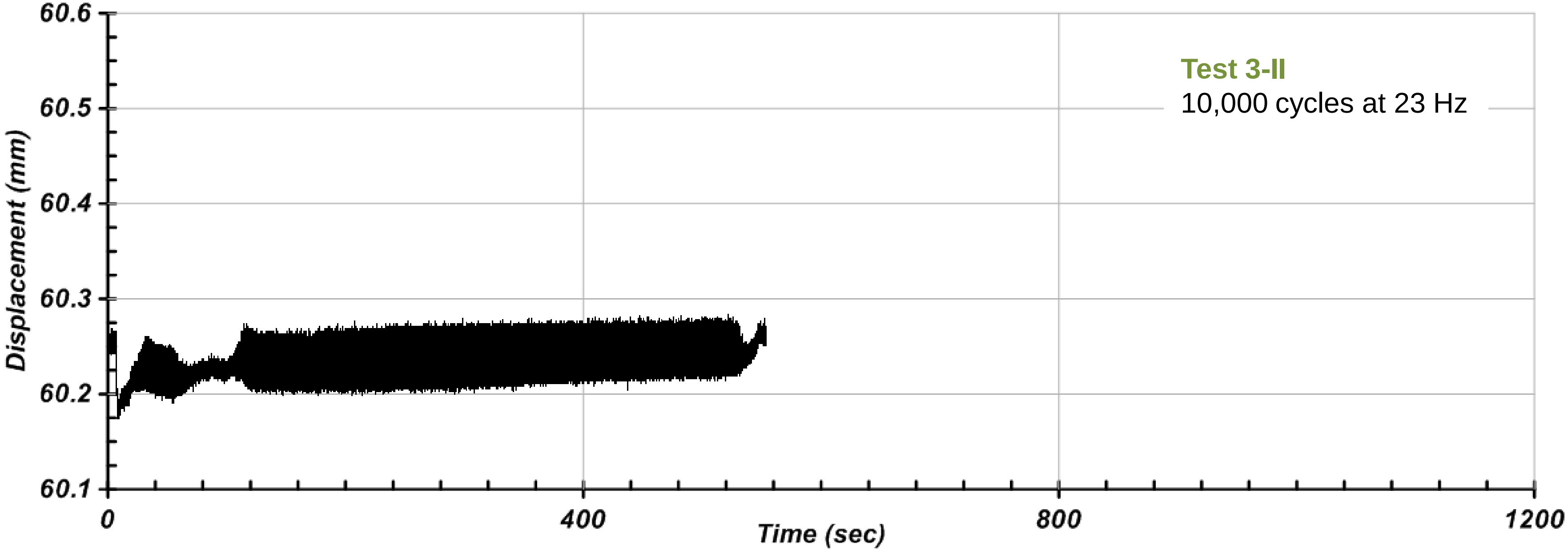

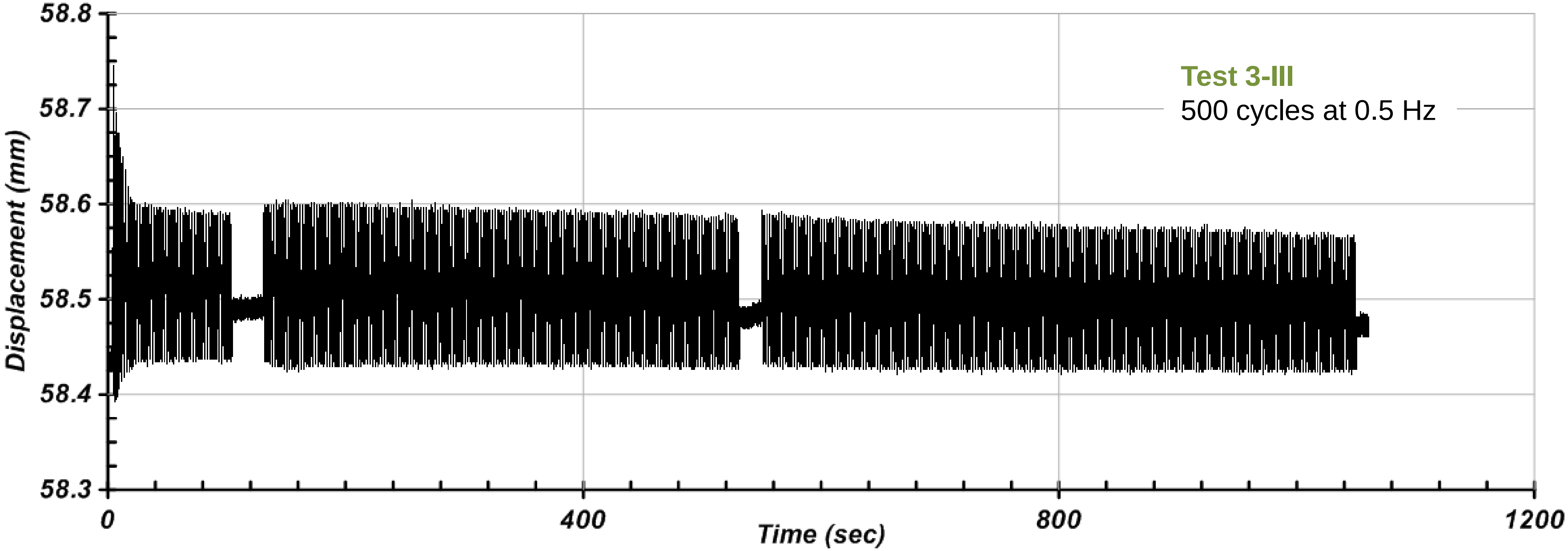

Displacement vs. Time

Centrifuge Test 3-II (10,000 cycles at 23 Hz) and Test 3-III (500 cycles at 0.5 Hz)

March 2016

MMI

engineers • scientists • innovators

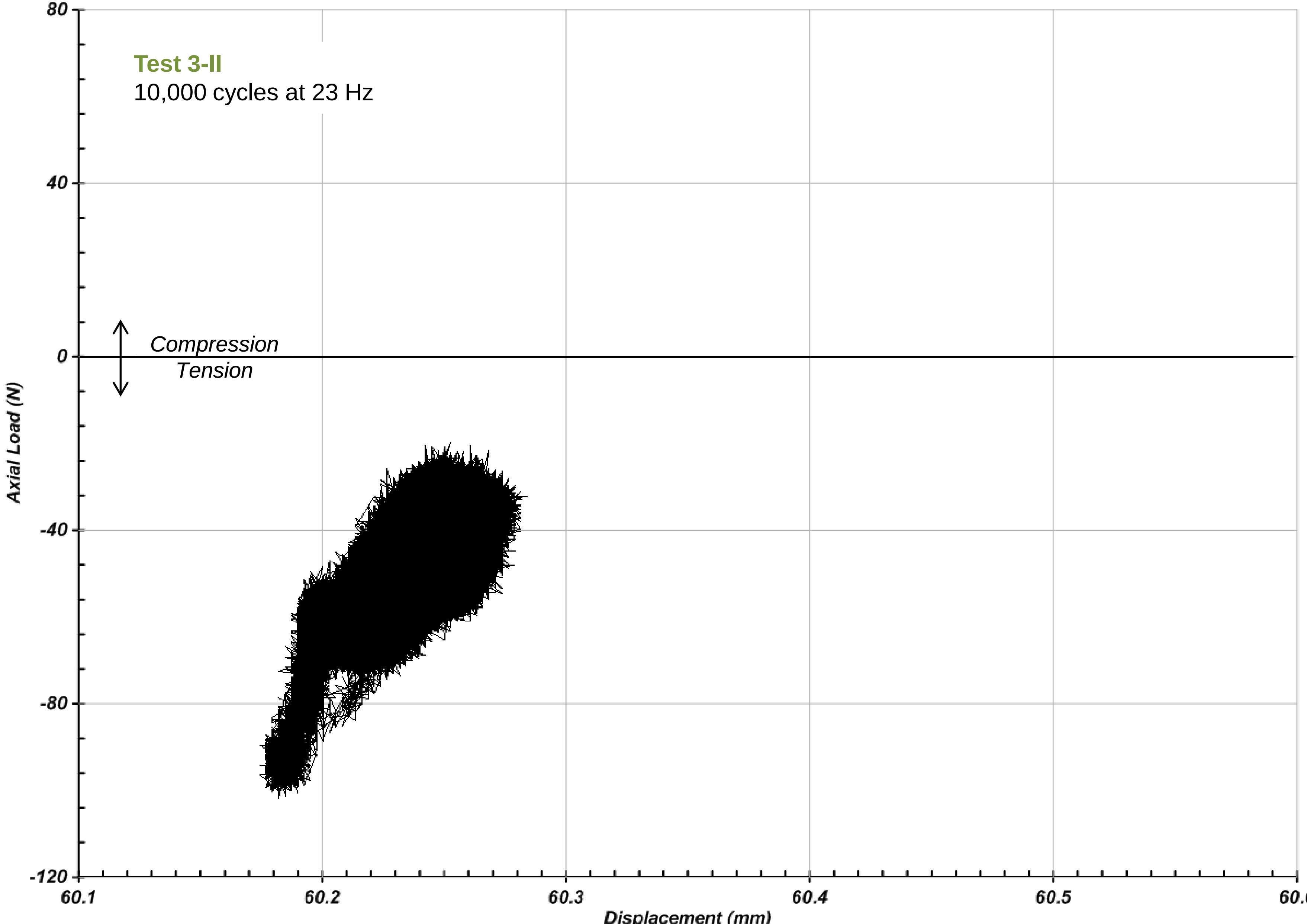

Axial Load vs. Displacement
Centrifuge Test 3-II (10,000 cycles at 23 Hz)

March 2016

engineers • scientists • innovators

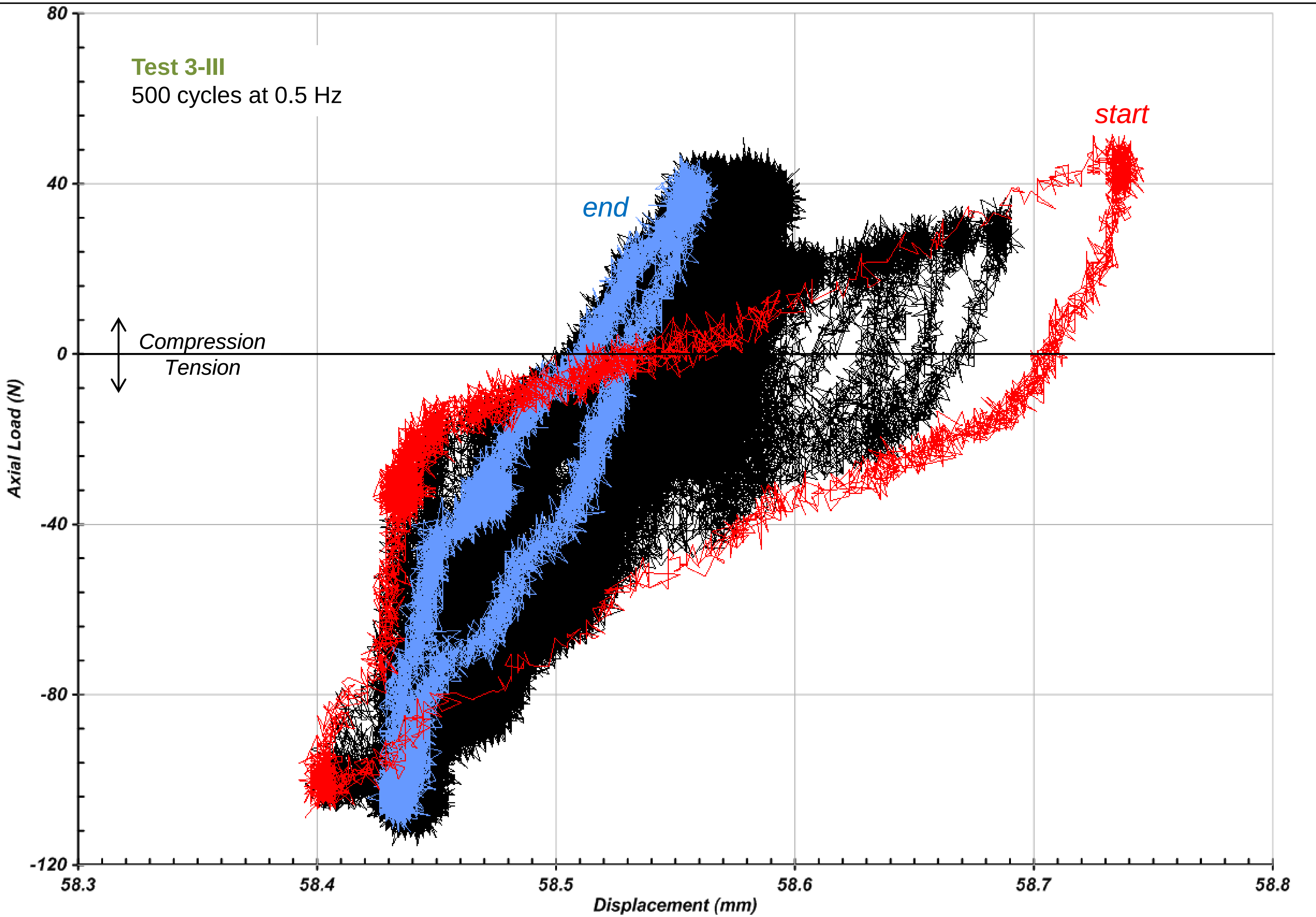

Axial Load vs. Displacement
Centrifuge Test 3-III (500 cycles at 0.5 Hz)

March 2016

MMI
engineers • scientists • innovators

CENTRIFUGE TEST 4

Load Packet	N_{cyc} =1000 cycles	Frequency	Q_S/Q_T	Q_{cyc}/Q_T	Static Load (N)	Cyclic Load (N)	Pre Tensile Capacity (N)	Post Tensile Capacity (N)	Residual Pullout (mm)	Residual Pullout Rate (RPR) (mm/N_{cyc})
4-I	100	23 Hz	0.39	0.04	109	11	281 (450*)	454	-0.04	-0.00044
4-II	10	23 Hz	0.24	0.08	109	36	454	411	0.02	0.0015
4-III	0.5	0.5 Hz	0.20	0.19	85	77.5	411	373	0.68	1.35

**Assumed value since 2mm displacement for pullout test was insufficient to fully mobilize pile capacity.*

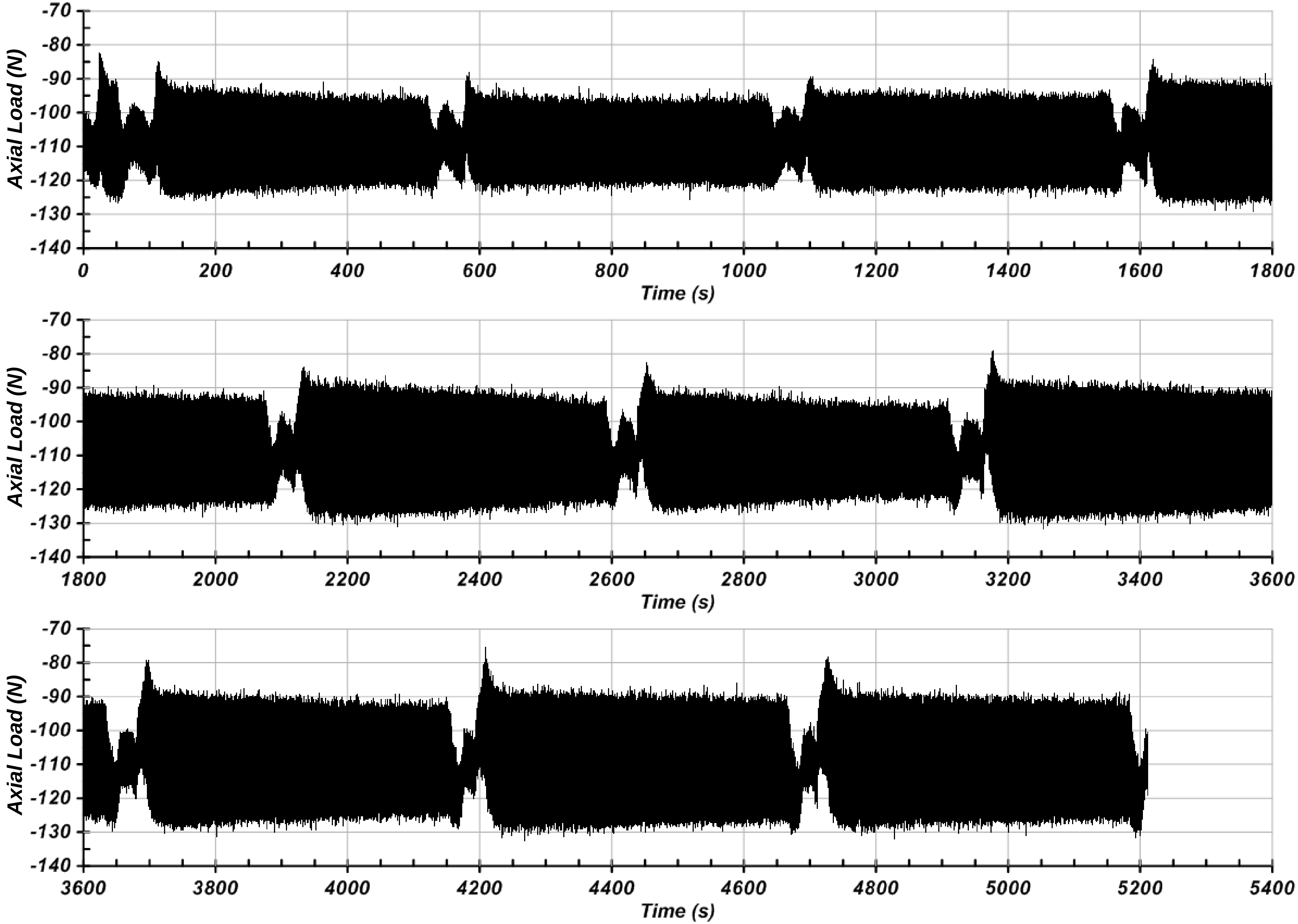

Axial Load vs. Time
Centrifuge Test 4-I (100,000 cycles at 23 Hz)

March 2016
B-23

engineers • scientists • innovators

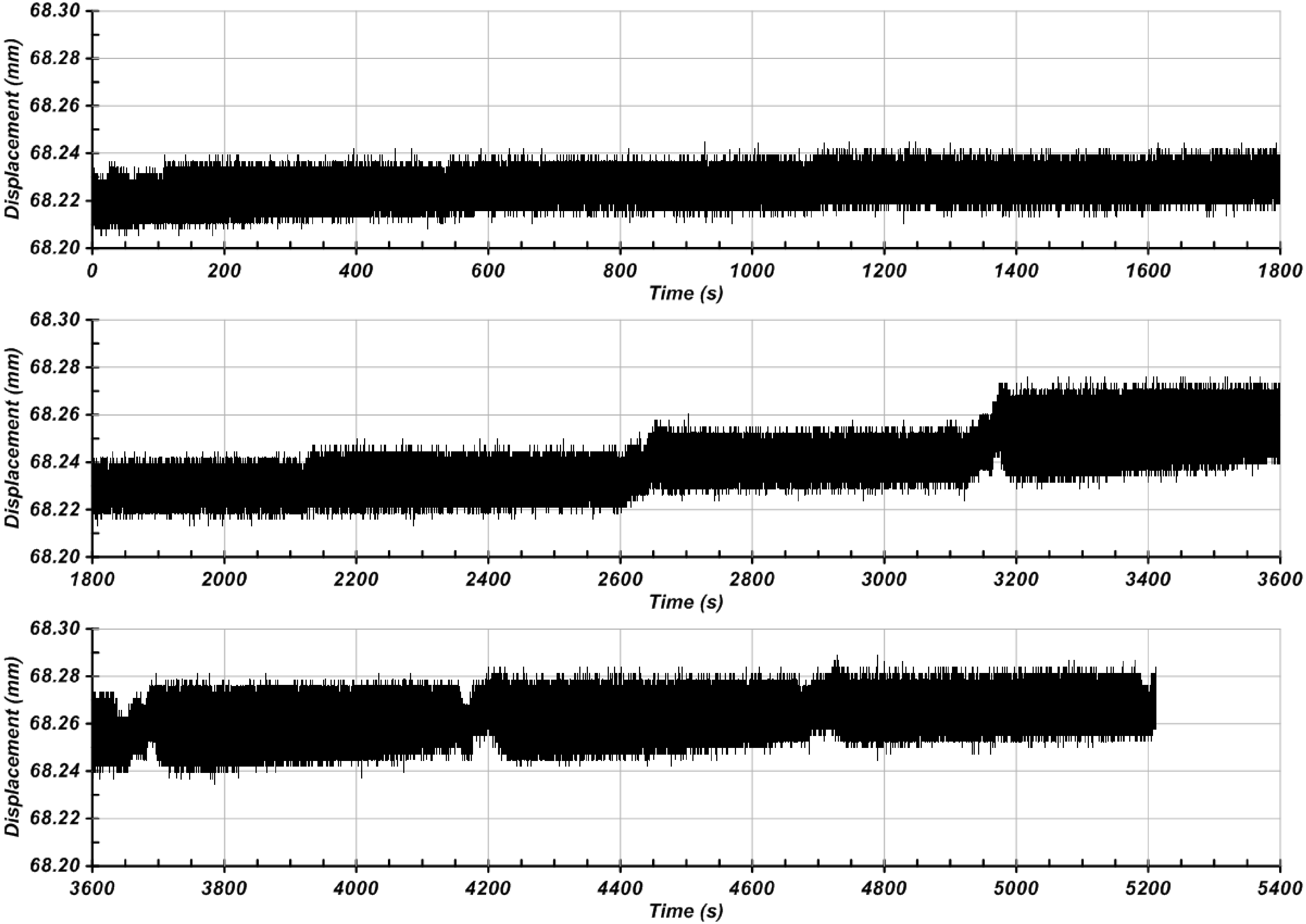

Displacement vs. Time
Centrifuge Test 4-I (100,000 cycles at 23 Hz)

March 2016

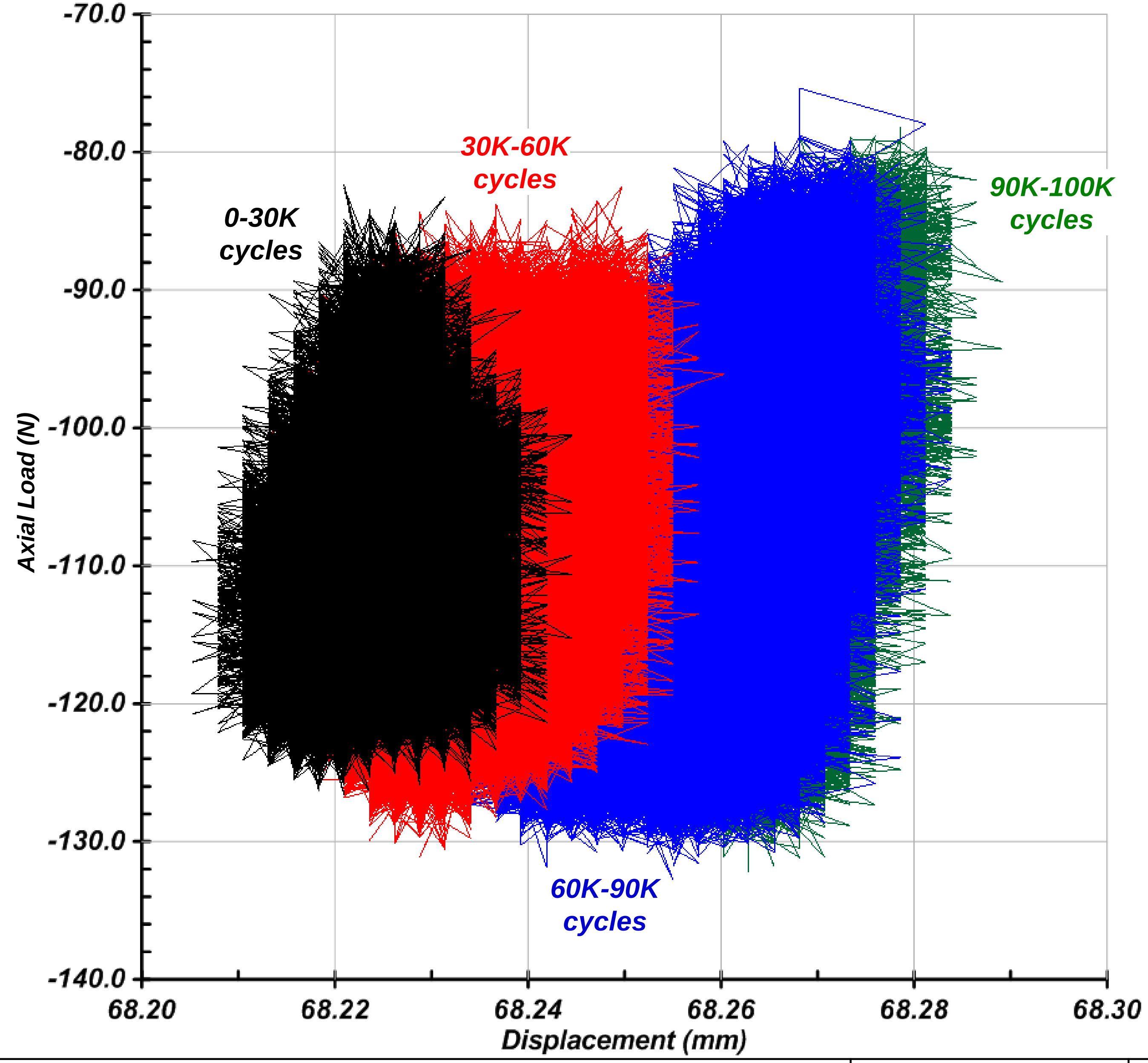

Axial Load vs. Displacement
Centrifuge Test 4-I (100,000 cycles at 23 Hz)

March 2016

MMI engineers • scientists • innovators

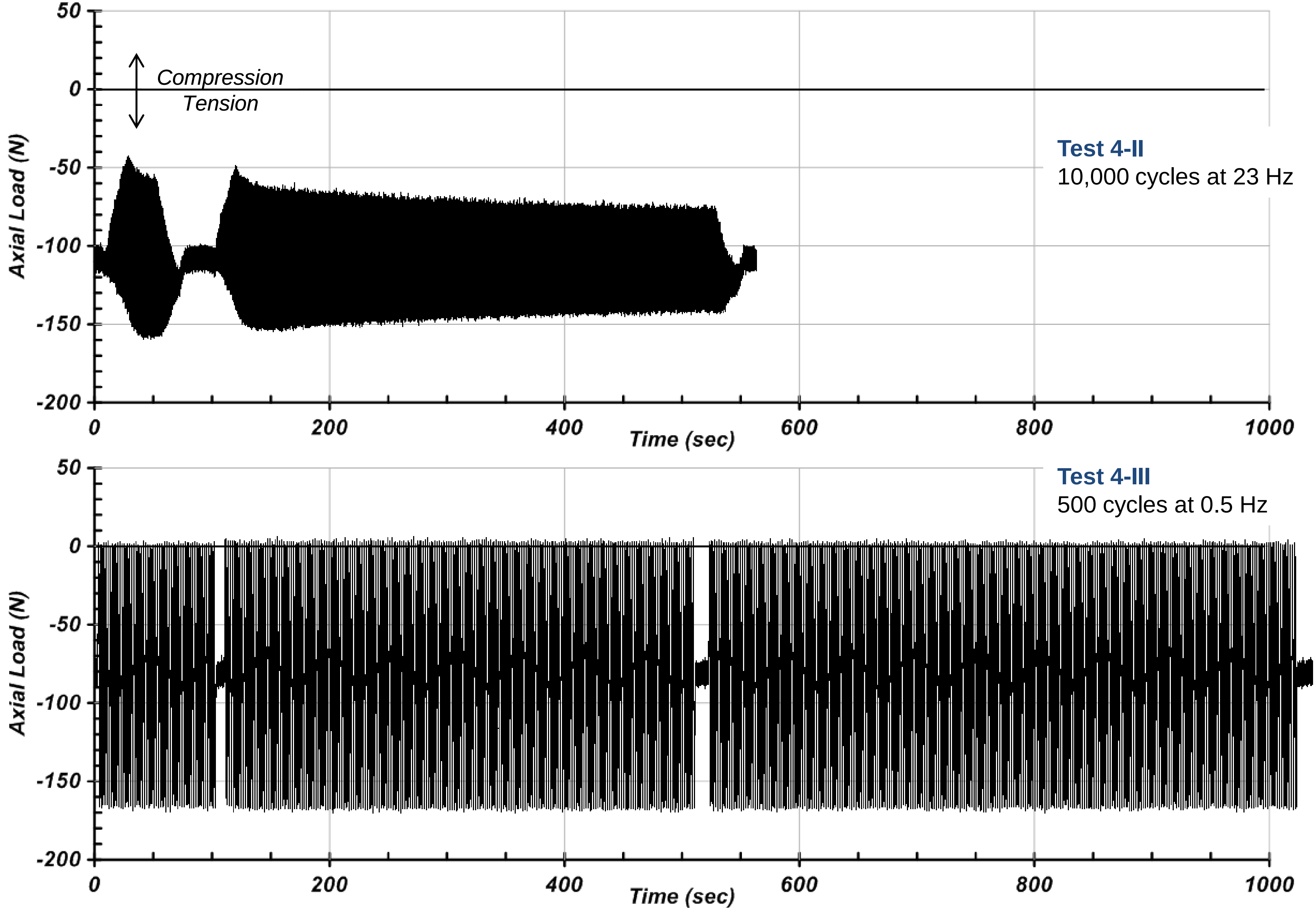

Axial Load vs. Time

Centrifuge Test 4-II (10,000 cycles at 23 Hz) and Test 4-III (500 cycles at 0.5 Hz)

March 2016

MMI engineers • scientists • innovators

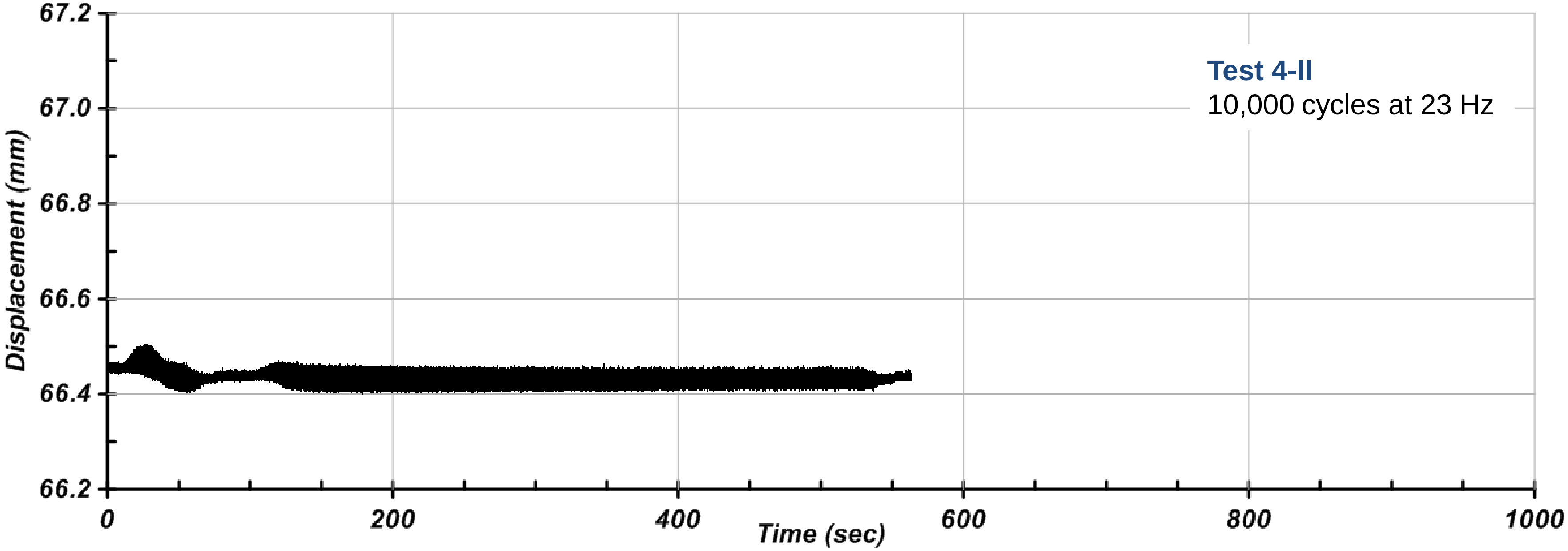

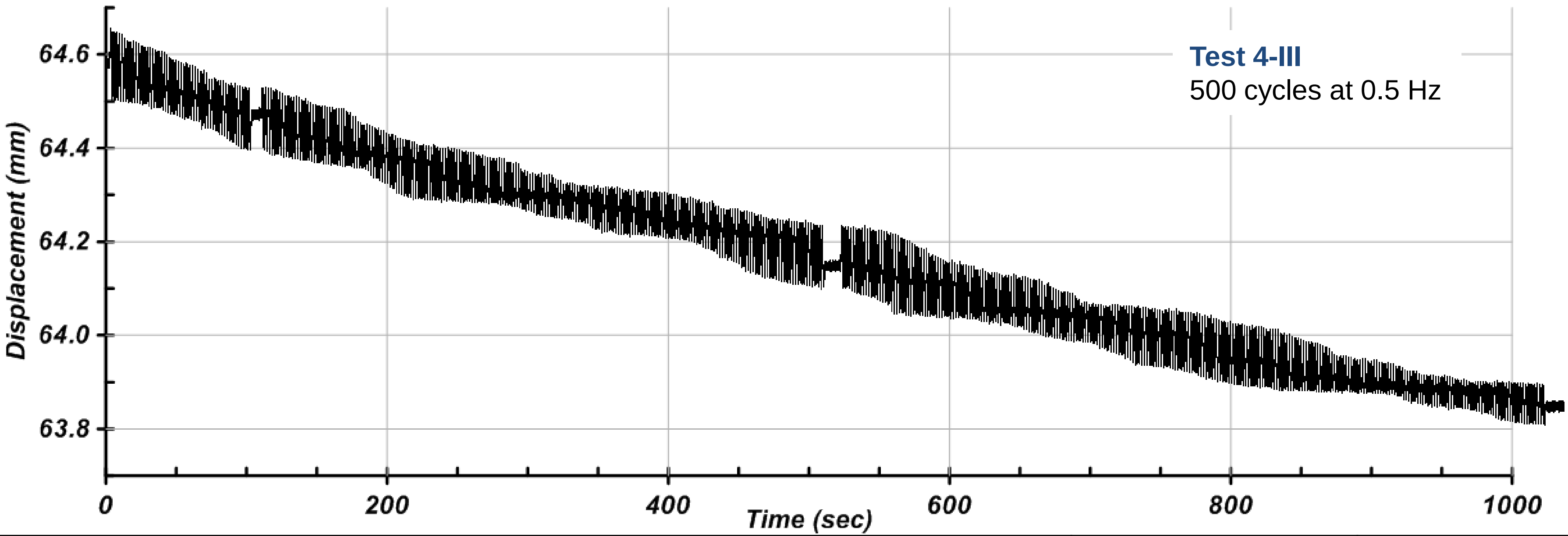

Displacement vs. Time **Centrifuge Test 4-II (10,000 cycles at 23 Hz) and Test 4-III (500 cycles at 0.5 Hz)**	**March 2016** B-27	MMI engineers • scientists • innovators

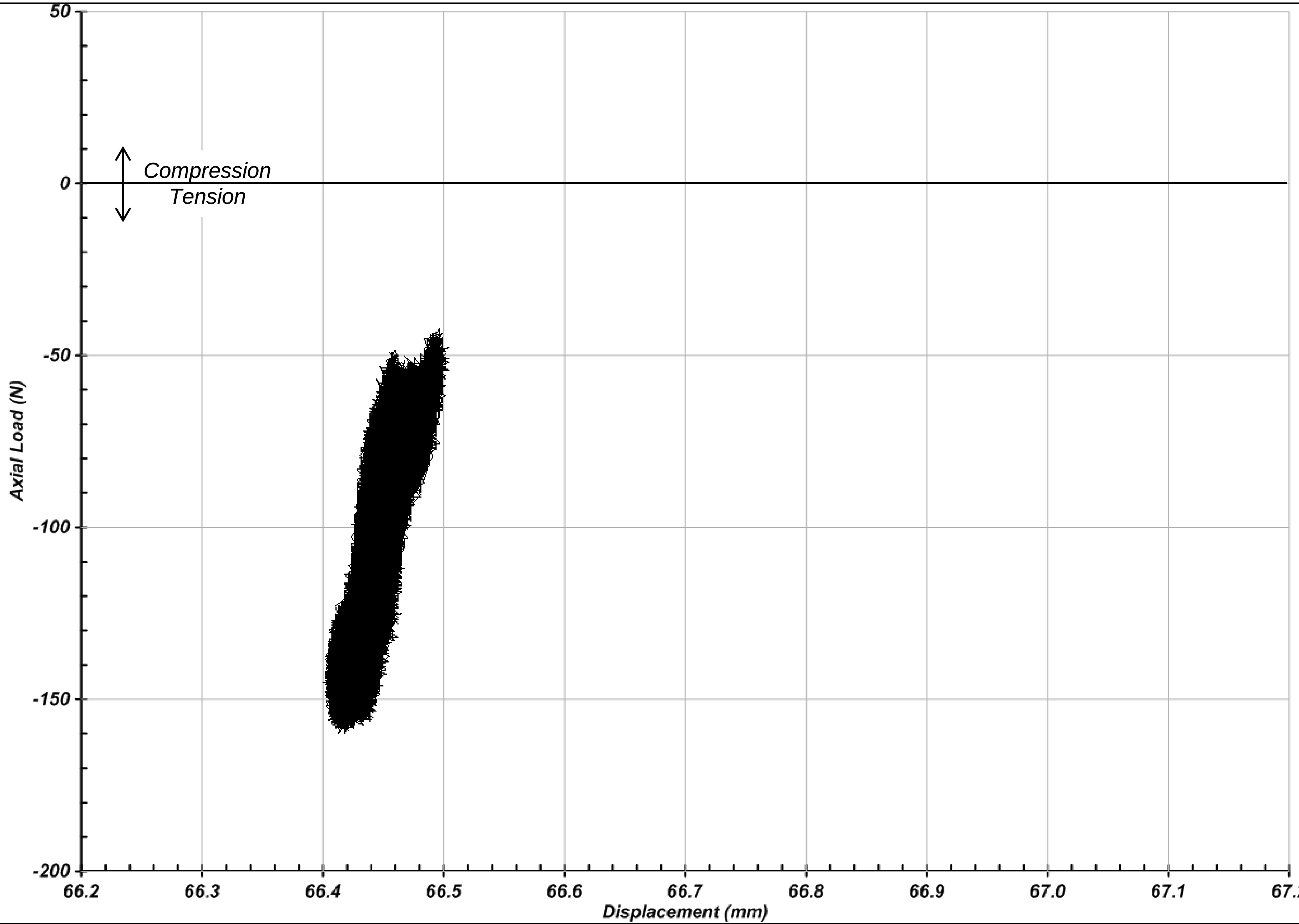

Axial Load vs. Displacement
Centrifuge Test 4-II (10,000 cycles at 23 Hz)

March 2016

engineers • scientists • innovators

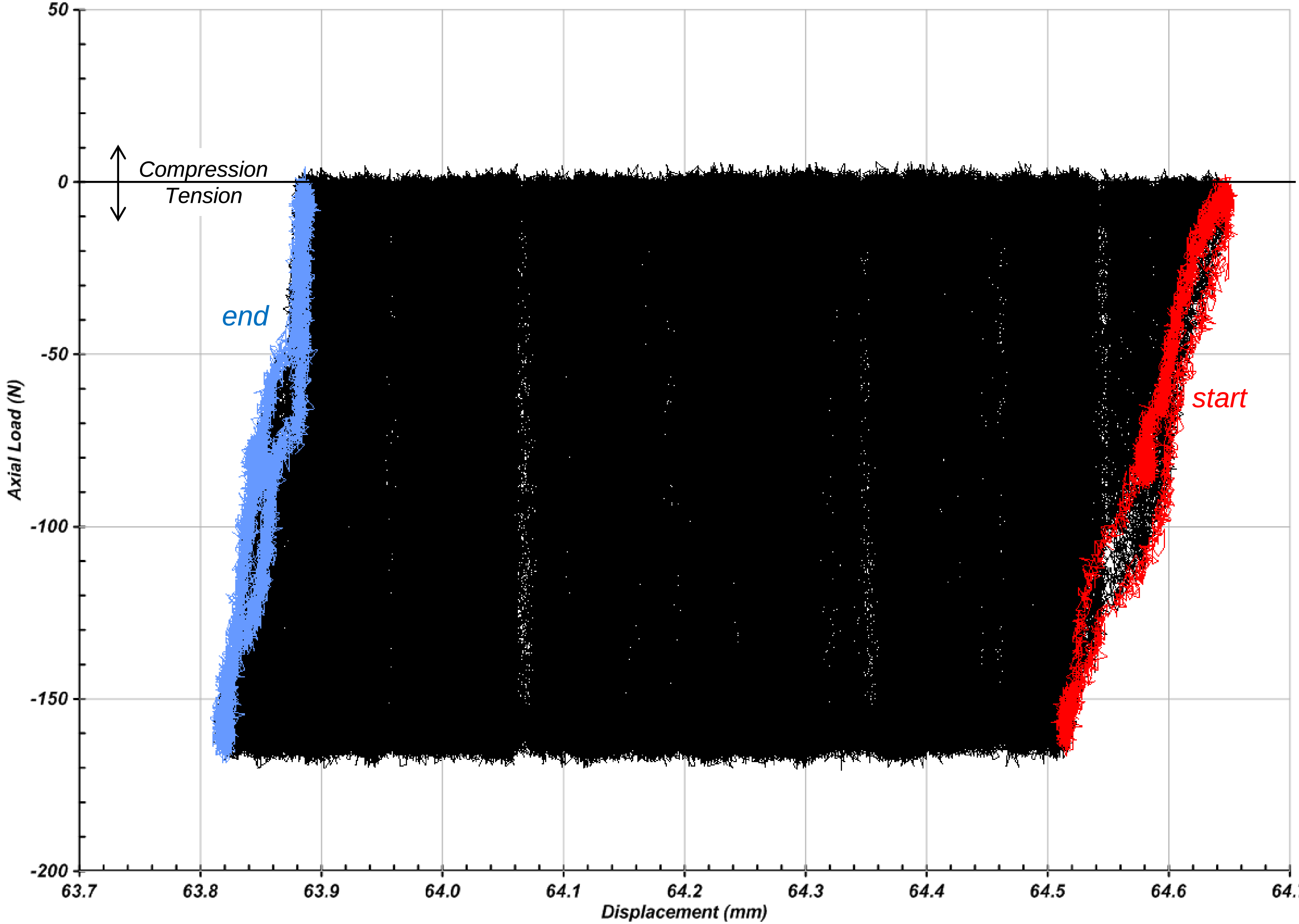

Axial Load vs. Displacement
Centrifuge Test 4-III (500 cycles at 0.5 Hz)

March 2016

engineers • scientists • innovators

CENTRIFUGE TEST 5

Load Packet	N_{cyc} =1000 cycles	Frequency	Q_S/Q_T	Q_{cyc}/Q_T	Static Load (N)	Cyclic Load (N)	Pre Tensile Capacity (N)	Post Tensile Capacity (N)	Residual Pullout (mm)	Residual Pullout Rate (RPR) (mm/N_{cyc})
5-IA	10,000	23 Hz	0.14	0.08	55	31	320 (400*)	(400*)	-0.001	-0.0001
5-IB	500	0.5 Hz	0.14	0.07	55	27	(400*)	340	-0.001	-0.002
5-II	500	0.5 Hz	0.16	0.23	56	78	340	375	0.20	0.4
5-III	50	0.5 Hz	0.29	0.21	107	79	375	200	54	54

**Assumed value since 2mm displacement for pullout test was insufficient to fully mobilize pile capacity and no pullout test was performed between Test 5-1A and 5-1B.*

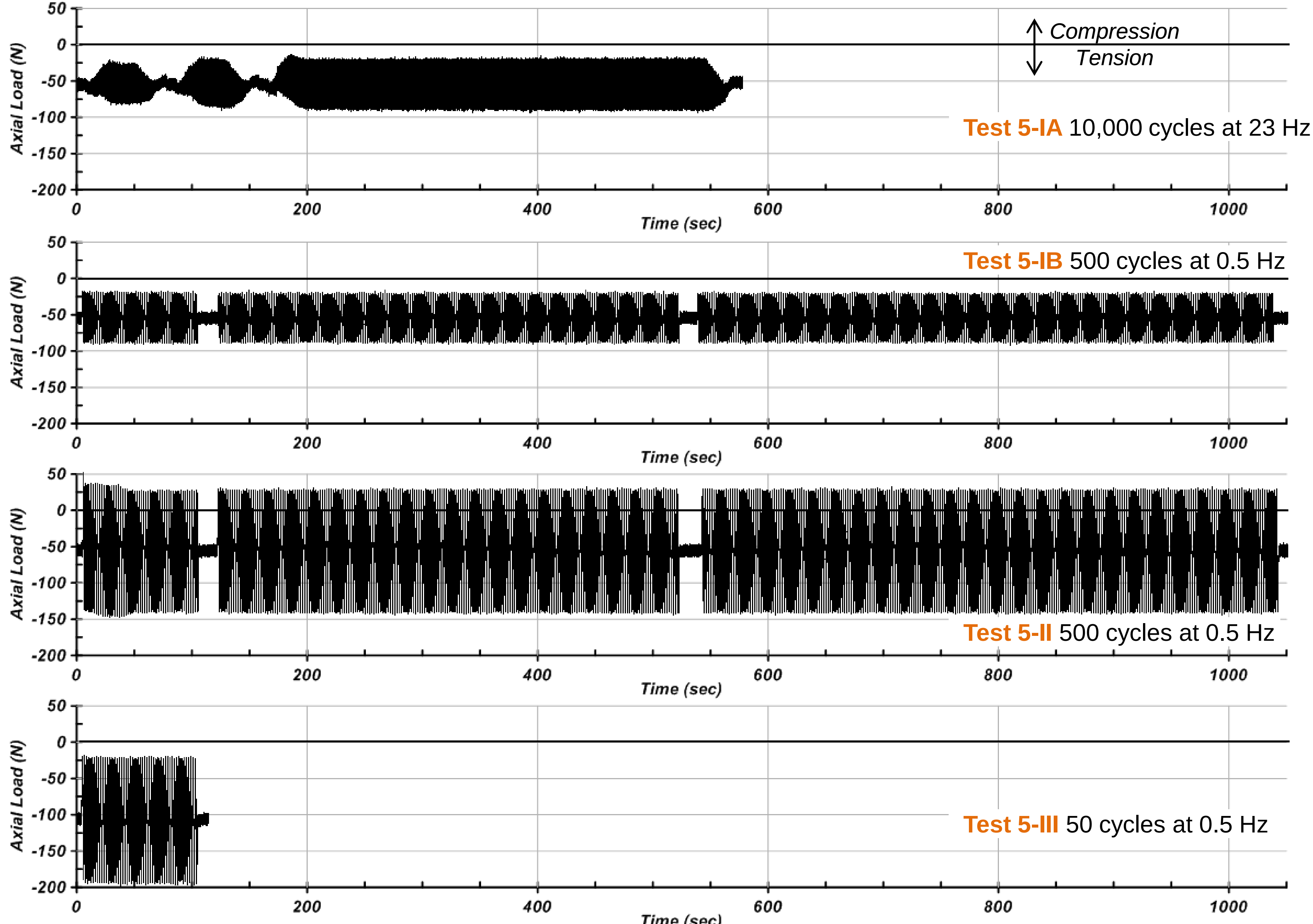

Axial Load vs. Time
Centrifuge Test 5

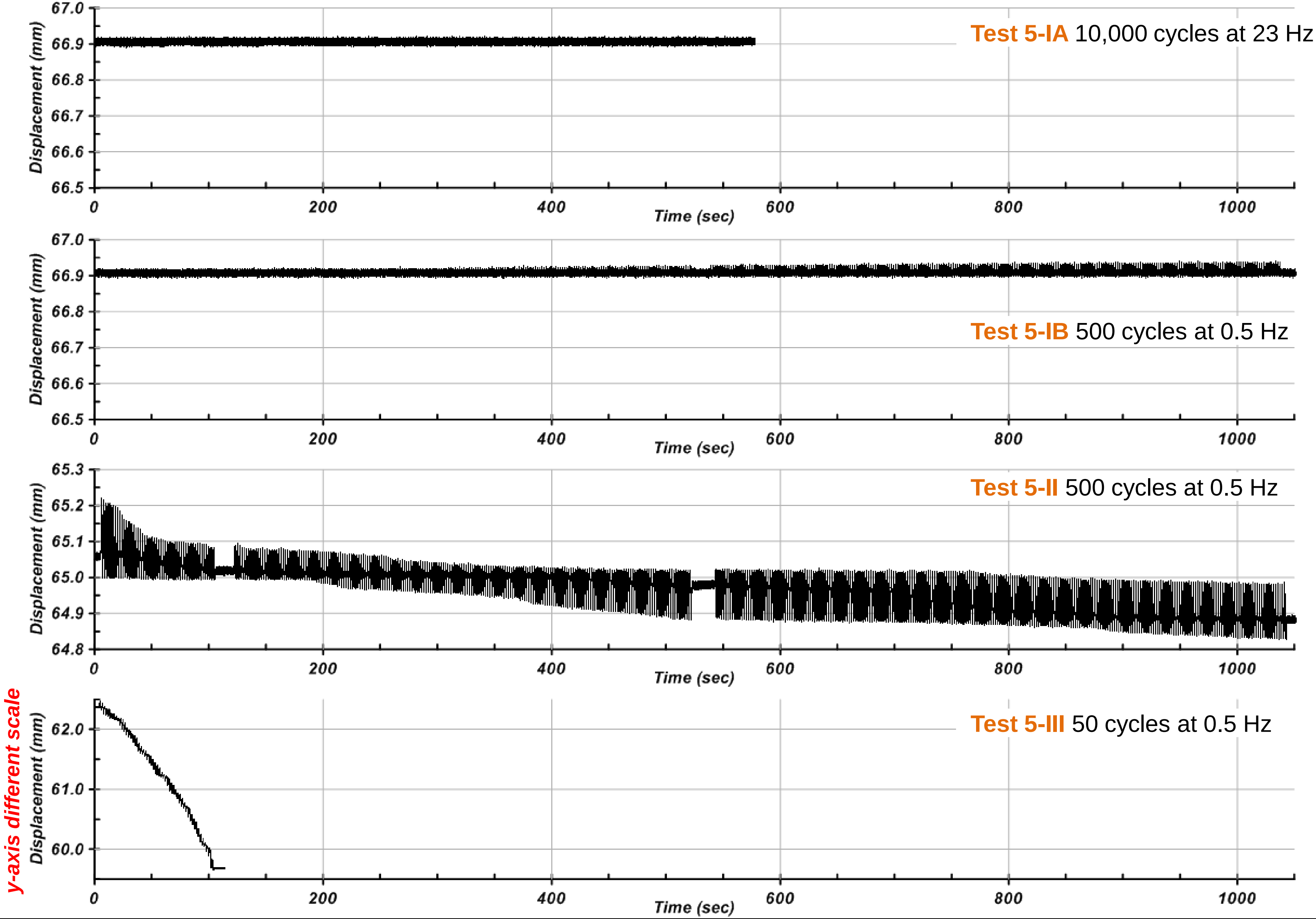

Displacement vs. Time
Centrifuge Test 5

March 2016

Test 5-IA
10,000 cycles
at 23 Hz

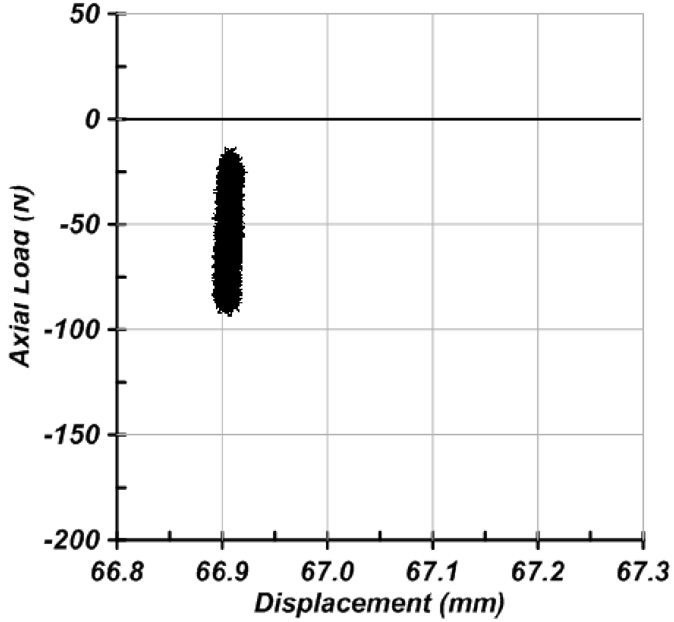

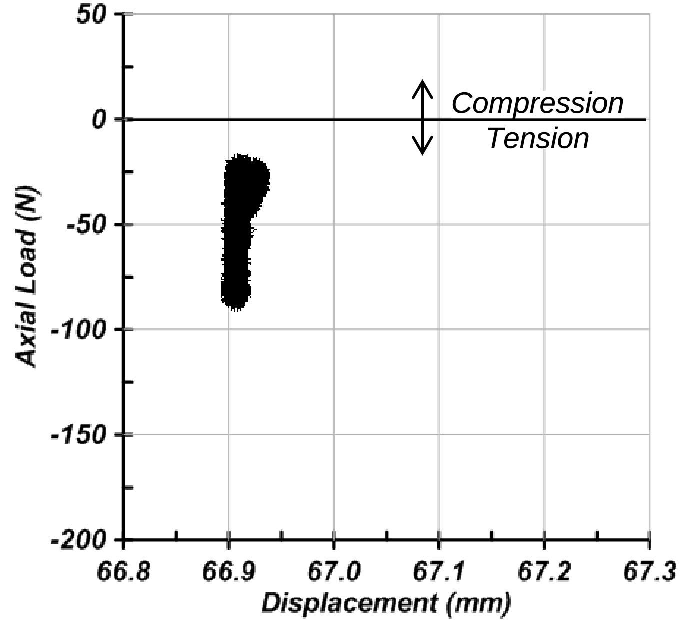

Test 5-IB
500 cycles
at 0.5 Hz

Test 5-II
500 cycles
at 0.5 Hz

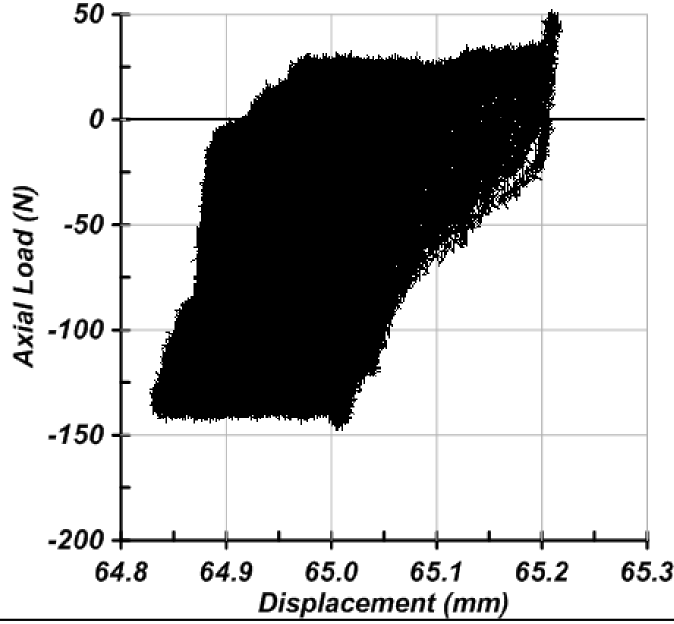

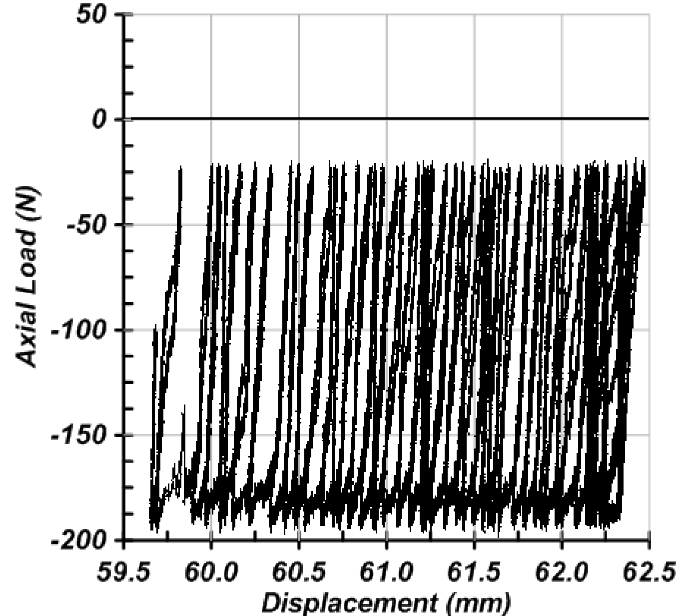

Test 5-III
50 cycles
at 0.5 Hz

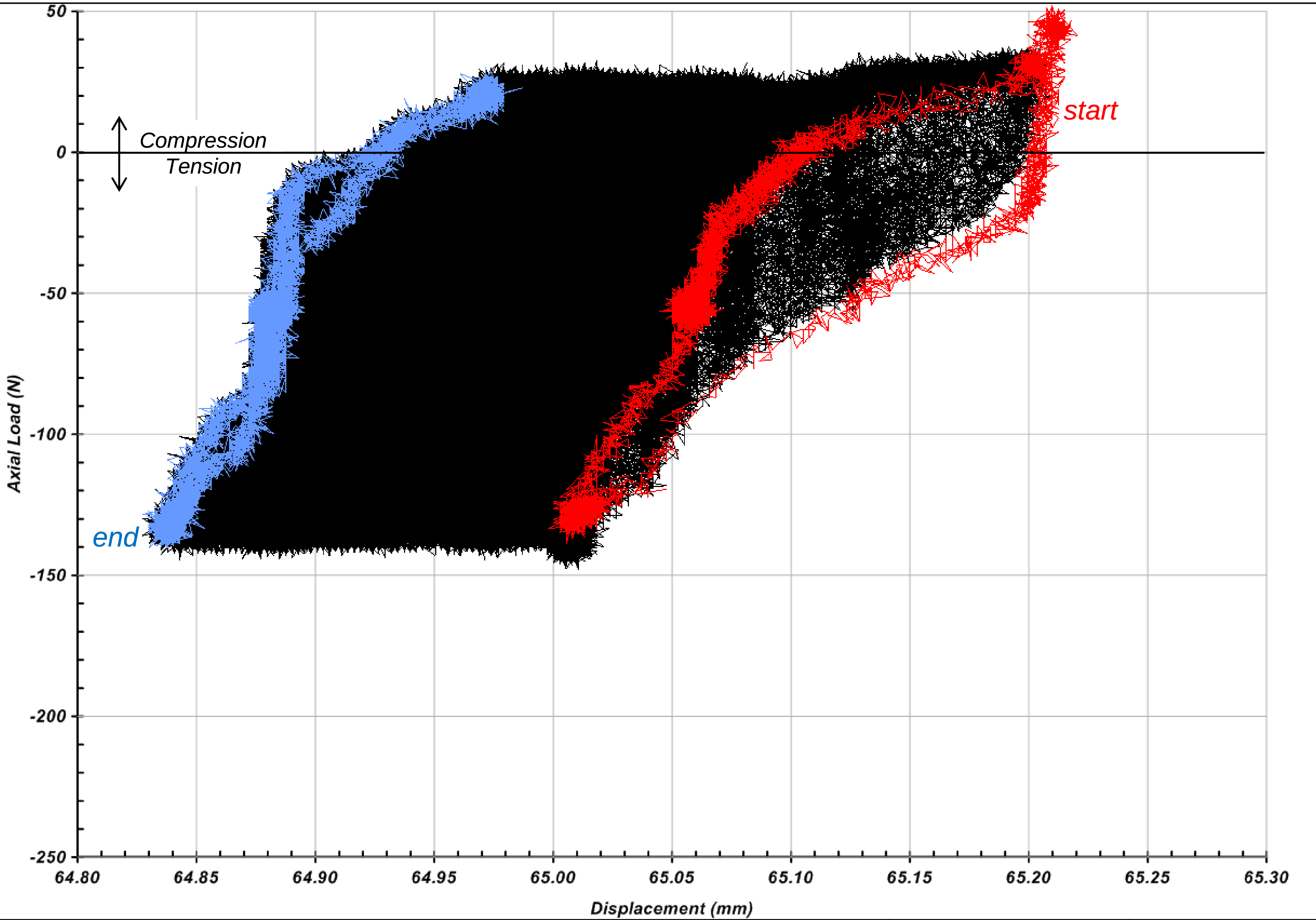

Axial Load vs. Displacement
Centrifuge Test 5-II

March 2016
B-34

engineers • scientists • innovators

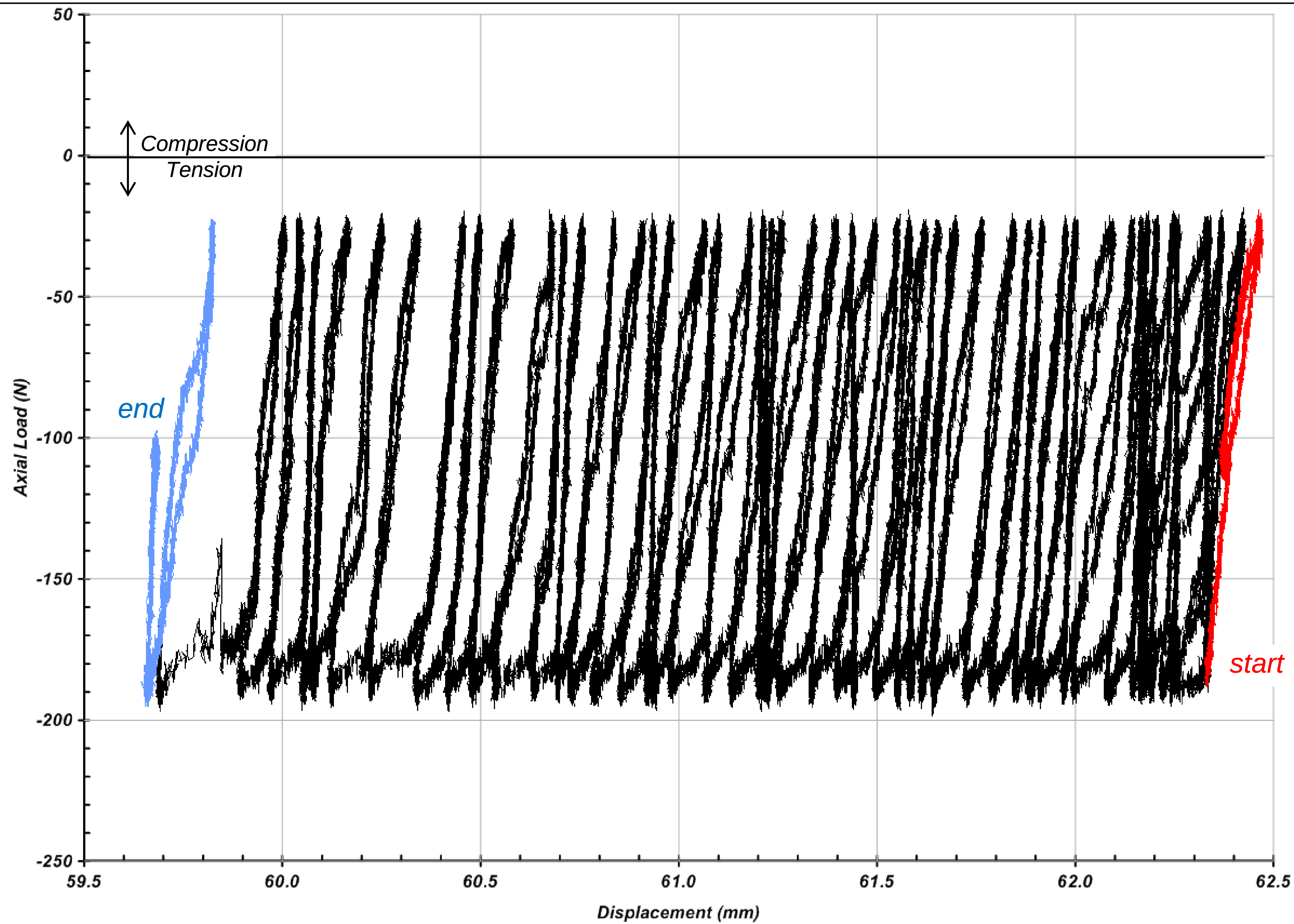

Axial Load vs. Displacement
Centrifuge Test 5-III

March 2016

MMI engineers • scientists • innovators

APPENDIX C: CYCLIC LOAD TIME HISTORIES

CENTRIFUGE TEST 2B

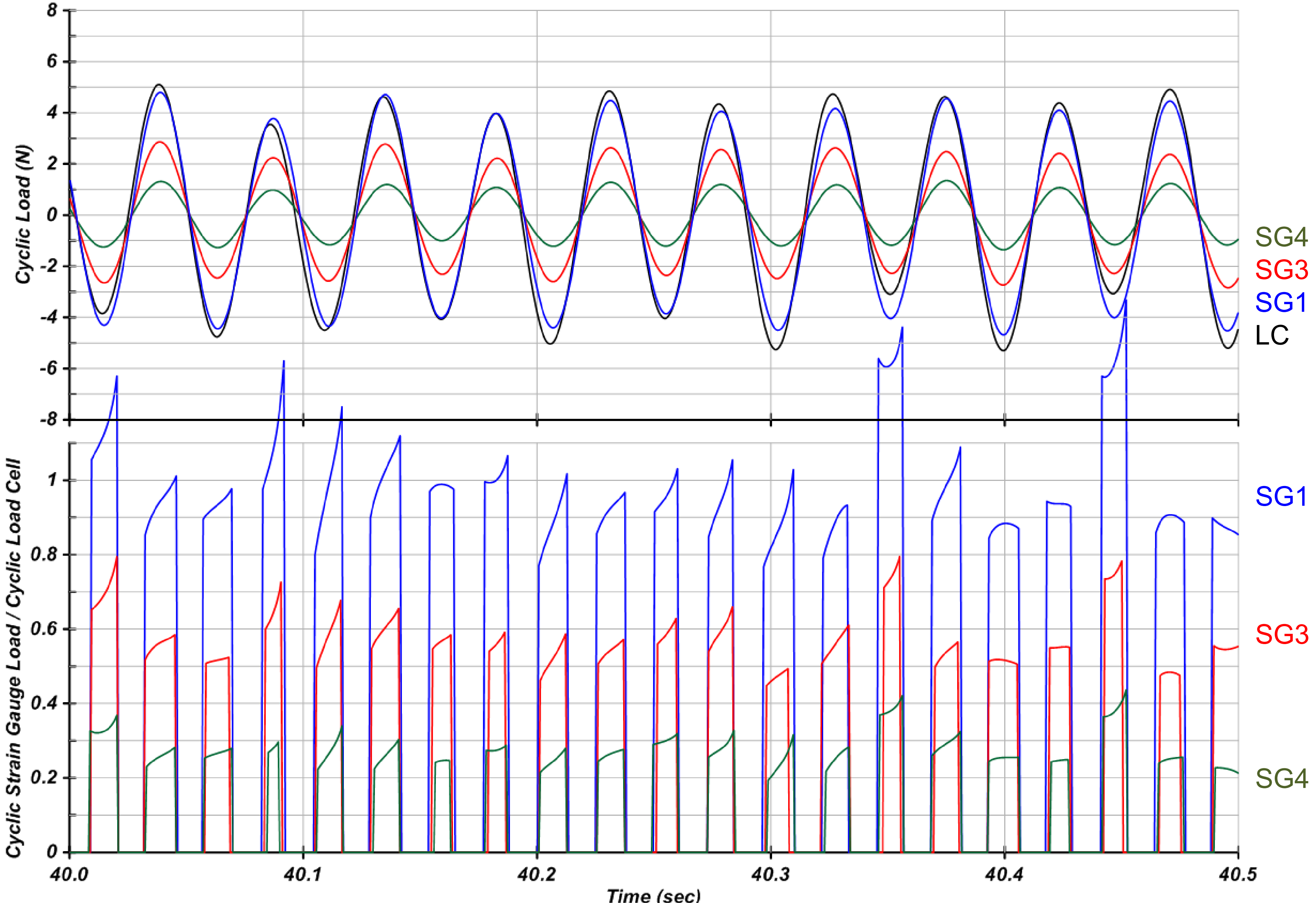

Cyclic Load Time Histories from Strain Gauges and Load Cell
Centrifuge Test 2B-I

upper 40% threshold

March 2016

C-3

MMI engineers • scientists • innovators

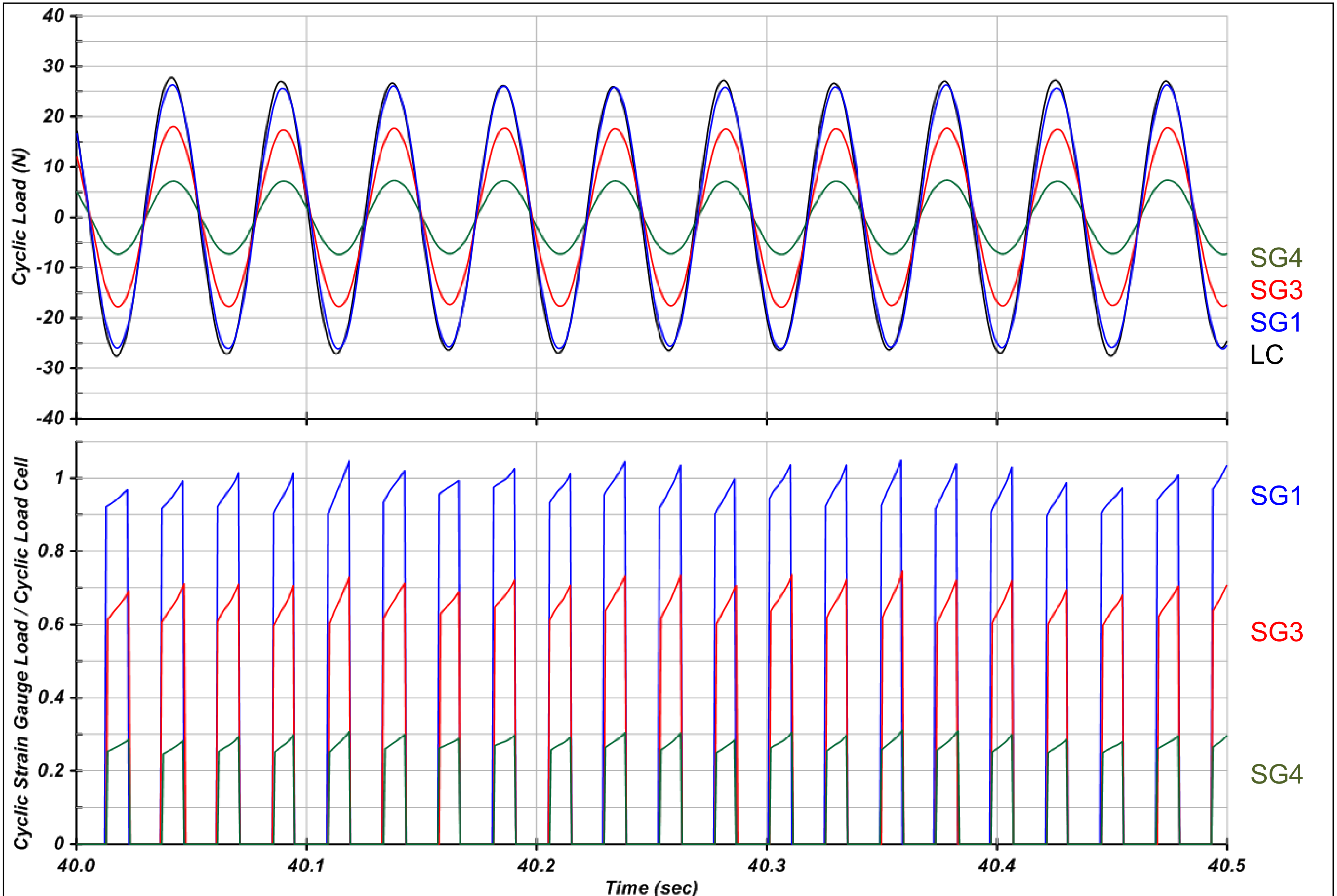

Cyclic Load Time Histories from Strain Gauges and Load Cell
Centrifuge Test 2B-IIA

upper 20% threshold

March 2016
C-4

MMI engineers • scientists • innovators

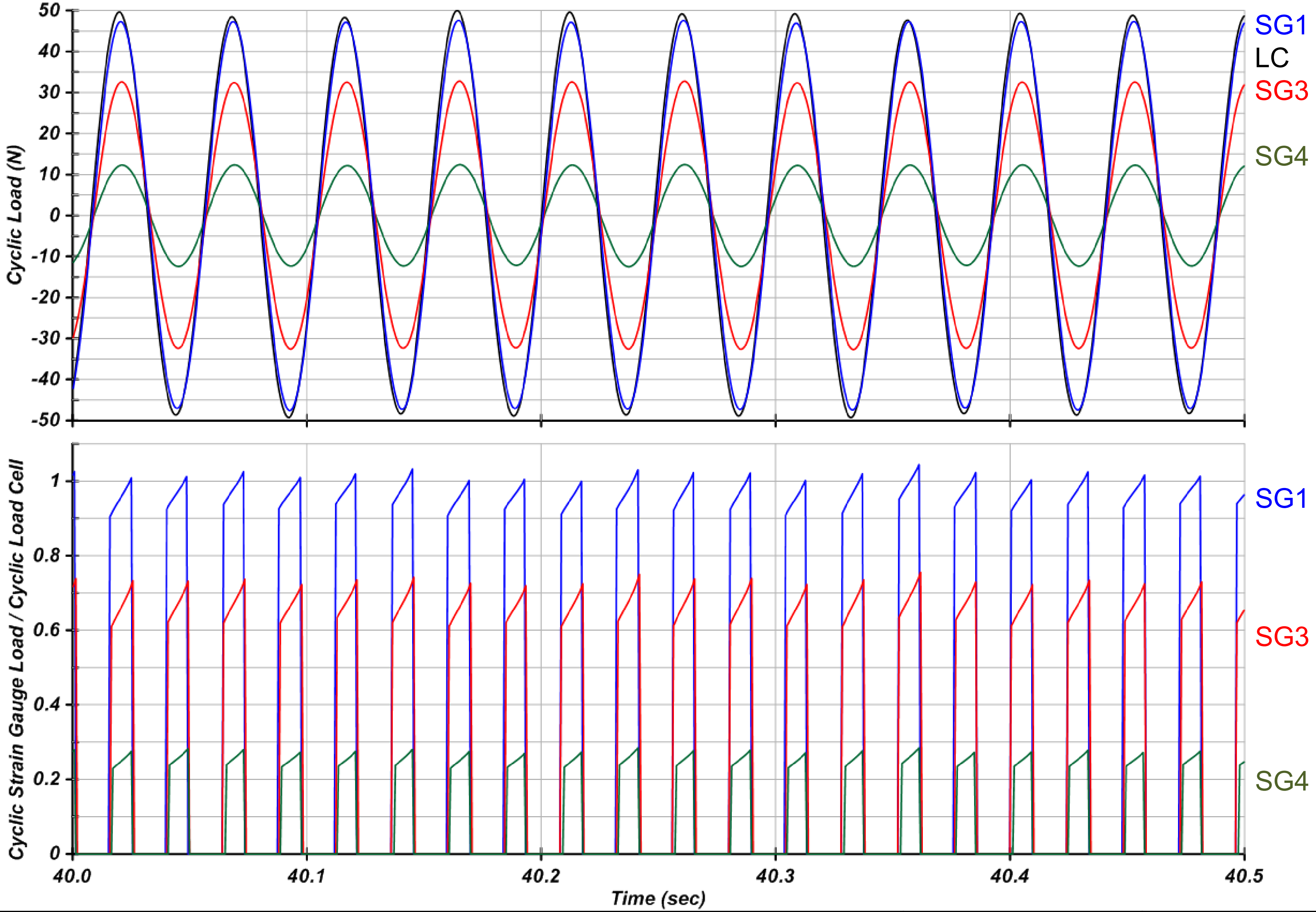

Cyclic Load Time Histories from Strain Gauges and Load Cell **Centrifuge Test 2B-IIB** *upper 20% threshold*	**March 2016** C-5	MMI engineers • scientists • innovators

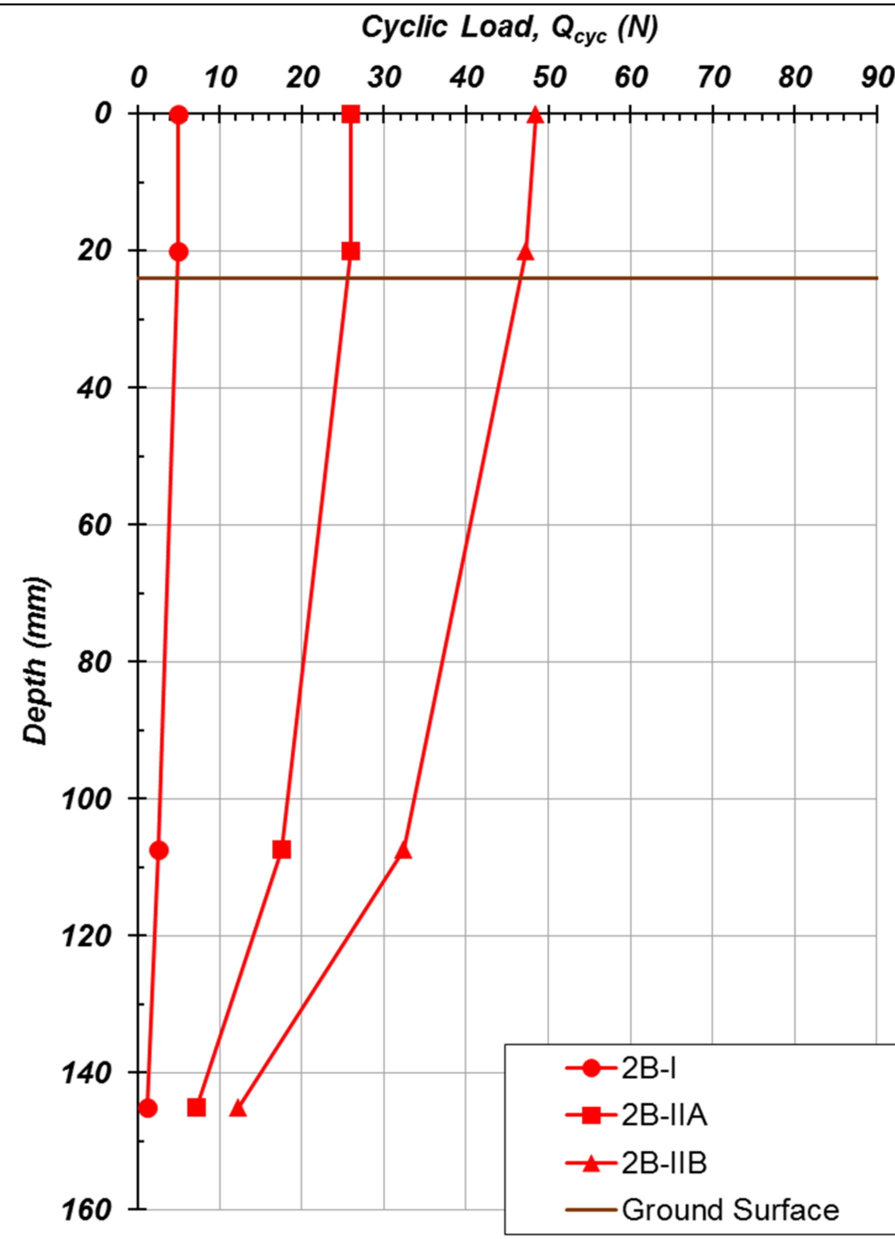

Cyclic Load from Strain Gauges with Depth
Centrifuge Test 2B

March 2016
C-6

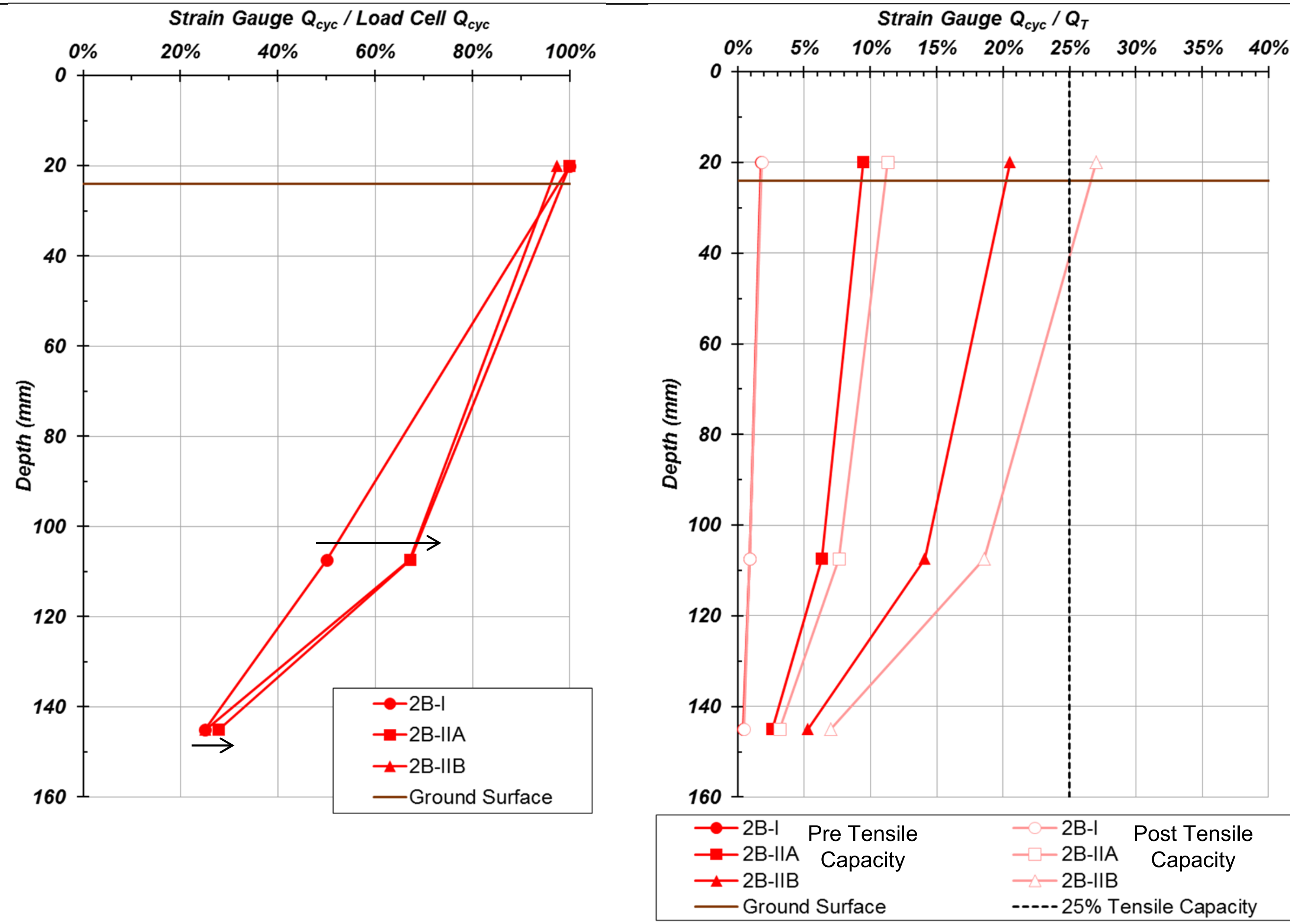

Normalized Cyclic Load from Strain Gauges with Depth

Centrifuge Test 2B

March 2016

C-7

MMI engineers • scientists • innovators

CENTRIFUGE TEST 3

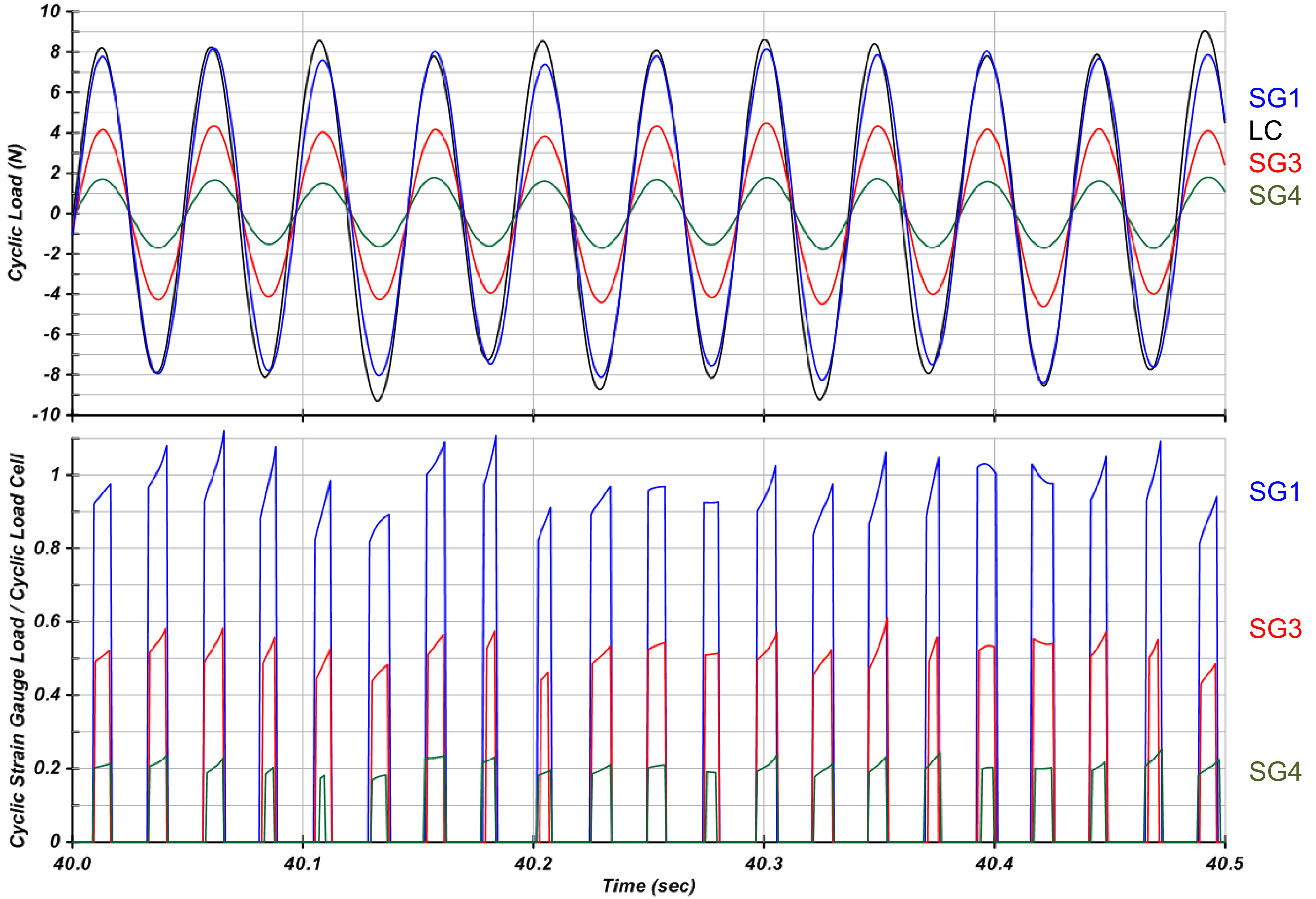

Cyclic Load Time Histories from Strain Gauges and Load Cell
Centrifuge Test 3-I

upper 20% threshold

March 2016
C-9

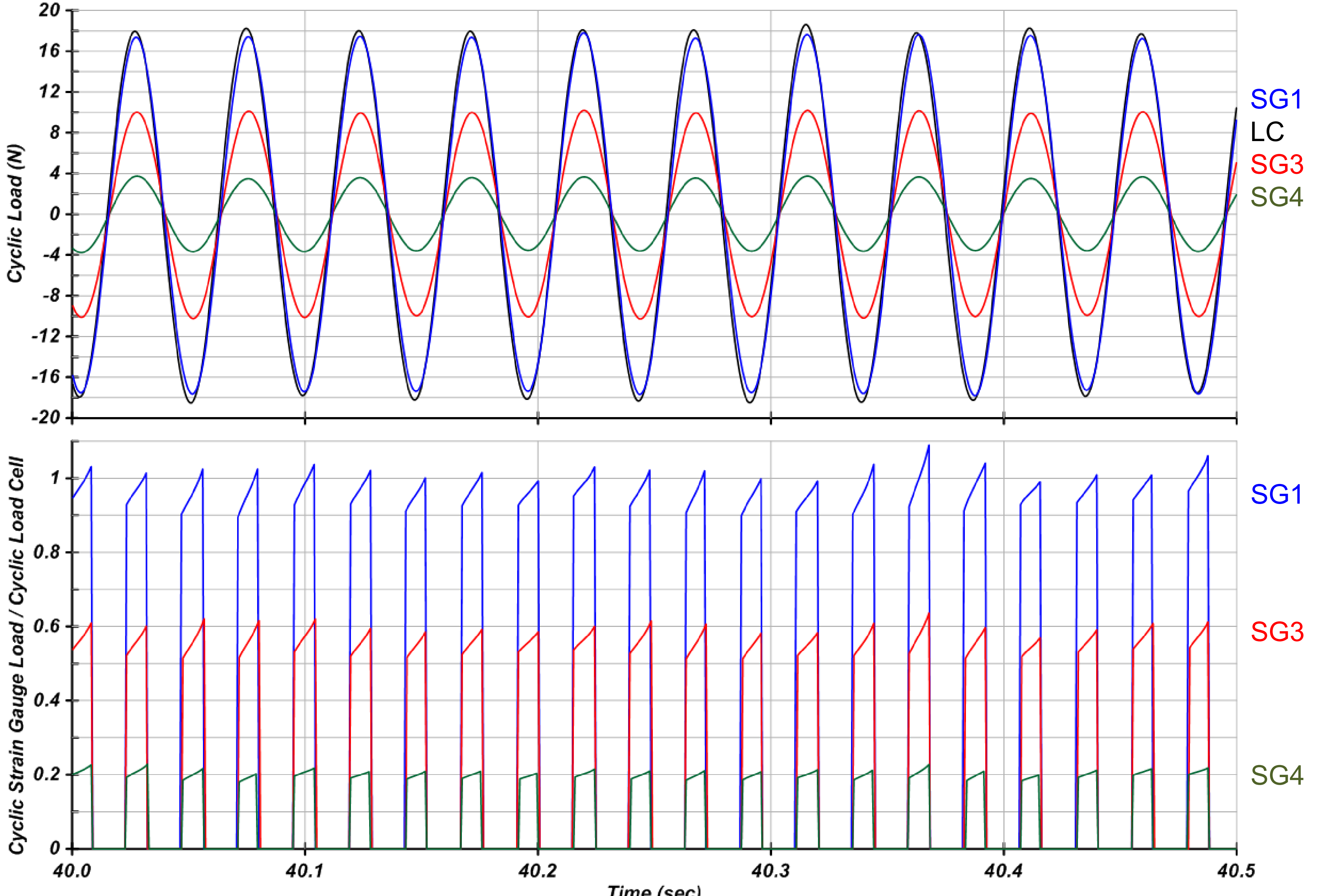

Cyclic Load Time Histories from Strain Gauges and Load Cell
Centrifuge Test 3-II

upper 20% threshold

March 2016

C-10

MMI
engineers • scientists • innovators

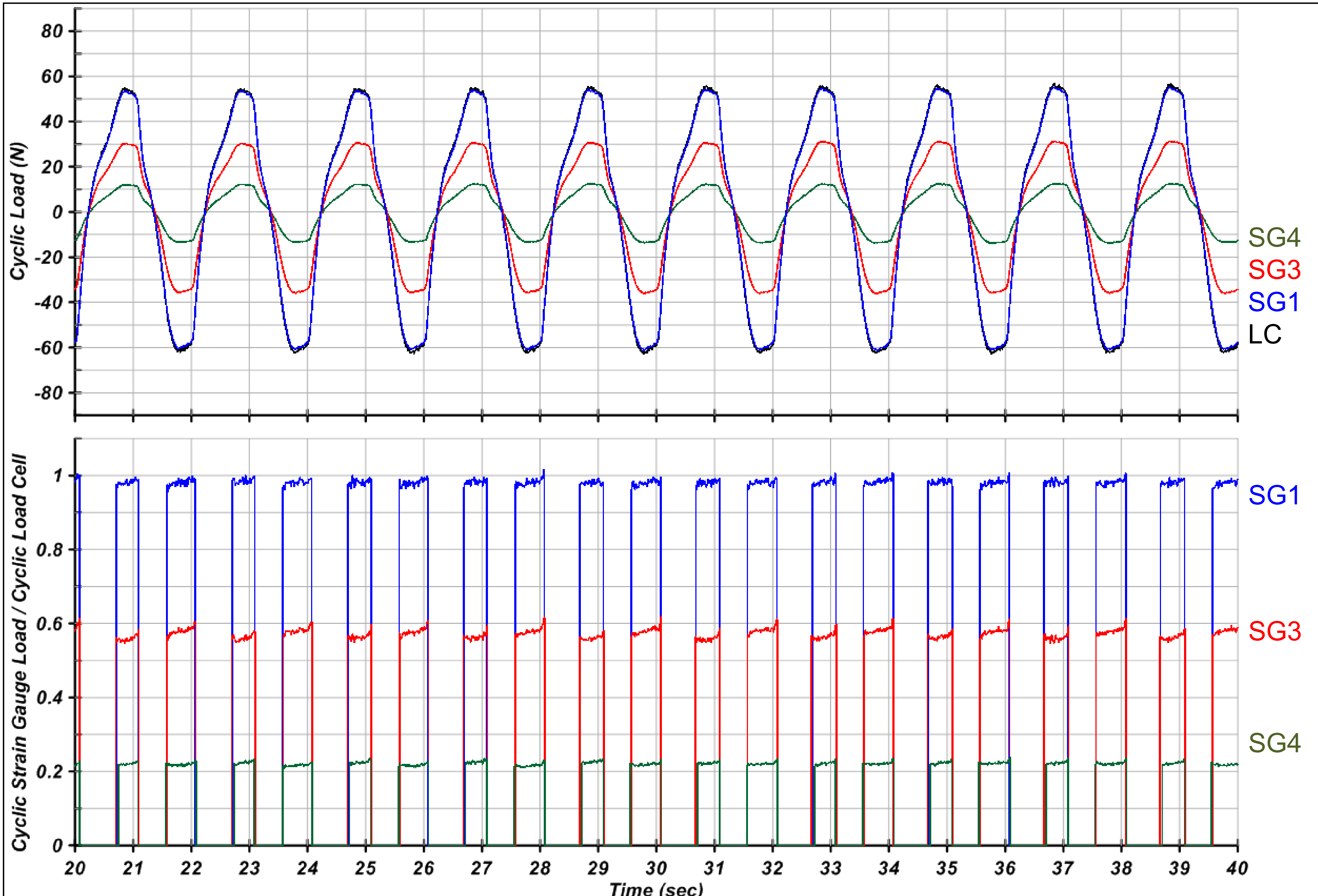

Cyclic Load Time Histories from Strain Gauges and Load Cell
Centrifuge Test 3-III

upper 40% threshold

March 2016

C-11

MMI
engineers • scientists • innovators

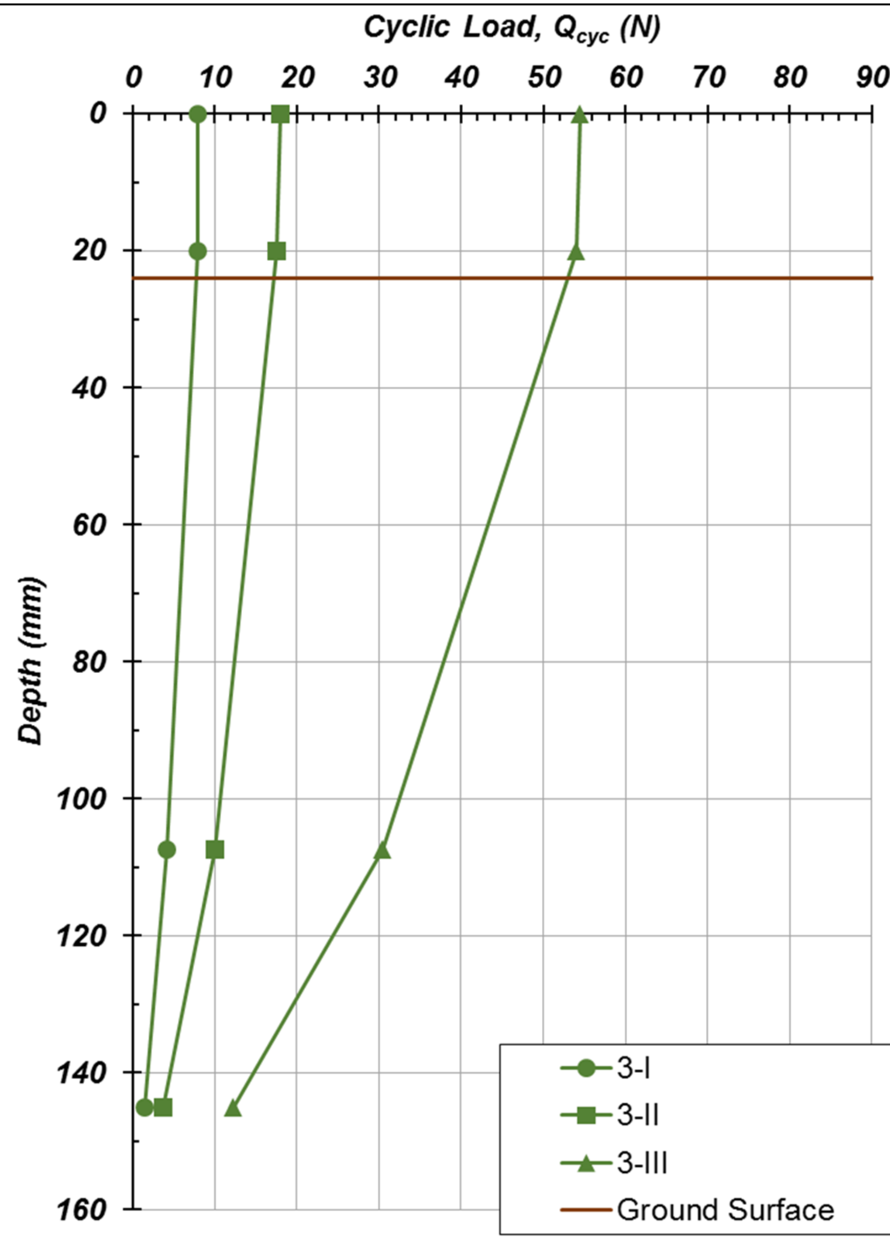

Cyclic Load from Strain Gauges with Depth
Centrifuge Test 3

March 2016
C-12

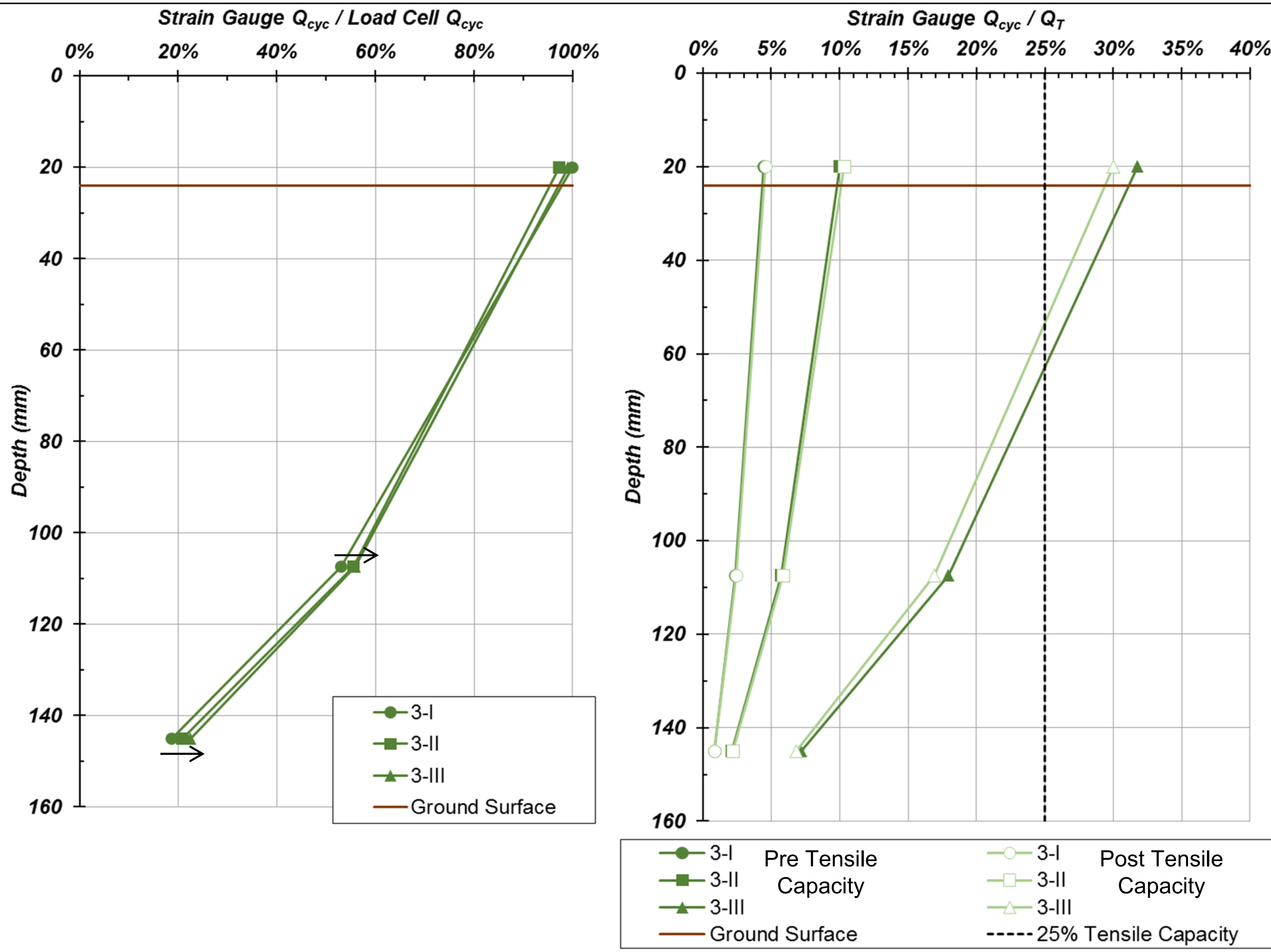

Normalized Cyclic Load from Strain Gauges with Depth

Centrifuge Test 3

March 2016

C-13

MMI engineers • scientists • innovators

CENTRIFUGE TEST 4

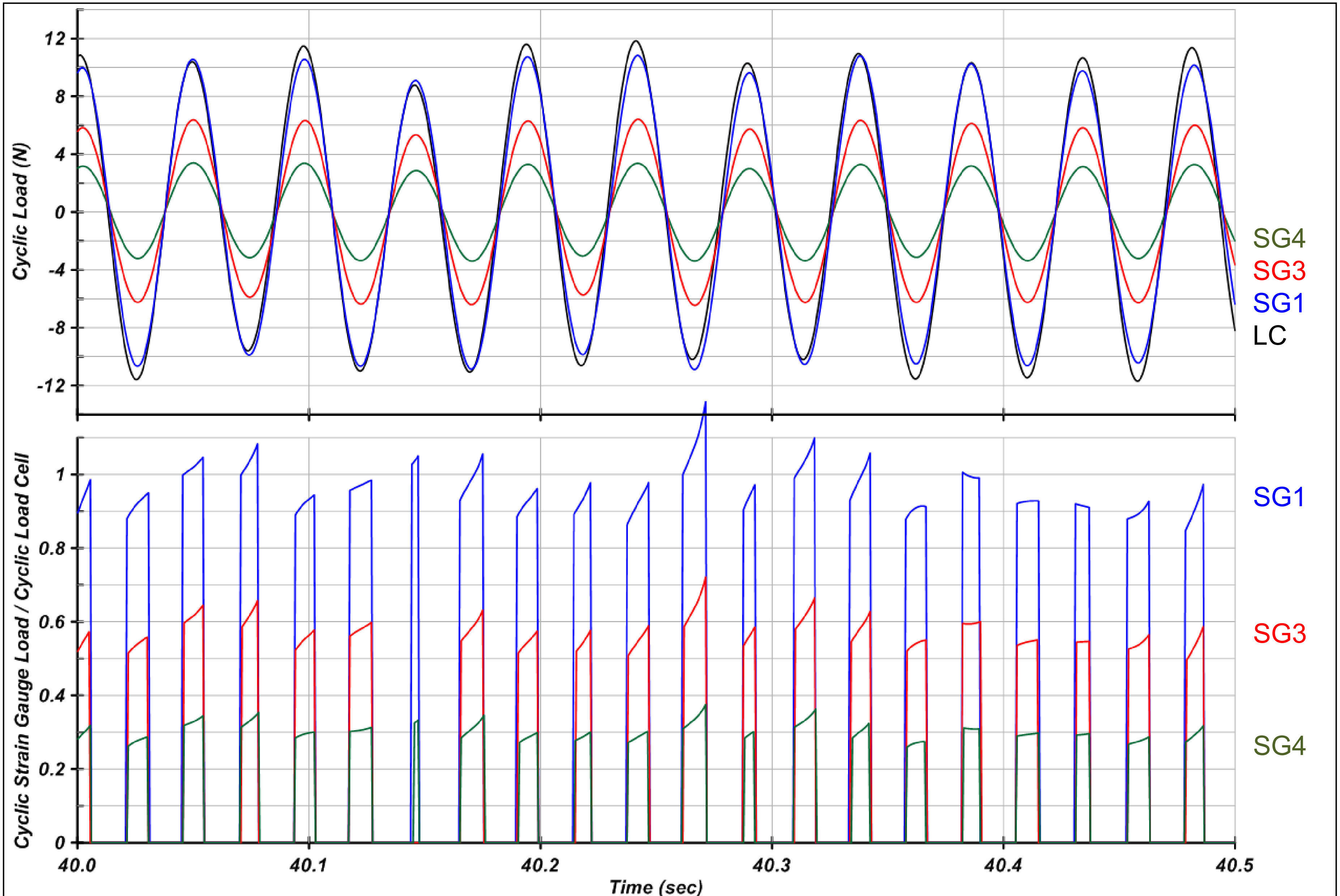

Cyclic Load Time Histories from Strain Gauges and Load Cell
Centrifuge Test 4-I

upper 30% threshold

March 2016

C-15

MMI
engineers • scientists • innovators

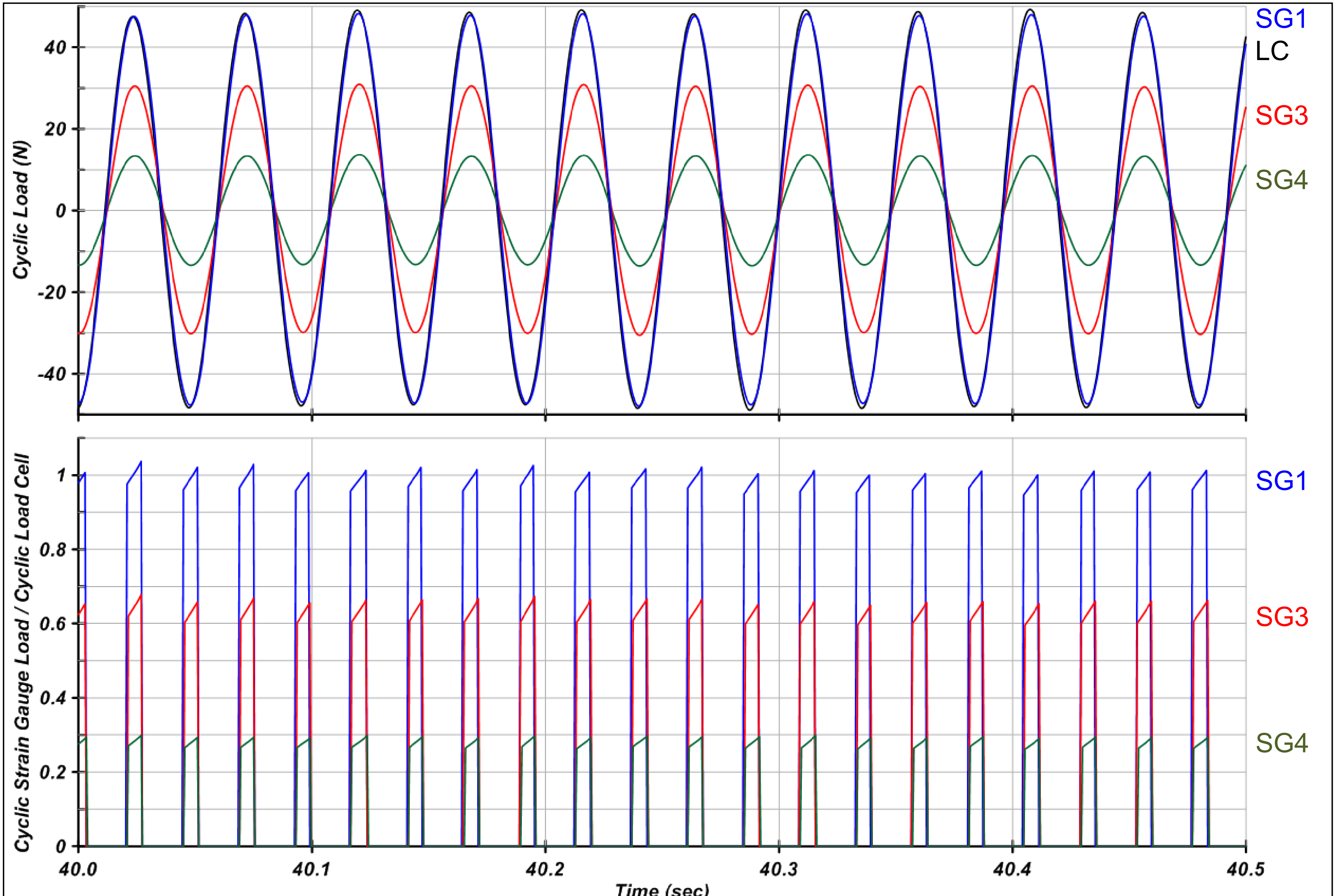

Cyclic Load Time Histories from Strain Gauges and Load Cell
Centrifuge Test 4-II

upper 10% threshold

March 2016

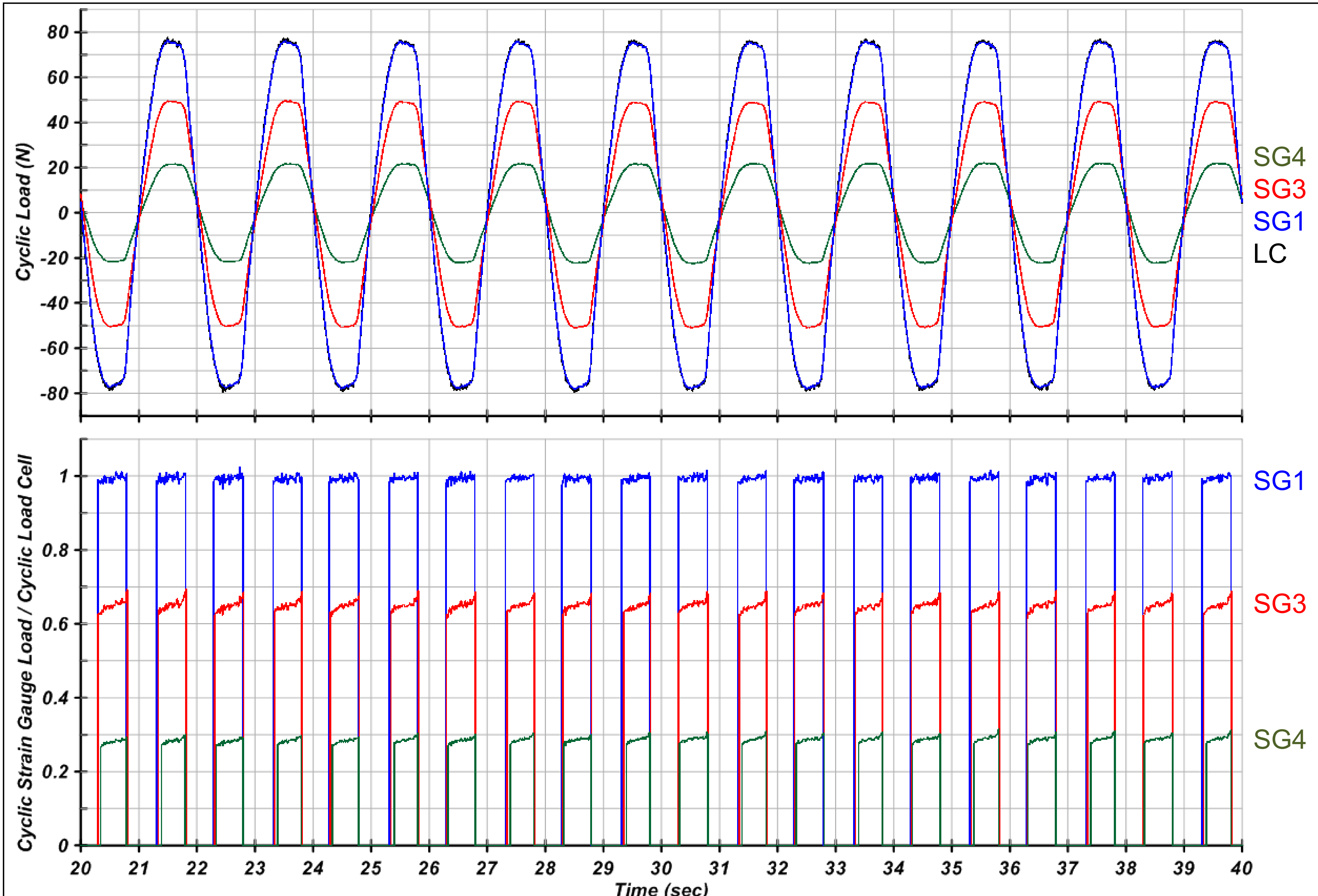

Cyclic Load Time Histories from Strain Gauges and Load Cell
Centrifuge Test 4-III

upper 20% threshold

March 2016

C-17

MMI
engineers • scientists • innovators

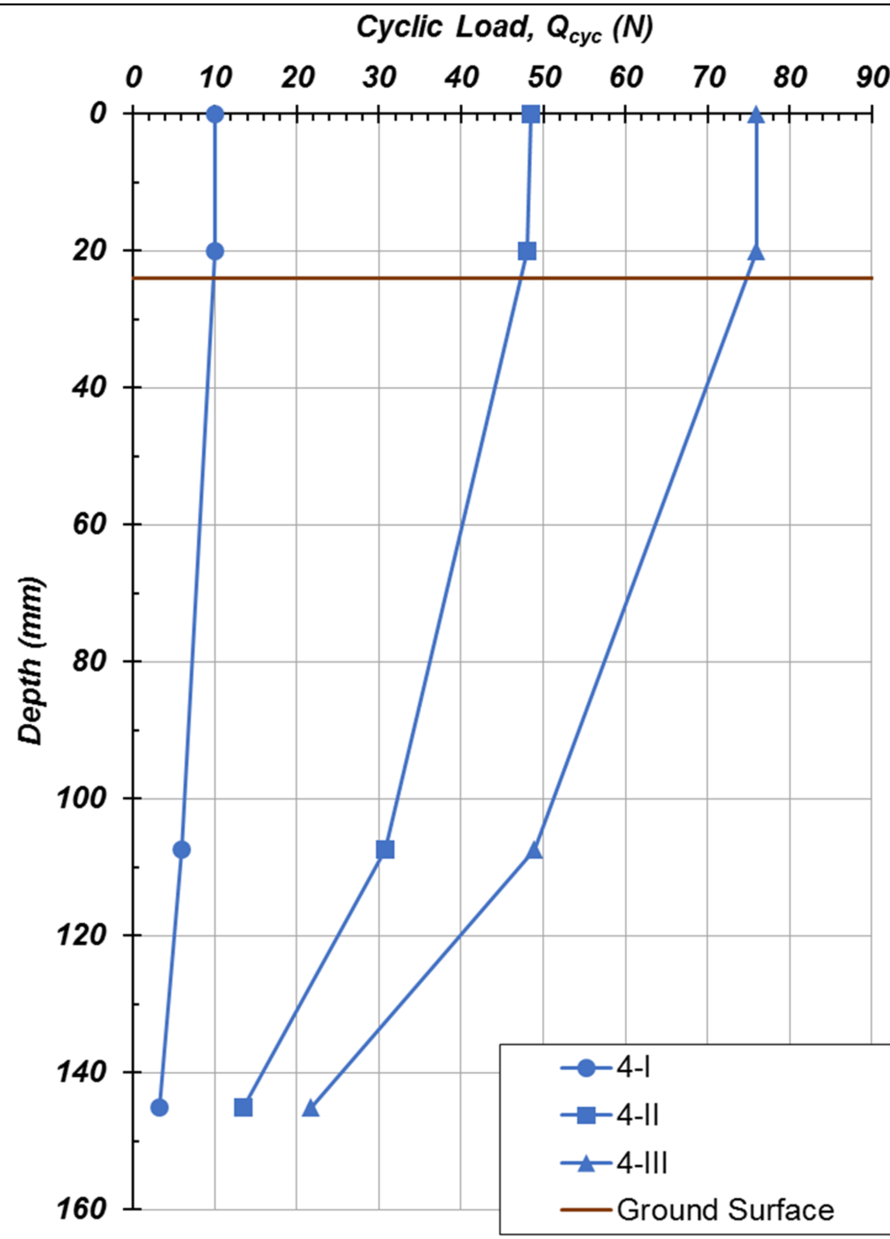

Cyclic Load from Strain Gauges with Depth
Centrifuge Test 4

March 2016
C-18

engineers • scientists • innovators

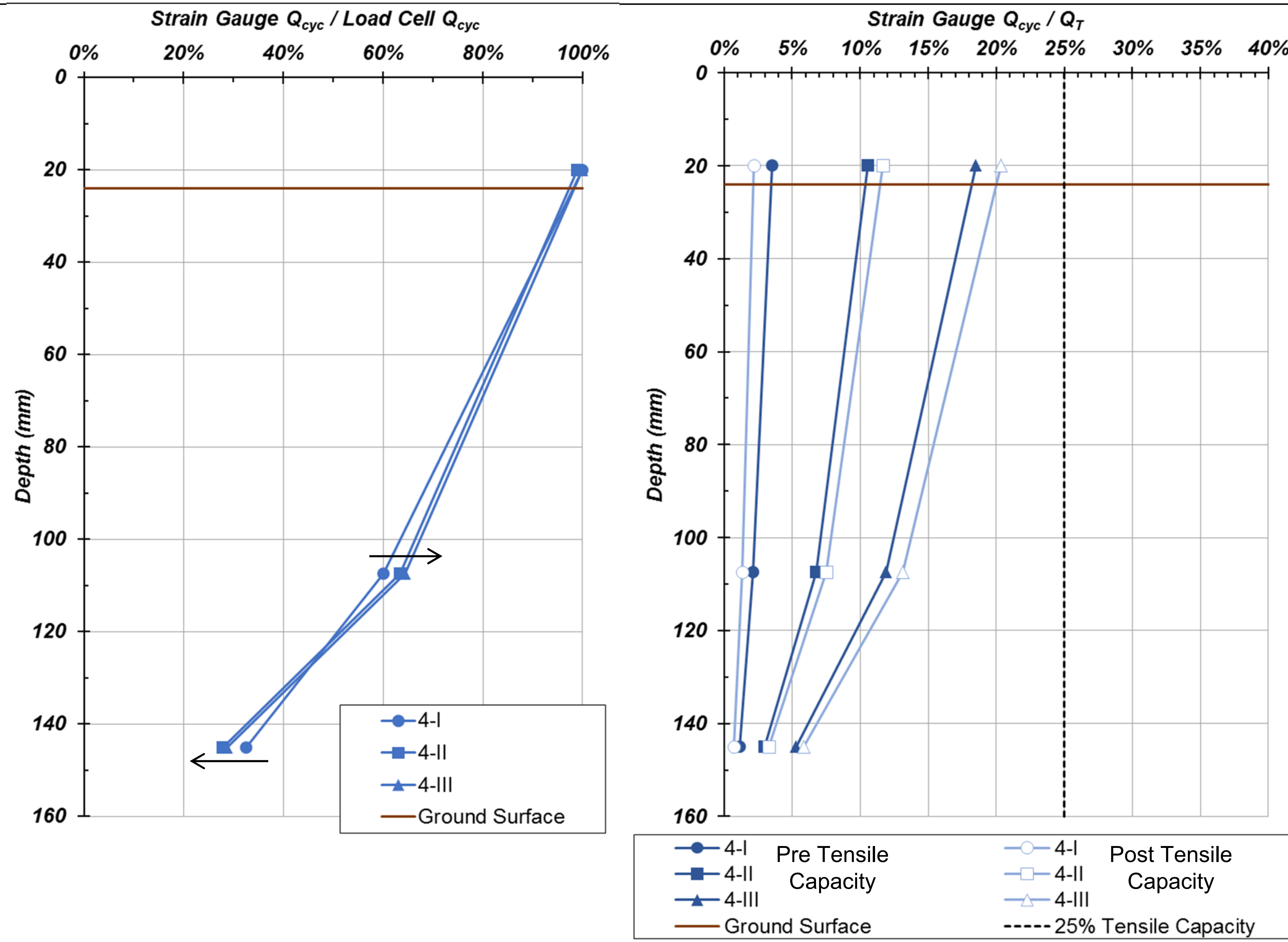

Normalized Cyclic Load from Strain Gauges with Depth
Centrifuge Test 4

March 2016

C-19

CENTRIFUGE TEST 5

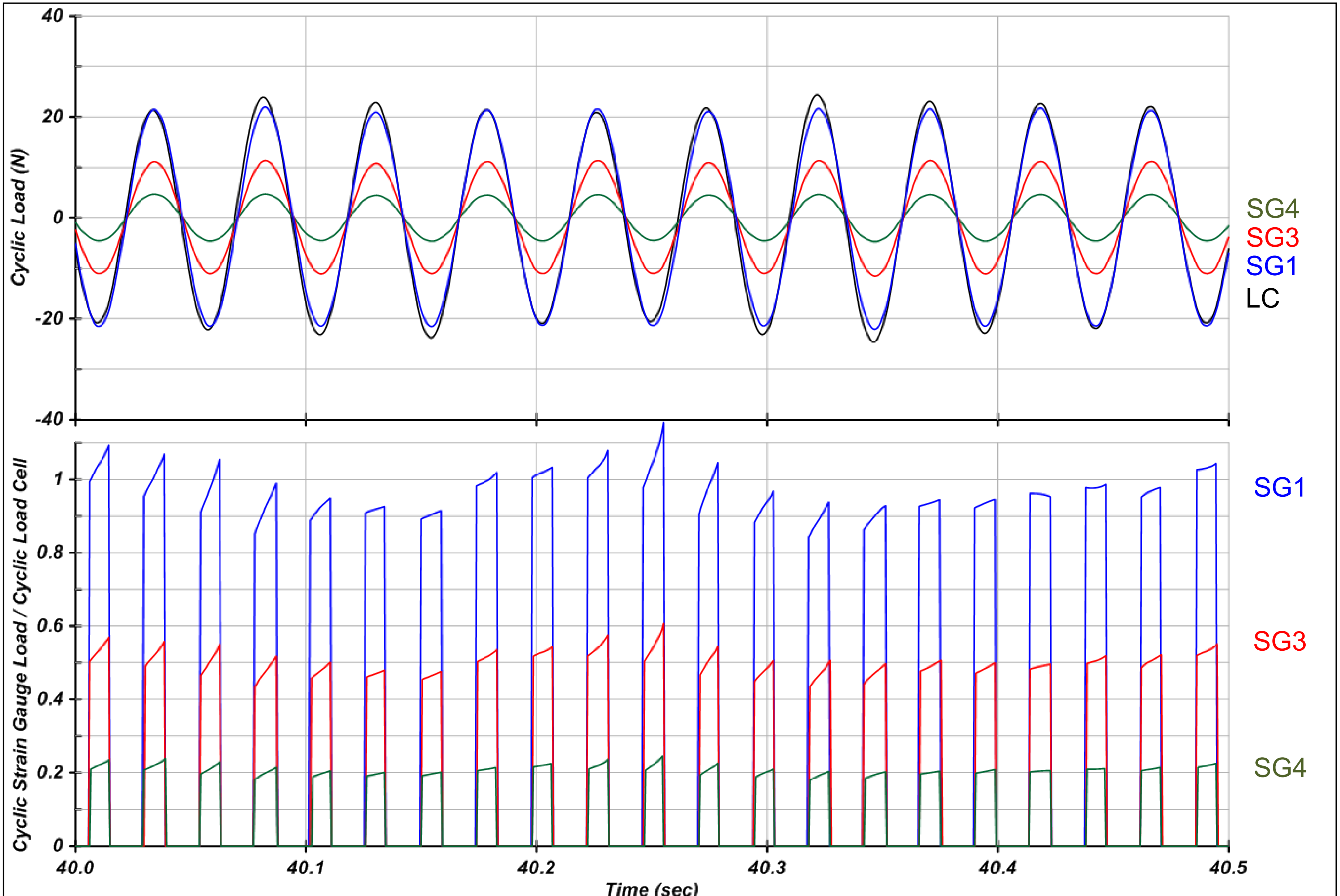

Cyclic Load Time Histories from Strain Gauges and Load Cell
Centrifuge Test 5-IA

upper 20% threshold

March 2016

C-21

MMI
engineers • scientists • innovators

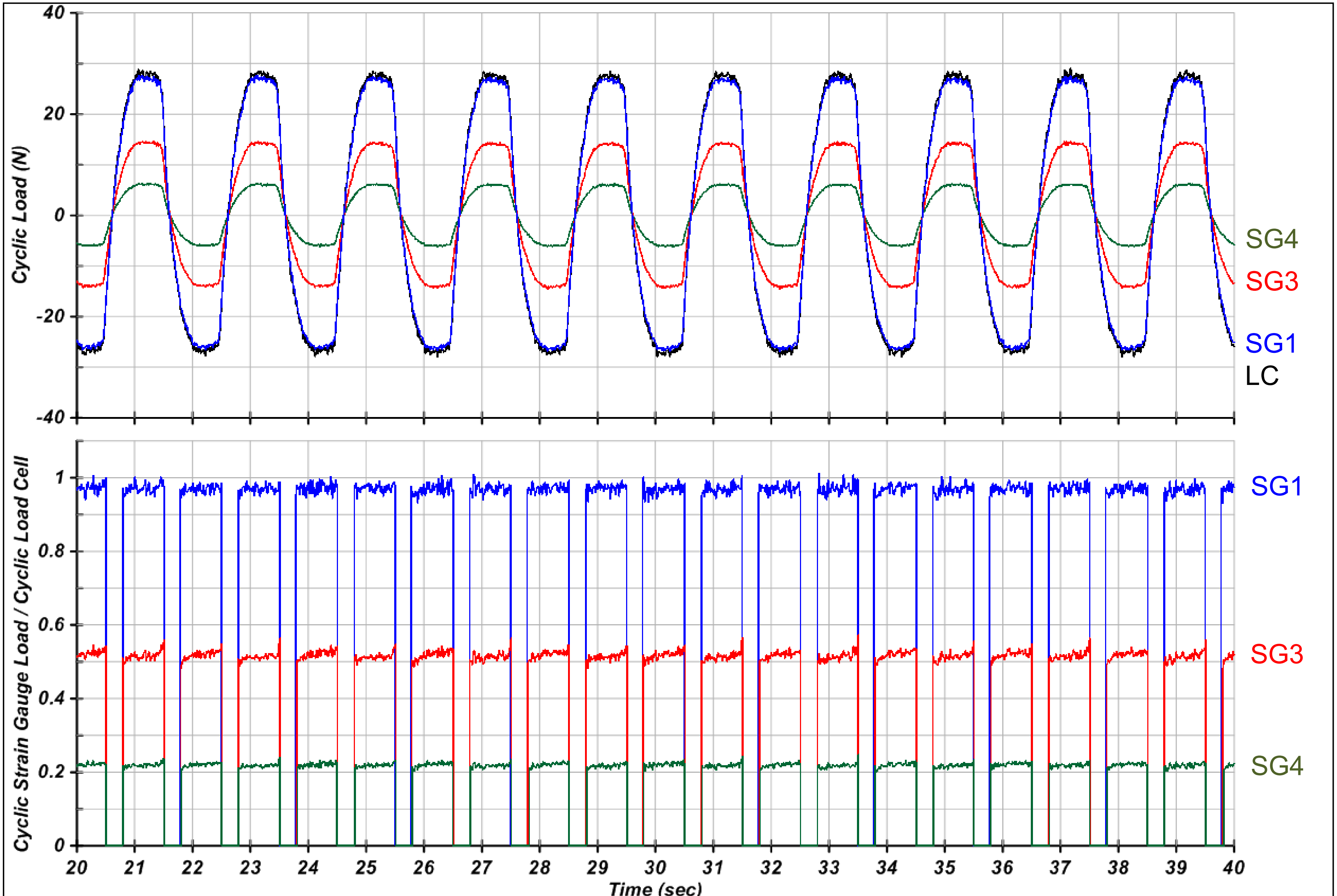

Cyclic Load Time Histories from Strain Gauges and Load Cell
Centrifuge Test 5-IB

upper 40% threshold

March 2016

C-22

MMI engineers • scientists • innovators

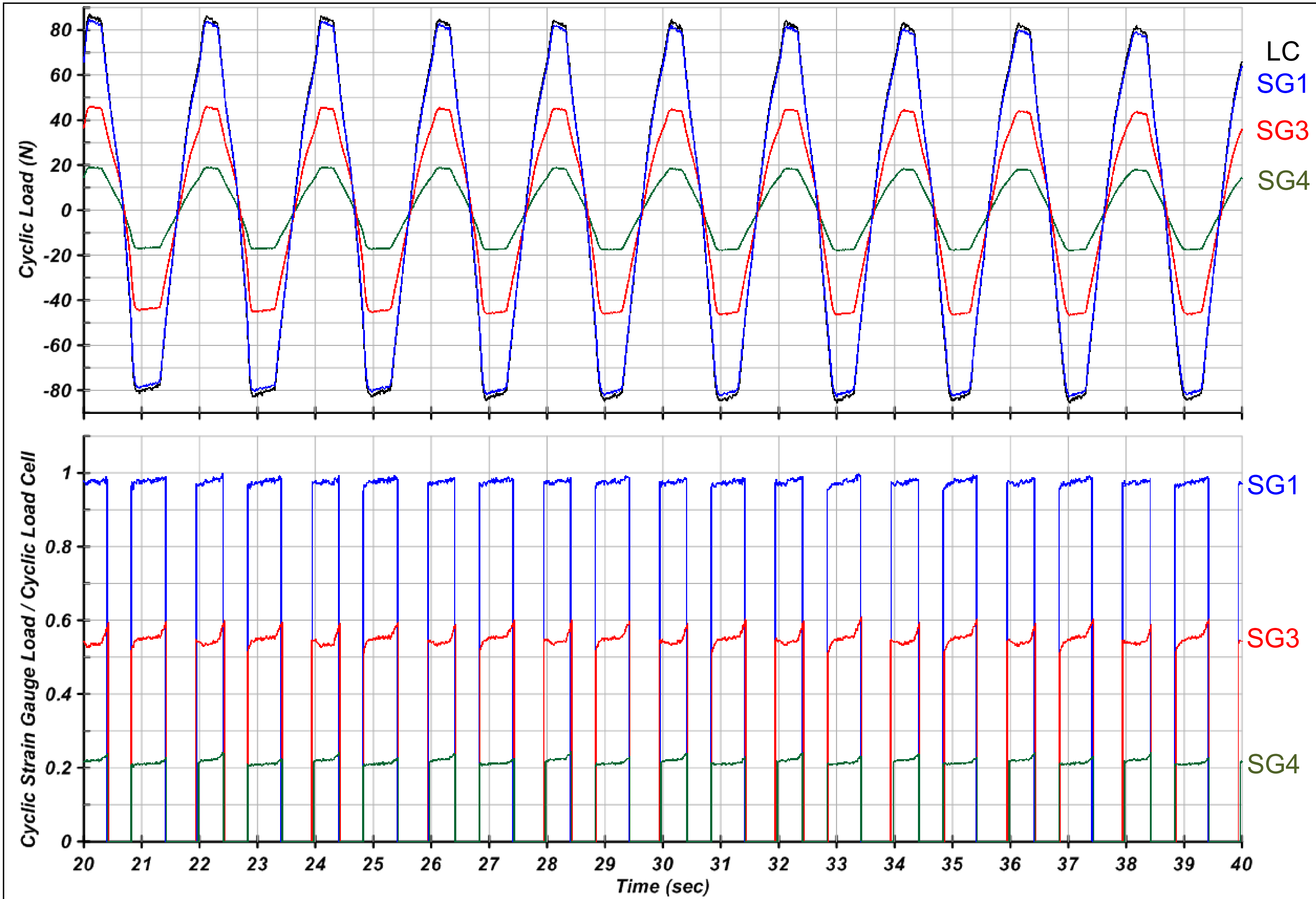

Cyclic Load Time Histories from Strain Gauges and Load Cell
Centrifuge Test 5-II

upper 40% threshold

March 2016

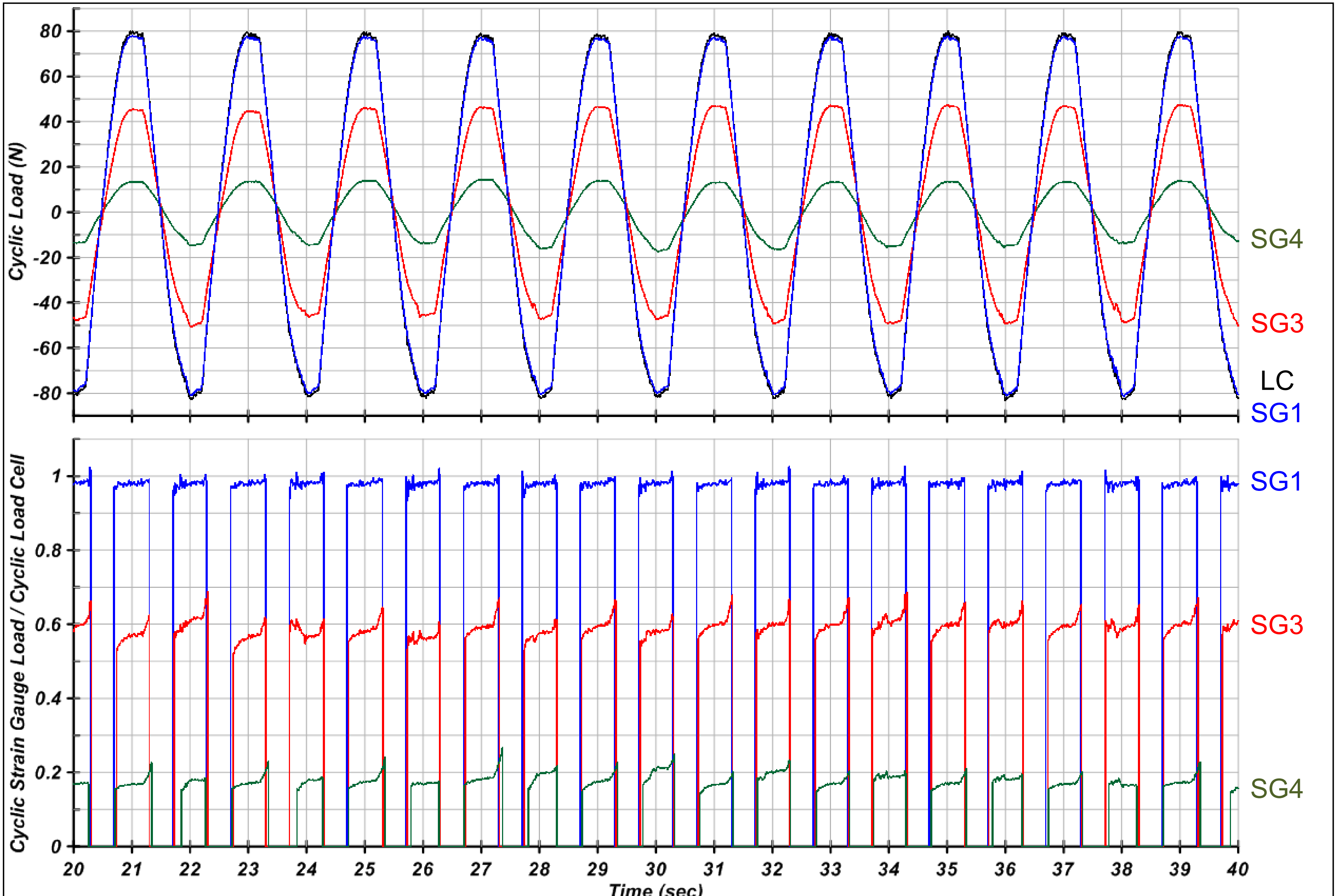

Cyclic Load Time Histories from Strain Gauges and Load Cell

Centrifuge Test 5-III

upper 40% threshold

March 2016

C-24

MMI
engineers • scientists • innovators

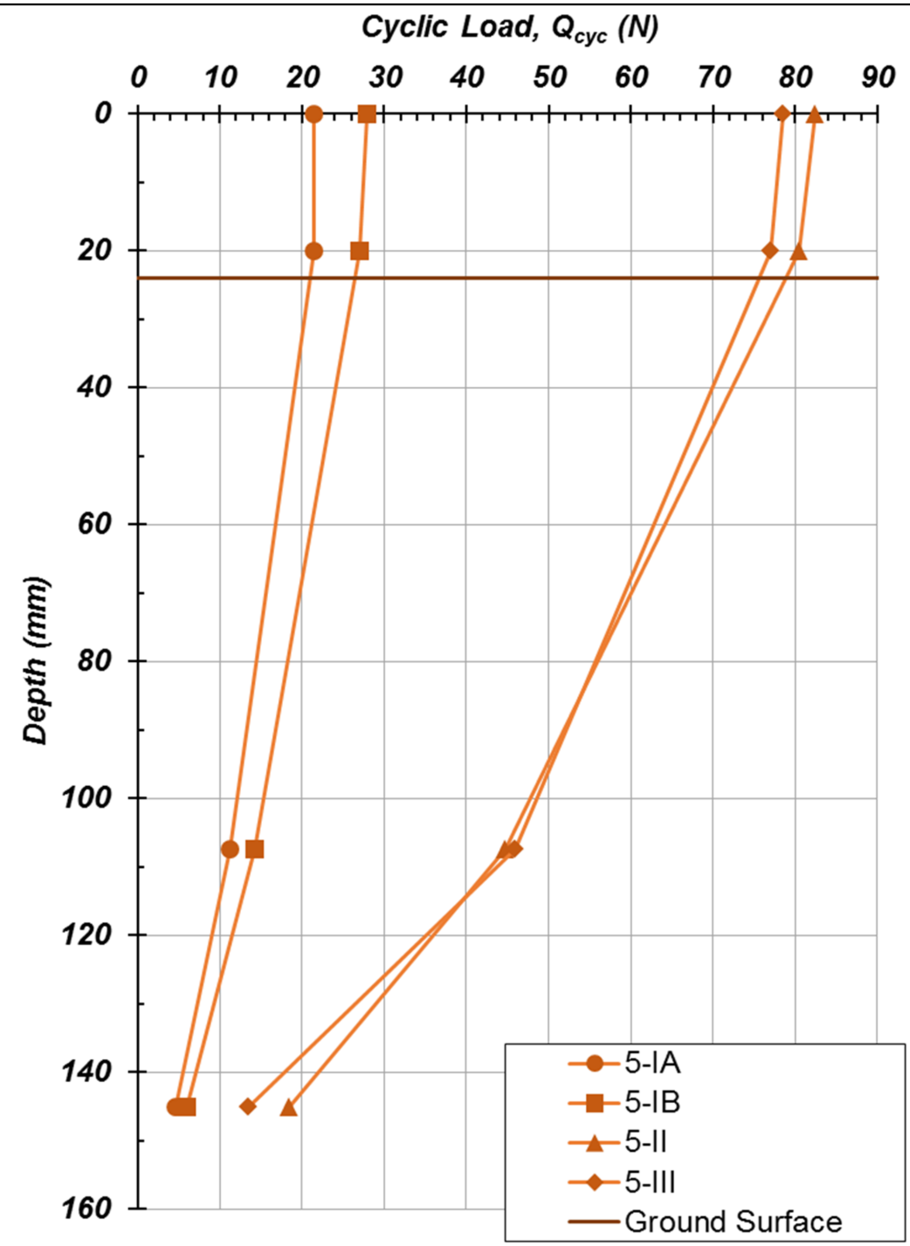

Cyclic Load from Strain Gauges with Depth
Centrifuge Test 5

March 2016
C-25

MMI
engineers • scientists • innovators

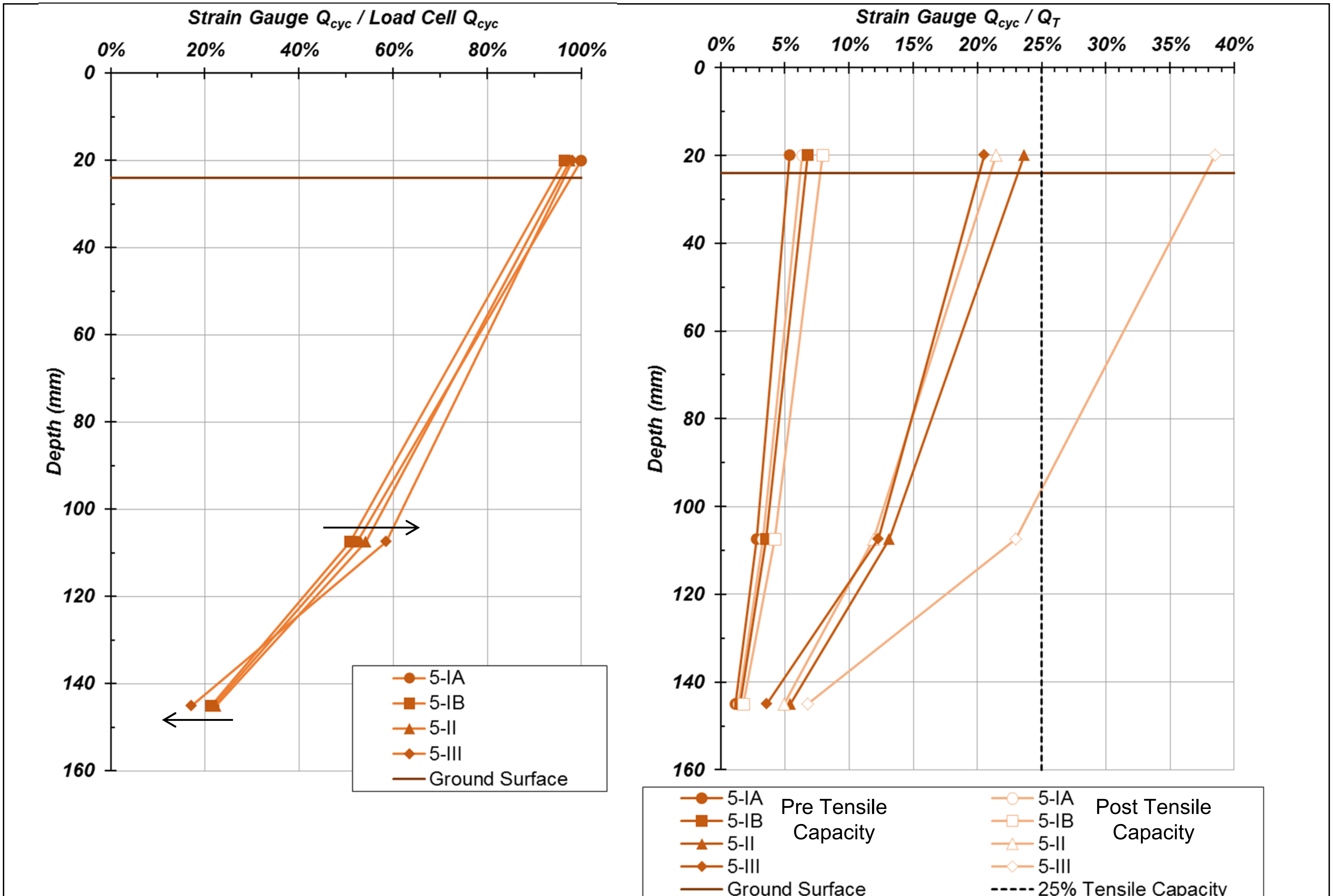

Normalized Cyclic Load from Strain Gauges with Depth
Centrifuge Test 5

March 2016
C-26

MMI engineers • scientists • innovators

APPENDIX D: RATZ MODEL ANALYSIS

PILE PARAMETERS			
Pile Length, Embedded	L_e	=	150 mm
Pile Diameter	D	=	6.92 mm
Pile Diameter with Composite	D_c	=	9.37 mm
[1]Modulus of Pile with Composite	E_c	=	41.7 GPa
Number of Elements	N	=	40

SOIL PARAMETERS BY LOAD PACKET			4-I	4-II	4-III
Load Transfer Parameter	ζ	=	4	4	4
Yield Parameter	χ_i	=	0	0	0
[2]Normalized Modulus	G/G_{max}	=	1/2	1/6.5	1/15
[3]Initial Tensile Capacity	Q_T	=	[5]450 N	454 N	411 N
[4]Final Tensile Capacity	Q_F	=	[6]450 N	411 N	373 N
[7]Shaft Friction Ratio (Residual/Peak)	τ_r/τ_{peak}	=	1	0.905	0.908
[8]Displacement to Residual	Δw_r	=	0.937 mm	0.937 mm	0.937 mm
Strain-Softening Parameter	η	=	1	1	1
[9]Cyclic Shaft Friction Ratio (Residual/Peak)	$\tau_{cyc,r}/\tau_p$	=	1	0.905	0.908

LAYER GEOMETRY AND PARAMETERS			Layer 1 *Dense Sand*	Layer 2 *Loose Sand*	Layer 3 *Modeling Clay*
Layer Depth (top)	z_{top}	=	0 mm	154 mm	161 mm
Layer Depth (bottom)	z_{bottom}	=	154 mm	161 mm	168 mm
Layer Thickness	Δh	=	154 mm	18 mm	7 mm
Initial Density	ρ_0	=	1665	1603	--
Initial Void Ratio	e_0	=	0.604	0.693	--
Initial Relative Density	$D_{R,0}$	=	70.7%	42.9%	--

NOTES:

1. E_c=F$(EA)_{pile}/A_c$, where F=1.6, observed increase in axial stiffness.
2. Matched initial pile head stiffness, G, with experimental data. G_{max} is obtained from empirical correlations.
3. The maximum tensile capacity is assumed as the measured residual tensile capacity before the packet.
4. The residual tensile capacity is assumed as the measured residual tensile capacity after the packet.
5. After installation, 2 mm pullout displacement was insufficient to fully mobilize pile capacity. A tensile capacity of 450 N was selected based on an assumption that limited degradation occurred during the course of the test.
6. The measured post-packet tensile capacity was 454 N, but set Q_r = Q_T to satisfy $Q_r \leq Q_T$ in RATZ.
7. Estimated to be equal to the ratio Q_F/Q_T.
8. Δw_r = 0.10D = required displacement to reach residual conditions.
9. Assumed no cyclic softening.

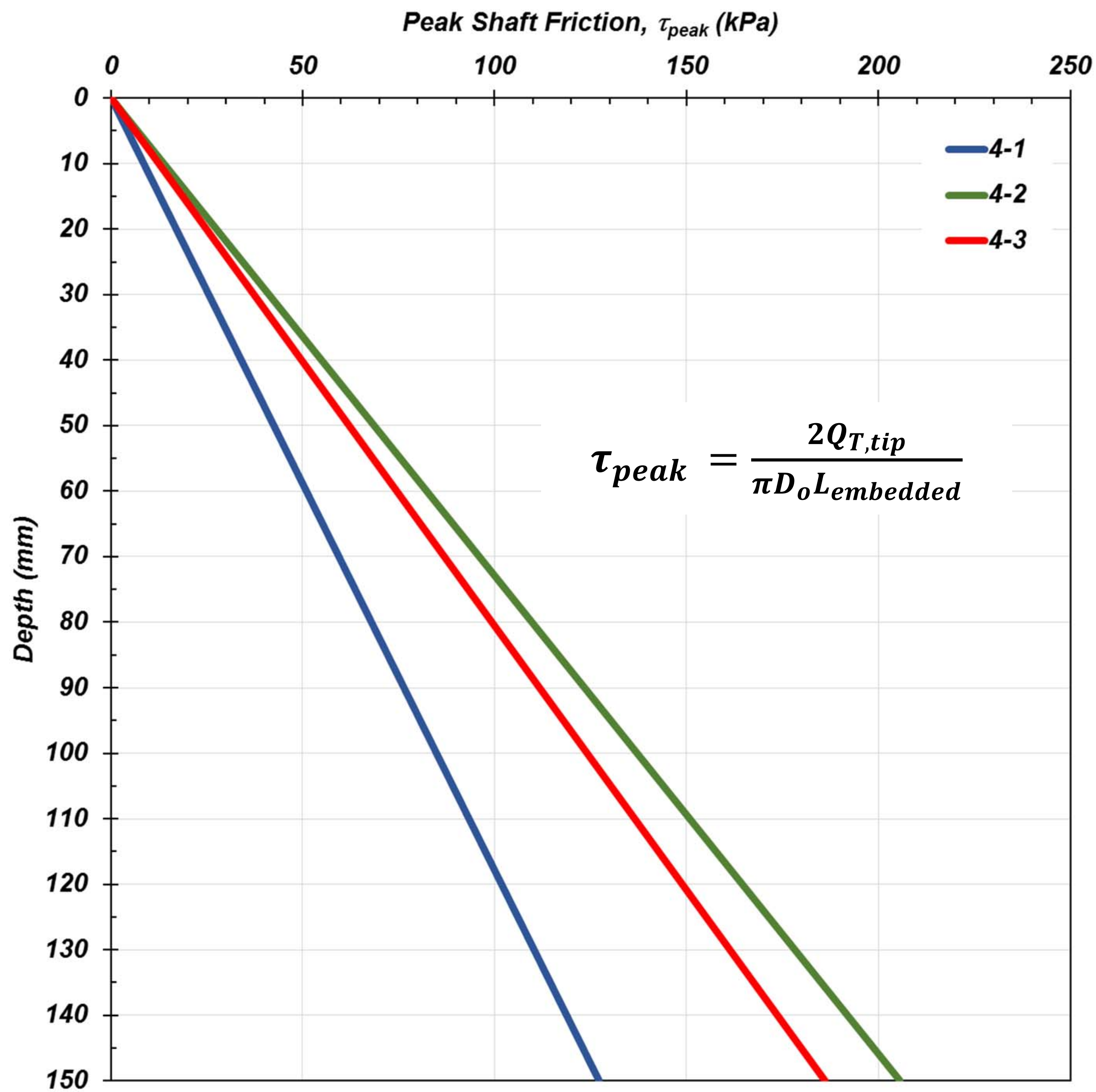

Calculated Peak Shaft Friction (τ_{peak}) with Depth

March 2016

D-3

MMI engineers • scientists • innovators

G_{max} MODEL INPUT ASSUMPTIONS

Method 1
Hardin (1978)

k_0 = 0.5

ν = 0.3

[1]S = 1350

OCR = 1

Method 2
Hardin & Drnevich (1972)

k_0 = 0.5

OCR = 1

Method 3
Carraro et al. (2003)

k_0 = 0.5

C_g = 611

e_g = 2.17

n_g = 0.437

NOTES:
1. Based on similar sand in Savidis & Vretto (1993)

z (mm)	σ_v' (kPa)	σ_m' (kPa)	$G_{max,1}$ (MPa)	$G_{max,2}$ (MPa)	$G_{max,3}$ (MPa)
0	0.0	0.0	0.00	0.00	0.00
5	6.5	4.4	19.65	23.54	23.94
10	13.1	8.7	27.79	33.29	32.41
15	19.6	13.1	34.03	40.78	38.69
20	26.1	17.4	39.29	47.08	43.87
25	32.7	21.8	43.93	52.64	48.37
30	39.2	26.1	48.13	57.67	52.38
35	45.7	30.5	51.98	62.29	56.03
40	52.3	34.8	55.57	66.59	59.39
45	58.8	39.2	58.94	70.63	62.53
50	65.3	43.6	62.13	74.45	65.48
55	71.9	47.9	65.16	78.08	68.26
60	78.4	52.3	68.06	81.55	70.91
65	84.9	56.6	70.84	84.88	73.43
70	91.5	61.0	73.51	88.09	75.85
75	98.0	65.3	76.09	91.18	78.17
80	104.5	69.7	78.59	94.17	80.41
85	111.1	74.0	81.01	97.07	82.57
90	117.6	78.4	83.36	99.88	84.65
95	124.1	82.8	85.64	102.62	86.68
100	130.7	87.1	87.87	105.28	88.64
105	137.2	91.5	90.03	107.88	90.55
110	143.7	95.8	92.15	110.42	92.41
115	150.3	100.2	94.22	112.90	94.23
120	156.8	104.5	96.25	115.33	95.99
125	163.3	108.9	98.24	117.71	97.72
130	169.9	113.2	100.18	120.04	99.41
135	176.4	117.6	102.09	122.33	101.06
140	182.9	122.0	103.96	124.57	102.68
145	189.5	126.3	105.80	126.78	104.27
150	196.0	130.7	107.61	128.95	105.83
155	202.5	135.0	95.51	115.03	90.49

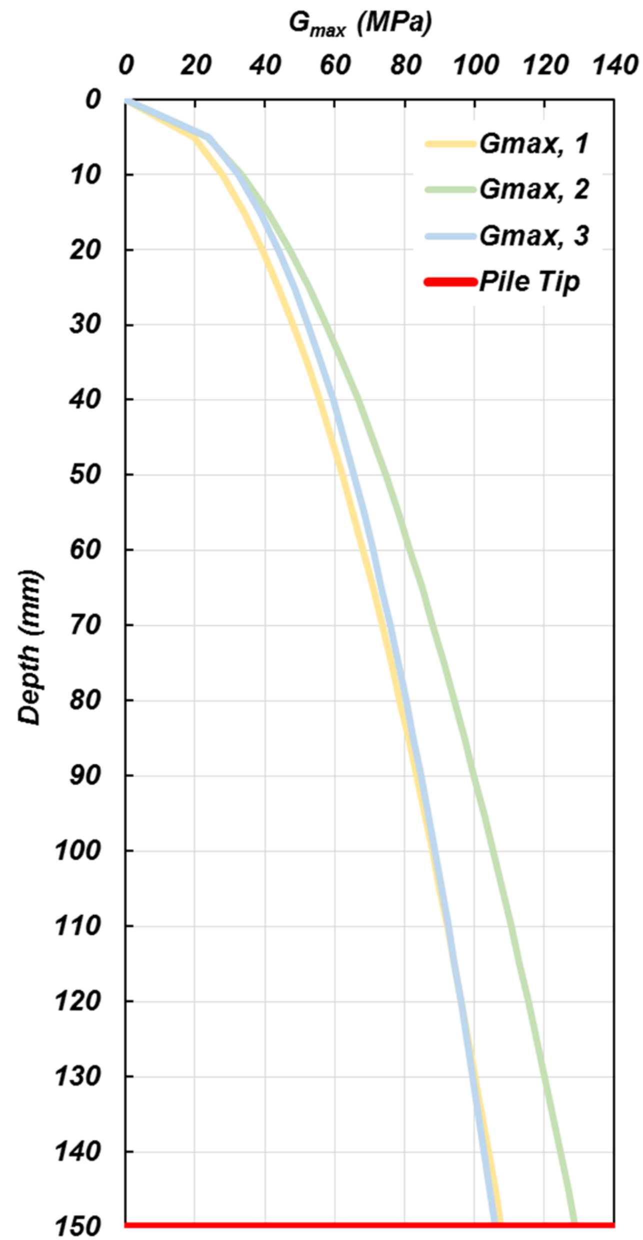

Calculated G_{max} with Depth for Test 4

March 2016
D-4

Test-Load Packet 4-II Cyclic Results

static component removed

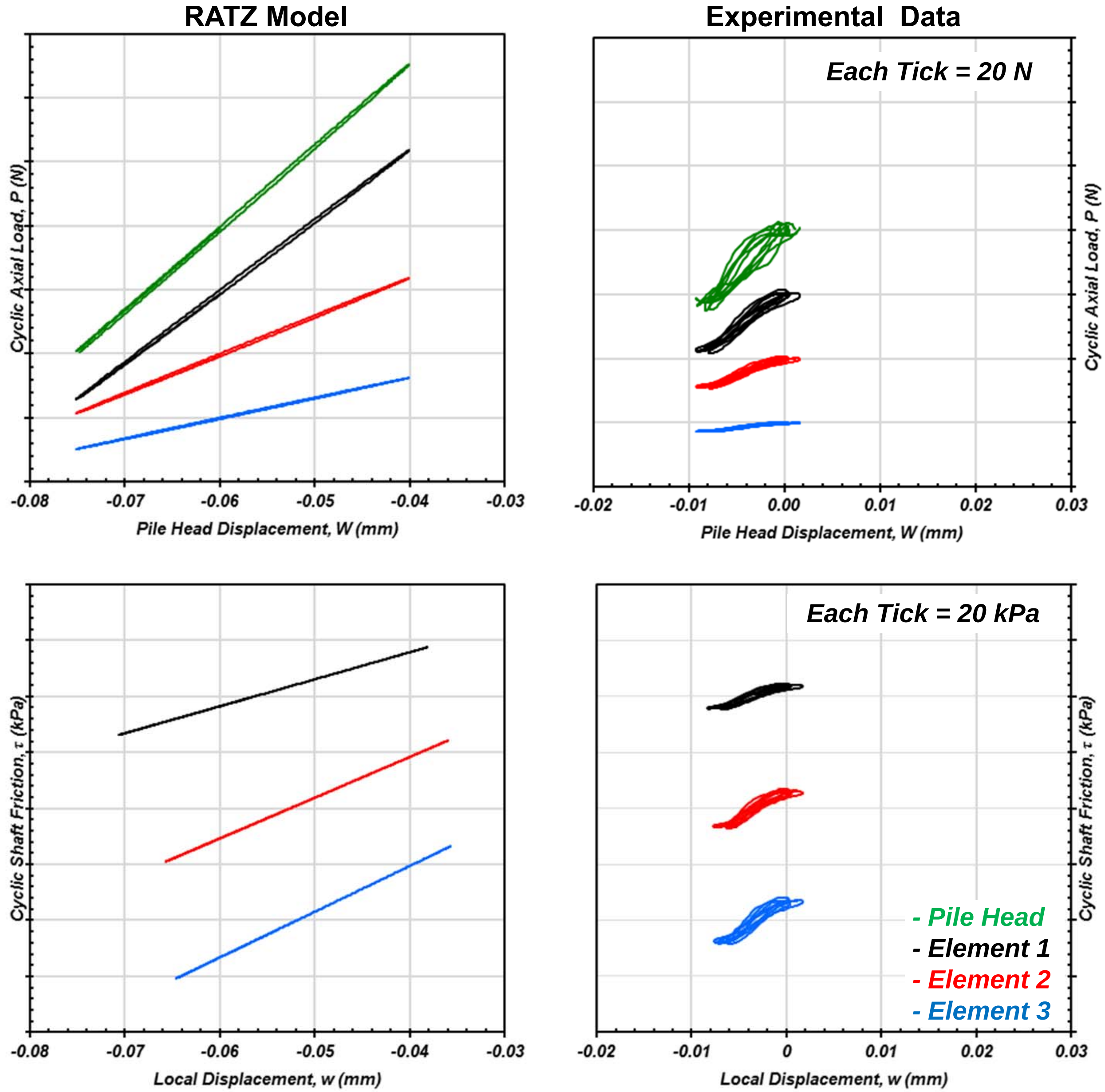

Comparison of Analytical RATZ Model and Experimental Centrifuge Data
1-50 cycles, first 50 cycles in full load packet

March 2016

Test-Load Packet 4-II Cyclic Results

static component removed

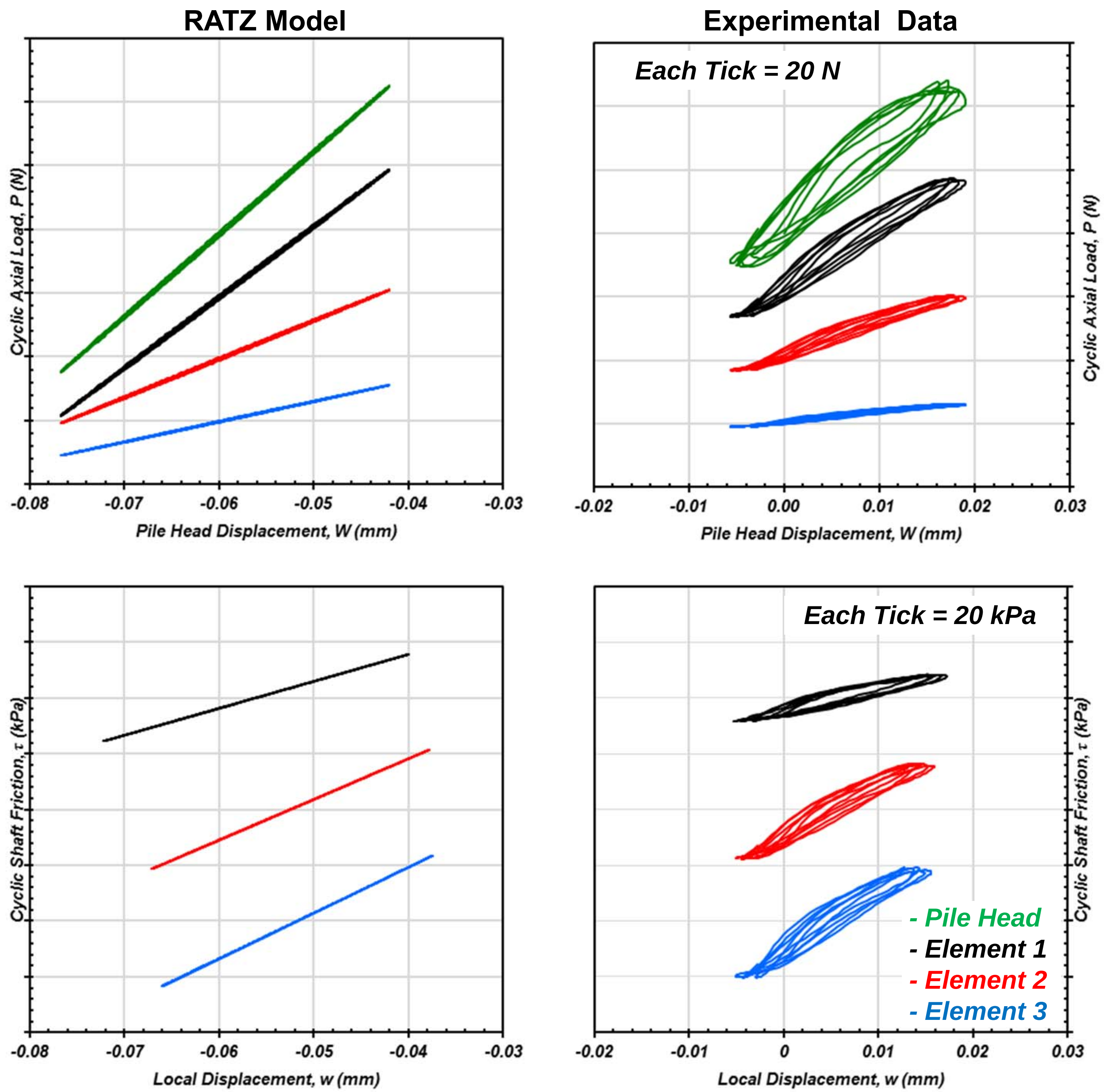

Comparison of Analytical RATZ Model and Experimental Centrifuge Data
9,950-10,000 cycles, last 50 cycles in full load packet

March 2016

engineers • scientists • innovators

Load Packet 4-I

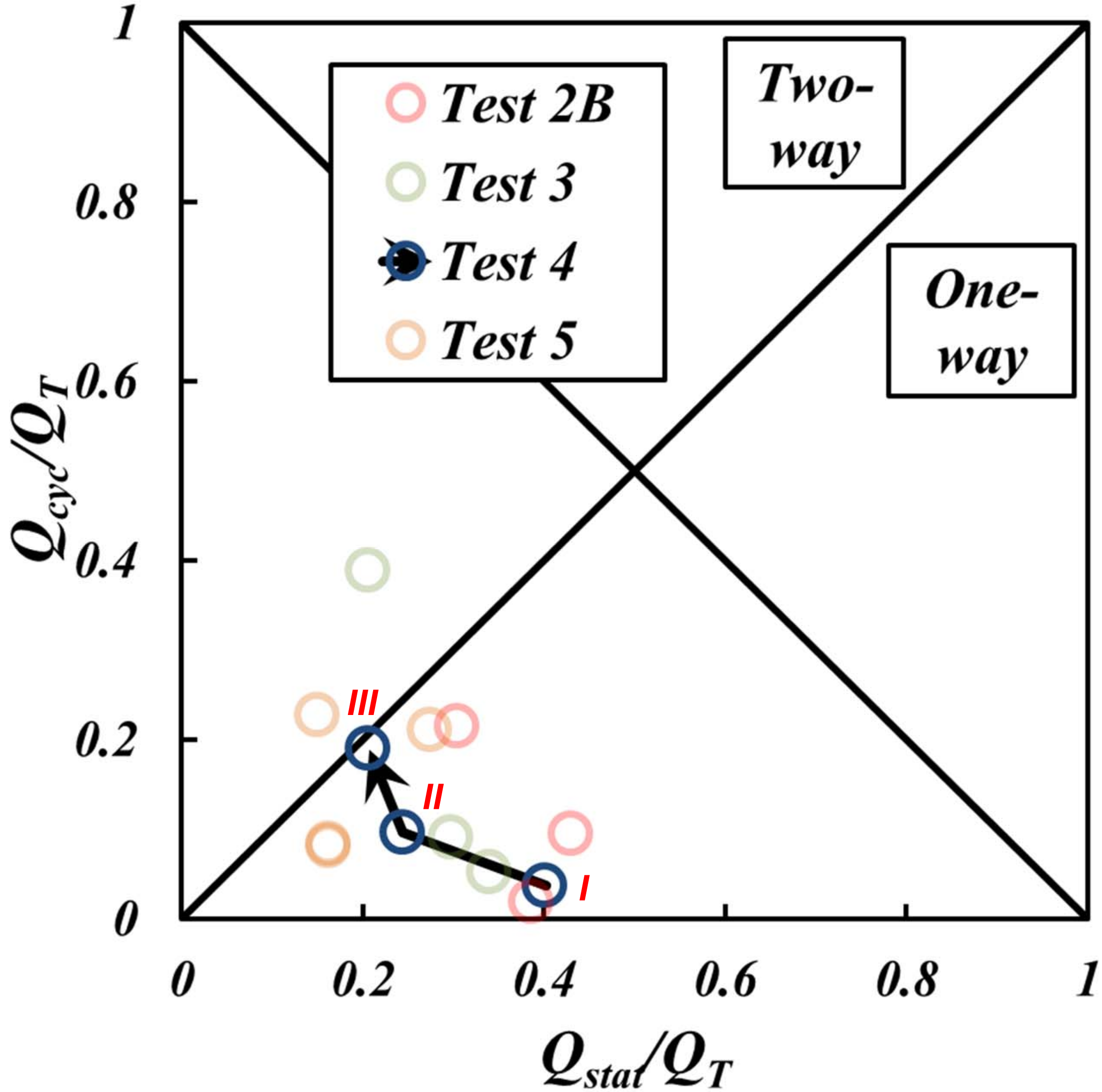

Analytical

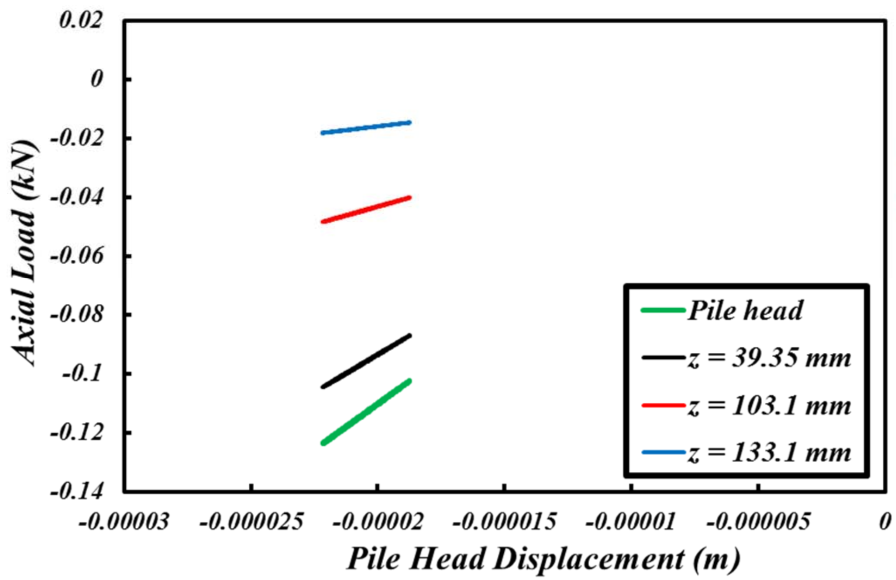

Experimental

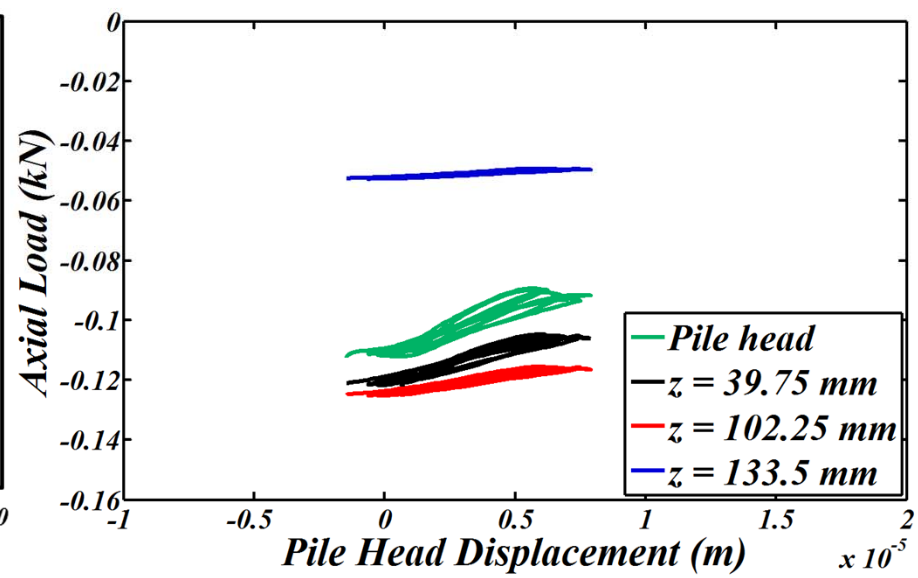

Analytical

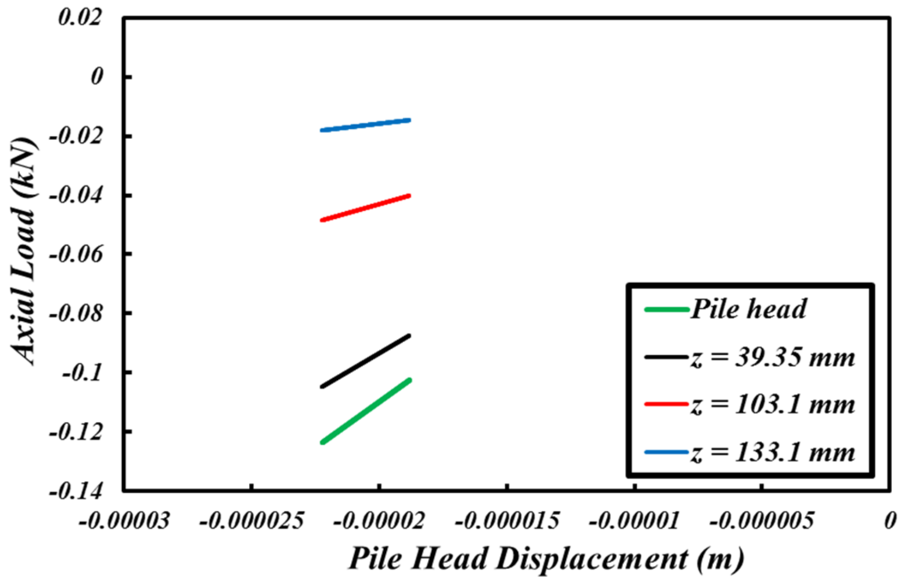

Experimental

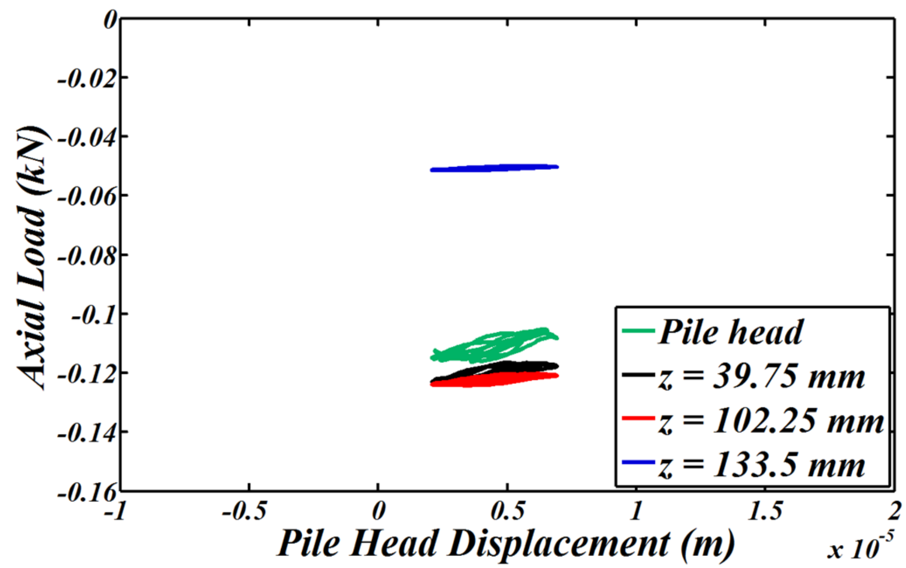

Pile Head Response (29,950-30,000 cycles, last 50 cycles in 30K packet) **Test-Load Packet 4-I**	**March 2016** D-9	MMI engineers • scientists • innovators

Analytical

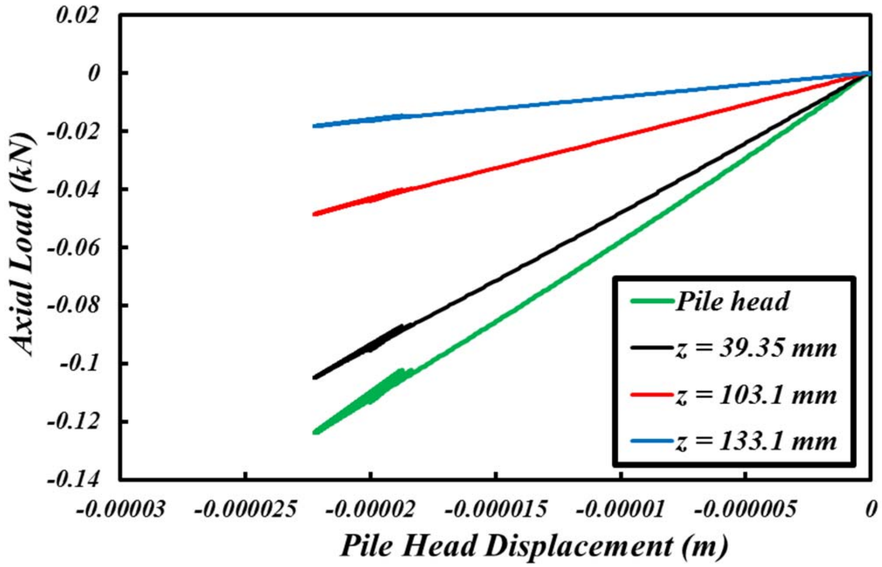

Experimental

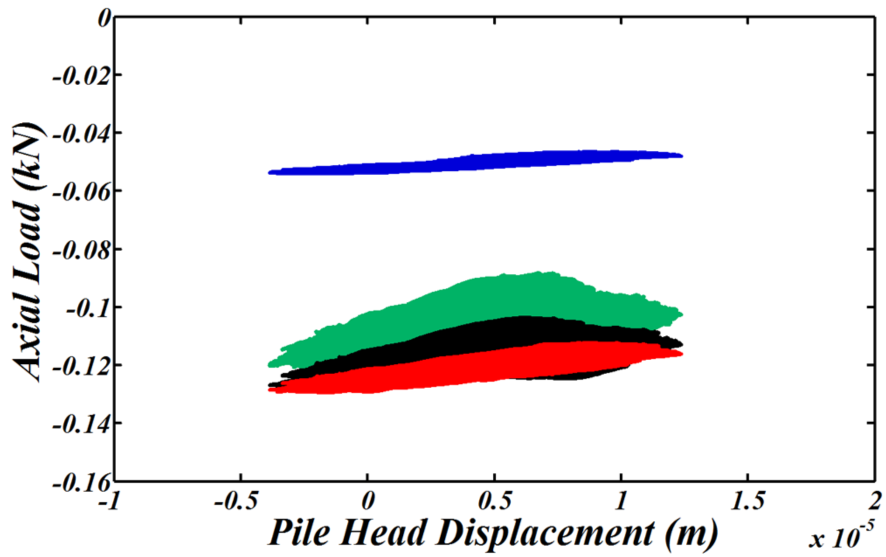

Analytical

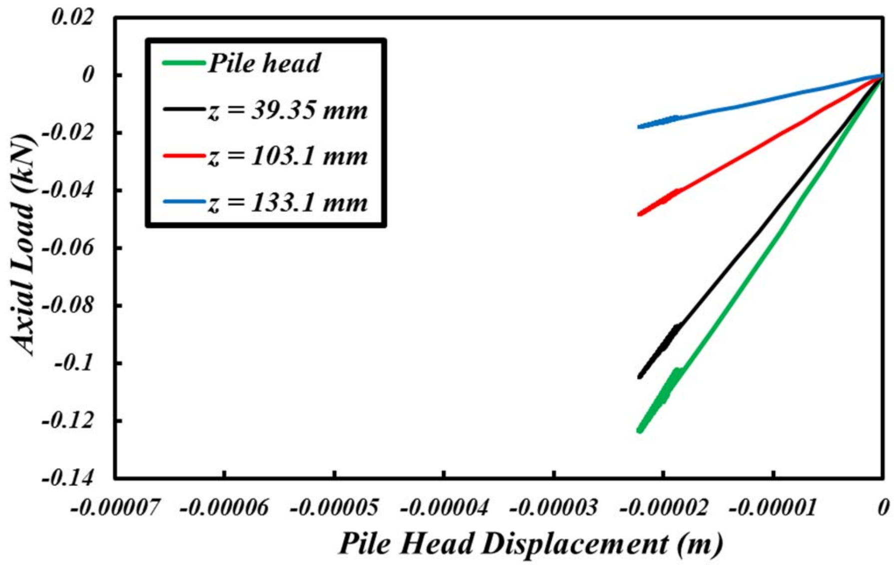

Experimental

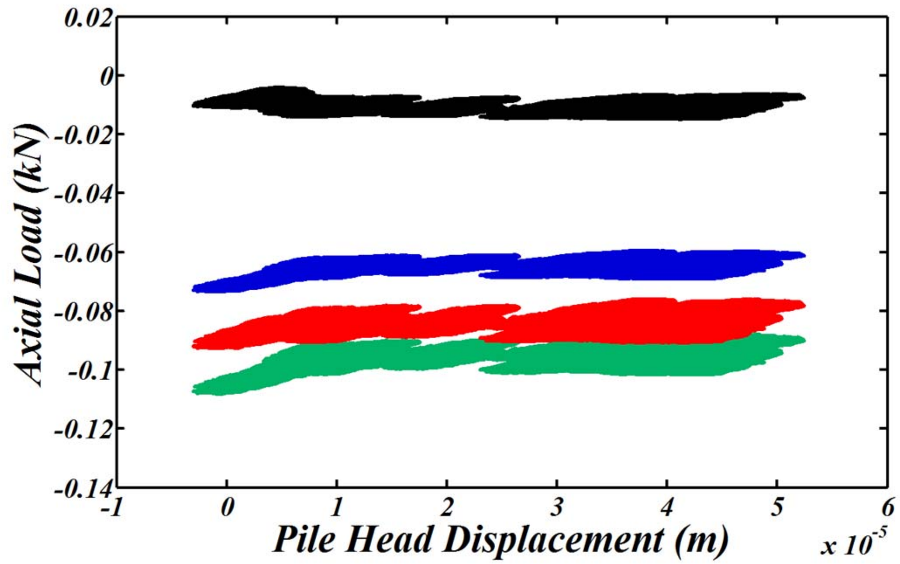

Analytical

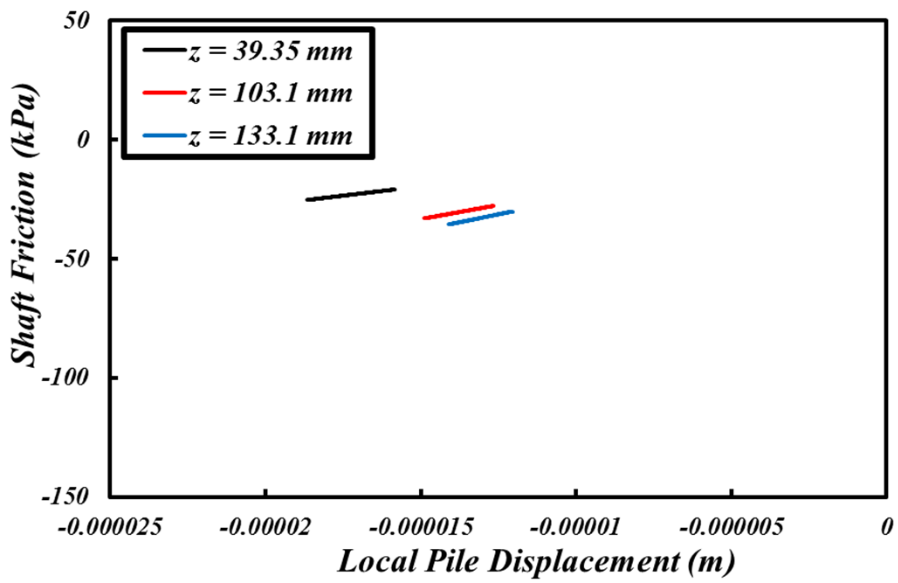

Experimental

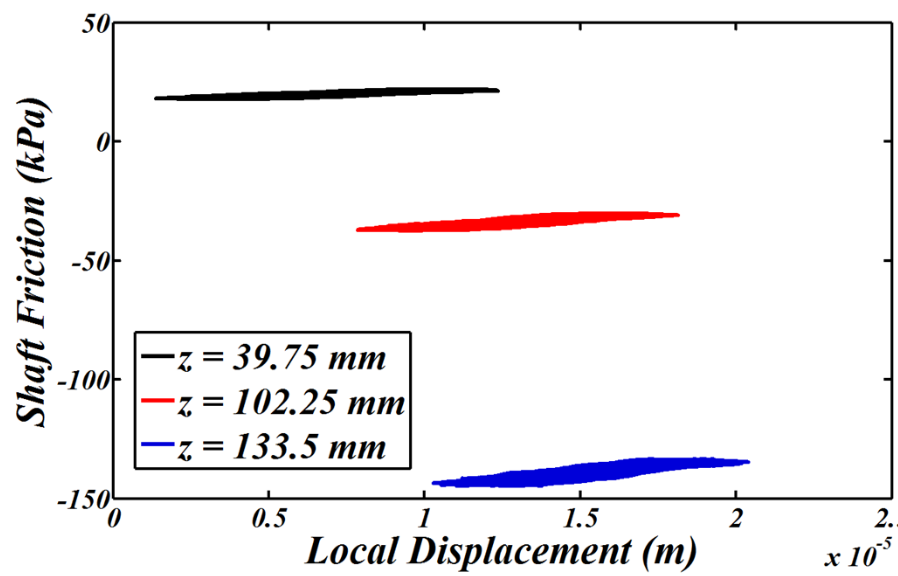

Analytical

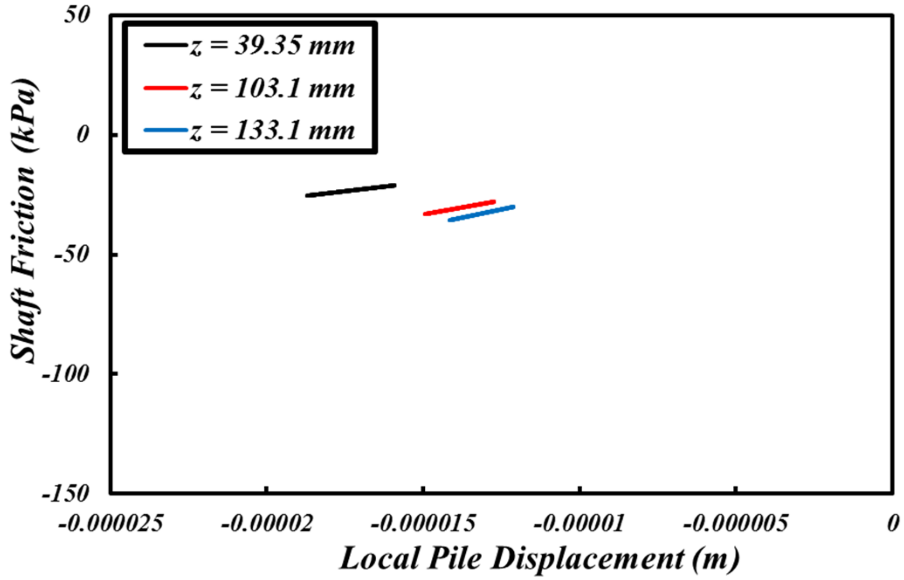

Experimental

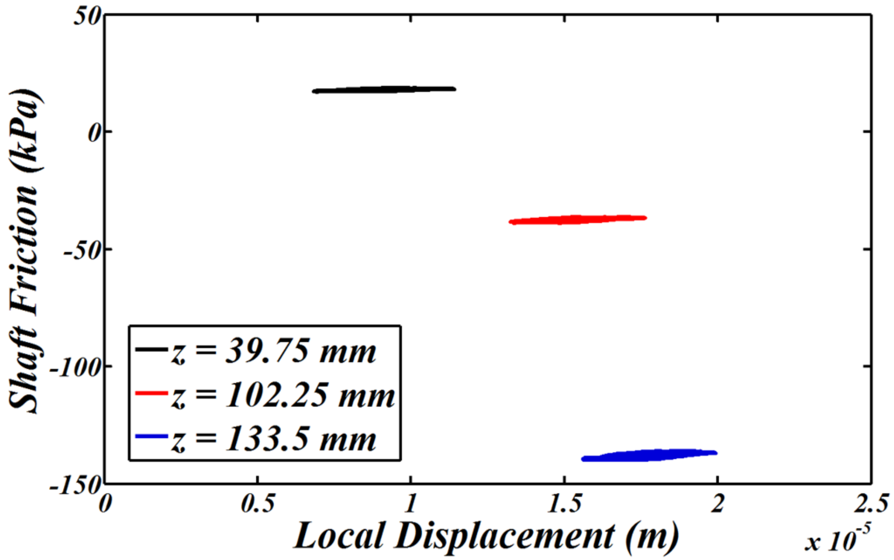

Analytical

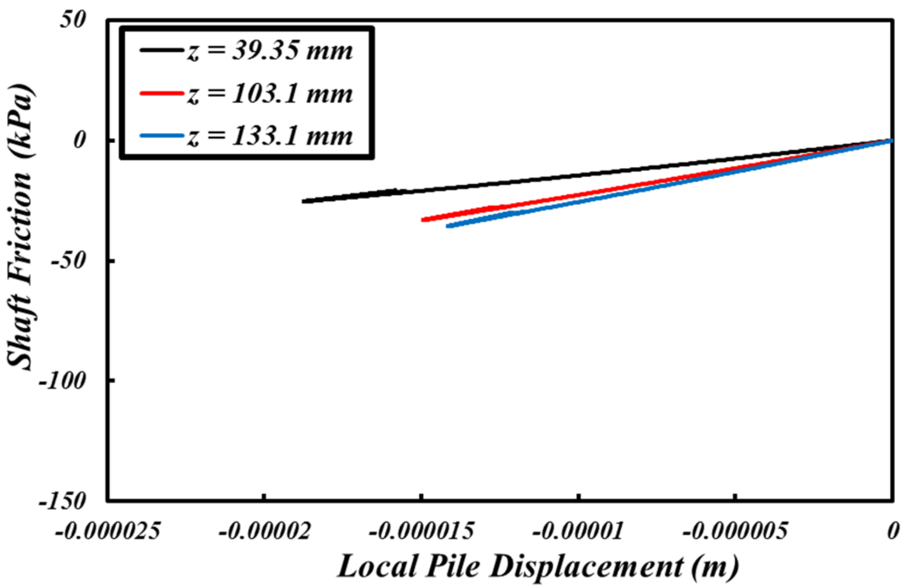

Experimental

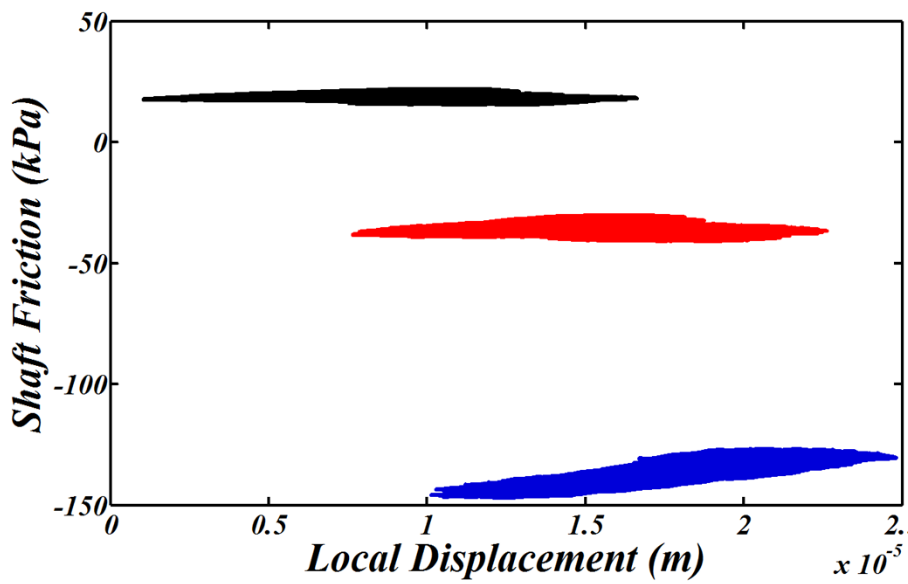

Analytical

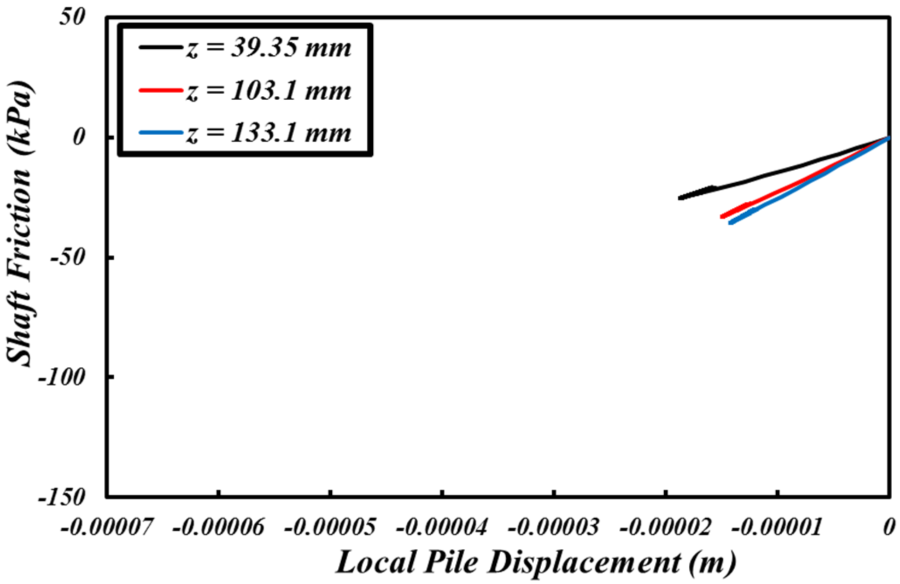

Experimental

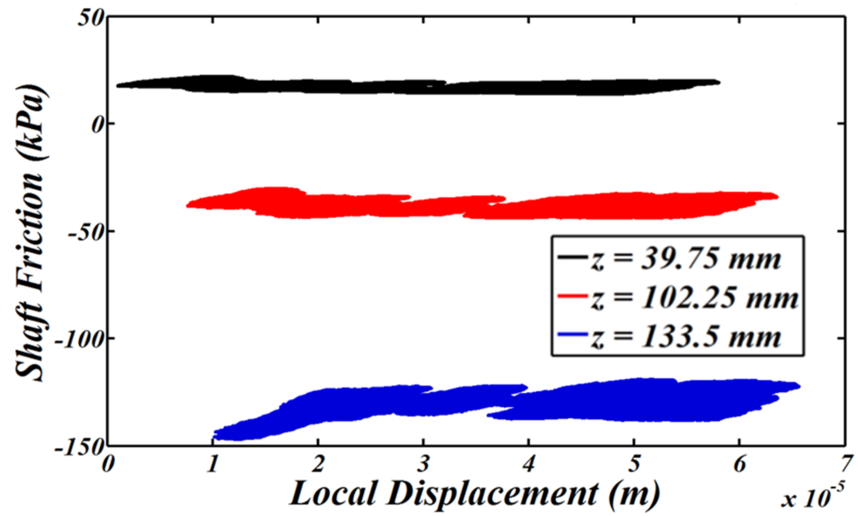

Load Packet 4-II

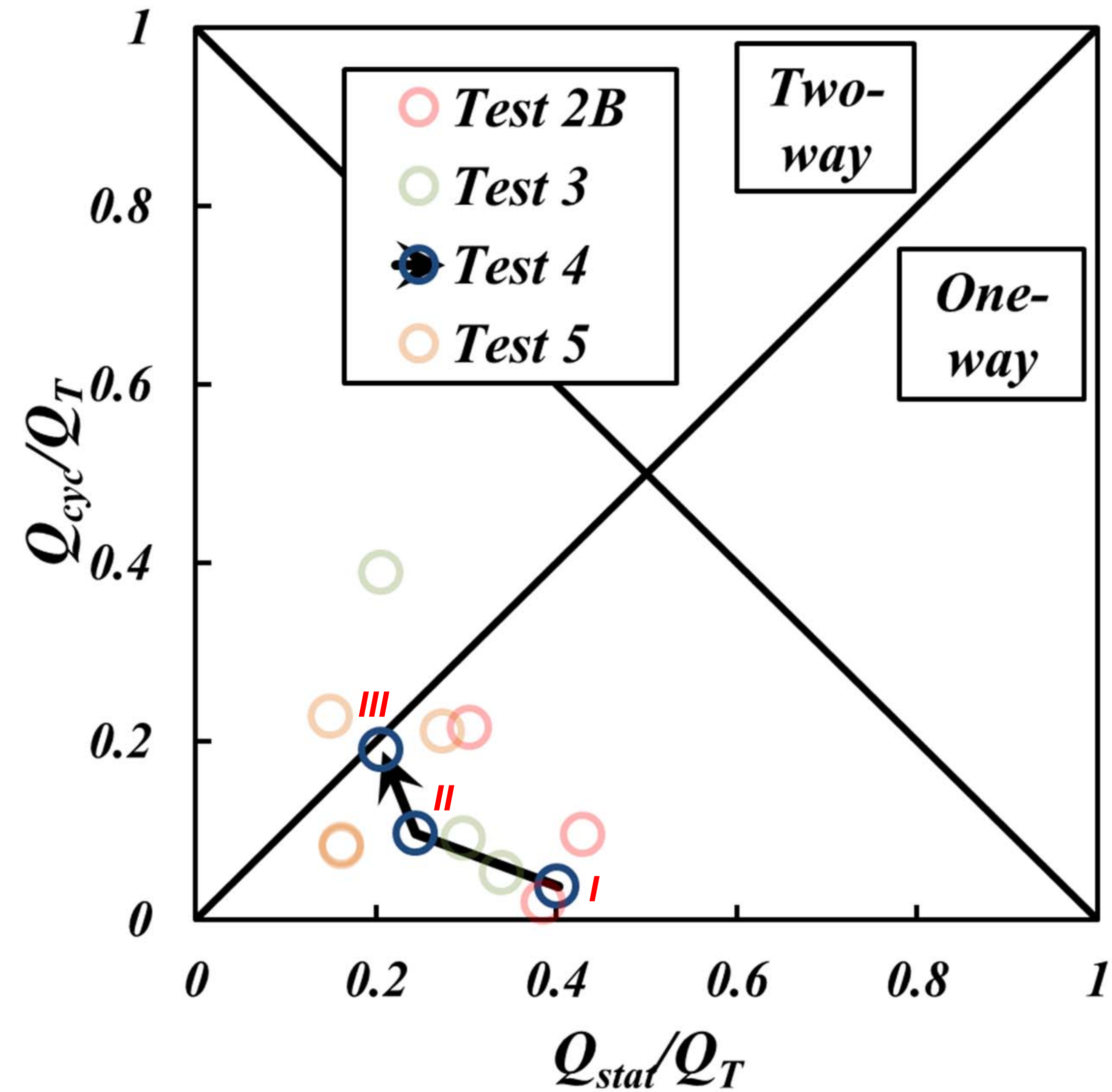

Analytical

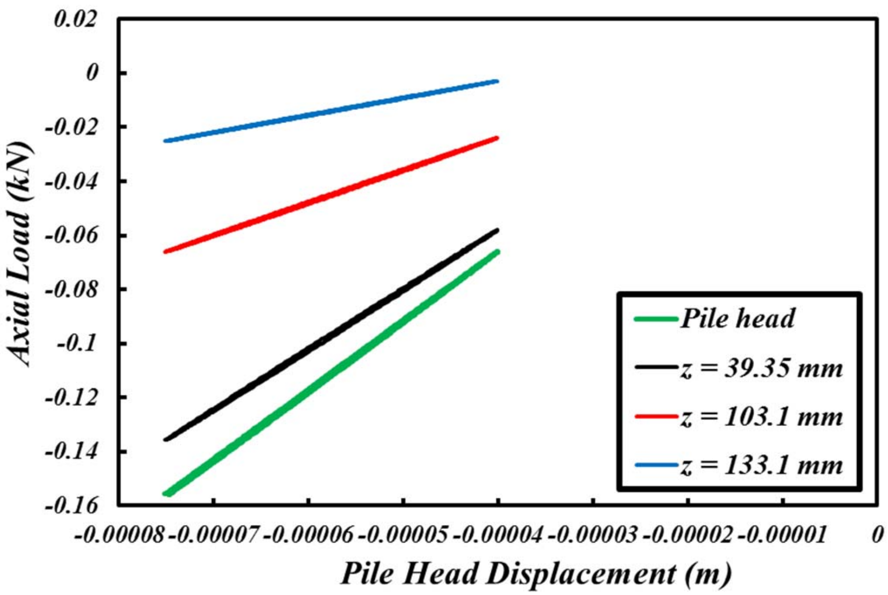

Experimental

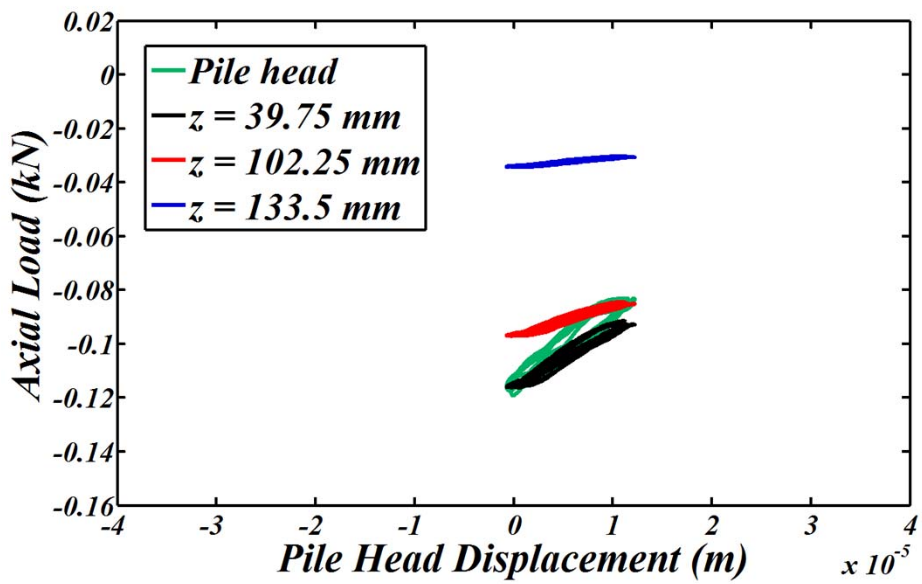

Analytical

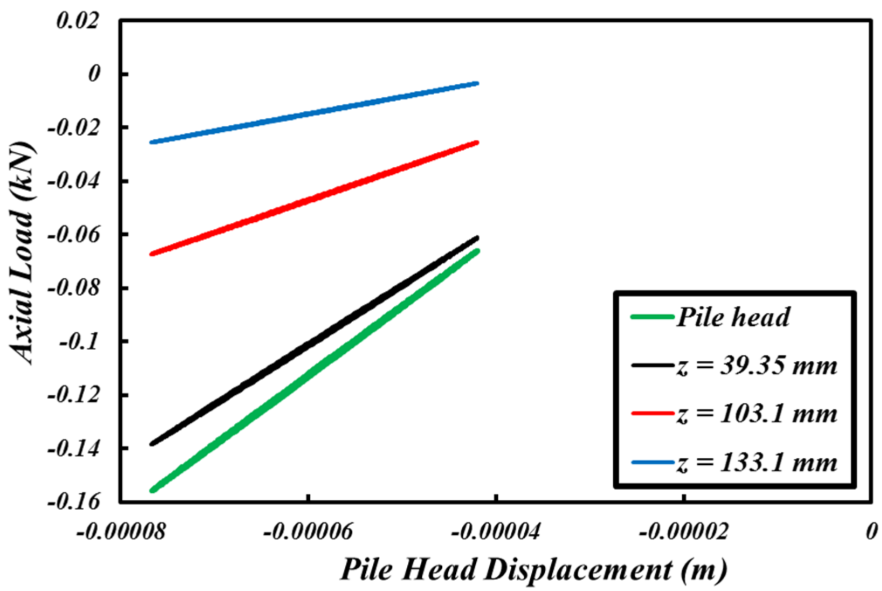

Experimental

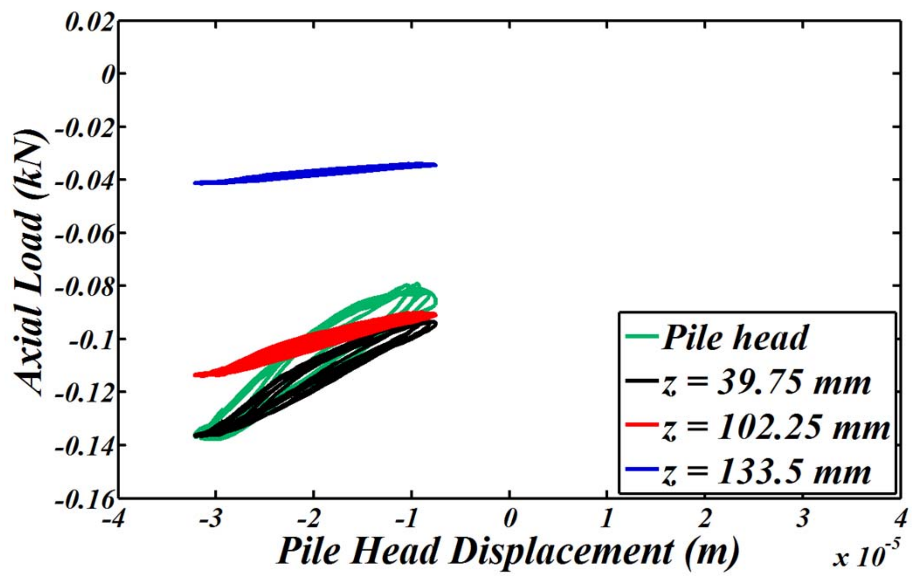

Pile Head Response (9,950-10,000 cycles, last 50 cycles in full load packet) **Test-Load Packet 4-II**	**March 2016** D-18	MMI engineers • scientists • innovators

Analytical

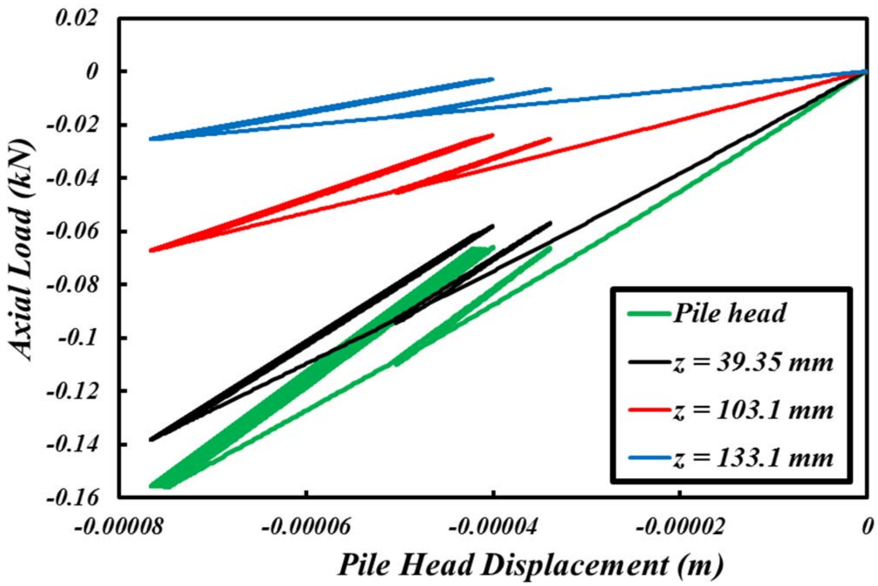

Experimental

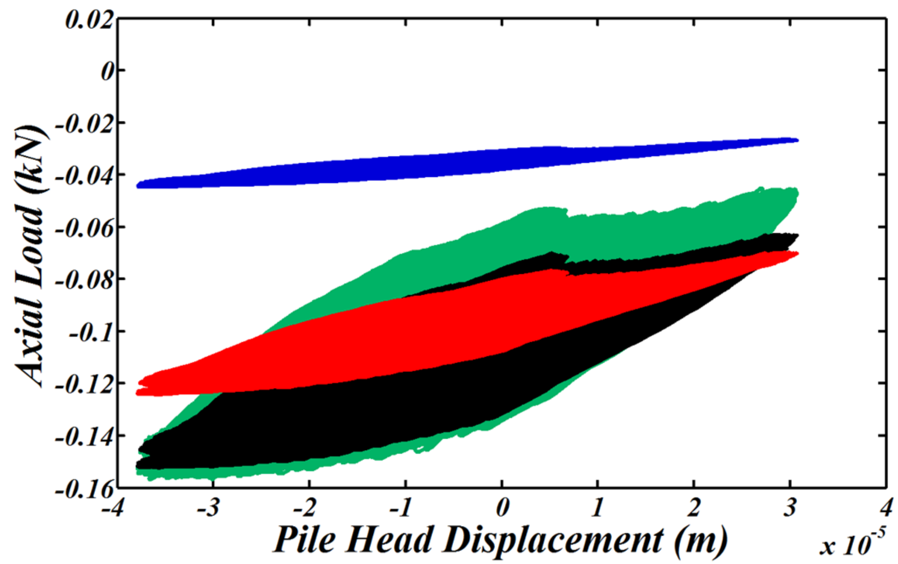

Analytical

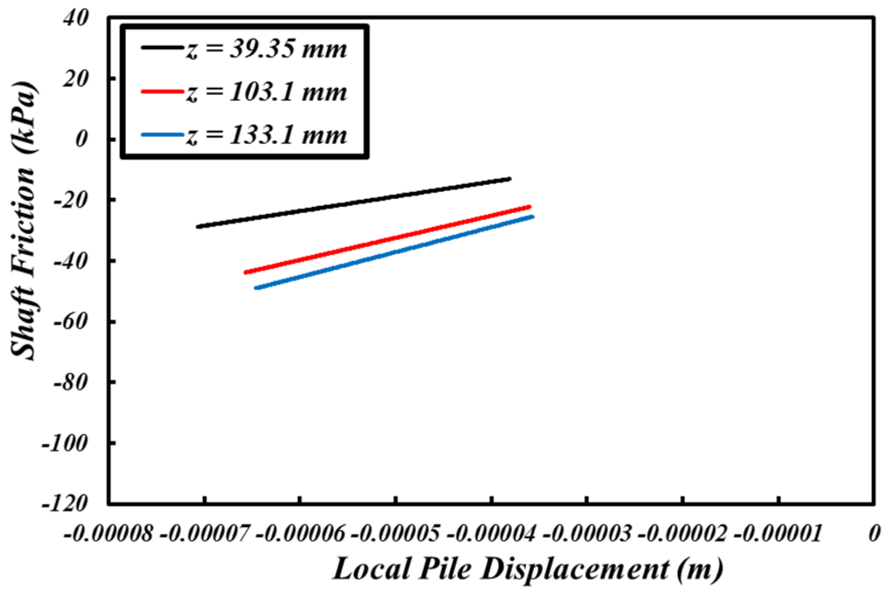

Experimental

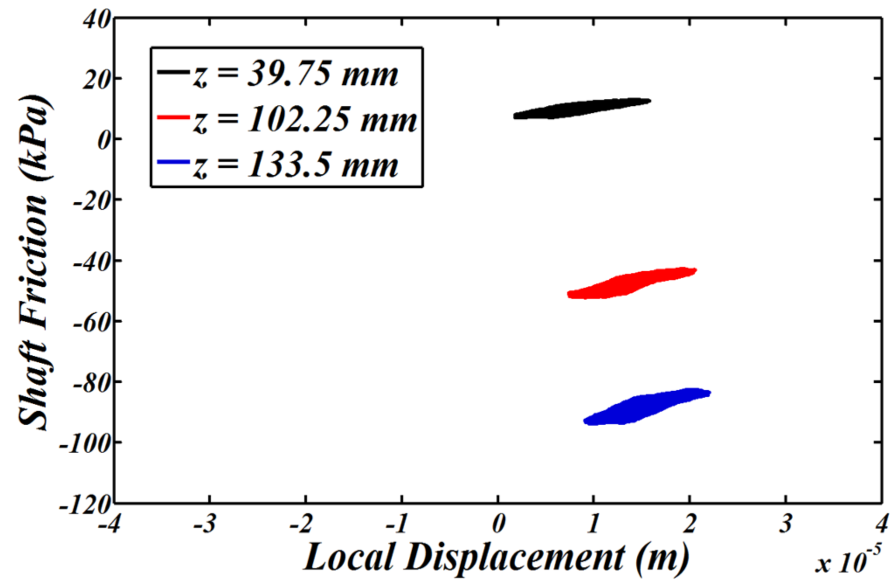

Analytical

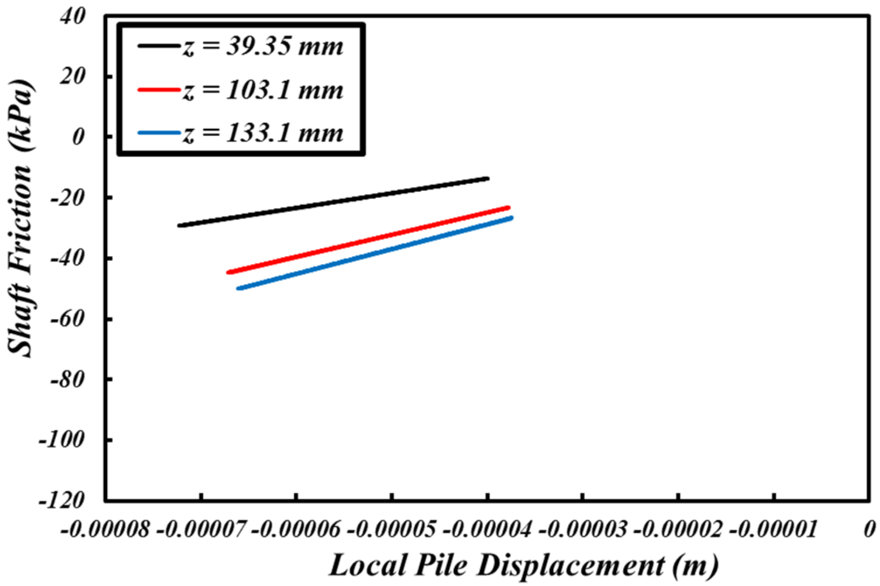

Experimental

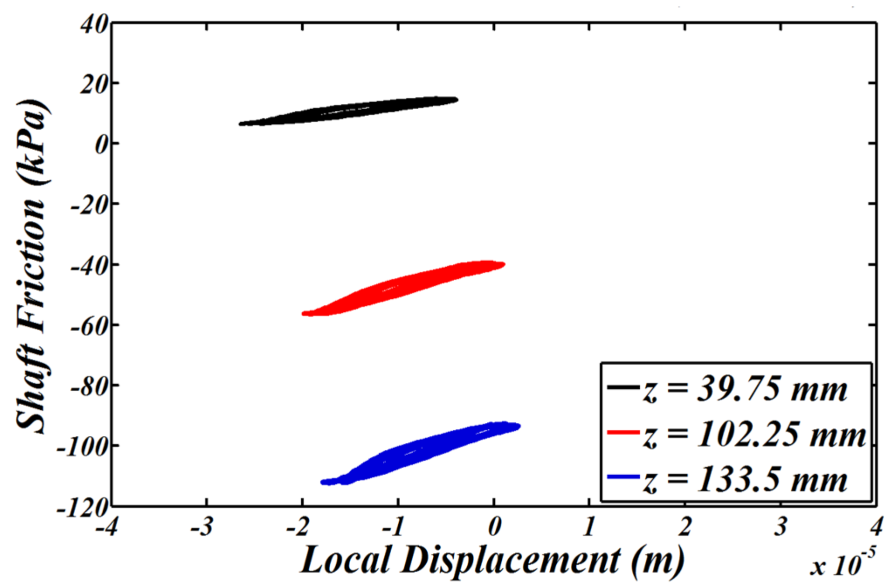

Shaft Friction Response (9,950-10,000 cycles, last 50 cycles in full load packet)
Test-Load Packet 4-II

March 2016

engineers • scientists • innovators

Analytical

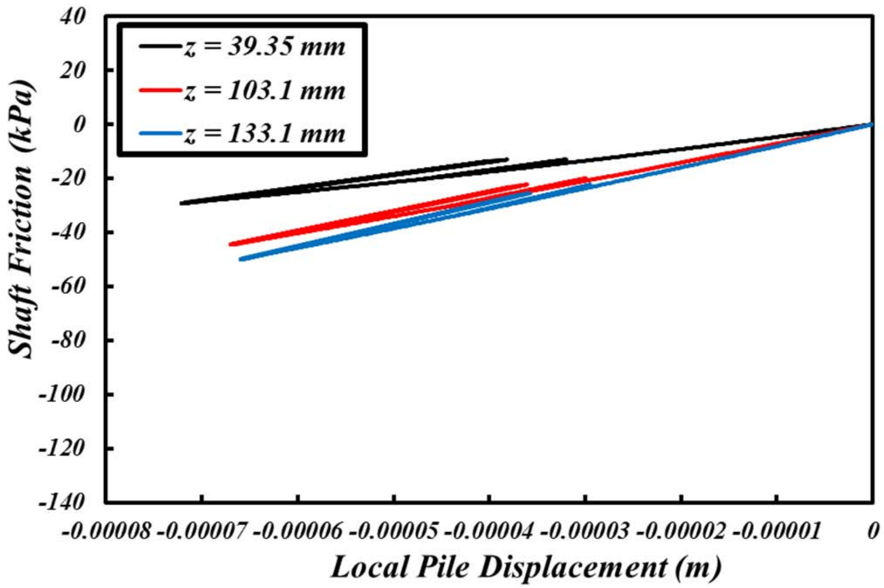

Experimental

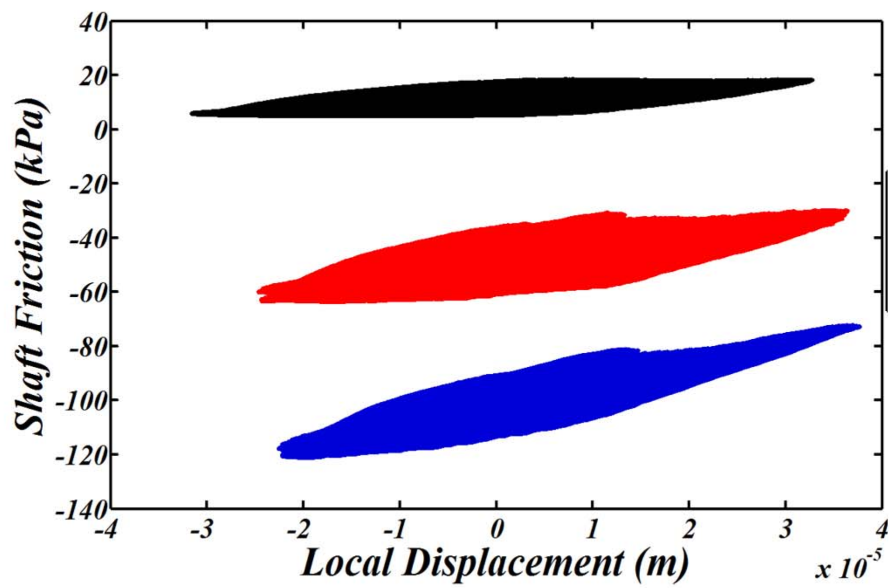

Load Packet 4-III

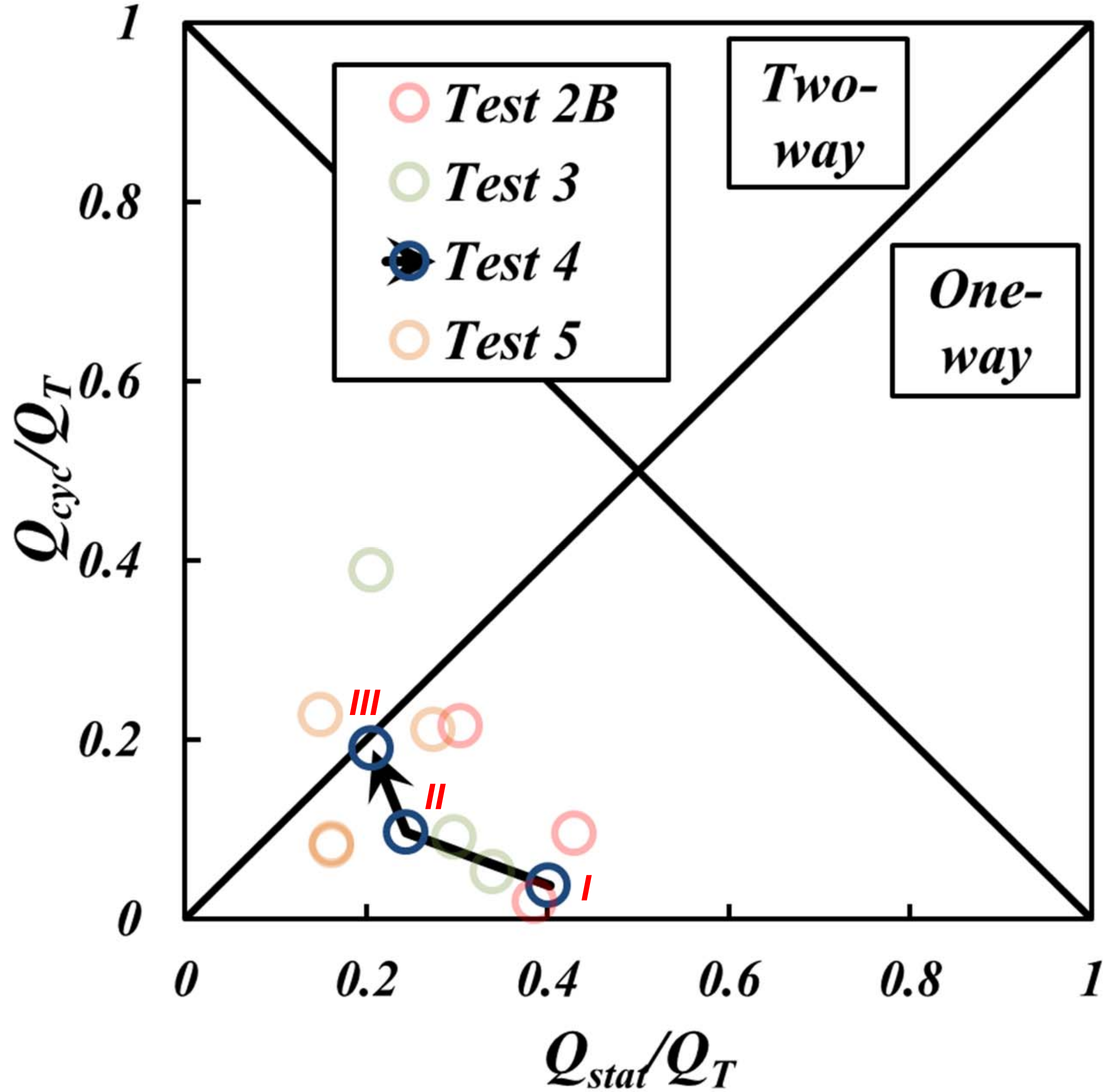

Analytical

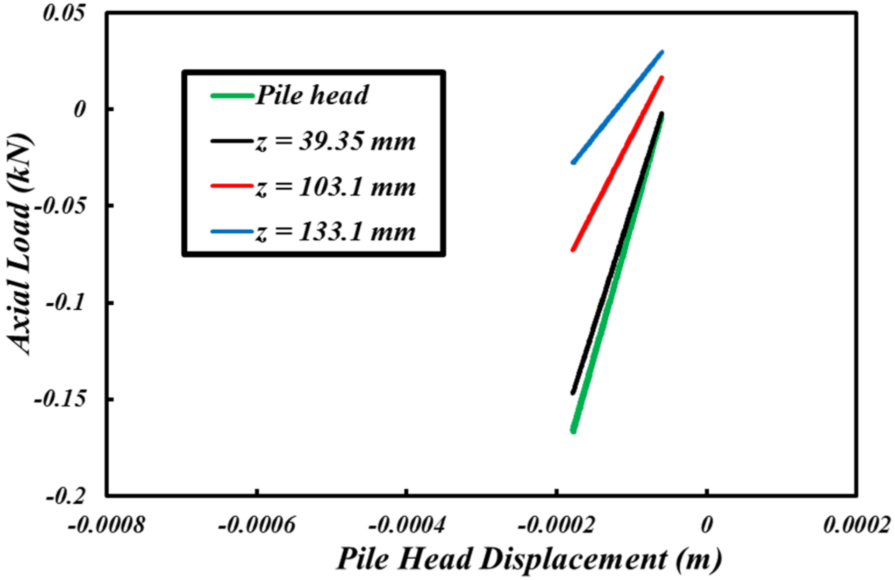

Experimental

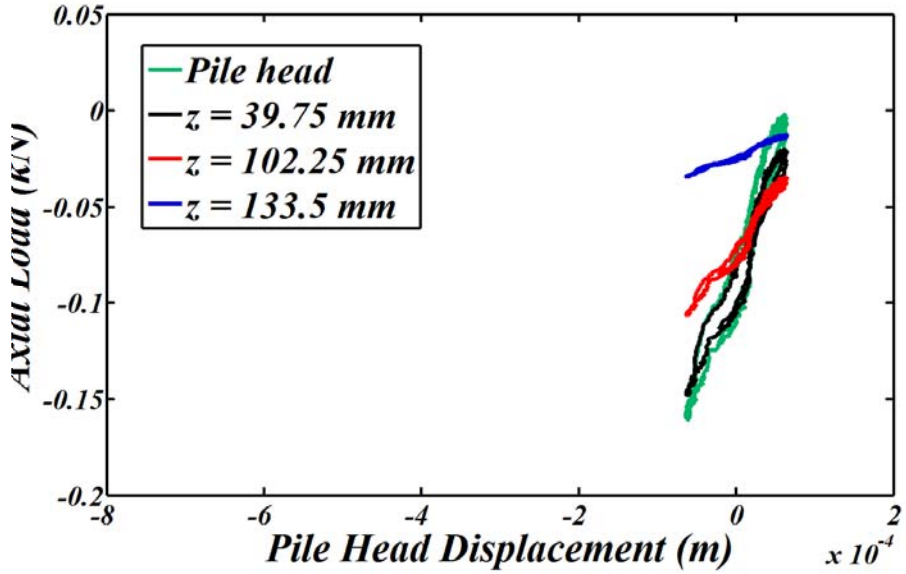

Analytical

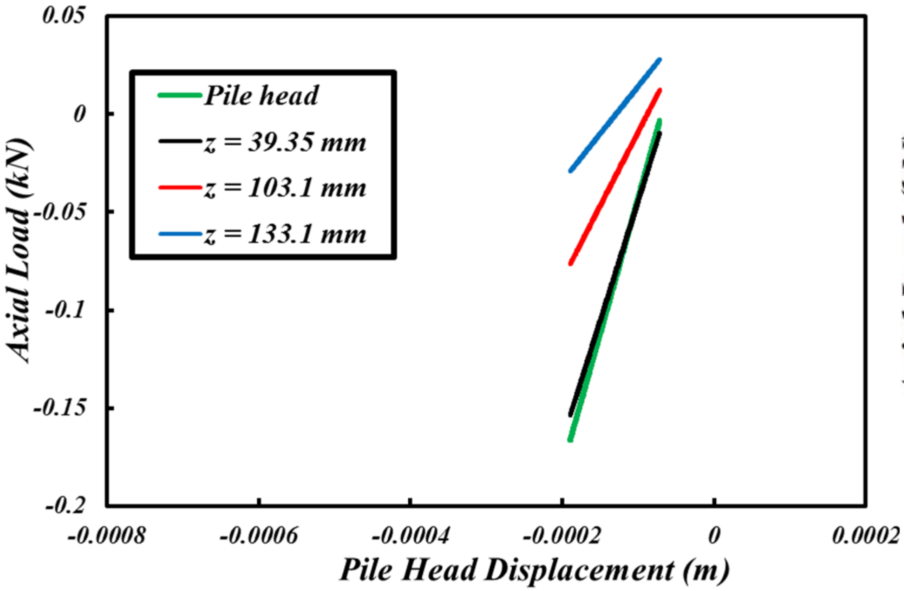

Experimental

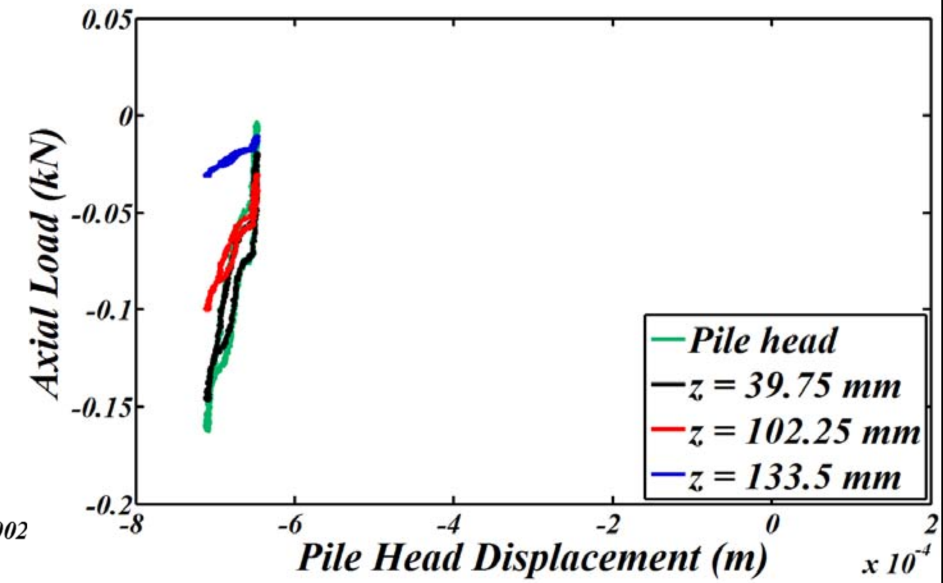

Pile Head Response (499-500 cycles, last 2 cycles in full load packet)
Test-Load Packet 4-III

Analytical

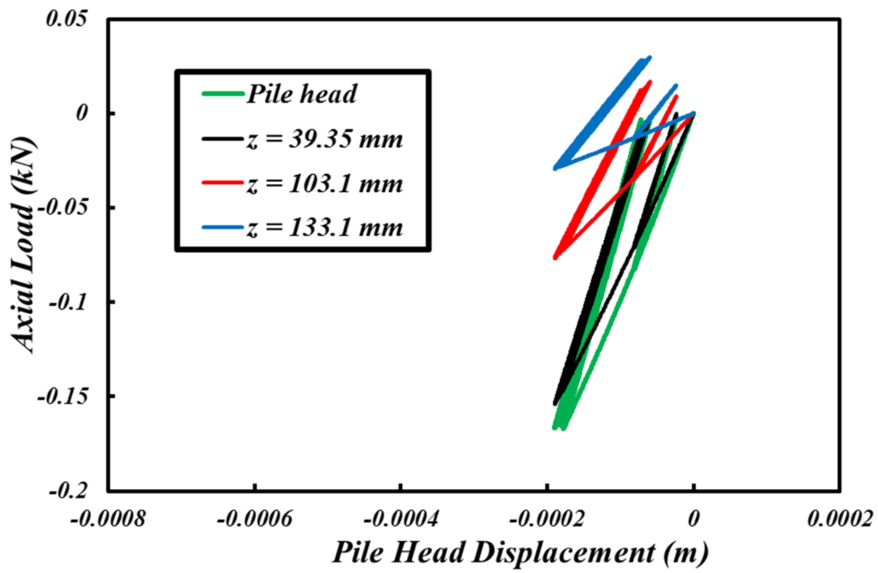

Experimental

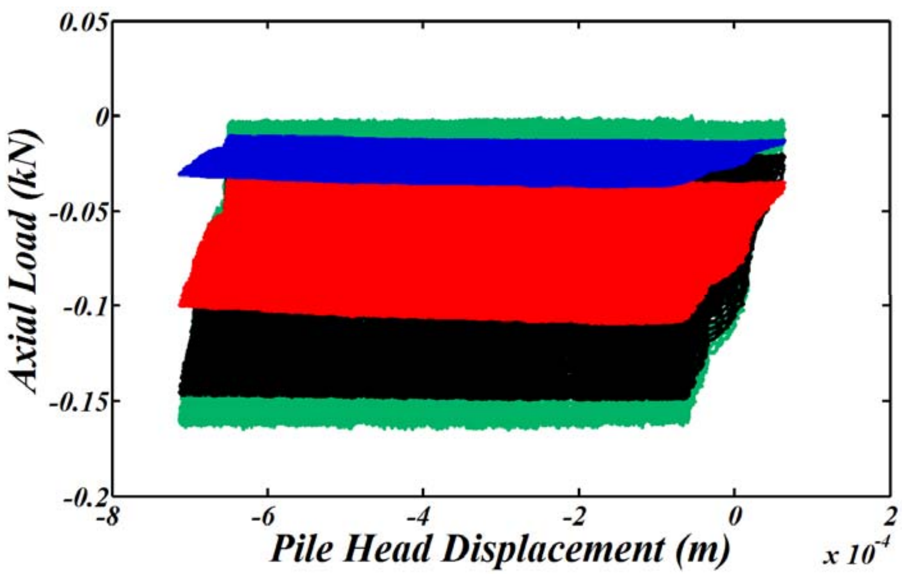

Analytical

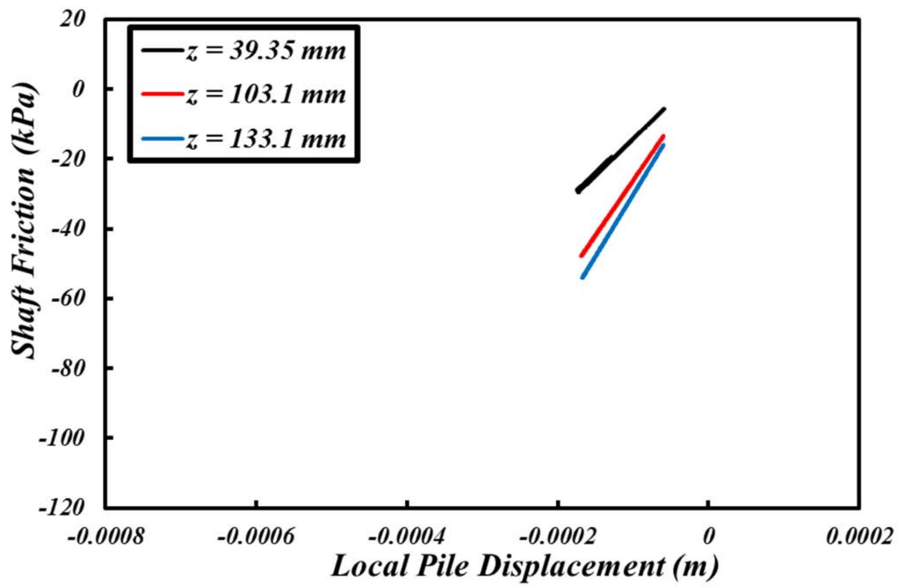

Experimental

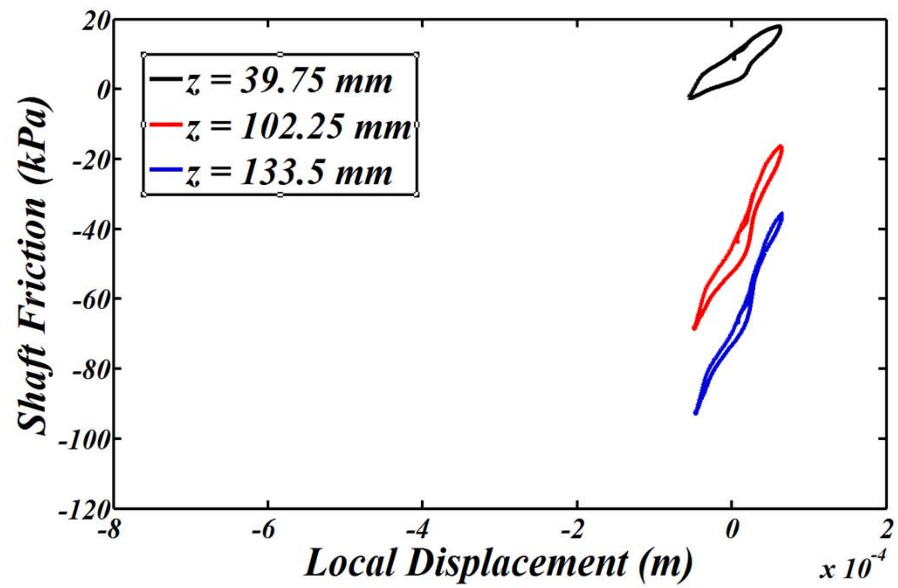

Analytical

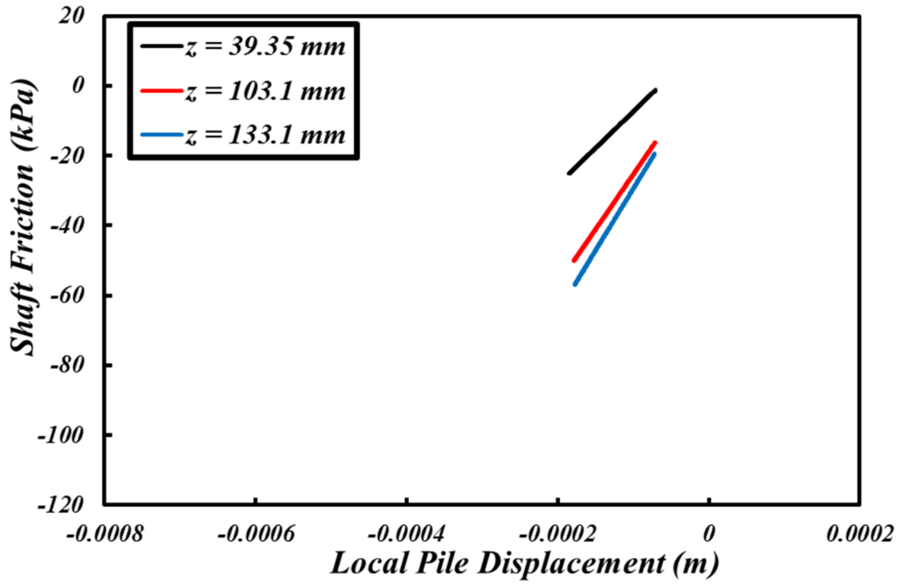

Experimental

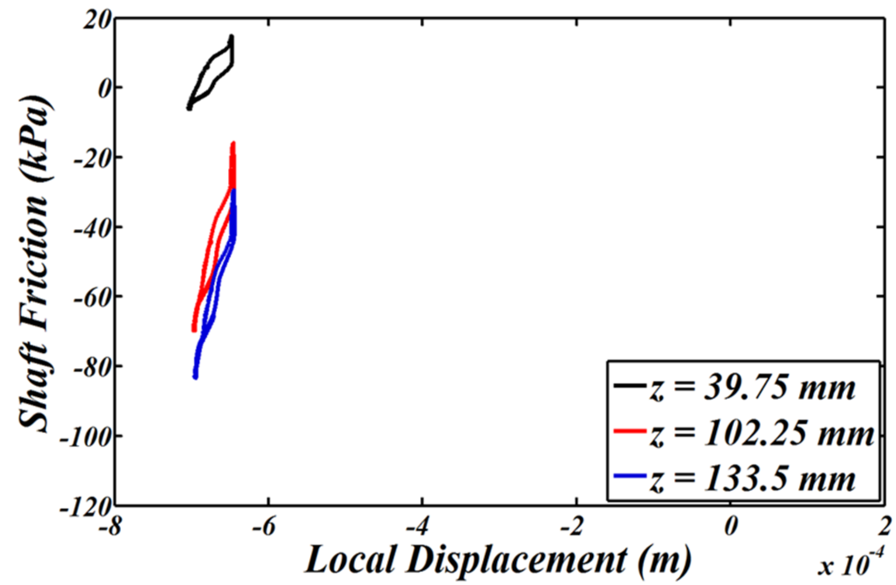

Shaft Friction Response (499-500 cycles, last 2 cycles in full load packet)
Test-Load Packet 4-III

engineers • scientists • innovators

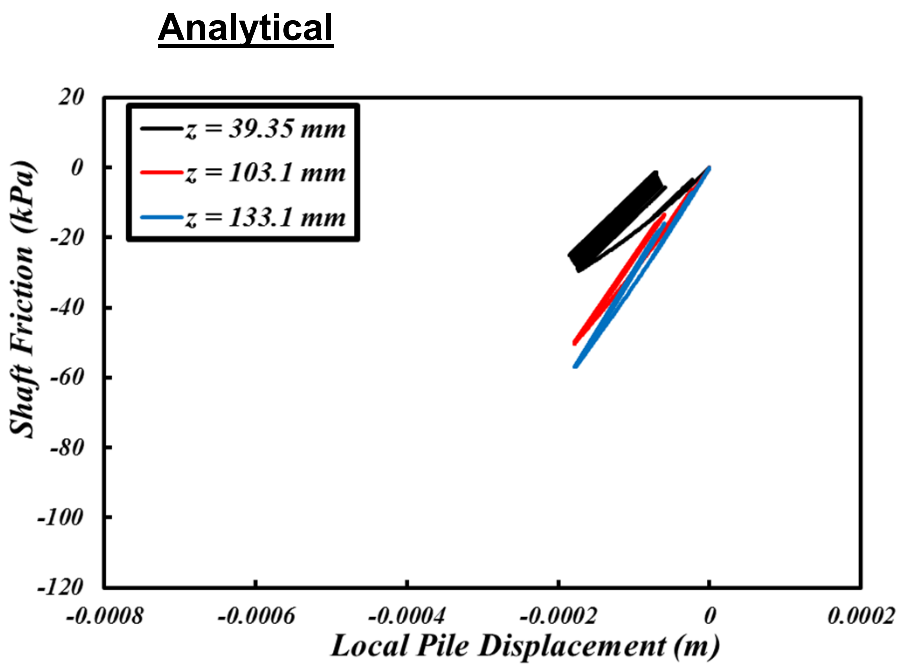

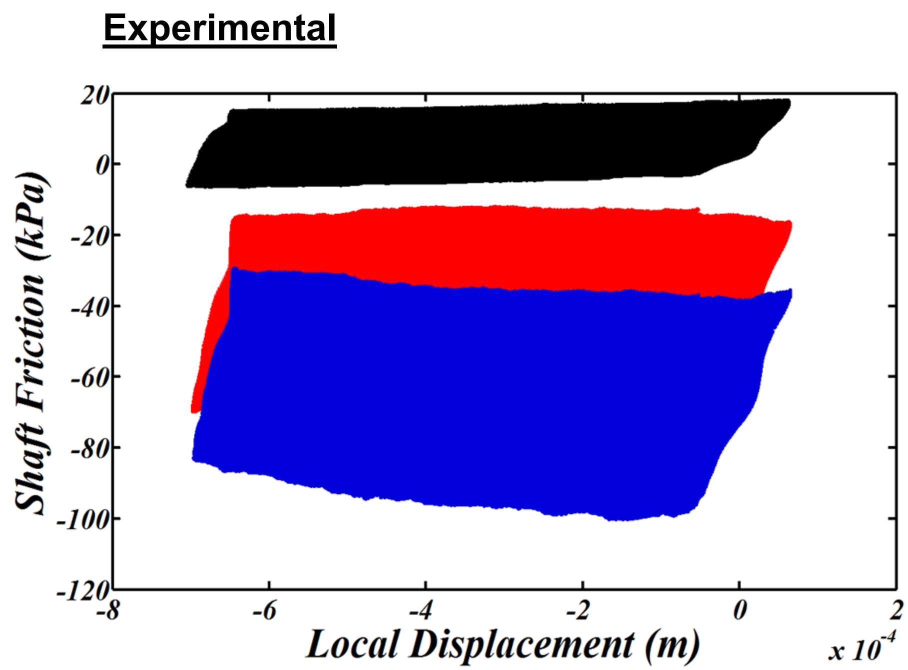

Shaft Friction Response (1-500 cycles, full load packet)
Test-Load Packet 4-III

MMI
engineers • scientists • innovators

APPENDIX E: SIMPLIFIED DAMAGE LAW ANALYSIS

Test-Load Packet	Number of Cycles, N_i	$\frac{Q_{stat}}{Q_T}$	$\frac{Q_{cyc}}{Q_T}$	Pre Tensile Capacity, Q_T (N)	Post Tensile Capacity (N)	Capacity Change (N)	Static Load, Q_{stat} (N)	Cyclic Load, Q_{cyc} (N)	Max Load, $Q_{max} = Q_{stat} + Q_{cyc}$ (N)	Residual Pullout (mm)	Residual Pullout Rate (mm/N_i/1,000)
2A-I	86,000	0.38	0.05	205	--	--	78	10	88	0.0	0.0
2B-I	100,000	0.39	0.02	285	275	10	110	6	116	0.0	0.0
2B-IIA	10,000	0.43	0.11	275	230	45	118	29	147	0.2	0.02
2B-IIB	10,000	0.30	0.22	230	175	55	70	51.5	121.5	9.5	0.95
3-I	100,000	0.32	0.06	180	175	5	58	10.5	68.5	0.0	0.0
3-II	10,000	0.29	0.10	175	170	5	50	17.5	67.5	0.0	0.0
3-III	500	0.19	0.42	170	180	-10	33	71.5	104.5	0.0	0.0
4-I	100,000	0.24	0.02	450[A]	454	-4	109	11	120	0.0	0.0
4-II	10,000	0.24	0.08	454	411	43	109	36	145	0.0	0.0
4-III	500	0.20	0.19	411	373	38	81	77.5	158.5	0.7	1.35
5-IA	10,000	0.14	0.08	400[B]	400[B]	0	55	31	86	0.0	0.0
5-IB	500	0.14	0.07	400[B]	340	60	55	27	82	0.0	0.0
5-II	500	0.16	0.23	340	375	-35	56	78	134	0.2	0.4
5-III	50	0.29	0.21	375	200	175	107	79	186	2.7	54

Note A: Test-Load Packet 4-I Pre-Tensile Capacity = 281N (tensile test did not complete, value above is assumed)
Note B: Test-Load Packet 5-I Pre-Tensile Capacity = 320N (tensile test did not complete, value above is assumed). No tensile test was performed between Test 5-1A and 5-1B.

Test-Load Packet	(a) Ultimate Residual Capacity, $Q_{T,f}$ (N)	(b) Total Capacity Reduction, D_T (%)	(c) Packet Capacity Reduction, D_i (%)	(d) Calculated Cycles to Failure, N_f (cycles)	(e) Selected Cycles to Failure, $N_{f\text{-}c}$ (cycles)
2A-I	--	--	--	--	--
2B-I	175	9.1%	5.9%	1,690,000	2,000,000
2B-IIA	175	45.0%	35.2%	28,444	30,000
2B-IIB	175	100.0%	50.7%	19,727	20,000
3-I	180	--	4.5%	2,230,000	2,000,000
3-II	180	-100.0%	4.7%	215,000	200,000
3-III	180	100.0%	-15.3%	-3,275	10,000,000[A]
4-I	200	-1.6%	-1.2%	-8,250,000	10,000,000[A]
4-II	200	16.9%	13.9%	71,860	70,000
4-III	200	18.0%	15.0%	3,322	3,000
5-IA	200	0.0%	0.0%	--	10,000,000[A]
5-IB	200	30.0%	18.9%	2650	3,000[B]
5-II	200	-25.0%	-17.0%	-2943	10,000,000[A]
5-III	200	100.0%	92.6%	54	50

Note A: Negative (or undefined) cycles to failure indicate an increase in pile capacity, therefore the selected cycles to failure ($N_{f\text{-}c}$) is set to 10,000,000 to essentially prevent reduction in capacity for these load packets.

Note B: 3,000 cycles to failure estimated for Test 5-IB may be an artifact of the assumed initial capacity of 400N, in tandem with the assumption that no degradation occurred over the 10,000 cycles applied during Test 5-IA. However, note that while Test 5-1A and Test 5-IB were performed at very similar load levels, Test 5-IB was performed at a lower frequency.

(a) Ultimate Residual Capacity = Measured residual capacity after the last load packet in the test ($Q_{T,f}$)

(b) Total Capacity Reduction = Capacity Change in Load Packet / (Pre-Tensile Capacity – Ultimate Residual Capacity)

$$D_T = \frac{\Delta Q_{T,i}}{Q_{T,i} - Q_{T,f}}$$

(c) Packet Capacity Reduction = Capacity Change in Load Packet / (Pre-Tensile Capacity – Maximum Load)

$$D_i = \frac{\Delta Q_{T,i}}{Q_{T,i} - Q_{max,i}}$$

(d) Calculated Cycles to Failure (N_f) = Number of Cycles / Packet Capacity Reduction

$$N_f = \frac{N_i}{D_i}$$

(e) Round Calculated Cycles to Failure ($N_{f\text{-}c}$)

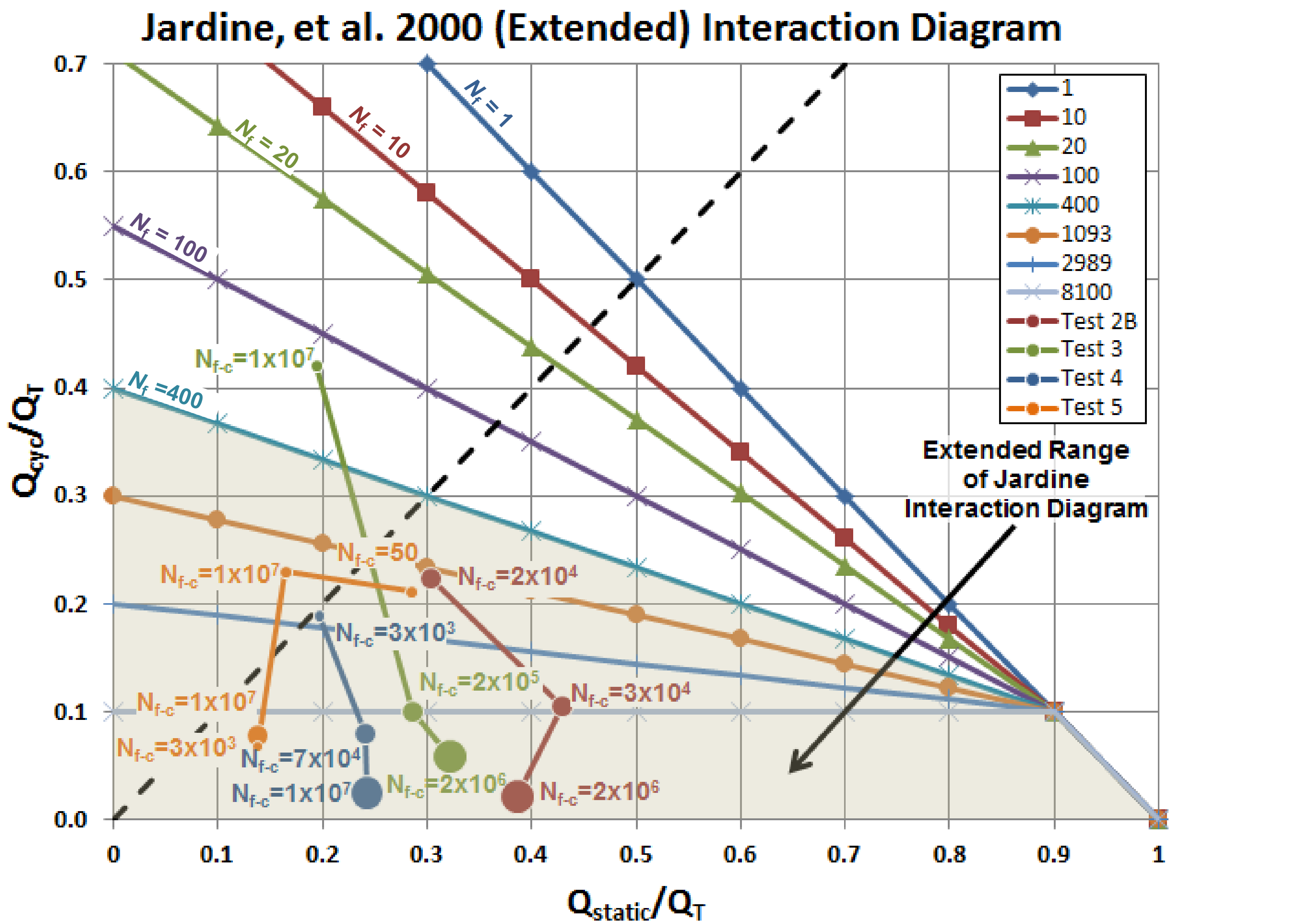

Interaction Diagram Calibration
Comparison of Test Results to Jardine, et al. 2000 “Extended” Interaction Diagram with Failure Curves

March 2016
E-4

MMI
engineers • scientists • innovators

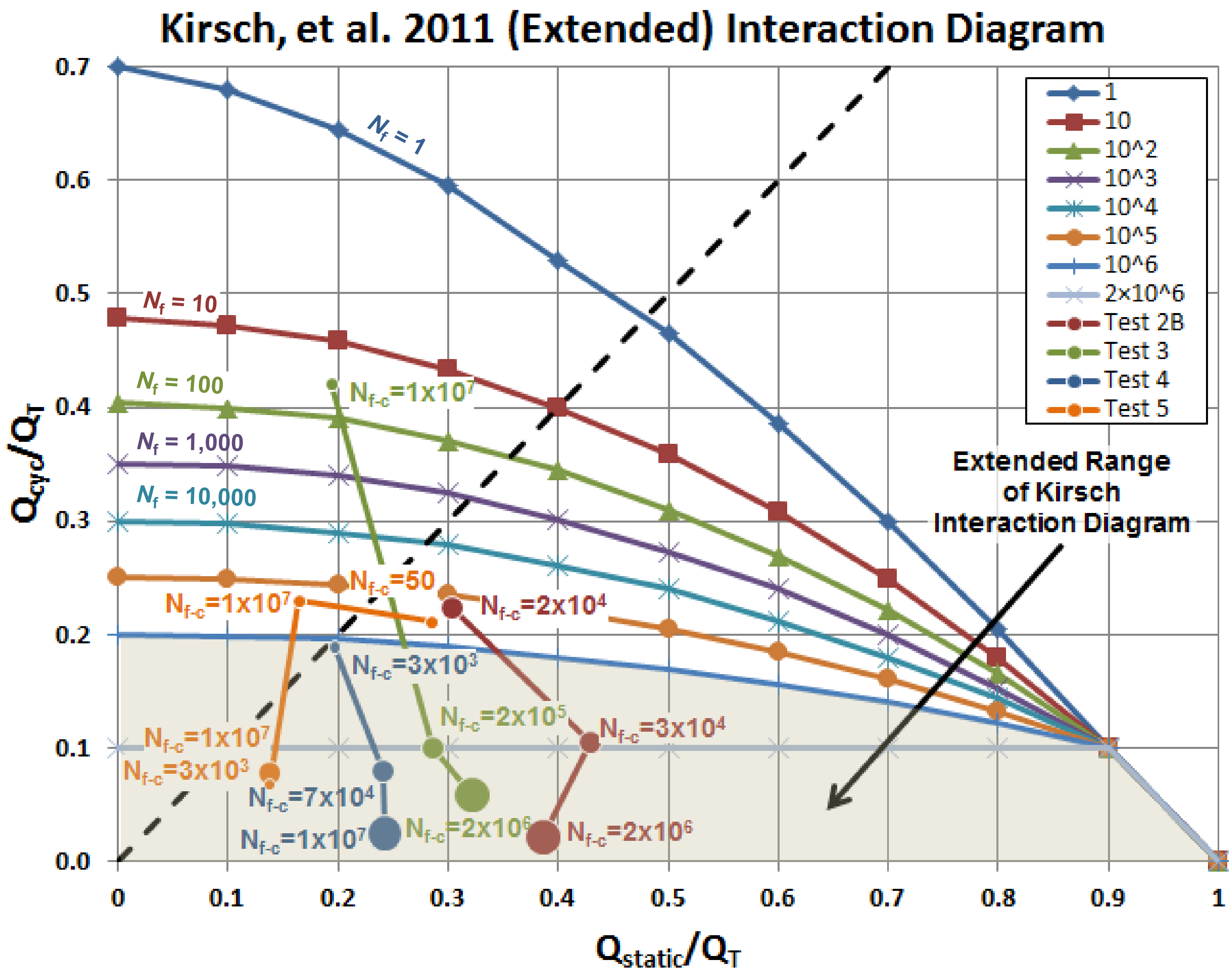

Interaction Diagram Calibration
Comparison of Test Results to Kirsch, et al. 2011 “Extended” Interaction Diagram with Failure Curves

March 2016

E-5

MMI engineers • scientists • innovators

Load Packet	Number of Cycles, N_i	Initial Tensile Capacity, $Q_{T,i}$ (N)	Q_{static} (N)	Q_{cyc} (N)	Selected Cycles to Failure, N_{f-c}	Damage, $D_i = N_i / N_{f-c}$ *Linear, failure if >1*	Q_{max} ($Q_{static}+Q_{cyc}$) (N)	Capacity Degradation, ΔQ_T D_i ($Q_{T,i}$ - Q_{max}) (N)	Final Capacity, $Q_{T,f}$: Calibrated *using known capacity change* ($Q_{T,i} - \Delta Q_T$) (N)	Final Capacity, $Q_{T,f}$: Measured in test (N)
2B-I	100000	285	110	6	2,000,000	0.050	116	8	277	275
2B-IIA	10000	277	118	29	30,000	0.333	147	43	233	230
2B-IIB	10000	233	70	51.5	20,000	0.500	122	56	177	175
3-I	100000	180	58	10.5	2,000,000	0.050	69	6	174	175
3-II	10000	174	50	17.5	200,000	0.050	68	5	169	170
3-III	500	169	33	71.5	10,000,000	0.000	105	0	169	180
4-I	100000	450	109	11	10,000,000	0.010	120	3	447	454
4-II	10000	447	109	36	70,000	0.143	145	43	404	411
4-III	500	404	81	77.5	3,000	0.167	159	41	363	373
5-IA	10000	400	55	31	10,000,000	0.001	86	0	400	400
5-IB	500	400	55	27	3,000	0.167	82	53	347	340
5-II	500	347	56	78	10,000,000	0.000	134	0	347	375
5-III	50	347	107	79	50	1.000	186	161	186	200

Load Packet	Number of Cycles, N_i	Initial Tensile Capacity, $Q_{T,i}$ (N)	Q_{static} (N)	Q_{cyc} (N)	Cycles to Failure, N_f	Damage, $D_i = N_i / N_f$ *Linear, failure if >1*	Q_{max} ($Q_{static}+Q_{cyc}$) (N)	Capacity Degradation, ΔQ_T D_i ($Q_{T,i}$ - Q_{max}) (N)	Final Capacity, $Q_{T,f}$: Failure Curves with Damage Law ($Q_{T,i} - \Delta Q_T$) (N)	Final Capacity, $Q_{T,f}$: Measured in test (N)
Jardine, et al. 2000 Extended Interaction Diagram										
5-IA	10000	400	55	31	2,000,000	0.005	86	2	398	400
5-IB	500	398	55	27	2,000,000	0.000	82	0	398	340
5-II	500	398	56	78	2,608	0.192	134	51	348	375
5-III	50	348	107	79	1,169	0.043	186	7	341	200
Kirsch, et al. 2011 Extended Interaction Diagram										
5-IA	10000	400	55	31	2,000,000	0.005	86	2	398	400
5-IB	500	398	55	27	2,000,000	0.000	82	0	398	340
5-II	500	398	56	78	1,009,899	0.000	134	0	398	375
5-III	50	398	107	79	699,391	0.000	186	0	398	200

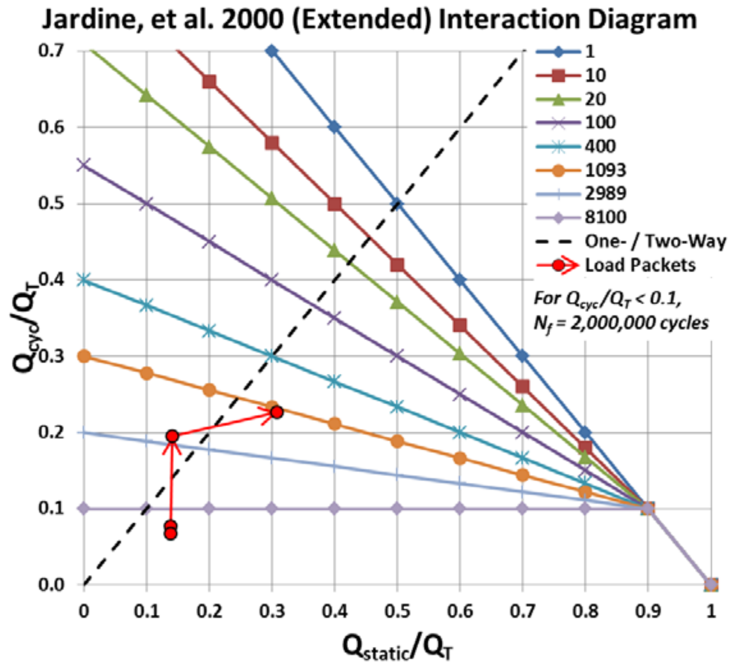

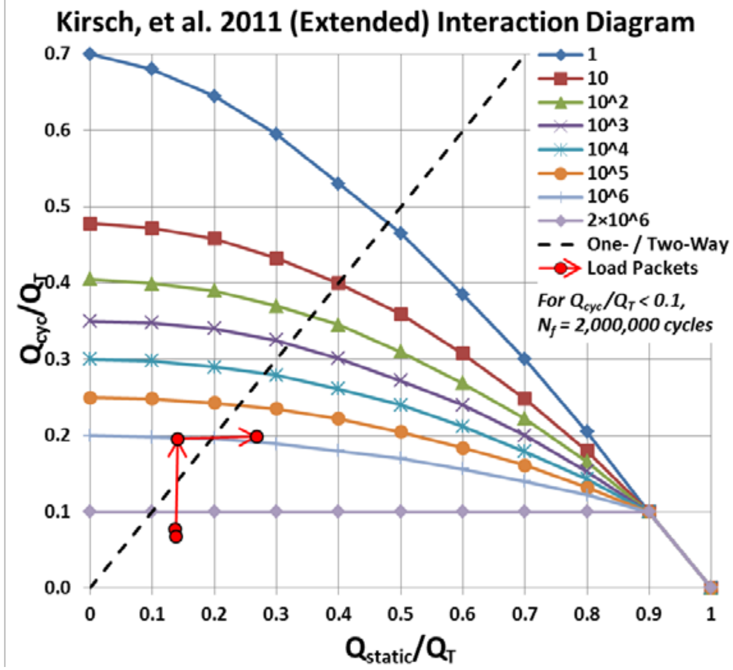

Implementing Damage Law using Interaction Diagram Failure Curves

Computing Final Capacity for <u>Test 5</u> Loading Conditions and Initial Capacity

(highlighted cells are used as input only)

March 2016

Load Packet	Number of Cycles, N_i	Initial Tensile Capacity, $Q_{T,i}$ (N)	Q_{static} (N)	Q_{cyc} (N)	Cycles to Failure, N_f	Damage, $D_i = N_i / N_f$ *Linear, failure if >1*	Q_{max} ($Q_{static}+Q_{cyc}$) (N)	Capacity Degradation, ΔQ_T D_i ($Q_{T,i}$ - Q_{max}) (N)	Final Capacity, $Q_{T,f}$: Failure Curves with Damage Law ($Q_{T,i} - \Delta Q_T$) (N)	Final Capacity, $Q_{T,f}$: Measured in test (N)
Jardine, et al. 2000 Interaction Diagram										
2B-I	100,000	285	110	6	2,000,000	0.050	116	8	277	275
2B-IIA	10,000	277	118	29	7,387	1.000	147	130	147	230
2B-IIB	10,000	147	70	51.5	44	1.000	122	26	122	175
Kirsch, et al. 2011 Interaction Diagram										
2B-I	100,000	285	110	6	2,000,000	0.050	116	8	277	275
2B-IIA	10,000	277	118	29	1,914,687	0.005	147	1	276	230
2B-IIB	10,000	276	70	51.5	1,042,655	0.010	122	1	274	175
Jardine, et al. 2000 Interaction Diagram										
3-I	100,000	180	58	10.5	2,000,000	0.050	69	6	174	175
3-II	10,000	174	50	17.5	8,061	1.000	68	107	68	170
3-III	500	68	33	71.5	1	1.000	105	68	0	180
Kirsch, et al. 2011 Interaction Diagram										
3-I	100,000	180	58	10.5	2,000,000	0.050	69	6	174	175
3-II	10,000	174	50	17.5	1,994,925	0.005	68	1	174	170
3-III	500	174	33	71.5	51	1.000	105	69	105	180
Jardine, et al. 2000 Interaction Diagram										
4-I	100000	450	109	11	2,000,000	0.050	120	17	434	454
4-II	10000	434	109	36	2,000,000	0.005	145	1	432	411
4-III	500	432	81	77.5	2,981	0.168	159	46	386	373
Kirsch, et al. 2011 Interaction Diagram										
4-I	100000	450	109	11	2,000,000	0.050	120	17	434	454
4-II	10000	434	109	36	2,000,000	0.005	145	1	432	411
4-III	500	432	81	77.5	1,129,228	0.000	159	0	432	373

Implementing Damage Law using Interaction Diagram Failure Curves
Computing Final Capacity for Test 2B, 3, and 4 Loading Conditions and Initial Capacity
(highlighted cells are used as input only)

Centrifuge Test 2B					Tensile Capacity (N)			
Test-Load Packet	Packet Cycles	Total Cycles	Q_{stat}/Q_T	Q_{cyc}/Q_T	Measured	Calibrated	Jardine, et al. (2000) Interaction Diagram	Kirsch, et al. (2011) Interaction Diagram
--	0	0	--	--	285	285	285	285
2B-I	100,000	100,000	0.39	0.02	275	277	277	277
2B-IIA	10,000	110,000	0.43	0.11	230	233	147	276
2B-IIB	10,000	120,000	0.30	0.22	175	177	122	274

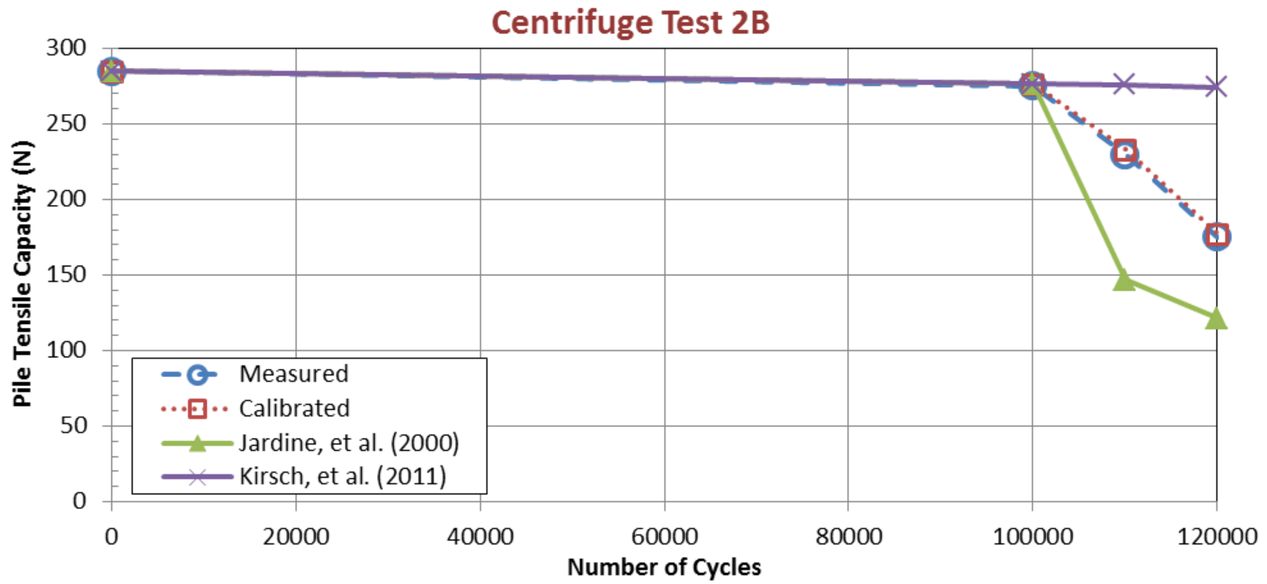

Centrifuge Test 3					Tensile Capacity (N)			
Test-Load Packet	Packet Cycles	Total Cycles	Q_{stat}/Q_T	Q_{cyc}/Q_T	Measured	Calibrated	Jardine, et al. (2000) Interaction Diagram	Kirsch, et al. (2011) Interaction Diagram
--	0	0	--	--	180	180	180	180
3-I	100,000	100,000	0.32	0.06	175	174	174	174
3-II	10,000	110,000	0.29	0.10	170	169	68	174
3-III	500	110,500	0.19	0.42	180	169	0	105

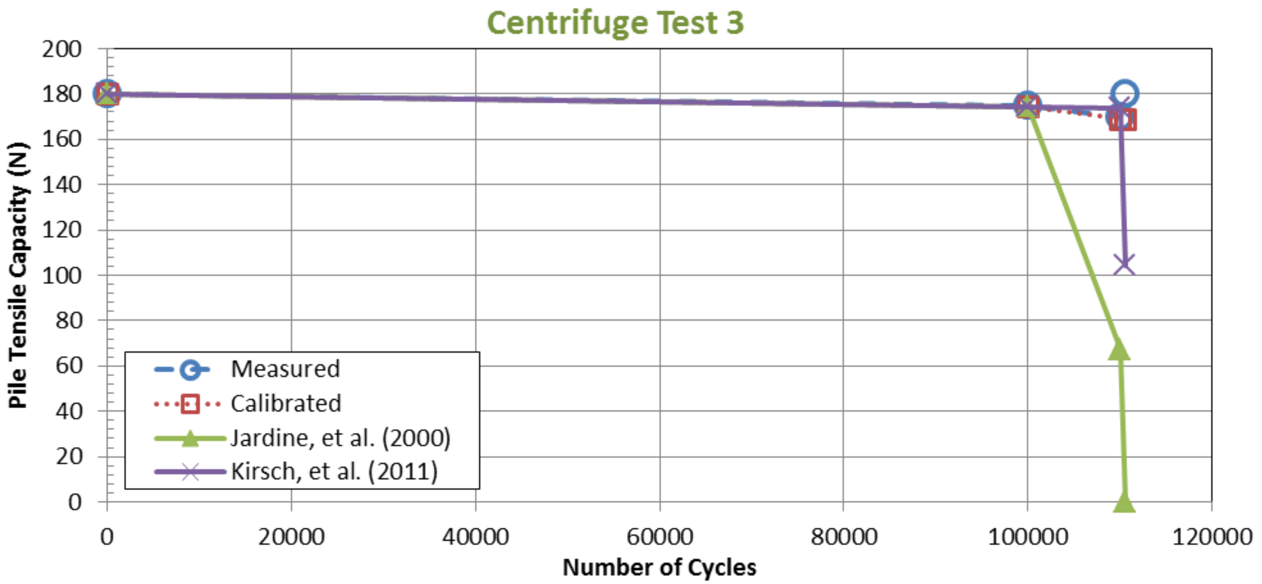

Centrifuge Test 4					Tensile Capacity (N)			
Test-Load Packet	Packet Cycles	Total Cycles	Q_{stat}/Q_T	Q_{cyc}/Q_T	Measured	Calibrated	Jardine, et al. (2000) Interaction Diagram	Kirsch, et al. (2011) Interaction Diagram
--	0	0	--	--	450	450	450	450
4-I	100,000	100,000	0.24	0.02	454	447	434	434
4-II	10,000	110,000	0.24	0.08	411	404	432	432
4-III	500	110,500	0.20	0.19	373	363	386	432

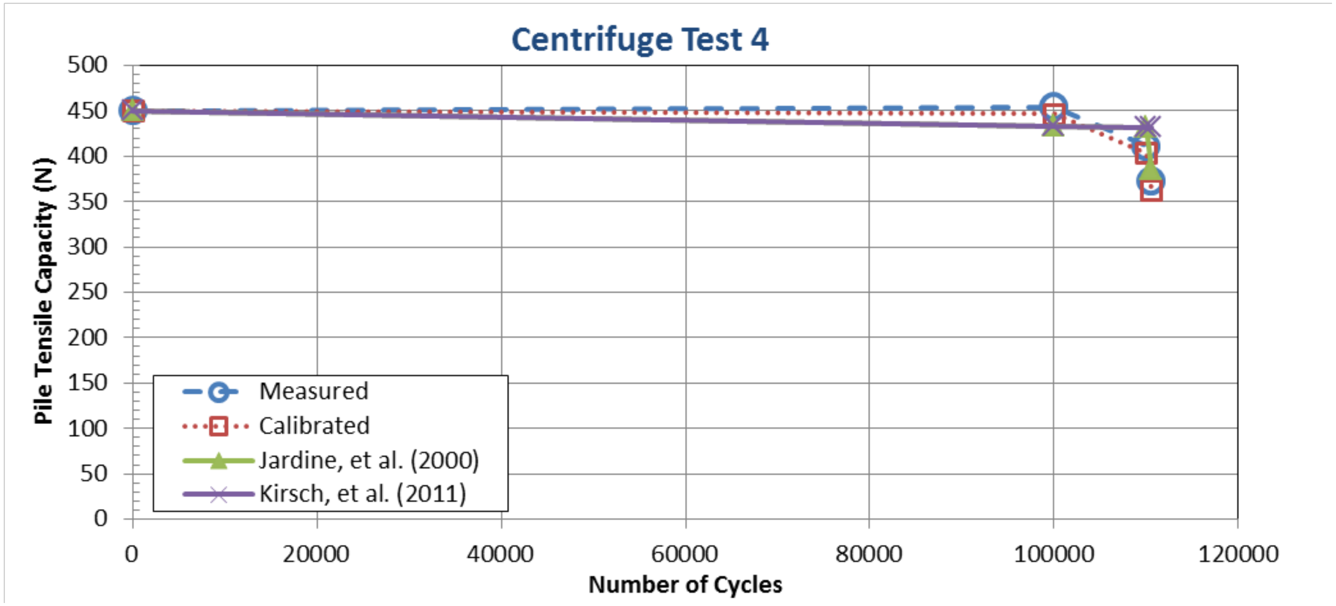

Centrifuge Test 5					Tensile Capacity (N)			
Test-Load Packet	Packet Cycles	Total Cycles	Q_{stat}/Q_T	Q_{cyc}/Q_T	Measured	Calibrated	Jardine, et al. (2000) Interaction Diagram	Kirsch, et al. (2011) Interaction Diagram
--	0	0	--	--	400	400	400	400
5-IA	10,000	10,000	0.14	0.08	400	400	398	398
5-IB	500	10,500	0.14	0.07	340	400	398	398
5-II	500	11,000	0.16	0.23	375	400	348	398
5-III	50	11,050	0.29	0.21	200	186	341	398